

The possibilities of hybrid steel-FRP bridges in movable highway spans

By

M. van der Wateren

In partial fulfilment of the requirements for the degree of

Master of Science

in Civil Engineering

at the Delft University of Technology, to be defended publicly on Thursday 5th of December, 2019 at 09:00 AM.

Student number: 4277945

Project duration: March 4th, 2019 - December 5th 2019

Thesis committee: Dr. M. Pavlovic TU Delft, supervisor and chair

Dr. Ir. M. Hendriks TU Delft, supervisor
Dr. Ir. R. Abspoel TU Delft, supervisor

Ing. B.S. Hylkema MSEng Witteveen+Bos, supervisor

Ir. L.J.M. Houben TU Delft, supervisor

An electronic version of this thesis is available at http://repository.tudelft.nl/.













Preface

This thesis is part of the requirements for the master structural engineering at the Civil Engineering faculty of the Technical University of Delft. Together with engineering firm Witteveen+Bos a subject was formulated around the usage of fibre reinforced polymers in bridge engineering to cope with weight problems in renovation projects.

In the first place I would like to thank Witteveen+Bos for the interesting topic and the support I have received during my graduation period. In specific Ing. Björn Hylkema who guided and supervised me through each step of the process and made time for me while there was none.

My sincere gratitude goes out to Dr. Marko Pavlovic whom I have had the pleasure to be supervised by for both my bachelor and master graduation works. By making me rethink my findings after each meeting he made me dig deeper and gain more knowledge than I could have on my own. I am thankful for the feedback from Dr. Ir. Roland Abspoel and Dr. Ir. Hendriks for their critical view at the structure and grammar of my thesis.

Last but not least, I would like to thank my parents and girlfriend for their patience and time they invested in helping me bring order in the chaos that my thesis was. Whilst having no civil engineering background they had a tremendous amount of tips and tricks on how to bring structure to my thesis and make it readable and understandable for a layman.





Abstract

The increasing number of vehicles does not stop, axle loads get higher and wheel contact surfaces have decreased causing bridges to show significant fatigue damage. Demolishing and building a new bridge is out of the picture due to the current ideas on sustainability and environmental impact. Therefore renovation is necessary, as much of the existing structures should be reused in the design of a new structure. This results in massive challenges especially in the design of new movable bridge leaves which should reuse the pillars and foundation of the current bridge. The weight of the new movable bridge is limited to the same or even less than the old one, but should outperform it by many years.

The old movable bridge leaf, often a steel orthotropic deck bridge, show significant fatigue damage. Designing a new steel orthotropic deck bridge which fulfils current safety regulations results in a large weight. This weight might be too much for the old already existing pillars and foundation so a lighter bridge leaf is desirable. A solution could be offered by a new hybrid bridge leaf consisting of a fibre reinforced polymer sandwich panel and a steel substructure. Especially when full hybrid interaction between the two materials (steel and fibre reinforced polymers) is considered a drastic decrease in weight of the bridge leaf is expected.

Hybrid bridge leaves consisting of steel and fibre reinforced polymers are already used nowadays, however these are bridge leaves without full hybrid interaction. Due to a lack of knowledge about the effects and safety of the full hybrid interaction engineering firms and contractors are still cautious to apply it. Quantifying the added value of hybrid bridge leaves with full hybrid interaction when considering weight will show the need for more research into the hybrid interaction. The goal of this report is to show this added value of hybrid bridge leaves with full hybrid interaction.

Parametric models have been created for both bridge types, orthotropic and hybrid, using finite element software RFEM to quantify this added. Both bridge models have been exposed to the same load cases stated in the Eurocode for traffic loads and fatigue loads. Maximum deflection and stresses have been verified in the steel of both bridges for the traffic loads. The sandwich panel has been verified for buckling and fatigue using a local model. The fatigue load cases have been used to verify the bridges steel frame. Global fatigue details in the connection between main girder and crossbeams have been investigated. An extra local detail has been investigated for the orthotropic bridge, namely the stiffener to crossbeam connection. Different bridge dimensions have been implemented to suit highway situations in the Netherlands to determine if the use of hybrid bridges is limited to specific bridge dimensions.





Results showed a clear favour towards the hybrid bridge for all of the spans and widths investigated. The difference in weight of the hybrid bridges showed a decrease of 15 to 30% as opposed to the orthotropic steel bridge. This decrease in weight was mainly caused by the difference in deck structure. The sandwich panel, with a weight of 85 kilograms per square meter, shows far less weight contribution in the hybrid bridge than the stiffeners and deck plate, with a combined weight of 256 kilograms per square meter, have in the steel orthotropic bridge.

However weight is not the only factor for which a design is chosen. Both costs and environmental impact have a big influence on the decision making process. The cost comparison showed that the OSD bridge and hybrid bridge are competitive in pricing in an early design stage. However there are many uncertainties that could result in one of the bridge types being significantly more expensive than the other. More experience with FRP and the hybrid interaction is needed to create better cost indications in such an early design stage.

The environmental impact showed a difference ranging from 10% to 30% in favour of the hybrid bridge for both the CO₂ impact analysis and the life cycle analysis by GWW. This difference was obtained when considering the production of the movable bridge including the counterweight and span. The difference is mainly due to the large amount of steel needed for the bridge leaf of the steel orthotropic bridge which also means that more material is needed for the counterweight. Other contributing factors to pollution such as transportation, installation, opening mechanism and maintenance have not been considered. It is expected that these factors further increase the difference due to the light weight of the hybrid bridge.

While this research showed a clear favour for hybrid bridges over steel orthotropic bridges in terms of weight and environmental impact and no significant difference in cost, more research is needed before this type of bridge is used more often. The full hybrid interaction between steel and FRP that has been modelled for the hybrid bridge comes with uncertainties due to the novelty of the connection type. Further research on this connection in bridge engineering, either bolted or adhered, is required before it can be implemented in norms and regulations.

An optimization of the sandwich panel is also recommended. In this research a slightly overdimensioned sandwich panel has been used. Optimizing this panel could result in a further decrease in weight. This optimization can easily be done on a local scale. However, when trying to optimize it on a global scale together with the steel substructure advanced software is needed to model the connection between the steel and the sandwich panel.

Although further research is necessary, this report shows the added value of hybrid bridges with full hybrid interaction and creates a step towards more use of hybrid steel and fibre reinforced polymer structures.





Table of content

Ta	able of	content	V
Α	bbrevia	ations	vii
Li	st of s	ymbols	viii
Li	st of fig	gures	x
Li	st of ta	ıbles	xiii
1	Intro	oduction	1
	1.1	Project motivation	1
	1.2	Problem statement	5
	1.3	Research objective	6
	1.4	Outline	9
2	Stat	te-of-the-art	11
	2.1	Bridges in the Netherlands	12
	2.2	Fibre reinforced polymers	21
	2.3	Norms and regulations	42
3	Fini	te element software	45
	3.1	Software requirements	45
	3.2	Conclusion	51
4	RFE	EM models	53
	4.1	Workflow	53
	4.2	Model design	56
	4.3	Model verification	83
	4.4	Conclusion	99
5	Loa	ding and results	101
	5.1	Load models	101
	5.2	Results export	109
	5.3	Analysis of load models	111
	5.4	Conclusion	121
6	Opt	imization	123
	61	Ontimization OSD model	124





6.2	Optimization nybrid model	130
6.3	Comparison	133
6.4	Conclusion	135
7 Co	mparison of results	137
7.1	Simulation parameters	137
7.2	Results	139
7.3	Comparison	151
8 Co	nclusion	159
8.1	OSD or hybrid	159
8.2	Finite element software	161
9 Re	commendation	163
10 E	Bibliography	165
Annex A	A Calculation elaborations	169
Annex E	Bridge data Rijkswaterstaat	173
Annex (Norms and regulations	175
C.1	Load models	176
C.2	FRP norms and regulations	198
Annex [Sandwich panel fatigue results	205
Annex E	Rain flow method	207
Annex F	FEM elements and analysis	211
Annex (S Validation of RFEM laminate	215
Annex I	Validation RFEM release mechanism	221
Annex I	Environmental impact (GWW)	229
Annex.	Graphic weight results	231





Abbreviations

Abbreviation Explanation

FLM Fatigue load model

FRP Fibre reinforce polymer

LM Load model

OSD Orthotropic steel deck

ROK Design guidelines for civil engineering works, "Richtlijnen Ontwerp

Kunstwerken"

RFEM finite element software, stands for "random finite element modelling"

SLS Serviceability limit state

TS Tandem system (in load models)

UDL Uniformly distributed load (in load models)

UD-plies Unidirectional plies, an FRP layer with fibres in one single direction

ULS Ultimate limit state





List of symbols

Symbol	Unit	Explanation
A	[-]	Matrix (bold non-italic)
A	[-]	Vector (bold italic)
A_{ij}	[-]	Value for elements of matrix (non-bold italic)
$\mathbf{A}, \mathbf{B}, \mathbf{D}, \mathbf{Q}$	[-]	Matrices used in the laminate theory
_	[-]	Inverse of A
a		Width of laminate
b	[mm]	
D	[-]	Fatigue damage (Palmgren-miner rule)
$D_{11}, D_{12}, D_{22}, D_{66}$	[Nmm]	Values obtained from D-matrix
E_1 , E_2	$\left[\frac{N}{mm^2}\right]$	In plane E-modulus in material main directions 1 and 2
E_{f1} , E_{f2}	$\lfloor \overline{mm^2} \rfloor$	E-modulus of fibres in main fibre directions 1 and 2
-117-12	$\lfloor \frac{1}{mm^2} \rfloor$	
$E_{\mathbf{r}}$	[N]	E-modulus of resin
ſ	$\lfloor \overline{mm^2} \rfloor$	Material yield point
$f_{\mathcal{Y}}$	$\left[\frac{1}{mm^2}\right]$	Material yield politi
G_{12}		In plane shear modulus
	$\lfloor \overline{m m^2} \rfloor$	·
G_r	[]	Shear modulus of resin
h	$\lfloor mm^2 \rfloor$	Total laminate thickness / height
k_s	[mm] [–]	Correction factor needed for certain detail categories
K K	[-]	Factor specific to laminate buckling
L	[m]	Span length
M	[N]	Moment vector
N	$[\underline{N}]$	Normal force vector
	$\lfloor mm \rfloor$	Number of evelop for a appoint attract range
n _{ei}	[-] [-]	Number of cycles for a specific stress range Endurance in cycles obtained from SN curve
$N_{Ri} \ Q_{ik}$	[kN]	Axle load
q_{ik}	$\lceil kN \rceil$	Distributed load
	$\lfloor \overline{m^2} \rfloor$	
t	[mm]	Thickness of laminate
$u_{z,max}$	[m]	Maximum deflection of the model in z-direction
V_f	[-]	Fibre volume percentage of ply
w_i	[m]	Width of lane i
α_Q , α_q	[-]	Adjustment factors for load models
γ_Q	[-]	Safety factor
$\Delta\sigma_{C}$	[N]	Detail category
3	$\lfloor \frac{1}{mm^2} \rfloor$	
$\Delta\sigma_D$	[N]	Constant amplitude fatigue limit
Λσ.	$\lfloor \overline{mm^2} \rfloor$	Cut-off limit
$\Delta\sigma_L$	$\left[\frac{1}{mm^2}\right]$	Out-on infint
	נוונוונ]	





Symbol	Unit	Explanation
$\Delta\sigma_R$	$\left[\frac{N}{mm^2}\right]$	Stress range
$\Delta\phi_{fat}$	[-]	Dynamic amplification factor
ε	[- <u>]</u>	Strain
η_2, η_g	[-]	Conversion factor for E_2 or G_{12}
κ	[]	Curvature
	\overline{mm}	
λ	[-]	Buckling factor
v	[-]	Factor specific to laminate buckling
v_{12}	[-]	In plane Poisson ratio in material main directions 1 and 2
v_r	[-]	In plane Poisson ratio of resin
v_f	[-]	In plane Poisson ratio of fibre in material main directions 1 and 2
ξ_2, ξ_g	[-]	Conversion factor for E_2 or G_{12}
σ	$\left[\frac{N}{mm^2}\right]$	Occurring stress
$\sigma_{cr,c}$	$[\underline{N}]$	Critical buckling stress
σ_{max}	$\begin{bmatrix} mm^2 \end{bmatrix}$	Maximum occurring stress
$ au_{xy,cr}$	$\begin{bmatrix} mm^2 \\ \frac{N}{mm^2} \end{bmatrix}$	Critical buckling stress for shear buckling
φ	[°]	Orientation of fibres
ϕ_{UD}	[-]	Empirical reduction factor equal to 0.97





List of figures

Figure 1.1 Traffic intensity	1
Figure 1.2 Super singles vs dual wheels	2
Figure 1.3 movable bridge weight trend line 1950-2000	2
Figure 1.4 Bascule bridge sideview	3
Figure 1.5 Bridge types(Li, 2014)	4
Figure 2.1 Typical bascule bridge (Koglin, 2003)	14
Figure 2.2 Swing bridge, Afsluitdijk (Afsluitdijk, 2017)	14
Figure 2.3 Vertical lift bridge, Botlek (NOS, 2015)	15
Figure 2.4 OSD bridge cross section (Freitas, 2011)	16
Figure 2.5 cope hole trapezoidal stiffener (Li, 2014)	17
Figure 2.6 Hybrid concrete leaf (SCIA, 2016)	19
Figure 2.7 FRP laminate (CUR 96, 2017)	21
Figure 2.8 Example: equation (2.11) clarification	26
Figure 2.9 FRP sandwich panel (Reis & Rizkalla, 2008)	34
Figure 2.10 Bridge deck beam model	36
Figure 2.11 bridge deck shear stress due to curvature	36
Figure 2.12 Leeghwaterbrug bridge geometry, top view (Souren, 2017)	37
Figure 2.13 Leeghwaterbrug sandwich panel cross-section (Souren, 2017)	39
Figure 2.14 Hierarchical order of norms and regulations	42
Figure 4.1 Model workflow	53
Figure 4.2 Model design	54
Figure 4.3 Model design: main girder to crossbeam flange connection	56
Figure 4.4 Parameters OSD bridge	57
Figure 4.5 Cross-sections OSD bridge	58
Figure 4.6 Dimensions stiffener and deck plate	59
Figure 4.7 Details to consider for OSD bridge	63
Figure 4.8 Hybrid model: rigid links	65
Figure 4.9 Parameters hybrid bridge	66
Figure 4.10 Cross-sections hybrid bridge	67
Figure 4.11 Details to consider for hybrid bridge	69
Figure 4.12 Buckling load locations and failure modes	72
Figure 4.13 Buckling sandwich panel parameters	75
Figure 4.14 Sandwich panel cross-section	80
Figure 4.15 Fatigue model sandwich panel side view	81
Figure 4.16 Parameters OSD model verification	83
Figure 4.17 side view OSD model verification	84





Figure 4.18 cross-section OSD model verification	84
Figure 4.19 Vertical deformation OSD model verification	86
Figure 4.20 Sigma_x deck plate OSD model verification	87
Figure 4.21 Strains OSD model verification	88
Figure 4.22 Strain diagram OSD model verification	88
Figure 4.23 Stresses OSD model verification	89
Figure 4.24 stress diagram OSD model verification	89
Figure 4.25 stress-strain diagram OSD model verification	89
Figure 4.26 Strain distribution OSD model verification	91
Figure 4.27 Parameters Hybrid model verification	92
Figure 4.28 cross-section hybrid model verification	93
Figure 4.29 Vertical deformation hybrid model verification	94
Figure 4.30 Strains hybrid model verification	95
Figure 4.31 Strain diagram hybrid model verification	95
Figure 4.32 Stresses hybrid model verification	
Figure 4.33 stress diagram hybrid model verification	96
Figure 4.34 stress-strain diagram hybrid model verification	
Figure 4.35 Strain distribution hybrid model verification	
Figure 5.1 Deck geometry top view, leading axle load location LM1	.102
Figure 5.2 bridge geometry top view, leading axle load location LM2	
Figure 5.3 RFEM database access workflow	
Figure 5.4 RFEM wheel track results OSD detail 1	
Figure 5.5 RFEM vehicle 4A_3 detail 1 influence line	
Figure 5.6 RFEM vehicle 4A_3 detail 1 influence line sorted	.115
Figure 5.7 RFEM vehicle 4A_1 detail 1 peak-valley distribution	.116
Figure 5.8 RFEM vehicle 4A_3 detail 1 four point counting	.117
Figure 7.1 OSD detail 1 vehicle 3 lane 1 and lane1 and 2 combined	
Figure 7.2 OSD detail 1 wheel influence lines	.141
Figure 7.3 OSD detail 1 vehicle 3 lane 1 spans 12, 15 and 20	
Figure 7.4 OSD detail 1 wheel A spans 12, 15 and 20	
Figure 7.5 OSD detail 1 vehicle 3 separate wheel influence lines	
Figure 7.6 OSD weight distribution in absolute values and percentages	
Figure 7.7 Case 4 and 5 sketch	
Figure 7.8 OSD and hybrid weight distribution	
Figure C.1 Application of tandem system	
Figure C.2 Load model 2(NEN-EN1991-2, 2015)	
Figure C.3 Dispersal of concentrated loads through pavement and structural top plate(NE	
EN1991-2, 2015)	
Figure C.4 Fatigue strength curve for direct stress ranges (EN1993-1-9 figure 7.1)	.186





Figure C.5 Frequency distribution (NEN-EN1991-2, 2015)	188
Figure C.6 Set of frequent lorries (FLM2) and wheel/axle type(NEN-EN1991-2, 2015)	189
Figure C.7 Fatigue load model 3(NEN-EN1991-2, 2015)	190
Figure C.8 Local detail 1 (NEN-EN1993-2NB, 2019)	193
Figure C.9 Local detail 2 (NEN-EN1993-2NB, 2019)	193
Figure C.10 Local detail 3 (NEN-EN1993-2NB, 2019)	194
Figure C.11 Local detail 4 (NEN-EN1993-2NB, 2019)	194
Figure C.12 Local detail 5 (NEN-EN1993-2NB, 2019)	195
Figure C.13 Local detail 6 (NEN-EN1993-2NB, 2019)	195
Figure C.14 General detail 1 (NEN1993-1-9, 2012)	195
Figure C.15 General detail 2 (NEN1993-1-9, 2012)	195
Figure C.16 General detail 3 (NEN1993-1-9, 2012)	196
Figure C.17 General detail 4 (NEN1993-1-9, 2012)	196
Figure C.18 General detail 5 (NEN1993-1-9, 2012)	197
Figure C.19 General detail 6 (NEN1993-1-9, 2012)	197
Figure E.1 Vehicle spectrum start at max	207
Figure E.2 Rainflow diagram from vehicle spectrum	208
Figure E.3 Stress range and rain flow for stress range	209
Figure F.1 FEM elements (Pillwein, 2015)	
Figure G.1 Validation beam model	215
Figure G.2 Validation beam model results	217
Figure G.3 Validation plate model results	218
Figure G.4 Validation sandwich model parameters	219
Figure G.5 Validation sandwich model results	219
Figure H.1 Node release example	221
Figure H.2 release mechanism example	222
Figure H.3 release mechanism 2D example results	223
Figure H.4 release mechanism 3D example results surface release	224
Figure H.5 release mechanism 3D example results nodal release	225
Figure H.6 release mechanism 3D example results single bolt	227
Figure J.1 OSD weight distribution	231
Figure J.2 Hybrid weight distribution	231
Figure J.3 OSD weight distribution	232
Figure J.4 Hybrid weight distribution	232
Figure J.5 OSD weight per square meter distribution	233
Figure J.6 Hybrid weight per square meter distribution	233





List of tables

Table 2.1 Highway bridges in the Netherlands (Rijkswaterstaat, 2019b)	13
Table 2.2 Characteristic E-glass and high strength carbon material properties (CUR 96,	
2017)	23
Table 2.3 Characteristic resin material properties (CUR 96, 2017)	24
Table 2.4 Characteristic stiffness properties of UD-plies with E-glass and polyester resin .	25
Table 2.5 Example: ply material properties	27
Table 2.6 Example: laminate Lay-up	27
Table 2.7 Example: transformed Q-matrix	28
Table 2.8 Example: A, B and D matrices	29
Table 2.9 Example: Laminate properties	31
Table 2.10 CUR Quasi-isotropic laminate properties	31
Table 2.11 Characteristic core material properties (CUR 96, 2017)	35
Table 2.12 effects of connection to crossbeams with or without main girder	38
Table 2.13 Leeghwaterbrug face sheet laminate (Souren, 2017)	39
Table 2.14 Leeghwaterbrug through thickness laminate (Souren, 2017)	40
Table 4.1 width over thickness ratio welded I-beams	60
Table 4.2 Sandwich panel lay-up and parameters	71
Table 4.3 Buckling sandwich panel parameters	75
Table 4.4 Buckling results	76
Table 4.5 Buckling sandwich panel final parameters	76
Table 4.6 Buckling final results	77
Table 4.7 FRP plate buckling under compression	78
Table 4.8 Sandwich panel dimensions	80
Table 4.9 FRP fatigue results	82
Table 4.10 Stress and strain data OSD model verification	90
Table 4.11 Stress and strain data hybrid model verification	97
Table 5.1 OSD bridge: SLS verification	.112
Table 5.2 ULS verification locations	.113
Table 5.3 OSD bridge: ULS verification	.113
Table 5.4 Vehicle 4A_3 detail 1 stress ranges	.118
Table 5.5 Vehicle 4A_3 excel results	.119
Table 5.6 Detail 1 excel results	.119
Table 6.1 OSD optimization: altered parameters	.124
Table 6.2 OSD optimization: fatigue damage results	.124





Table 6.3 OSD optimization: influence line stress range	125
Table 6.4 Boundaries for changing parameters	127
Table 6.5 OSD optimization parameters	128
Table 6.6 Hybrid optimization result	128
Table 6.7 Hybrid optimization: fatigue damage results	130
Table 6.8 Hybrid optimization: influence line stress range	131
Table 6.9 Hybrid optimization parameters	132
Table 6.10 Hybrid optimization result	132
Table 6.11 OSD versus hybrid results comparison	133
Table 7.1 Vehicles in the Netherlands (CBS, 2019)	137
Table 7.2 General bridge parameters for comparison	138
Table 7.3 OSD bridge configuration results	139
Table 7.4 OSD stiffener results case 4 per lane	140
Table 7.5 OSD stiffener stress ranges case 4 - 6	144
Table 7.6 OSD weight per part	145
Table 7.7 Hybrid bridge configuration results	147
Table 7.8 Weight comparison OSD vs hybrid	152
Table 7.9 OSD and hybrid weight distribution	153
Table 7.10 Cost comparison material weight	154
Table 7.11 Cost comparison results	155
Table 7.12 Environmental impact (GWW) OSD vs hybrid	157
Table 7.13 CO ₂ footprint OSD vs hybrid	157
Table C.1 Number and width of notional lanes (NEN-EN1991-2, 2015)	176
Table C.2 Correction factors (NEN-EN1991-2NB, 2011)	177
Table C.3 Partial factors for fatigue strength	178
Table C.4 Load model 1: characteristic values (NEN-EN1991-2, 2015)	179
Table C.5 Assessment of groups of traffic loads (NEN-EN1991-2NB, 2011)	183
Table C.6 Indicative number of heavy vehicles expected per year and per slow lane (NEN-
EN1991-2NB, 2011)	187
Table C.7 Deck thickness as a function of design life (NEN-EN1993-2NB, 2019)	187
Table C.8 Set of equivalent lorries for load model 4A (NEN-EN1991-2NB, 2011)	191
Table C.9 Set of equivalent lorries for load model 4B (Rijkswaterstaat, 2017)	191
Table C.10 FRP plate buckling $ab > 5$	200
Table C.11 FRP plate buckling $ab < 5$	202
Table C.12 Regression parameters k and B for UD-laminates	204
Table D.1 Sandwich panel fatigue results	205
Table E.1 Stress range overview	210





Table G.1 Validation material properties	215
Table I.1 GWW environmental impact values	229
Table I.2 Case results GWW impact values	230
Table J.1 OSD weight distribution	231
Table J.2 Hybrid weight distribution	231
Table J.3 OSD weight percentage distribution	231
Table J.4 Hybrid weight percentage distribution	232
Table J.5 OSD weight per square meter distribution	233
Table J.6 Hybrid weight per square meter distribution	233





1

1

Introduction

A brief explanation on the motivation and goals of this thesis will be given in this chapter. First of is a project motivation from which a problem statement is created. The problem statement is transformed into a research question which in turn is divided in several sub-questions. At the end of this chapter is an outline of this report which shows a flow diagram and the contents of each chapter.

1.1 Project motivation

Many traffic bridges have been built in the 50's and 60's. Since then the load intensity on the bridges have increased due to several reasons (TU-Delft, n.d.). The amount of traffic has increased tremendously over the years as is shown in Figure 1.1 for two Dutch highway bridges.



Figure 1.1 Traffic intensity





Furthermore, the introduction of the so called super singles tires caused an increased surface load due to a decrease in surface area. This can be seen in Figure 1.2 which shows the super singles on the left and the old dual wheels (duals) on the right.



Figure 1.2 Super singles vs dual wheels

The third and most important reason of increased load intensity is a minimalization of weight which has mainly been accomplished by decreasing the thickness of the steel deck plate. In the early 60's the minimum bridge weight per square meter has been found. From that point onwards it became clear that this decrease in material caused problems. In the early 90's the effects of fatigue became clearer and as a result the thickness of plates have been increased again. These key points are illustrated in Figure 1.3.

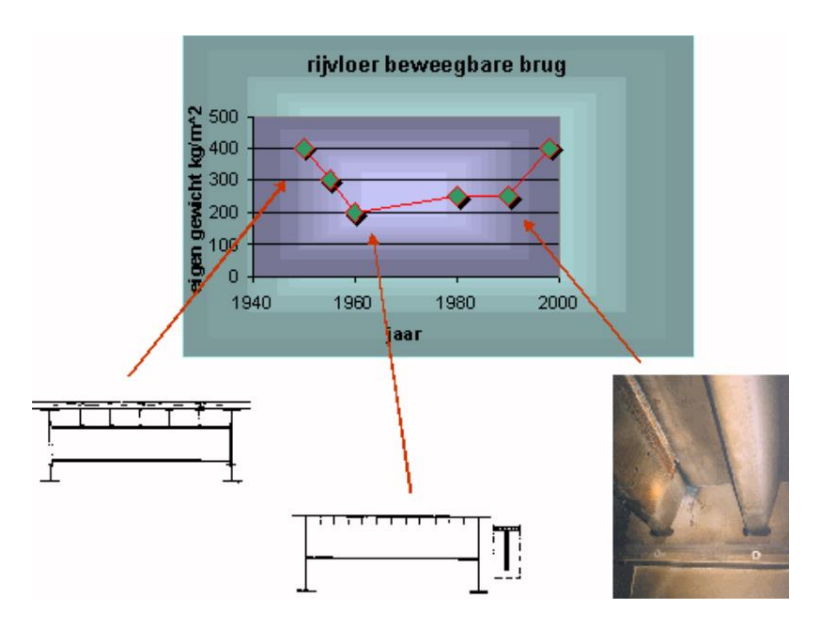


Figure 1.3 movable bridge weight trend line 1950-2000

2





As a result of these three contributing factors many bridges build in the 50's and 60's are at the end of their service life and replacement is required, especially for the bridge spans.

Building a new bridge would solve the issue, however with climate policies in mind, maintaining the existing structure as much as possible is desired. The foundation and pillars are often still in good conditions and therefore suited for an extended lifetime. Life time extension of these parts of the bridge comes with a downside, the weight of the new bridge span is limited to the weight that the foundation and pillars can carry. The new span should have the same weight, or preferably even less, as the old one whilst still being able to carry the increased traffic loads. This results in a challenge in the design of new bridge spans, especially for the movable bridges.

A side view of a bascule bridge is given in Figure 1.4 in which the bridge parts are named. The leaf of the movable span is given in green, this is the part that will be replaced during renovation. Often a new counterweight, trunnion and trunnion drive are needed as well, however that will be outside of the scope for this thesis.

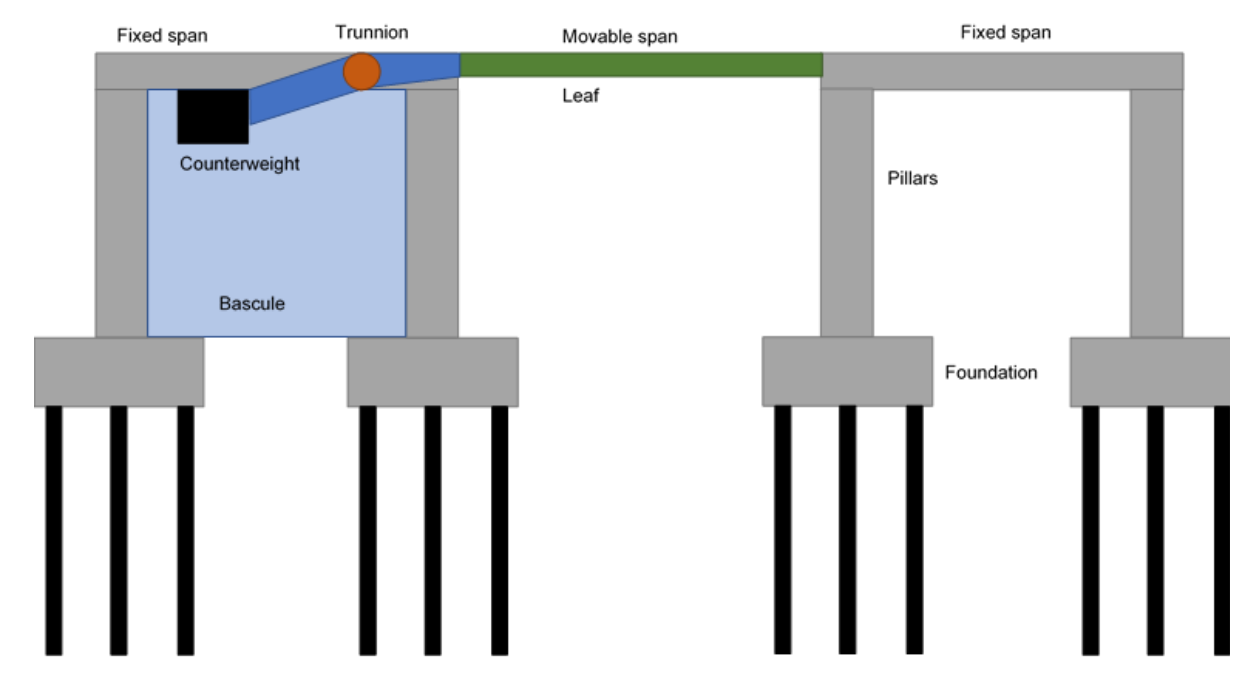


Figure 1.4 Bascule bridge sideview

The existing movable spans have been designed to be light to decrease waiting time for road traffic when the bridge is opened for water traffic. The classic solution for these light weight bridge spans is an Orthotropic Steel Deck bridge (OSD bridge). Replacing this bridge which has already been designed to be light-weight by a new bridge with higher load bearing capacity but the same or even less weight is challenging. However, new materials might give a better

^[1] Different hybrid bridges exist. When "hybrid" is mentioned in this report it refers to a steel-FRP hybrid construction unless specified otherwise.





solution than the OSD bridge, namely a hybrid^[1] bridge made up of steel and Fibre Reinforced Polymer (FRP). Both the OSD and hybrid bridge are shown in Figure 1.5.

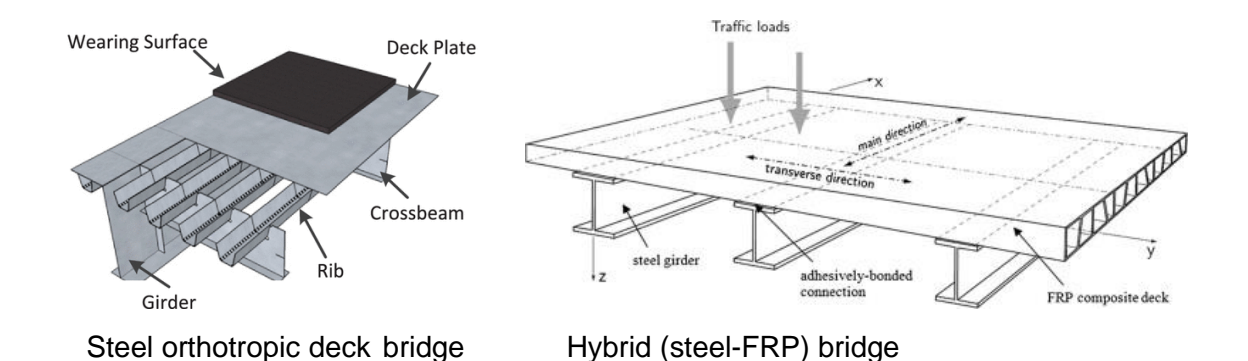


Figure 1.5 Bridge types(Li, 2014)

An orthotropic steel deck consists of 4 main parts, the main girders and the crossbeams for the overall load bearing capacity and stiffeners (ribs) and a deck plate to transfer wheel loads to the crossbeams and main girders. The stiffeners are used to minimize local deflections in between crossbeams and also create torsional stiffness due to their U-shape which is connected to the deck plate. The crossbeams transfer the loads from the stiffeners to the main girders, their bottom flange prevent excessive bending to maintain a flat road surface. The main girders transfer the loads back to pillars and foundation, stiffness is mainly caused by the bottom flanges and the deck plate and stiffeners.

In the hybrid bridge the steel stiffeners and deck plate are substituted by an FRP sandwich panel (composite deck). The load baring structure of main girders and crossbeams is still maintained. The reason why FRP could be a good substitute is mainly due to its high strength to weight ratio. This enables creating a movable bridge deck lighter than the classic steel orthotropic bridge deck whilst still ensuring structural safety.

However, for many renovation projects a classic OSD bridge is still used. The reason behind this is that hybrid bridge decks are still new and more research is needed to persuade contractors to chose this new type of deck. This thesis aims to create a better understanding of the possibilities of hybrid bridges in an early design stage so engineers can make a well justified decision on which bridge deck to design.





5

1.2 Problem statement

There have been multiple feasibility studies, (Flink, 2015; Souren, 2017; Mouroulis, 2018), looking into weight saving of movable bridges by using FRP. Each of them showed positive results with a weight reduction of up to 25% of the bridge span by using a hybrid bridge instead of OSD bridge (Mouroulis, 2018). These results have been produced for certain case studies of existing bridges and showed the potential of hybrid steel-FRP bridges. Yet engineering firms still opt for OSD bridges instead.

There are multiple reasons behind this choice, one of which is the time and money that is needed to do a complete bridge design, often more than a few months. Both bridge spans (OSD and hybrid) should be designed and verified to make a fair comparison and chose which solution is best. Designing both bridge types is often labour intensive which results in engineering firms choosing the known and established OSD bridge. More information is needed to make a well educated decision in an early design stage to choose the hybrid bridge.

Automated parametric models can be used to make this well educated decision possible. This requires two models, one for each bridge type, which can be altered easily in their dimensions such as width, height and span. To ensure the best bridge can be chosen in an early design stage a number of verifications must be done. For an orthotropic bridge this will be done using the norms and regulations stated in the Eurocode. However, for hybrid (Steel-FRP) bridges there is no Eurocode yet. Therefore recommendation documents such as the CUR (CUR 96, 2017) will be used instead.

As a result of these calculation models a recommendation can be given to chose for either an OSD or a hybrid (steel-FRP) bridge. This will be done with the help of general verifications. After the recommendation the chosen model needs to be verified in further detail to ensure safety for local details.





1.3 Research objective

The goal is to give a recommendation on which bridge type to chose for certain dimensions. The hypothesis is that for certain dimensions a tipping point will be found where a hybrid bridge becomes more favourable than an OSD bridge. This result can be found as an answer to the following research question:

For which dimensions of movable highway bridges in the Netherlands is a hybrid bridge favourable as opposed to an orthotropic steel deck bridge when comparing weight?

A highway bridge has been chosen since this has the highest occurring traffic load. When a design can be made for these high loads it will ensure the possibility of hybrid bridge spans for other vehicle bridges with a lower intensity as well.

1.3.1 Literature study

To achieve an answer to the research question a literature study is needed to research the state-of-the-art in movable bridge building and Fibre Reinforced Polymers. This literature study has been divided in several sub-questions which will be stated below.

Firstly, the boundary conditions and dimensions have to be established for highway bridges in the Netherlands. The different structural dimensions will result in a list of parameters that should be adaptable in the model within a certain range.

1) What are the boundary conditions and structural dimensions of current highway bridges in the Netherlands?

This information will be obtained from the database of Rijkswaterstaat (Rijkswaterstaat, 2019a).





The second part of this literature study will focus on FRP. First some basic knowledge on fibre materials will be stated including laminate theory which is the basis of every laminated material. Then a brief explanation on the structural usage of FRP in bridge building is given. In the last part an analysis on hybrid bridges in general and the type of interaction that occurs between the two materials is given.

- 2.1) What is FRP and how can material properties be determined for fibrous materials?
- 2.2) How is FRP used most in bridge building?
- 2.3) Which hybrid bridge decks exist and what interaction occurs between steel and FRP?

The information about what FRP is will mainly come from the CUR96 (CUR stands for "Civieltechnisch centrum Uitvoering research en Regelgeving") recommendation document which is a set-up for an actual Eurocode which is being made at the moment. The CUR96 has been used by different engineering companies and is accepted by the Dutch government. Literature will be used to answer sub guestions 2.2 and 2.3.

With the materials and boundary conditions set the next step is to determine all design verifications for bridge design. This will follow the rules and regulations as stated in different norms such as the Eurocodes (also known as NEN-norms in Dutch) and the CUR-recommendations. This will determine the design verifications that will be implemented in the model and can be found by answering the following sub-question:

3) What are the design verifications for movable bridge spans in the Netherlands for orthotropic and hybrid bridges?

With the three sub questions stated above it is possible to create a model and determine if the structure is safe or unsafe. However, which modelling software is most appropriate for the task at hand? A brief comparison will be made in chapter 3 between two different software packages namely RFEM and SOFiSTiK. This chapter will determine the software to be used and answers the following sub question.

4) Which FEM software package is most appropriate to model both an orthotropic and hybrid bridge including traffic loads?





1.3.2 Modelling

The previous sub-questions conclude the desk research and give all the necessary information to create an adequate model and therefore start the design-phase of this thesis. A model must be made for an OSD bridge and a hybrid (steel-FRP) bridge including the boundary conditions and load cases needed for the design verifications. These models should result in a correct verification according to the regulations.

FE-software will be used to create the models to obtain stresses, strains and deformations in the material and overall weight values. The validity of the models will be verified with hand calculations using classic laminate theory and beam theory.

These finite element models will be coupled with excel for pre- and postprocessing. The post processing consists verification of the load models and a simple model optimization.

1.3.3 Results analysis

The next step is to run the models for several configurations and compare the results of the bridge designs. The question which design is better (OSD or hybrid) can be different in each situation. For certain renovation projects weight is most important, for others the material cost might be decisive. For this project the weight of the bridge will be decisive, however other criteria such as costs or environmental impact will be considered as well.

A tipping point is expected for which one bridge type is favourable as opposed to the other depending on the dimensions. The goal is to determine this tipping point for a few cases and summarise the results in a table. If the results are conclusive this table can be used to have a better understanding of the choice, OSD or hybrid, in an early design stage.

Besides this comparison the goal is to create a model and calculation method that can be used by engineers. By inserting project specific boundary conditions a calculation must be done and as a result the preferred choice of bridge type should be given. This should be the result of the modelling part of this thesis, which is explained above in paragraph 1.3.2.





1.4 Outline

A brief outline of this thesis will be stated below with the use of a flow diagram shown on the next page.

Literature study

The Literature study is conducted in chapter 2 and 3. These chapters give answer to subquestions 1 to 4 and give an overview of the boundaries of this thesis. Initial decisions on what will or will not be included in this thesis are made and elaborated in these chapters.

Paragraph 2.1	Bridges in the Netherlands	Sub-question 1
Paragraph 2.2	Fibre reinforced polymers	Sub-question 2
Paragraph 2.3	Norms and regulations	Sub-question 3
Chapter 3	Finite element software	Sub-question 4

Modelling

Models to design the different bridge types will be the core of this thesis and will be explained in Chapters 4 to 6. A brief workflow of the calculation models can be found in the first chapter. Chapter 4 focusses on the development of the finite element models and a verification of them. Chapter 5 elaborates on the development of load models and the result analysis conducted in excel. Chapter 6 shows how the model will be optimized and how the optimized results are compared.

Chapter 4 RFEM model

Chapter 5 Loading and results

Chapter 6 Optimization

Result analysis

Different bridge configurations are chosen to run the models for. The results from these configurations are shown in tables for each bridge type to create a clear overview. These tables are then compared and the most optimal bridge type will be chosen for each configuration.

Chapter 7 Comparison of results

Conclusion and recommendations

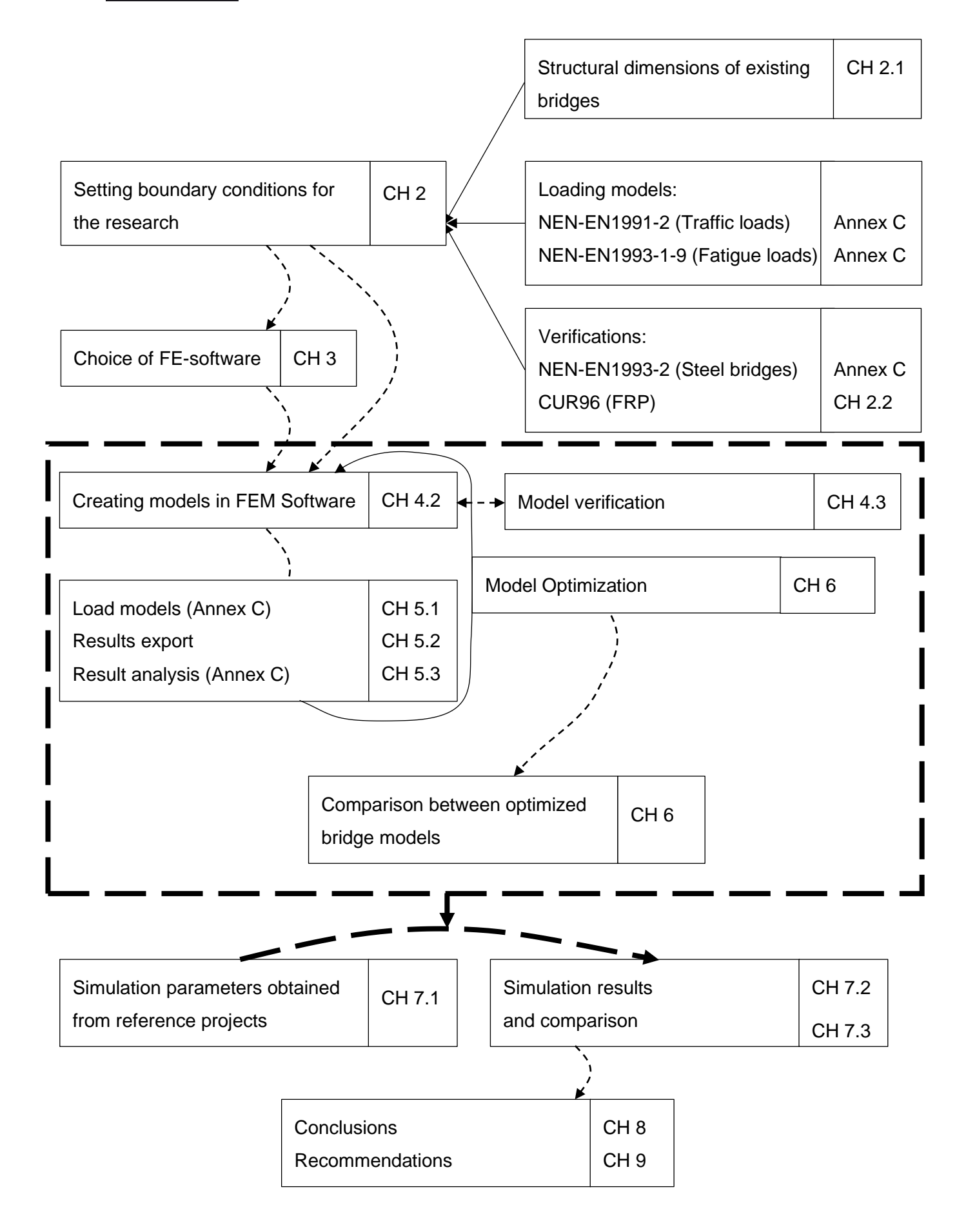
The final chapters are dedicated to conclusions and recommendations.

Chapter 8 Conclusion

Chapter 9 Recommendation











2

State-of-the-art

This chapter contains background knowledge needed for the research and is divided in three paragraphs. The first paragraph consists of a brief summary of the history of bridges in the Netherlands followed by an explanation on different types of movable bridges. The last part of this paragraph will elaborate more on the history of two types of bridge spans, namely orthotropic and hybrid bridges.

The second paragraph will give some more insights on Fibre Reinforced Polymers (FRP). This paragraph will show material properties of the separate materials and how to determine properties of laminates. Besides that, a brief explanation on the usage of FRP in bridge engineering will be given. The third part of this paragraph will show the structural usage of FRP in bridge engineering and the special interaction that occurs between FRP and steel. At last a short conclusion will be given to answer sub-questions 2.1 to 2.3.

The final paragraph of this chapter is about the existing norms and regulations for bridges. This will mainly focus on vehicle loads that have to be considered and the verifications that must be done for different bridge types. This paragraph will answer sub-question 3.





2.1 Bridges in the Netherlands

Bridges have been used for many centuries to cross obstacles such as water, valleys or roads. Starting as simple brick structures to pass small obstacles, bridges have evolved to massive structures spanning immense valleys or rivers. Since people first set sail, bridges also had to have a certain clearance for ships to pass and reach their destination. The bigger the ships became, the bigger the clearance had to be, which resulted in the first movable bridges to be erected to obtain infinite clearance (Partov, Pasternak, Petkov, et al, 2018).

To ensure the least possible hindrance for both road and water traffic these movable bridges are designed as light as possible to ensure quick opening and closing times. As a result these bridges are made of steel and not with concrete slabs as is often used for fixed spans. The bridge leaves of these bridges are all Orthotropic Steel Deck (OSD) bridges except for the vertical lift bridge.

An explanation on different movable bridges will be given in the first part of this paragraph. Two different types of movable bridge spans, orthotropic and hybrid, will be elaborated in the second and third part. This paragraph will finish with a short conclusion on the first subquestion.





2.1.1 Movable bridges

Different types of movable bridges have been built in the past, such as the classic drawbridge at castle entrances, bascule bridges or swing bridges. Bascule bridges are most common in movable highway bridges due to the quick opening and closing times. Table 2.1 shows all the movable highway bridges in the Netherlands. It shows that 16 out of the total of 19 bridges used on Dutch highways are single leaf bascule bridges. More details on the dimensions on these bridges are given in Annex B and are obtained from the database of Rijkswaterstaat.

Table 2.1 Highway bridges in the Netherlands (Rijkswaterstaat, 2019b)

road	Bridge name	bridge type	lanes	span	intensity (2019)	
				[m]	[cars/day]	[cars/lane]
A6	Ketelbrug	Bascule	2x2	18	47,100	11,775
A6	Scharsterrijnbrug	Bascule	2x2	7	40,300	10,075
A7	Stevinsluizen	Swing	2x2	unknown	19,500	4,875
A7	Lorentzsluizen	Swing	2x2	unknown	19,500	4,875
A7	Kruiswaterbrug	Bascule	2x2	7.88	24,900	6,225
A7	A7-brug	Bascule	2x2	~13	12,600	3,150
A8	Coenbrug	Bascule	2x3	14	unknown	unknown
A9	Schipholbrug	Bascule	2x3	16	unknown	unknown
A9	Brug over het Zijkanaal C	Bascule	2x3 (spits)	14	unknown	unknown
A10	Schinkelbrug	Bascule	2x5 (spits)	14	224,300	22,430
A15	Suurhoffbrug	Bascule	2x2	24	24,600	6,150
A15	Botlekbrug	Vertical lift	2x2	45 & 87.3	21,600	5,400
A16	Van Brienenoordbrug	Bascule	4x3 (2 bridges)	60	229,600	19,133
A20	Giessenbrug	Bascule	2x3	10.7	115,600	19,267
A27	Merwedebrug	Bascule	2x2	30	93,800	23,450
A29	Haringvlietbrug	Bascule	2x2	35	54,400	13,600
A29	Volkerakbrug	Bascule	2x2	24.1	unknown	unknown
A44	Kaagbrug	Bascule	2x2	8	70,100	17,525
A44	Oude Rijnbrug	Bascule	2x2	~24	46,800	11,700





Bascule bridges owe their names from the French word "bascule" translating to "seesaw" which refers to the balance of the bridge pivoting on a horizontal axis. A typical bascule bridge consists of the leaf, which is the section of the bridge that spans the gap, a counterweight and a pivot also known as a trunnion. When closed, the leaf often rests on live load shoes to support the weight of the bridge and traffic. For a double leafed bascule bridge, as shown in Figure 2.1, there is only one live load shoe at the heel of the leaf. Single leaf spans often have two live load shoes, one at each end (Koglin, 2003).

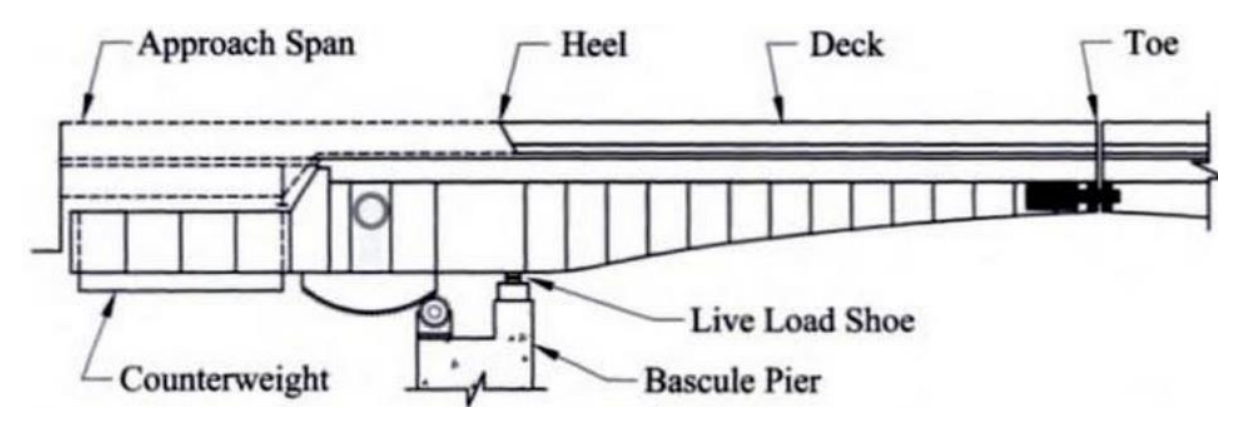


Figure 2.1 Typical bascule bridge (Koglin, 2003)

The counterweight in the bridge works as a balancing weight to lower the force needed to rotate (open) the bridge. If the balance weight keeps the bridge closed the bridge is called "span heavy", if the balance weight would keep the bridge in an open position it is called "counterweight heavy". Usually bridges are span heavy making sure that in case of malfunction road traffic can continue using the bridge.

The two swing bridges are situated in the "Afsluitdijk" and have been built in the 1930's. The choice at that time to build swing bridges instead of another type is based on military motivation. Bridges that would open to a vertical position would be an easy target during war, whereas swing bridges rotate horizontally and therefore don't show on the horizon when in an "open" position (see Figure 2.2). This is still a demand during current renovations of the Afsluitdijk which is done by several engineering firms including Witteveen+Bos.



Figure 2.2 Swing bridge, Afsluitdijk (Afsluitdijk, 2017)





The Botlekbrug is a vertical lift bridge situated in the port of Rotterdam. Due to the large ships passing the bridge a big movable span was necessary and the choice was made to do this with a vertical lift bridge spanning 87.3 meters. Nowadays there is a tunnel next to the bridge which is used by most vehicles, with the exception of local traffic and trucks that carry dangerous substances.



Figure 2.3 Vertical lift bridge, Botlek (NOS, 2015)

The other bridges are bascule bridges with most of them consisting of two traffic lanes in each direction. Each bridge is split up into two movable spans, one for each direction, to ensure traffic can still transit during maintenance. These bridges span between 7 and 60 meters and most bridges have two traffic lanes and an emergency lane. Nowadays these emergency lanes are often used as an extra traffic lane during rush hour.





2.1.2 Orthotropic Steel Deck bridge

At the end of World War II resources were scarce and more efficient use of materials was needed. This resulted in new discoveries including the orthotropic steel deck bridge. Before this time bridges usually consisted of a beam grid with a concrete slap on top. Transverse and longitudinal beams were calculated as independent components as was the concrete slap. This type of bridge design did not include any shear interaction between steel and concrete. This lack of interaction means that the high compressive strength of concrete was not used to its full capacity.

Connecting the concrete slab to the beam grid with studs made shear transfer between the concrete and steel possible. This was the first hybrid (steel-concrete) bridge which used the strengths and weaknesses of different materials to its full extend. However, to save weight the concrete slap was later switched for a lighter steel plate of 12-16 mm. This reduced the self-weight tremendously and made welding possible, ensuring a constant connection between beams and deck plate (Partov et al., 2018). Optimization and new calculation methods resulted specific build up of the steel bridge. Nowadays this steel bridge build-up is most commonly known as the Orthotropic Steel Deck (OSD) bridge, Figure 2.4 shows a cross-section.

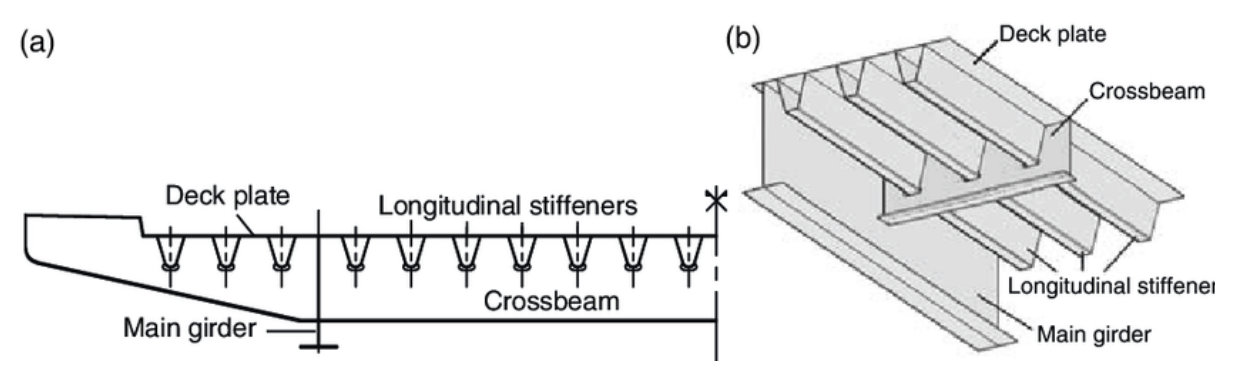


Figure 2.4 OSD bridge cross section (Freitas, 2011)

An OSD bridge consists of a deck plate supported by stiffeners (also known as troughs) in longitudinal direction. This deck structure is supported by crossbeams in transverse direction and main girders in longitudinal direction to create a structure that can span large gaps. Orthotropic refers to the orthogonal structure of beams and the anisotropic behaviour due to this structure. The definition according to the oxford dictionary: "three mutually perpendicular planes of elastic symmetry that exists at each point". Due to this set-up mechanical properties of the leaf can be used to its full extend without wasting to much material in places where it is irrelevant.





In this build-up the main girders and cross beams are inverted T-beams. Stiffeners can have many shapes with the trapezoidal being most common. Trapezoidal stiffeners have advantages over plain strips or angle stiffeners since they create extra torsional stiffness. To prevent high risk fatigue locations cope holes can be used in the crossbeams at the bottom flange of the stiffeners as shown in Figure 2.5.

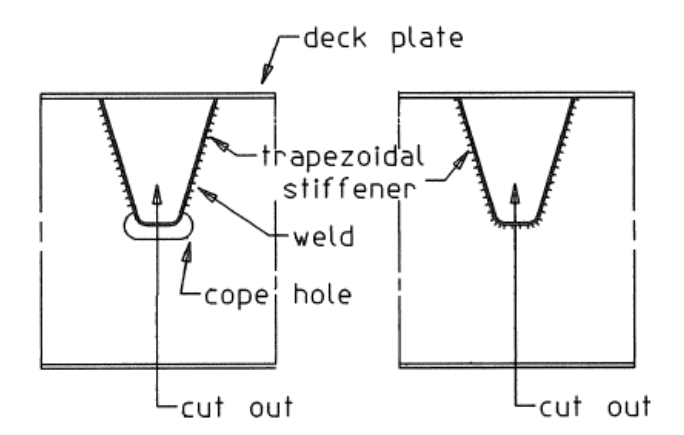


Figure 2.5 cope hole trapezoidal stiffener (Li, 2014)





2.1.3 Hybrid bridge

While orthotropic leaves are most used in practice, current renovation projects call for a new solution. To re-use the foundation of existing bridges a weight limitation occurs for the new bridge leaf. In many cases this results in the need of a lighter solution for which steel orthotropic deck bridges or steel-concrete hybrid bridges are not sufficient.

Replacing the concrete in a hybrid leaf by a lighter material such as FRP might be the solution. This "new" hybrid bridge leaf, the steel-FRP hybrid bridge, is an already used bridge that has been implemented on provincial road bridges (Souren, 2017). However, even for provincial road bridges there are challenges using FRP let alone for highway bridges. A quick review on the developments of the first hybrid bridge (steel-concrete) will give insight on the challenges for new hybrid bridges.

Hybrid bridge bridges are composed of two or more materials that act together as one, so load transfer is possible between the two materials. In the more classic bridge engineering this refers to steel-concrete hybrid bridges as mentioned before. Hybrid bridges make use of the strengths of each material. Concrete is a cheap material with great compressive properties and is placed in the compressive zone of the cross-section. By using the compressive strength of the concrete, less steel is needed in the tensile zone to carry the loads and as a result a cheaper bridge can be designed.

The main challenge in hybrid bridges however, is to create a strong bond between the two elements. To make optimal use of both components a bond is needed that ensures transfer of shear stresses and not only forces perpendicular to the contact area, this is called hybrid interaction. Years of knowledge resulted in strong bonding between steel and concrete by using studs as shown in Figure 2.6.





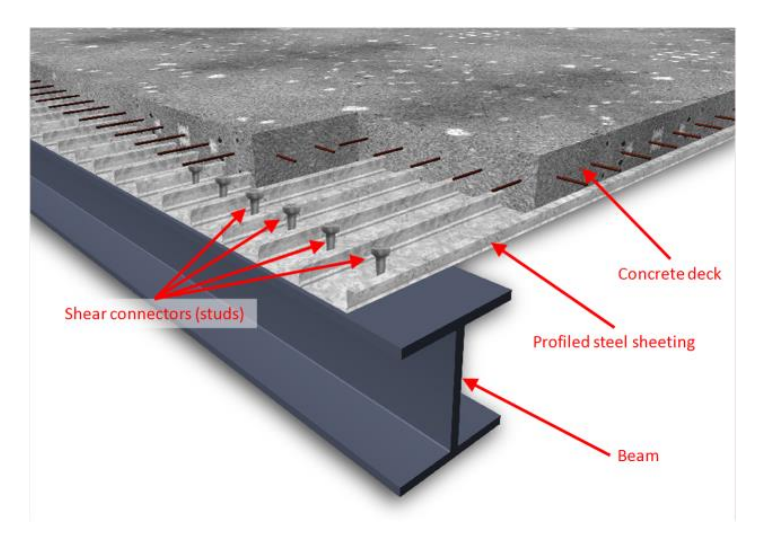


Figure 2.6 Hybrid concrete leaf (SCIA, 2016)

These studs transfer the shear stresses between the concrete and steel beam that occur during bending. As shown in this figure the concrete is poured on sight on top of the profiled sheeting. Another option is using pre-fabricated concrete slabs with holes for the studs. These holes are filled with concrete on sight to create the shear connection between steel and concrete.

These types of hybrid bridges (steel-concrete) are still used today for fixed spans, however for movable spans these bridges tend to be too heavy due to the weight of the concrete. The steel-FRP combination seems to be more promising since FRP is many times lighter than concrete but still has great material properties. Just as in hybrid steel-concrete bridges the connection between materials seems to be the biggest issue. More on what FRP is and how this connection can be made will be elaborated in the next paragraph (2.2).





2.1.4 Conclusion

A conclusion can be written for the first sub-question with the information given in the previous paragraphs.

What are the boundary conditions and structural dimensions of current highway bridges in the Netherlands?

There are many highway bridges in the Netherlands where most of the fixed spans consist of concrete or steel-concrete bridges. There are 19 bridges that have a movable span in them, of which 16 are bascule bridges build up as an Orthotropic Steel Deck (OSD). These are all single leaf bridges with a span ranging from 7 to 60 meters. Most of them consist of two separate bridges with each two traffic lanes. Further structural dimensions of these OSD bridges can be found in Annex B.





2.2 Fibre reinforced polymers

FRP is a composite material that consists of fibres (e.g. glass or carbon) and a resin (e.g. polyester or epoxy). FRP is most used as a layered material or a so called laminate, laminates are often used for timber as well such as plywood or laminate floorboards. Such a laminate usually consists of unidirectional layers, also known as UD-plies. In the case of timber each ply is close to unidirectional due to the fibre directions of the wood. This results in different strength properties in each direction. Stacking these UD-plies in different orientations can create a material that has (almost) the same properties in the in-plane directions.

The main strength properties for these FRP UD-plies come from the fibrous material which is oriented in one single direction, hence the "unidirectional". There are different fibres that can be used, E-glass is most used in civil engineering. The resin is there to create a bond between the fibres to ensure interaction. As for the fibres there are different types of resin that can be used to suit different conditions, most used are polyester and epoxy. Information on the material properties for FRP can be found in the first part of this paragraph (2.2.1).

Stacking these UD-plies in different directions create a laminate as shown in Figure 2.7. Due to the layered nature of FRP laminates it can be modelled to fit the conditions at hand. For instance, in bridge design the main forces occur in longitudinal direction thus adding fibres in that direction add in strength without wasting material in the other direction as holds for isotropic materials. Classic laminate theory can be used to determine the material properties of an FRP laminate and will be elaborated in paragraph 2.2.1.4.

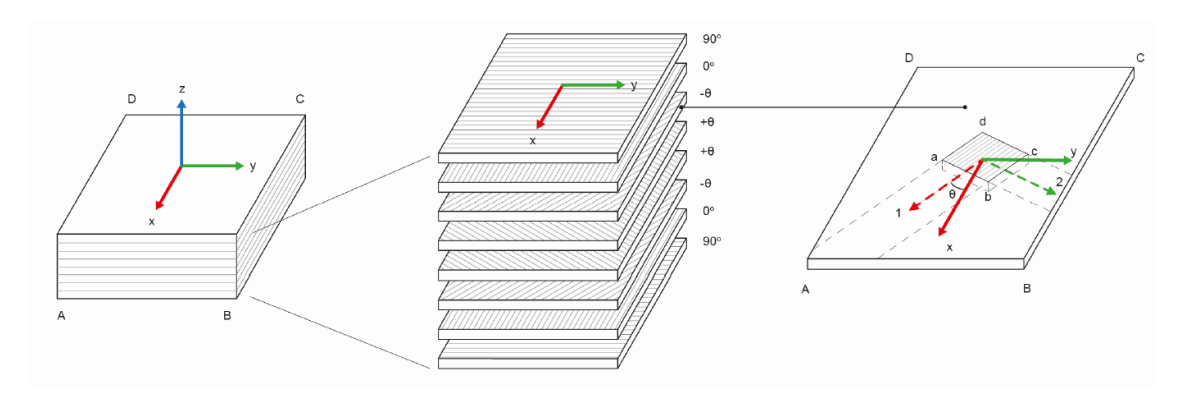


Figure 2.7 FRP laminate (CUR 96, 2017)

Nowadays FRP is often used in bridges as facade panelling due to its capabilities to be formed in any way required. Other ways FRP can be used is as reinforcement of existing structures. Another usage of FRP in bridges has a more structural nature, namely as bridge deck. This has already been used in many bicycle and pedestrian bridges but also in vehicle bridges in





the form of sandwich panels. More on the usage of FRP in bridge engineering can be found in paragraph 2.2.2.

For vehicle bridges these sandwich panels are combined with a steel sub-structure to form a hybrid bridge. The build up and usage of these sandwich panels will be elaborated in the final part of this paragraph (2.2.3). Also the hybrid interaction between steel and FRP will be considered together with a proof of concept.





2.2.1 Material properties

FRP consists of two materials, fibres and resin. The properties of both materials will be elaborated in this paragraph as well as the properties of an uni-directional (UD) ply. The last part of this paragraph shows how to determine material properties for a laminate consisting of UD plies.

2.2.1.1 Fibre properties

Different types of fibres are used in building engineering with E-glass being the most common. This type of glass was first used for electrical applications, hence the "E", and was the first glass used in FRP (AZoM.com, 2001). Since it has been around for a long time it is a cheap material which is produced all around the world. Carbon is another type of fibre which is often used. This type is used if very light laminates need to be produced, for instance in aerospace or nautical engineering. Characteristics of both fibres can be found in Table 2.2. E-glass will be used in this research due to its cheap nature and the fact that many FRP manufacturers for civil engineering purposes use it.

Table 2.2 Characteristic E-glass and high strength carbon material properties (CUR 96, 2017)

		E-glass	Carbon (HS)
Tension in fibre	Poisson ratio $[v_f, -]$	0.24	0.3
direction	Stiffness $[E_{f1}, N/mm^2]$	73100	238000
	Max strain [ε_{f1} , %]	3.8	1.5
	Strength $[f_{f1}, N/mm^2]$	2750	3600
Tension orthogonal to	Poisson ratio $[v_f, -]$	0.24	0.02
fibre direction	Stiffness $[E_{f2}, N/mm^2]$	73100	15000
	Max strain $[\varepsilon_{f2}, \%]$	2.4	0.9
	Strength $[f_{f2}, N/mm^2]$	1750	135
Pressure in fibre	Max strain [ε_{f1} , %]	2.4	0.9
direction	Strength $[f_{f1}, N/mm^2]$	1750	2140
Shear	Shear modulus $[G_f, N/mm^2]$	30000	50000
	Max shear strain $[\gamma_r, \%]$	5.6	2.4
	Shear strength $[\tau_r, N/mm^2]$	1700	1200
Density $[kg/m^3]$	2570	1790	
Thermal expansion coef	ficient $[\alpha_f, 10^{-6}/^{\circ}C]$	5.0	-0.4

2.2.1.2 Resin properties

The second material used in FRP is the resin to bind the fibres together. There are multiple resins that could be used and the choice depends on the conditions it will be used in. Most common materials are polyester, vinyl ester and epoxy. The advantage of Polyester is that other resins adhere really well to hardened polyester, the other way around requires a pre-





treatment. Since the FRP panels are often bonded together on sight polyester resin will be used in this report. Characteristic values of the three resins can be found in Table 2.3.

Vinyl ester Polyester Ероху Density $[\rho_r, kg/m^3]$ 1.2 1.25 1.1 Poisson ratio $[v_r, -]$ 0.38 0.26 0.39 Glass transition temperature 60 - 10080 - 15080 - 150 $[T_q, {}^{\circ}C]$ Tensile or compression 75 55 75 strength $[f_r, N/mm^2]$ Tensile stiffness $[E_r, N/mm^2]$ 3550 3350 3100 Maximum strain [ε_r , %] 1.8 2.2 2.5 Shear modulus $[G_r, N/mm^2]$ 1350 1400 1500 Shear strength $[\tau_r, N/mm^2]$ 80 50 65 Max shear strain $[\gamma_r, \%]$ 3.8 3.7 5 Thermal expansion coefficient 50 - 12050 - 7545 - 65 $[\alpha_r, 10^{-6}/^{\circ}C]$

Table 2.3 Characteristic resin material properties (CUR 96, 2017)

Polyester resin will be used in this research. It is cheaper then the other resins and is therefore widely used in the civil engineering field. Vinyl ester resins have a higher chemical and impact resistance which could be necessary in specific situations. Epoxy has this properties as well but also outperforms the other resins in the other material properties but is slightly more expensive.

2.2.1.3 *UD-plies*

UD-plies (Figure 2.7) are the most used plies due to their possibility to design strength properties per direction. The properties of a UD-ply depends on the fibres and resin that are used. To calculate the ply-properties the CUR gives equations (2.1) to (2.7) (CUR 96, 2017).

$$E_1 = [E_r + (E_{f1} - E_r) * V_f] * \phi_{UD}$$
 (2.1)

$$E_{1} = \left[E_{r} + \left(E_{f1} - E_{r}\right) * V_{f}\right] * \phi_{UD}$$

$$E_{2} = \left[\frac{1 + \xi_{2}\eta_{2}V_{f}}{1 - \eta_{2}V_{f}} * E_{r}\right] * \phi_{UD}$$
(2.1)

$$\eta_2 = \frac{\frac{E_{f2}}{E_r} - 1}{\frac{E_{f2}}{E_r} + \xi_2} & \xi_2 = 2$$
 (2.3)

$$G_{12} = \left[\frac{1 + \xi_G \eta_G V_f}{1 - \eta_G V_f} * G_r^{[1]} \right] * \phi_{UD}$$
 (2.4)

$$\eta_g = \frac{\frac{G_f}{G_r} - 1}{\frac{G_f}{G_r} + \xi_2} \& \xi_G = 1$$
 (2.5)

$$v_{12} = v_r - (v_r - v_f) * V_f \tag{2.6}$$





$$V_f = \frac{volume\ of\ fibres}{volume\ of\ resin} \tag{2.7}$$

Multiplying by G_r has been forgotten in the CUR-recommendations Where

VV ILCI C		
E_1, E_2	$\left[\frac{N}{mm^2}\right]$	in plane $E-modulus$ in material main directions 1 and 2
G_{12}	$\left[\frac{N}{mm^2}\right]$	in plane shear modulus
v_{12}	[-]	in plane poisson ratio in material main directions 1 and 2
ϕ_{UD}	[-]	empirical reduction factor equal to 0.97
v_r	[-]	in plane poisson ratio of resin
v_f	[-]	in plane poisson ratio of fibre in material main directions 1 and 2
E_r	$\left[\frac{N}{mm^2}\right]$	$E-modulus\ of\ resin$
E_{f1} , E_{f2}	$\left[\frac{N}{mm^2}\right]$	$E-modulus\ of\ fibres\ in\ main\ fibre\ directions\ 1\ and\ 2$
G_r	$\left[\frac{N}{mm^2}\right]$	Shear modulus of resin
V_f	[-]	fibre volume percentage of ply

The fibre properties and resin properties can be found in the previous two paragraphs (2.2.1.1 and 2.2.1.2). Some characteristic values for E-glass plies with a polyester resin are given in Table 2.4 depending on the fibre volume percentage. These values can be determined using equations (2.1) to (2.7) and the information from Table 2.2 and Table 2.3.

Table 2.4 Characteristic stiffness properties of UD-plies with E-glass and polyester resin

V_f	$E_1[kN/mm^2]$	$E_2[kN/mm^2]$	$G_{12}[kN/mm^2]$	<i>v</i> _12
40%	30.4	8.9	2.7	0.30
45%	33.8	10.1	3.0	0.29
50%	37.2	11.4	3.4	0.29
55%	40.5	12.9	3.8	0.28
60%	43.9	14.6	4.3	0.27
65%	47.3	16.8	5.0	0.27
70%	50.7	19.4	5.8	0.26





2.2.1.4 Laminate theory

The laminate theory is used to determine the properties of materials made up of multiple layers, so called laminates. These layers, also called plies, each have their own properties and are usually anisotropic. Stacking these anisotropic plies will result in a laminate, a well known example is plywood. Plywood has quasy-isotropic properties though the plies have strictly orthotropic properties due to the fibre direction in wood.

In this paragraph each step from the laminate theory will be explained and shown for an example laminate. This example consisting of a symmetric lay-up of 8 glass fibre layers with polyester resin with a fibre volume of 50%. The direction of fibres is $[0,45,90,-45]^s$ with a ply thickness of 0.125 cm as shown in Figure 2.8.

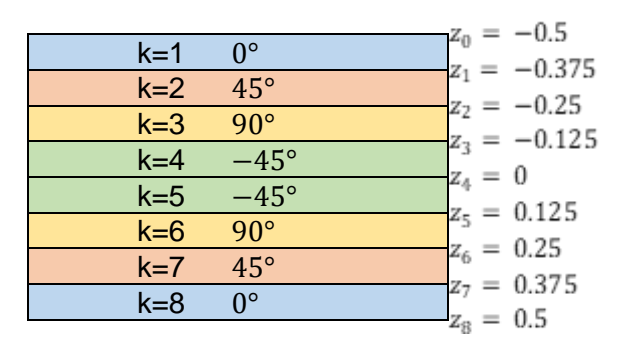


Figure 2.8 Example: equation (2.11) clarification

Laminate theory consists of the following steps and will be elaborated below.

- 1. Define ply materials
- 2. Define laminate orientation
- 3. Determine reduced stiffness matrix Q
- 4. Determine transposed reduced stiffness matrix Q
- 5. Determine laminate stiffness matrix **Q**
- 6. Determine laminate strength properties

1. Define ply material properties

The ply material properties depend on the material composition of the ply. For fibre reinforced polymers these materials are the fibres and the resin.

The properties needed for this calculation are the E-modulus in fibre direction and transverse direction, the shear modulus and the Poisson ratio. The values given in Table 2.5 can be found for a UD-ply made up of E-glass fibres and a polyester resin with a volume fraction of 50%.





Table 2.5 Example: ply material properties

	unit	value
E_1	$\lfloor N \rfloor$	37200
	$\lfloor mm^2 \rfloor$	
E_2	$\lfloor N \rfloor$	11400
	$\lfloor mm^2 \rfloor$	
G_{12}	$\lceil N \rceil$	3400
	mm^2	
v_{12}	[-]	0,29

2. Define laminate lay-up orientation

The next step is to determine the lay-up of the different plies. Most common is to create a symmetric lay-up which prevents torsion due to in plane stresses. A quasy-isotropic material can be created using the lay-up given by Table 2.6. A lay-up where the fibre orientation from layer to layer differs as little as possible forms the best interaction between plies and prevents early delamination.

Using a symmetric lay-up ensures that normal forces occur solely due to strains and moments occur solely due to curvature. This effect can be viewed later on in equation (2.14).

Table 2.6 Example: laminate Lay-up

Layer nr	1	2	3	4	5	6	7	8
$t_k [mm]$	0,125	0,125	0,125	0,125	0,125	0,125	0,125	0,125
φ [°]	0°	45°	90°	-45°	-45°	90°	45°	0°

3. Calculate reduced stiffness matrix Q

The Q-matrix can be calculated using the material properties given by Table 2.5. This is a 3x3 matrix which consists of four different values if a symmetric laminate is considered. The composition of this matric can be found in equation (2.8).

$$\mathbf{Q} = \begin{bmatrix} Q_{11} & Q_{12} & Q_{16} \\ Q_{21} & Q_{22} & Q_{26} \\ Q_{61} & Q_{62} & Q_{66} \end{bmatrix} = \begin{bmatrix} \left(\frac{E_{11}^{2}}{E_{11} - v_{12}^{2} E_{22}}\right) & \left(\frac{v_{12} E_{11} E_{22}}{E_{11} - v_{12}^{2} E_{22}}\right) & 0 \\ \left(\frac{v_{12} E_{11} E_{22}}{E_{11} - v_{12}^{2} E_{22}}\right) & \left(\frac{E_{11} E_{22}}{E_{11} - v_{12}^{2} E_{22}}\right) & 0 \\ 0 & 0 & (G_{12}) \end{bmatrix}$$

$$Q_{12} = Q_{21}$$

$$Q_{16} = Q_{61} (= 0 \text{ if } lay - up \text{ is symmetric})$$

$$Q_{26} = Q_{62} (= 0 \text{ if } lay - up \text{ is symmetric})$$

Where





With the values used for this example the Q-matrix shown in equation (2.9) can be found.

$$\mathbf{Q} = \begin{bmatrix} Q_{11} & Q_{12} & Q_{16} \\ Q_{21} & Q_{22} & Q_{26} \\ Q_{61} & Q_{62} & Q_{66} \end{bmatrix} = \begin{bmatrix} (38184) & (3393) & 0 \\ (3393) & (11701) & 0 \\ 0 & 0 & (3400) \end{bmatrix} \frac{N}{mm^2}$$
(2.9)

4. Calculate transformed reduced stiffness matrix Q

The **Q**-matrix given in equations (2.8) and (2.9) are correct for fibres with a fibre angle (theta) of 0. For the other fibre angels a transformation is needed. This can be done with a transformation matrix T or with a set of equations as is shown in equation (2.10). This results in the transformed matrix Q which is given by \bar{Q} .

$$\frac{\overline{Q_{11}}}{\overline{Q_{12}}} = \frac{Q_{11}C^4 + 2(Q_{12} + 2Q_{66})C^2S^2 + Q_{22} * S^4}{Q_{12}} = Q_{12}(C^4 + S^4) + (Q_{11} + Q_{22} - 4Q_{66})C^2S^2
\overline{Q_{16}} = \overline{Q_{61}} = (Q_{11} - Q_{12} - 2Q_{66})C^3S - (Q_{22} - Q_{12} - 2Q_{66})CS^3
\overline{Q_{22}} = Q_{11}S^4 + 2(Q_{12} + 2Q_{66})C^2S^2 + Q_{22} * C^4
\overline{Q_{26}} = \overline{Q_{62}} = (Q_{11} - Q_{12} - 2Q_{66})CS^3 - (Q_{22} - Q_{12} - 2Q_{66})C^3S
\overline{Q_{66}} = (Q_{11} + Q_{22} - 2Q_{12} - 2Q_{66})C^2S^2 + Q_{66}(C^4 + S^4)
C = Cos(\varphi)
S = Sin(\varphi)$$
(2.10)

Where

The results for the example can be found in Table 2.7 for each of the layers.

Table 2.7 Example: transformed Q-matrix

Layer number	1	2	3	4	5	6	7	8
$t_k [mm]$	0.125	0.125	0.125	0.125	0.125	0.125	0.125	0.125
φ [°]	0	45	90	-45	-45	90	45	0
$\overline{Q_{11}}$	38184	17568	11702	17568	17568	11702	17568	38184
$\overline{Q_{12}}$	3393	10768	3393	10768	10768	3393	10768	3393
$\overline{Q_{16}}$	0	6621	0	-6621	-6621	0	6621	0
$\overline{Q_{22}}$	11702	17568	38184	17568	17568	38184	17568	11702
$ \frac{\overline{Q_{12}}}{\overline{Q_{16}}} $ $ \frac{\overline{Q_{22}}}{\overline{Q_{26}}} $	0	6621	0	-6621	-6621	0	6621	0
$\overline{Q_{66}}$	3400	10775	3400	10775	10775	3400	10775	3400





5. Calculate laminate stiffness matrix ABD

The next step is to calculate the ABD-matrix. This matrix can be split up in three separate matrices A, B and D. Matrix A, B and D can be constructed following equation .

$$\mathbf{A} = \sum_{k=1}^{n} \overline{\mathbf{Q}_{n}} (z_{k} - z_{k-1}) \left[\frac{N}{mm} \right]$$

$$\mathbf{B} = \sum_{k=1}^{n} \overline{\mathbf{Q}_{n}} (z_{k}^{2} - z_{k-1}^{2}) [N]$$

$$\mathbf{D} = \sum_{k=1}^{n} \overline{\mathbf{Q}_{n}} (z_{k}^{3} - z_{k-1}^{3}) [Nmm]$$
(2.11)

Where

k = number of layers

z = vertical position of ply edges measured from midplane

Figure 2.8 gives a clarification on the k and z numbering.

Implementing the example values in these equations results in Table 2.8 and equation (2.12). As can be seen in this table and equation, the B-matrix will always be 0 if a symmetric lay-up is used.

Table 2.8 Example: A, B and D matrices

		z_0	z_1	z_2	z_3	z_4	z_5	z_6	z_7	z_8
		-0,5	-0,375	-0,25	-0,125	0	0,125	0,25	0,375	0,5
t (z_k-	z_k-1)	=	0,125	0,125	0,125	0,125	0,125	0,125	0,125	0,125
A_11	=	21255,496	4773,0129	2196,0187	1462,697	2196,019	2196,019	1462,697	2196,019	4773,0129
A_12	=	7080,804	424,18227	1346,0187	424,1823	1346,019	1346,019	424,1823	1346,019	424,18227
A_16	=	0	0	827,57884	0	-827,579	-827,579	0	827,5788	0
A_22	=	21255,496	1462,6975	2196,0187	4773,013	2196,019	2196,019	4773,013	2196,019	1462,6975
A_26	=	0	0	827,57884	0	-827,579	-827,579	0	827,5788	0
A_66	=	7087,3458	425	1346,8365	425	1346,836	1346,836	425	1346,836	425
t (z_k^2-z_	_k-1^2) / 2	=	-0,0546875	-0,0390625	-0,02344	-0,00781	0,007813	0,023438	0,039063	0,0546875
B_11	=	0	-2088,1931	-686,25585	-274,256	-137,251	137,2512	274,2558	686,2559	2088,1931
B_12	=	0	-185,57974	-420,63085	-79,5342	-84,1262	84,12617	79,53418	420,6309	185,57974
B_16	=	0	0	-258,61839	0	51,72368	-51,7237	0	258,6184	0
B_22	=	0	-639,93015	-686,25585	-894,94	-137,251	137,2512	894,9399	686,2559	639,93015
B_26	=	0	0	-258,61839	0	51,72368	-51,7237	0	258,6184	0
B_66	=	0	-185,9375	-420,88639	-79,6875	-84,1773	84,17728	79,6875	420,8864	185,9375
t (z_k^3-z_	_k-1^3) / 3	=	0,0240885	0,0123698	0,004557	0,000651	0,000651	0,004557	0,01237	0,0240885
D_11	=	2403,7576	919,79935	217,31435	53,32751	11,4376	11,4376	53,32751	217,3144	919,79935
D_12	=	474,83744	81,743459	133,19977	15,46498	7,010514	7,010514	15,46498	133,1998	81,743459
D_16	=	155,17103	0	81,895823	0	-4,31031	-4,31031	0	81,89582	0
D_22	=	1369,2841	281,874	217,31435	174,0161	11,4376	11,4376	174,0161	217,3144	281,874
D_26	=	155,17103	0	81,895823	0	-4,31031	-4,31031	0	81,89582	0
D_66	=	475,38259	81,901042	133,28069	15,49479	7,014773	7,014773	15,49479	133,2807	81,901042





$$\mathbf{A} = \begin{bmatrix} 21256 & 7081 & 0 \\ 7081 & 21256 & 0 \\ 0 & 0 & 7087 \end{bmatrix}$$

$$\mathbf{B} = \begin{bmatrix} 0 & 0 & 0 \\ 0 & 0 & 0 \\ 0 & 0 & 0 \end{bmatrix}$$

$$\mathbf{D} = \begin{bmatrix} 2404 & 475 & 155 \\ 475 & 1369 & 155 \\ 155 & 155 & 475 \end{bmatrix}$$
(2.12)

This laminate stiffness matrix creates the connection between strains in the laminate and the applied loads and can be used as shown in equation (2.13)

$$\begin{bmatrix} N \\ M \end{bmatrix} = \begin{bmatrix} A & B \\ B & D \end{bmatrix} \begin{bmatrix} \varepsilon_0 \\ \kappa \end{bmatrix}$$
 (2.13)

Where

$$N = normal force vector$$
 $M = moment vector$
 $\varepsilon = strain[-]$
 $\kappa = curvature \left[\frac{}{mm}\right]$
 $For \mathbf{B} = 0:$
 $N = \mathbf{A} \varepsilon_0$
 $M = \mathbf{D} \kappa$ (2.14)

6. Calculate laminate strength properties

The properties of the laminate can now be determined by using the inverse of the A-matrix as is shown in equation (2.15).

$$A^{-1} = a = \begin{bmatrix} a_{11} & a_{12} & a_{16} \\ a_{21} & a_{22} & a_{26} \\ a_{61} & a_{62} & a_{66} \end{bmatrix}$$

$$E_{x} = \frac{1}{ha_{11}}$$

$$E_{y} = \frac{1}{ha_{22}}$$

$$G_{xy} = \frac{1}{ha_{66}}$$

$$v_{xy} = -\frac{a_{12}}{a_{11}}$$

$$h = total \ laminate \ thickness$$

$$(2.15)$$

where





For the example this results in the values given in Table 2.9.

Table 2.9 Example: Laminate properties

2D properties					
t_{tot}	=	1,00	mm		
E_{x}	=	18,9	Gpa		
$E_{\mathcal{Y}}$	=	18,9	GPa		
G_{xy}	=	7,1	GPa		
v_{xy}	=	0,33	_		

The Young's moduli are the same for the in-plane direction which is to be expected for a symmetric lay-up with evenly distributed fibres in each direction. The CUR gives the stiffness properties for this lay-up as well but with slightly different results, see Table 2.10. This is due to a round-off which is used in the CUR for the UD-plie properties.

Table 2.10 CUR Quasi-isotropic laminate properties

Stijfheidseigenschappen	Quasi-isotroop GVK laminaat 0° (25 %) / 90° (25 %) / +45° (25 %) / -45° (25 %)
E_{\times} [kN/mm ²]	18,6
$E_{\rm y}$ [kN/mm ²]	18,6
G_{xy} [kN/mm ²]	7,0
$ u_{xv}$	0,33





2.2.2 Structural usage in bridge engineering

FRP can be used as a structural component in many ways. Different usages will be elaborated shortly in this paragraph and follow from lectures of an FRP course at the TU Delft (Pavlovic, 2018a).

2.2.2.1 Internal FRP reinforcement

FRP reinforcement in the form of rebar has been used since 1975. Glass fibre reinforced polymers were used as rebar in a glue laminated timber bridge in Russia (Engineering, 2018). Here FRP replaced steel rebar for the first time. Downsides of steel rebar such as corrosion and high density (weight) are resolved by FRP. Besides these advantages FRP has a large tensile strength and it has no thermal or electrical conductivity.

To this day steel rebar is still used more often that FRP rebar. FRP rebar is only used if very specific material properties are needed.

2.2.2.2 External FRP reinforcement

FRP reinforcement can also be used externally to strengthen already existing structures. In seismic areas, prone to earthquakes, external strengthening is done to increase ductile behaviour by wrapping of columns. A different applications are shear strengthening of (masonry) walls and concrete walls can be accomplished by bonding FRP to the wall in the direction needed. Flexural strengthening is also possible by adhering FRP to the tension side of beams or slabs (Alkhrdaji, 2015).

2.2.2.3 Factory moulded structures

Free moulded structures such as windmill turbines or ships hulls are also possible to make with FRP. To create the specific structural forms a mould has to be created in which the fibres can be laid. Different processes exist to add the resin, one that is often used is vacuum infusion where resin is placed in the mould through an inlet and spread through the mould through a vacuum outlet (Vacmobiles, 2012).

2.2.2.4 Bridge decks

FRP bridge decks can be made by using different processes such as vacuum infusion, pultrusion or a sandwich structure. Pultrusion is a process where fibres are pultruded through a die which applies resin to form a reinforced panel with FRP face sheets and FRP webs which are used as spacers between the face sheets. This process can create beam or plate structures and cannot be used for free forms.





A sandwich structure is a bridge deck that consists of FRP face sheets and a foam core such as PVC. Here the spacers between the face sheets is the foam core bonded to the face sheets. A downside of this process is the bonding between face sheets and core. This bond can fail easily due to impact loads.

A combination of both aforementioned decks can be made through vacuum infusion where the face sheets are spaced by webs and a foam core. This type of sandwich panel can be tailored to the specific load conditions at hand and is still easy to produce. This type of panel has been used by engineering firm Witteveen+Bos and is designed and made by Delft Infra Composites. This type of sandwich panel is intended upon mentioning of a sandwich panel in this report.





2.2.3 Hybrid bridges

Hybrid bridges, as explained in paragraph 2.1.3, consist of at least two different materials that determine the load baring capacity. In the case of hybrid steel-FRP bridges the load baring capacity is determined by the steel sub-structure and an FRP sandwich deck. An explanation on what an FRP sandwich deck consists of can be found in the first part of this paragraph.

Two different types of hybrid bridges exist, bridges with and without shear interaction. Both bridge types will be explained in the second and third paragraph respectively. The last part of this paragraph shows an example of a hybrid steel-FRP bridge that is already built in the Netherlands.

2.2.3.1 Sandwich panels

The most used form of FRP with a load baring value in bridge engineering are sandwich panels as bridge decking. These sandwich panels are composed of two FRP face sheets with a core in between to create spacing. This spacing can be created by a plate material in a certain pattern such as a honeycomb or wave patterns. Another option is to us a solid material such as foam to create the spacing with added webs or so called through thickness fibres. This latter option is most used with FRP decking and is shown in Figure 2.9.

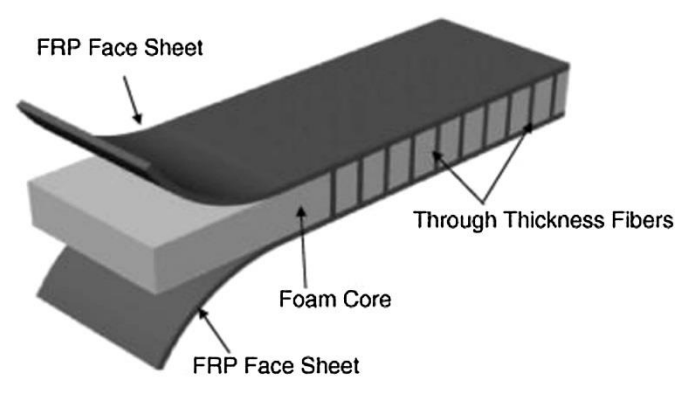


Figure 2.9 FRP sandwich panel (Reis & Rizkalla, 2008)

The lay-up of the face sheets and webs depend on the loads that will occur. Therefore the choice of lay-up will be made later on in paragraph 4.2.3.

Core materials

Different core materials are used in the industry such as PVC, PUR or PMI each having their own set of material properties. In many applications the foam core is not considered as a load baring material and left out of the calculations, this will also be done in this thesis. The weight





of the material will be considered. The characteristic values for several materials as shown in Table 2.11 are given in the CUR.

Table 2.11 Characteristic core material properties (CUR 96, 2017)

Material	Density $\left[\frac{kg}{2}\right]$	Compression strength $\left[\frac{N}{2}\right]$	Shear strength [_N]	E-modulus [_N_]	Shear modulus [_N_]
	$\lfloor m^3 \rfloor$		$\lfloor mm^2 \rfloor$	$\lfloor mm^2 \rfloor$	$\lfloor mm^2 \rfloor$
PUR	50	0.3 - 0.5	~0.2	6 - 10	4 - 5
	100	0.6 - 1.0	0.3 - 0.5	~30	~10
PVC	40	0.5 - 0.8	0.3 - 0.4	20 - 30	~10
	80	1.2 - 2.0	0.7 - 1.0	60 – 90	20 - 30
	80	~0.9	0.5 - 1.0	~50	20
PMI	30	~0.5	~0.3	~30	~15
	70	~1.5	~1.0	~90	~30

2.2.3.2 Hybrid bridge without interaction

Without shear interaction means that the deck is free to translate horizontally for small displacements in relation to the steel substructure. Only vertical forces are transferred from panel to sub-structure. In this case the load baring capacity of the bridge is solely dependent on the steel sub-structure and the sandwich panel only transfers wheel loads to the substructure by contact pressure.

For verification purposes this is the easiest option. Calculations are fairly simple and since there will always be some interaction between panel and substructure this calculation results in a safe design. A downside of this lack of interaction is that the load carrying capacity of the sandwich panel is not used for global deformations. As a result the steel substructure has to have large dimensions causing an increase in weight.

This process has been used for a recent bridge designed by Witteveen+Bos despite these disadvantages. This was a 2x2 highway bridge called the "Leeghwaterbrug" near Alkmaar. More on the Leegwaterbrug can be found in paragraph 2.2.3.4.

2.2.3.3 Hybrid bridge with interaction

When ensuring a hybrid interaction between deck panel and sub-structure a decrease in material usage can be established since the deck panel acts as an added top flange. This hybrid interaction can be accomplished either by using bolts or by bonding the deck to steel with adhesive.

Taking a cross-section along the longitudinal axis the bridge can be seen as a continuous beam on supports (deck plate on crossbeams) as shown in Figure 2.10. When applying a load





in span 1 a splitting force will occur in at the third support between deck (blue) and support reaction (black). This splitting force should be carried by the adhesive or the bolts.

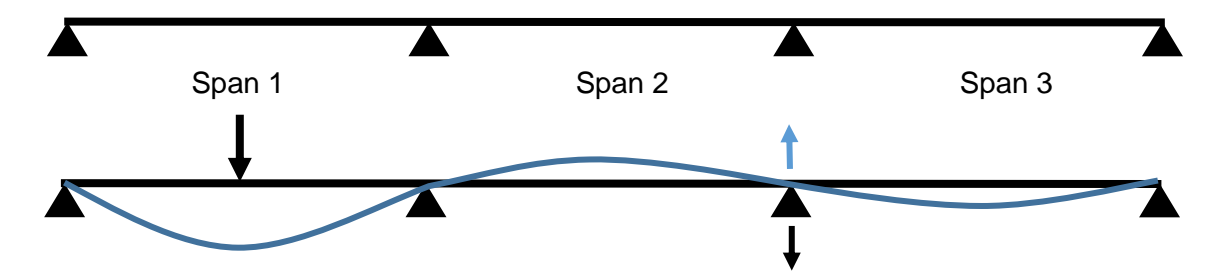


Figure 2.10 Bridge deck beam model

Besides that shear forces will occur in the adhesive layer due to curvature of the deck. When looking at the two different materials in a close up as shown in Figure 2.11 shear stresses occur between the FRP panel (blue) and steel flange (black). At the edges of a beam the deformation of the adhesive layer (red) is largest.

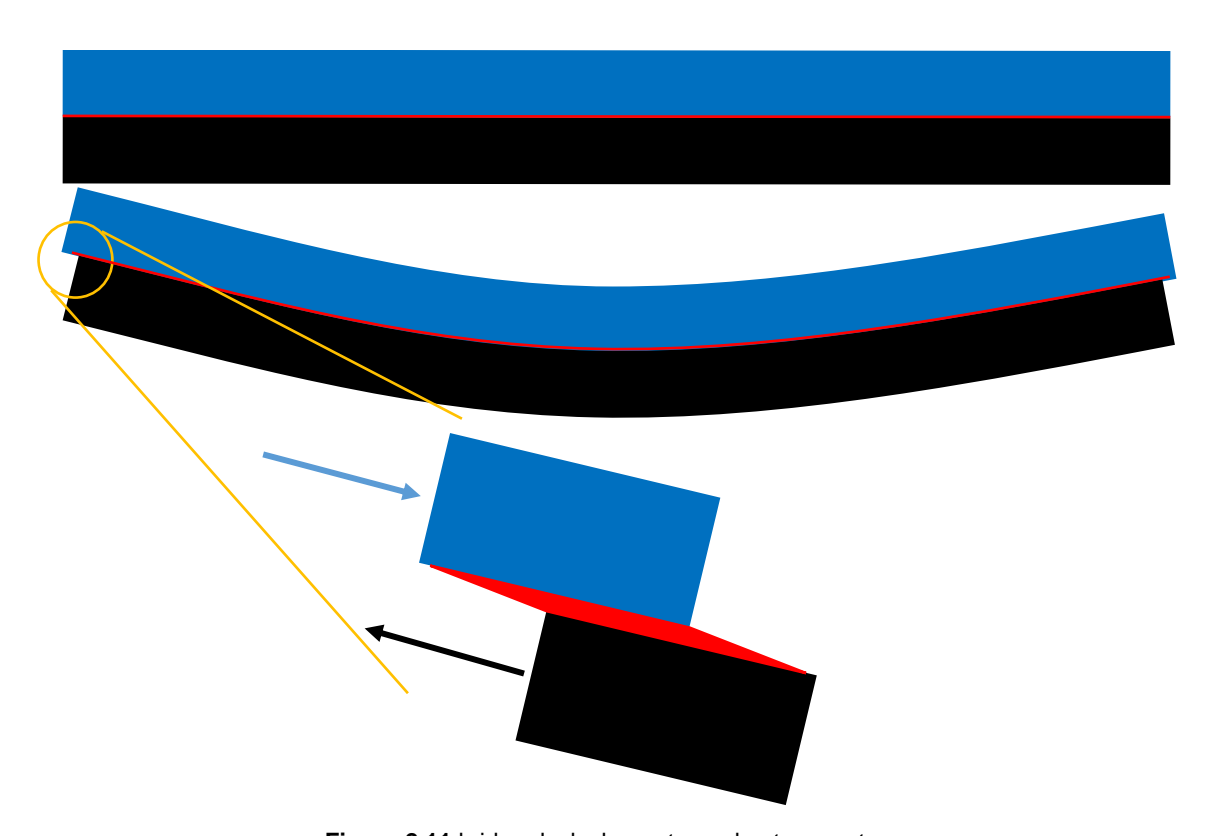


Figure 2.11 bridge deck shear stress due to curvature

This shear effect can occur either due to global deformation of the complete bridge span or as a local deformation in between crossbeams. This is the other challenge in hybrid bridge interactions. Both the splitting force and shear stresses should be verified for the bond.





2.2.3.4 Leeghwaterbrug

The Leeghwaterbrug near Alkmaar is a traffic bridge consisting of two movable bridge spans with each two traffic lanes. It is currently (2019) being renovated, the movable bridge in the direction of Heerhugowaard has already been replaced for a new hybrid steel-FRP movable bridge. The bridge in the other direction, to the AFAS stadium, is still under construction due to the fact that the foundation and pillars have to be replaced as well (Provincie Noorhd-Holland, 2018).

Across the Leeghwaterbrug runs the N242, a medium intensity road with a design value of 500.000 vehicles per year. The dimensions, as shown in Figure 2.12, are similar to movable highway bridges since it has a span of almost 16 meters and 2 traffic lanes in each direction (Souren, 2017).

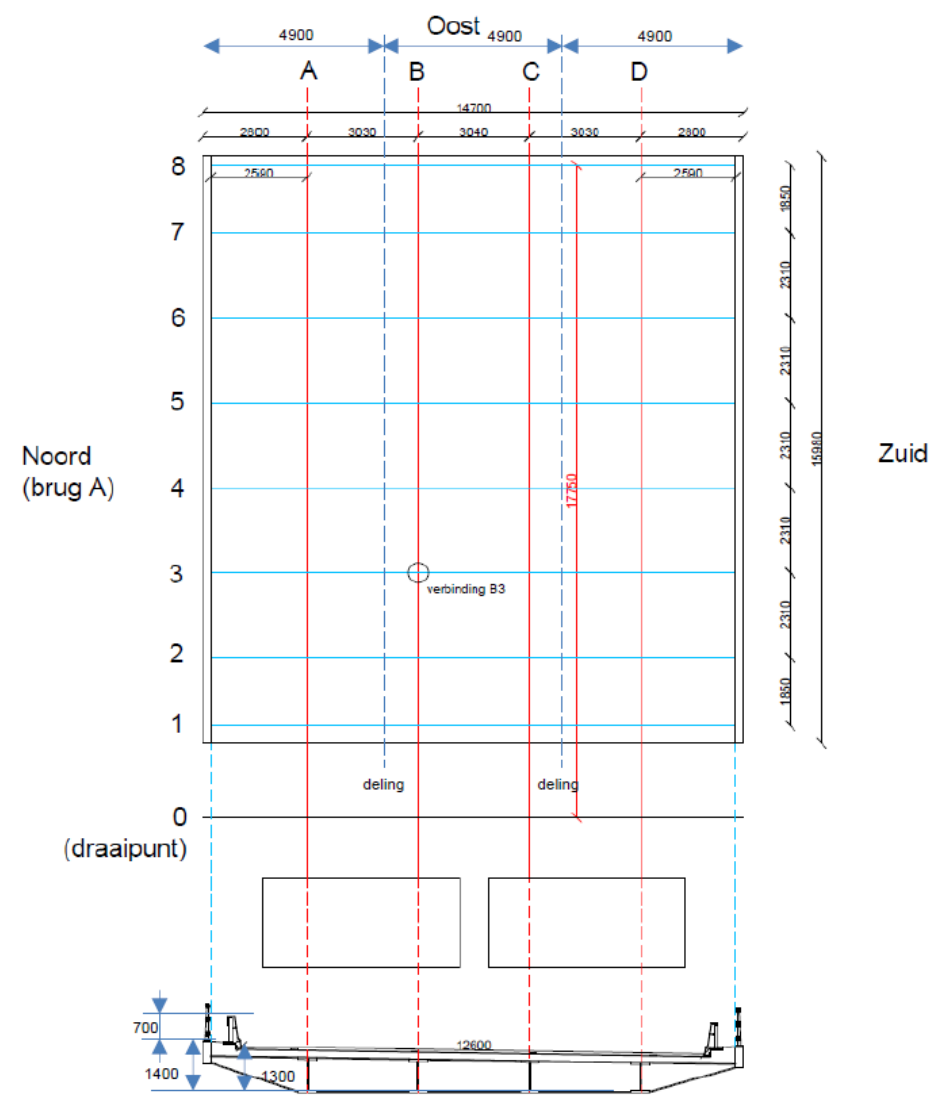


Figure 2.12 Leeghwaterbrug bridge geometry, top view (Souren, 2017)





This bridge consists of a steel subframe made up of four main girders and eight crossbeams. An FRP sandwich panel of E-glass fibres and polyester resin is placed on top of this. The sandwich panel is only in contact with the cross beams and consists of three parts attached together at the dashed blue lines shown in Figure 2.12. To ensure the sandwich panel does not come in contact with the main girders an extra layer of laminate is attached to the panel at crossbeam location.

During the design phase the assumption was made that the panel did not interact with the steel at all. The panel was bolted to the crossbeams, which means when deflecting enough the bolts will transfer loads from the panel to the steel and interaction will occur. Therefore, designing the bridge without any interaction can be viewed as a conservative approach since interaction will occur in some situations.

In Table 2.12 a model comparison can be found for a bridge with full hybrid interaction when attaching the sandwich panel only to the crossbeams or to the crossbeams and main girders. This comparison has been done for a bridge with a span of 20 meters, width of 12 meters and height of 1.5 meters. This showed that, although there are effects, the effects of the extra connection to the main girders is rather small as shown in Table 2.12.

Table 2.12 effects of connection to crossbeams with or without main girder

Connected to	Only crossbeams	Crossbeams and main girders
Max displacement	50,12 mm	45,8 mm
Max steel stress	87,8 N/mm^2	85,4 N/mm^2
FRP buckling factor	2,14	2,2
Max fatigue damage	0,947	0,859





Different load cases have been taken into account for this bridge and are stated below.

- Self-weight
- Mobile loads in accordance with EN1991-2
- Braking forces
- Wind forces
- Temperature loads
- Fatigue load model 4B in accordance with NEN-EN1991-2NB
- Loads on handrails (will not be taken into account)
- Loads on guardrails (will not be taken into account)

Sandwich panel

The sandwich panel used on the bridge has dimensions as shown in Figure 2.13. The extra blue layer at the bottom is only placed at crossbeam location to ensure no contact occurs between sandwich panel and main girders.

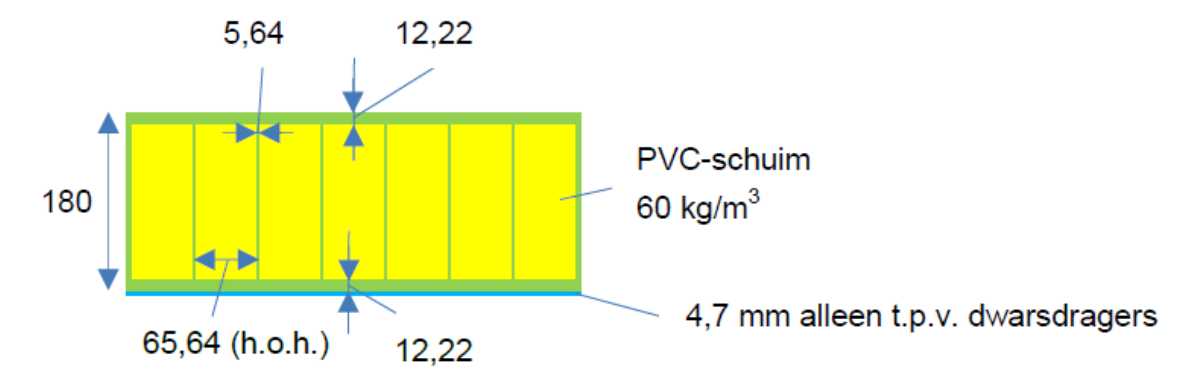


Figure 2.13 Leeghwaterbrug sandwich panel cross-section (Souren, 2017)

Both face sheets are identical and consist of plies in a layup as stated in Table 2.13, composition of the through thickness laminate can be found in Table 2.14.

Table 2.13 Leeghwaterbrug face sheet laminate (Souren, 2017)

i	arphi [°]	$t_k [mm] (0.94116 mm total)$	
8	0	0.17647	50% E

i	arphi [°]	$t_k [mm] (0.94116 mm total)$	ply
8	0	0.17647	50% E − glass UD
7	45	0.05882	50% E − glass UD
6	90	0.17647	50% E − glass UD
5	-45	0.05882	50% E – glass UD
4	-45	0.05882	50% E – glass UD
3	90	0.17647	50% E – glass UD
2	45	0.05882	50% E − glass UD
1	0	0.17647	50% E - alass UD





Table 2.14 Leeghwaterbrug through thickness laminate (Souren, 2017)

i	φ [°]	$t_k [mm] (1.88 mm total)$	ply
8	0	0.235	50% E - glass UD
7	45	0.235	50% E - glass UD
6	90	0.235	50% E - glass UD
5	-45	0.235	50% E - glass UD
4	-45	0.235	50% E - glass UD
3	90	0.235	50% <i>E</i> − <i>glass UD</i>
2	45	0.235	50% <i>E</i> − <i>glass UD</i>
1	0	0.235	50% <i>E</i> − <i>glass UD</i>

The PVC foam core hasn't been including in any strength calculation, self-weight of the foam however has been taken into account in the load models.

The sandwich panel has been verified for all applied load cases and the bridge has been constructed. This is one of few hybrid steel-FRP vehicle bridges in existence at the moment.





2.2.4 Conclusion

The answers to sub-questions 2.1 to 2.3 can be found below.

2.1) What is FRP and how can material properties be determined for fibrous materials.

FRP, Fibre Reinforced Polymers, are composite materials made up of fibres and resin. The fibres can be oriented in different directions to create resistance to the specified needs. Most common combination of fibre and resin in civil engineering is E-glass fibres with polyester resin. These components are often used in uni-direction plies (UD-plies) where all fibres are oriented in one direction. When combining these UD-plies and stacking them a laminate is created. To determine the properties of a laminate the laminate theory must be used.

Specific material properties of the fibres, resin and UD-plies can be found in Table 2.2, Table 2.3 and Table 2.4 respectively. Properties of a laminate highly depend on the build up of the laminate, how to determine the properties is elaborated in paragraph 2.2.1.4.

2.2) How is FRP used most in bridge building?

Structural applications of FRP in civil engineering can be found all around. Examples are internal reinforcements in the form of rebar, external reinforcements in the form of strips or wrapping of beams or columns and moulded structures such as turbine blades.

Different types of bridge decking exist for FRP, one of which is the vacuum infused sandwich panel. This panel consists of FRP face sheets and uses FRP webs combined with a foam core as spacers. This panel can be tailored to resist specific load conditions and will be used in this report.

2.3) Which hybrid bridge decks exist and what interaction occurs between steel and FRP.

As explained in paragraph 2.1.3 a hybrid bridge is a bridge that consists of multiple materials. The hybrid bridge type that will be focused on in this report is the steel-FRP hybrid bridge which consists of a steel structure of main girders and crossbeams with a FRP deck on top.

A bridge with or without shear interaction can be made depending on the connection between the FRP and steel. A bridge with shear interaction makes the best use of all the material in the bridge and will therefore be considered in this report.





2.3 Norms and regulations

There are many norms and regulations to be considered to verify the structural requirements of a movable bridge. In Europe these regulations are stated in the Eurocode. Since FRP is a rather new material in civil engineering no Eurocode exists yet. There are however several recommendation documents, one of which is the Dutch recommendation CUR. This is used as a basis for the Eurocode under construction for FRP.

Besides the Eurocode and the CUR many countries have additions or alterations to the Eurocode. In the Netherlands there are two, the national annex to the Eurocode (NEN-NB) and the ROK (design guidelines for civil engineering works, Dutch: Richtlijnen ontwerp kunstwerken). The ROK is the leading document for civil engineering works in the Netherlands.

There is a certain hierarchical order in which these documents overrule each other. The Eurocodes (EN and NEN) state all the basic norms. The Dutch national annex (NEN-NB) overrules these documents by stating certain changes or additions to the Eurocode, these are documents that cannot be used on their own. The ROK has even more changes or additions to the Eurocode and the Dutch national annex. This is not a stand alone document and can therefore only be used in combination with the Eurocode and the Dutch national annex.

The CUR is a Dutch recommendation document acknowledged by the Dutch government, Eurocodes are in the making but not yet finished. Therefore this is a stand alone document without any other documents that state changes or additions. Figure 2.14 shows the hierarchy of these documents, the most important at the top.

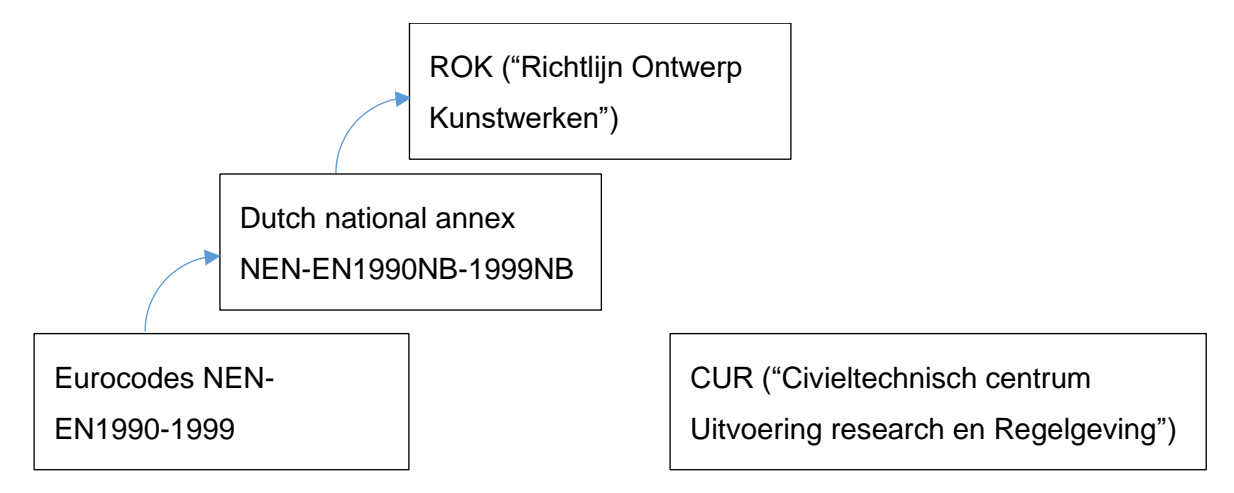


Figure 2.14 Hierarchical order of norms and regulations





The following list of rules and regulations are needed to conduct a thorough research on highway bridge design.

• EN1990	\rightarrow	Basis of structural design	
• EN1991	\rightarrow	Actions on structures	
o Part 1-1		→ General actions	
o Part 1-2		→ exposed to Fire	
o Part 1-3		→ Snow loads	
o Part 1-4		→ Wind actions	
o Part 1-5		→ Thermal actions	
o Part 1-6		→ During construction	
o Part 1-7		→ Accidental actions	
o Part 2		→ Traffic loads on bridges	
• EN1993	\rightarrow	Design of steel structures	
o Part 2		→ Steel bridges	
 NEN 6786 (Dutch) 	\rightarrow	Rules for the design of movable parts of civil structures	
o Part 1		→ Movable bridges	
 CUR 96 (Dutch) 	\rightarrow	FRP in structural and civil engineering structures	
 ROK (Dutch) 	\rightarrow	Design guidelines for civil engineering works	

Considering all types of loading would result in an unnecessarily extensive model for an early design stage. The focus of this thesis will be on the leaf of the bridge. It is expected that the traffic loads will be leading for the design of the leaf. Therefore other actions are not taken into account. This results in the consideration of EN1990, EN1991-2, EN1993, CUR96 and the ROK. An overview of the necessary parts can be found in Annex C.









3

Finite element software

Finite element software can be used to examine load cases, buckling modes, reaction to temperature, stability, vibrations, etcetera. Depending on the goal different types of analyses must be done and depending on the structure and materials different elements should be used. There are many finite element packages in existence and each one has its pros and cons. Depending on the requirements a software package can be chosen.

First requirements will be stated for the software. After that two finite element packages will be compared, one of which will be chosen to use for further model design and thereby answering the final sub-question. Background information on the type of finite elements and analysis is given in Annex F.

3.1 Software requirements

Choosing a certain software package depends on the goal of the FE-model. For global structural analysis with many different load cases simple software packages that use 1D or 2D elements will suffice. SCIA is one of the more well-known software packages that can do this and is used often in engineering firms. Other software packages are for instance SOFiSTiK (used by RHDHV) and RFEM (used by Witteveen+Bos).

More research and advanced detail related models call for sophisticated 3D elements. Software packages such as Abaqus, Ansys and Diana offer this but have their limitations in other parts such as defining numerous load cases. Abaqus is one of the most used FE-software used for detailed FRP modelling. The scope of this thesis is on a global scale, therefore sophisticated 3D software is not necessary.

For the 2D software both SOFiSTiK and RFEM offer a bit more for engineers then SCIA does. More in depth analysis can be done and simple 3D elements are incorporated in the software. Therefore these two software packages will be compared in this chapter and a





decision will be made on which one to use. Certain requirements have to be met by the program to make sure it is applicable for this thesis. These requirements follow from the information given in chapter 2.

FE-software requirements:

- Option to use textual input to create parametric models
- Laminate modelling to model FRP
- Ways to model the interface (bolted or adhered)
- Design multiple load models
 - Global loads (self-weight)
 - Stepwise loads (traffic loads)
- Multiple types of analysis
 - Linear analysis (global analysis)
 - Buckling analysis (local and global for FRP)
- Clear results export to do post calculations/verifications





3.1.1 SOFISTIK

SOFiSTiK is a FE-program designed in Germany and can be used in many different ways. Graphical input is possible by using other programs such as AutoCAD or BIM models.

3.1.1.1 Textual input

For textual input it uses it's own text editor called TEDDY which runs on a unique programming code. However, this programming code has a lot of similarities with more known codes such as Python. Furthermore it offers an extensive guide for all possible commands and there are many example files to help learn the language. This text editor can be coupled and run from other programs such as Python or excel to create a more user friendly input program instead of changing actual data in the code.

This text editor works with different modules for different parts of the analysis. There are a few main modules for material definition (aqua), meshing (sofimshc), load definition (sofiload) and analysis (ase). When an analysis is finished there are multiple modules or extra programs that can be used for results visualization.

3.1.1.2 Laminate modelling

Laminate modelling in SOFiSTiK is a possibility and is based on timber laminates. Recently glass, carbon or synthetic fibres are included as are epoxy, polyester and vinyl ester resins. If these standard values are not valid for the used material possibilities are there to define anisotropic materials. This makes it possible to define laminate properties for a global load bearing analysis.

3.1.1.3 Interface modelling

There are interface elements for the interface between layers and between laminate and steel. Currently, only spring elements are supported by SOFiSTiK.

3.1.1.4 Load modelling

Load module Sofiload has many different loading possibilities. Dead weight of the structure can be implemented by the program which uses the density of the material to define the weight. For area loads such as crowd loading or wheels the command LAR can be used. By using a set of loops in the code this area load can be configured in such a way to form a step-wise load model as if a wheel is driving along the bridge deck which is needed for fatigue calculations.





Thermal loading is possible using EVAL and can be quantified in several temperature steps along the height of the structure. Furthermore, there are no limitations to the number of load cases that SOFiSTiK can evaluate.

3.1.1.5 Analysis types

Several types of analysis are possible in SOFiSTiK. The user is free to create load models for example vehicle loading or temperature loading. Besides those "simple" loads SOFiSTiK offers different ways of dynamic loading for earthquake simulations. Train loading for vehicles is also possible with a pre-made program to simplify usage. Modelling wind, wave and snow loads is also made simpler with pre-made programs within SOFiSTiK.

SOFiSTiK also offers a buckling analysis both linear and non-linear. This analysis can find all sorts of buckling for beam and shell elements. All of these analysis can also be initiated from the text editor Teddy.

3.1.1.6 Result visualisation

SOFiSTiK has different results processors depending on the demands of the user. It has an inbuild tool for colourful visuals of deformations or stresses which is useful for a quick overview of the results. For a more detailed picture an external tool, WinGRAF, can be used. This tool can show both 3D and 2D figures with results along a line or at nodes or cross-sections.

The Result Viewer will be most useful for post calculation. This module (RESULTS) can export specific data to excel sheets. Export data can be selected by the user and can include or exclude load cases, stresses, strains, support reactions etcetera. These exports are easy to categorise and name so a post calculation can be done with ease.





3.1.2 RFEM

RFEM is a FE-program also designed in Germany and can be used for many different applications such as plant and mechanical engineering or dynamic analysis. Various CAD and BIM programs can be combined with RFEM

3.1.2.1 Textual input

Parametric modelling can be done in multiple ways with RFEM. One is by using the parametric option in the program itself. Data points in the model can be linked to certain parameters, if a parameter is changed the model changes as well. Although this is a strong tool it will not be applicable for this project since it is impossible to create (or delete) nodes by changing parameters which should be done if for instance the width of the bridge is changed.

The other way of creating a parametric model is by using excel and importing excel sheets into RFEM. Models in RFEM can be created by solely implementing excel tables. These tables can be created by for instance using programming languages such as vba or Python to create data points, lines and surfaces for the model. Programming languages vba and Python are well known and a lot of support can be found for problems within these languages making it fairly easy to learn and understand it.

There are limitations to this way of parametric modelling which lies in the way RFEM works. Certain "add-ons" or so called modules cannot be used by importing excel sheets. Dlubal Software, the developers of RFEM, are working on this problem but at the moment modules such as RF-laminate and RF-move cannot be used with this method.

The last way to create a parametric model is using RFEM commands within vba. This works similarly as the previous option however the data is created in RFEM immediately instead of creating an excel sheet and importing it later. Several add-on modules have been incorporated in the vba commands and can be used remotely. Unfortunately not every module can be used this way yet but Dlubal is working on this.

3.1.2.2 Laminate modelling

Laminate modelling in RFEM is possible with the module RF-laminate. Unfortunately this cannot be combined with parametric modelling yet. It has no limitation to the number of layers or the thickness of each layer. It is also possible to add an eccentricity making it possible to model sandwich panels.





3.1.2.3 Interface modelling

RFEM offers several ways to model interfaces with the help of surface-, line- or nodal releases. These can be modelled width different constraints to model a release that happens at a certain tension or shear force for example.

3.1.2.4 Load modelling

Load modelling in RFEM can be done in two ways. The first is by creating load combinations by hand. This process can be done parametrically using the vba commands.

The other option is to use the RF-move module. This add-on creates load trains by setting a load area and setting a step size. This is a simple process and works perfectly however it cannot be invoked from vba yet making it impossible to use for a parametric model.

3.1.2.5 Analysis types

Several types of analysis are possible in RFEM. The user is free to create load models for example vehicle loading or temperature loading. Besides those "simple" loads RFEM offers different ways of dynamic loading for earthquake simulations. Train loading for vehicles is also possible with a module which already has the Eurocode load cases implemented. Modelling wind, wave and snow loads is also made simpler with modules within RFEM.

RFEM also offers a buckling analysis both linear and non-linear. This analysis can find all sorts of buckling modes for both beam and shell elements.

3.1.2.6 Result visualisation

Results can be visualised in many ways using RFEM. The visual results can be shown by using isobands, isolines or as a difference percentage. Many different results can be shown including stresses, strains, deformation, moments, normal forces and shear forces. Numerical results can be obtained on so called "grid points" This grid can be set by the user and does not coincide with the mesh.

To obtain results on a mesh point located inside a surface vba is needed. Each nodal result can be obtained for different load cases making it easy to obtain the desired results.





3.2 Conclusion

Both SOFiSTiK and RFEM have the capabilities needed for this project with each their own strong and weak points. The main difference is in the way the input is required, SOFiSTiK uses their own coding software whereas RFEM uses visual basics. SOFiSTiK has created an extensive manual for their programming language to help users understand and use the software efficiently. RFEM doesn't have any manual for the programming part of their software since it is mainly focused on visual input instead of textual.

Besides this disadvantage RFEM has better capabilities of modelling laminates since there is no limitation to the number of layers. Interface modelling seems to be more extensive in RFEM than it is in SOFiSTiK which is a big advantage for this research since the interface between steel and FRP is very important. For load modelling and the different types of analysis these programs do not show significant differences. Also the result visualisation seems to be able to do the same in each of the programs.

RFEM has more possibilities for interface modelling which together with the fact that RFEM is the program used by Witteveen+Bos results in the decision to use RFEM as modelling software.









4

RFEM models

An explanation of the RFEM models will be given in this chapter. First of a workflow will be given which shows the steps taken to create, verify, calculate and analyse the complete calculation model. Figure 4.1 shows this workflow of the complete model. Steps one to seven will be elaborated in this chapter and show how to create the finite element model and how its validity has been verified. Steps eight to ten will be elaborated in chapter 5 and show the model calculation and result analysis. The optimization will be elaborated in chapter 6 together with the comparison between the two bridges.

4.1 Workflow

Starting at the top left of Figure 4.1 are the global parameters of the bridge such as span, width and traffic type. These parameters are used to set-up the model data for calculation. The model data is then exported to RFEM and the calculations can be started. After this the required results must be exported from RFEM to conduct a results analysis. The final step will be to determine possible optimizations in the model and loop back to the start to begin another run of the model.

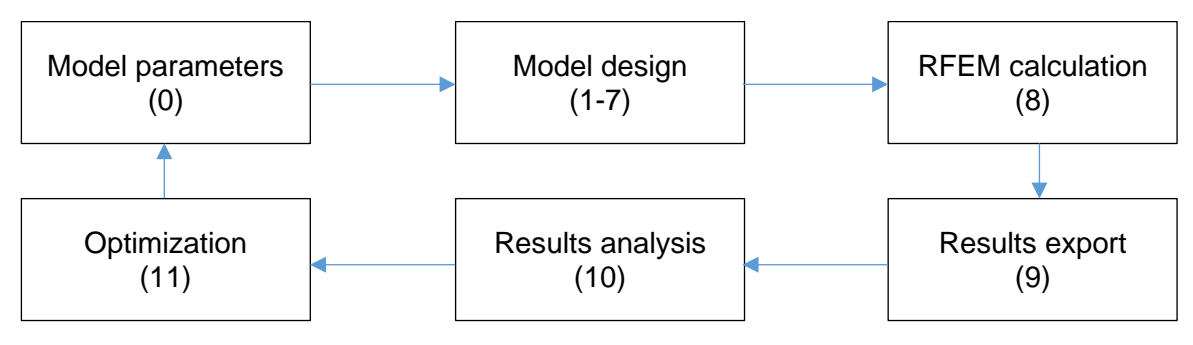


Figure 4.1 Model workflow





Model design (step 1 to 7)

The model design and the results export will both be done using visual basics and will be the core of the model. The model design can be split up in two parts and follows a fixed path that will be explained using a simple OSD bridge with 2 main girders and three stiffeners.

The first part starts by reading all the necessary parameters given by the user. With these parameters all the nodes can be created (step 1) on their correct location. The next step is to draw lines (step 2) between the nodes to create the edges of the plates. The material has to be defined next (step 3), with the materials defined it is possible to create the plates (step 4) surrounded by the previously defined lines. The final step of the model set-up is defining the supports (step 5) and the mesh refinements (step 6). These 6 steps are illustrated in Figure 4.2. Mesh refinements can be implemented to further increase the accuracy of the model. This can be done by setting a mesh refinement for a surface, a line or around a node.

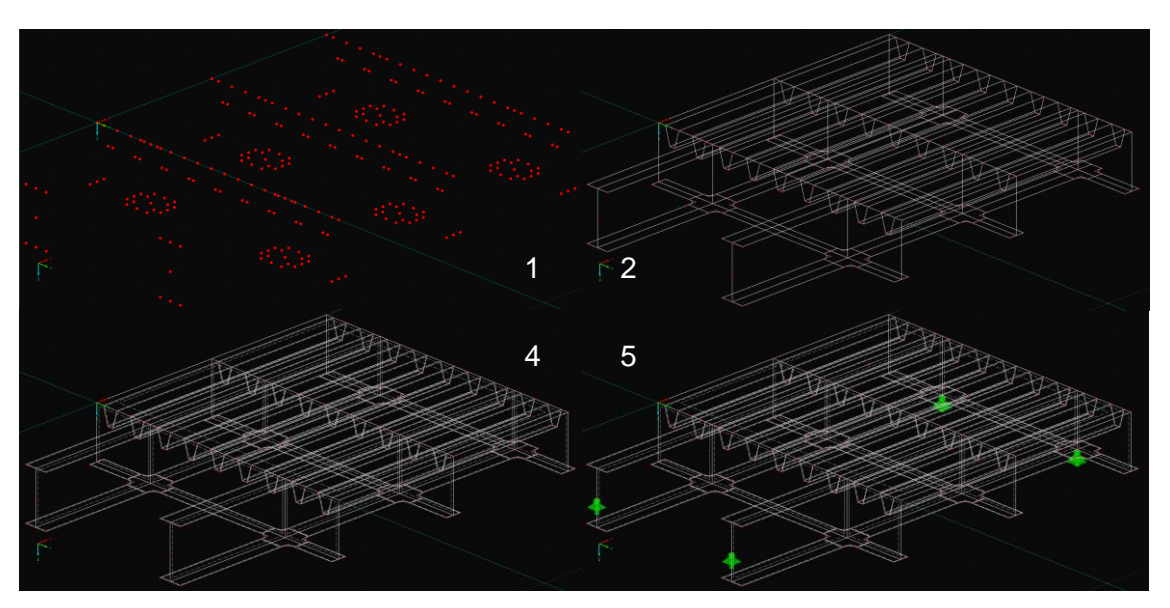


Figure 4.2 Model design

The second part (step 7) of the model design is the definition of load cases. This includes the traffic load models and the fatigue load models. For this process load cases need to be created and for each load case the different loads must be defined using free rectangular loads which can be placed on the deck plate.





RFEM calculation (step 8)

The previously mentioned model set-up has created everything for RFEM to start the calculations. The calculation starts by creating the mesh, including refinements if specified. Extra mesh specification can be implemented if necessary. Each different load case will be analysed after the mesh has been determined. The calculation time depends on the size of the model and mesh refinements.

Results export (step 9)

The results can be exported using vba. The results can be obtained by "requesting" a variable for a certain mesh node within a plate element. Nodes can be defined in the model set-up and can be given a fixed node number making it easier to read out variables in the correct location.

Results analysis (step 10)

The next step is to analyse the results. By means of a post calculation verifications can be done. This will include a fatigue damage calculation for the fatigue load models using the rainflow method. For the other load cases a ULS and SLS (maximum deflection) verification will be conducted.

Optimization (step 11)

The final step is to optimize the model. There are multiple types of optimization possible, the simplest of which is to start with one model and change certain parameters depending on the results. Some of the parameters will be fixed by the first model, from there on a few parameters will be altered for each new iteration. This optimization does not look into previous results but only works of the latest iteration and alters from there. This type of optimization is simple to implement but will probably not give the most optimal solution. Nonetheless it will result in an optimization good enough to compare the two different models.

An optimization will be done if the verification with the Eurocode and CUR results in negative results but also when it results in an unnecessarily safe design.





4.2 Model design

Both models are build up of plate elements and follows the steps shown at the start of this paragraph. The plates are connected at their centroid and do not take into account any round-off or weld material. The welded connections are considered to be rigid which means that rotations in a connection are all the same.

The build-up of both models will be elaborated in this paragraph together with the needed input parameters and detail locations needed for the fatigue calculation. A separate paragraph is dedicated to the creation of the load cases.

4.2.1 OSD model

The OSD model consists of 4 main parts, namely the deck plate, stiffeners, crossbeams and main girders. The main girders and crossbeams are inverted T-beams and the stiffeners will have a trapezoidal shape. Each part will have a constant dimension for the complete leaf of the bridge. The main girders and crossbeams are connected to each other by means of welding. Different configurations of this connection can be created and depend on the height of the crossbeams and main girders. For bridge spans with a limited height, which is often the case for renovation projects, the height of the crossbeams and main girders are the same. This means that the flanges of both parts are connected to each other as well as the webs, a close up of the connection can be seen in Figure 4.3.

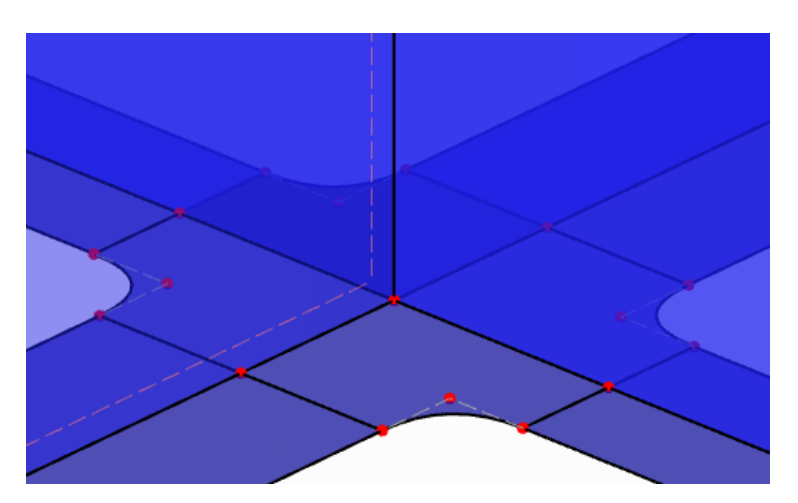


Figure 4.3 Model design: main girder to crossbeam flange connection





The configuration of the stiffeners also depends on the height. Nowadays trapezoidal stiffeners are used most of the time. These stiffeners can be continuous, which means they run through a hole in the crossbeams, or they are cut and placed in between the crossbeams. For bridges with a limited height the cut-outs in the crossbeams would result in stress concentrations, therefore the stiffeners are cut and welded to the crossbeams. As a result the crossbeam webs are simple plates spanning from the deck plate to the bottom flanges of the bridge without any cut-outs.

Most of the dimensions of these parts will differ for different designs. Each of the parameters (thicknesses, width, height, etc.) will be elaborated in the next paragraph.

4.2.1.1 Parameters

There are many parameters that can be thought of for an OSD bridge. Most of them are standardized such as the dimensions of the stiffeners or the thickness of the deck plate, others depend on the global dimensions. A list of all the parameters can be found in Figure 4.4, Figure 4.5 shows cross-sections of the bridge including the parameters for a clear overview. All parameters can be altered but for simplicity recommended values are given.

Values in the green boxes are the general dimensions and must be given by the user. Values in the yellow boxes may be altered by the user and the program will still function. Values in the orange boxes may be altered by the user but might cause errors. Values in the red boxes must not be altered or the model will not fulfil the general dimensions.

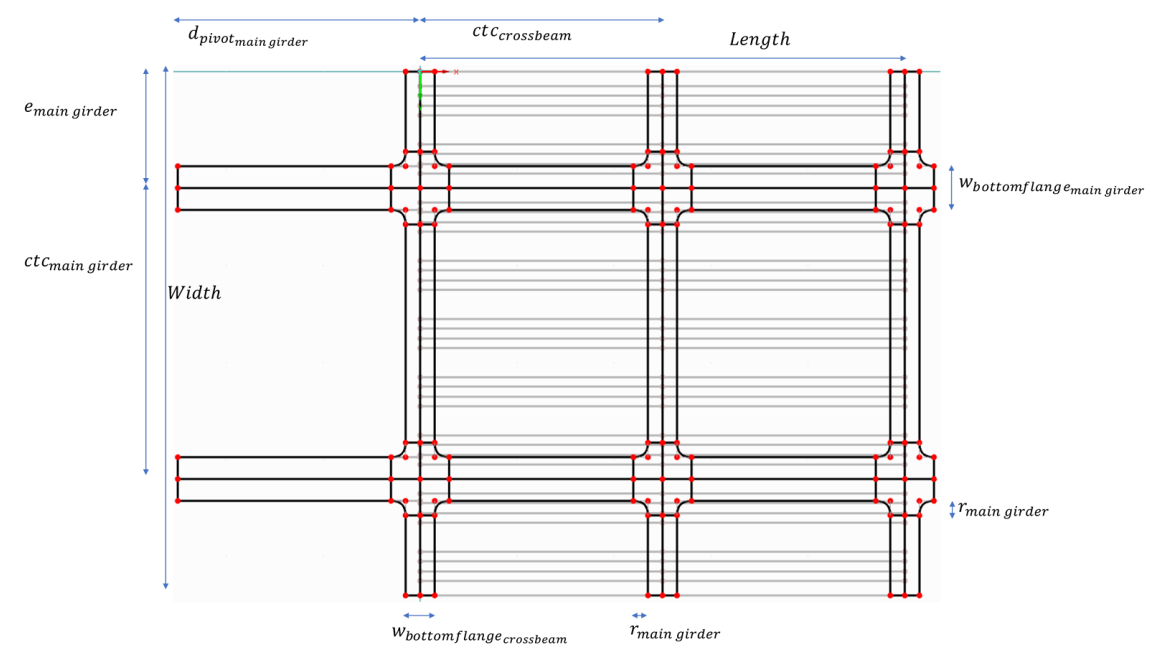
Input Parameters	In code	value	Unit	Input Parameters	In code	value	Unit
General				Main girders			
Span	br_l		m	Main girder height	br_h_mg		m
Width	br_w		m	Main girder connection radius	br_r_mg		m
Height	br_h		m	Main girder distance to pivot	br_piv_mg		m
Deck				Main girder web thickness	br_t_web_mg		m
Deck thickness	br_t_deck		m	Main girder bottom flange width	br_w_bfl_mg		m
Stiffeners				Main girder bottom flange thickness	br_t_bfl_mg		m
Number of stiffeners	br_n_stif		-	Number of main girders	br_n_mg		-
Stiffener centre-to-centre cantilever	br_ctc_stif_can1		m	Main girders centre-to-centre distance	br_ctc_mg		m
Stiffener centre-to-centre distance	br_ctc_stif		m	Main girder distance to edge	br_e_mg		m
Stiffener centre-to-centre cantilever	br_ctc_stif_can2		m	Load cases			
Stiffener top width	br_w_tstif		m	Lanewidth	ld_w_lane		m
Stiffener bottom width	br_w_bstif		m	Side parapet (zijberm)	ld_w_par		m
Stiffener height	br_h_stif		m	nr_lanes	ld_nr_lanes		-
Stiffener thickness	br_t_stif		m				
Crossbeams							
Crossbeam height	br_h_cb		m				
Crossbeam-stiffener geometry	br_geom_cb		-				
Number of crossbeams	br_n_cb		-				
Crossbeam ctc distance first spans	br_ctc_cb2		m				
Crossbeam web thickness	br_t_web_cb		m				
Crossbeam bot flange width	br_w_bfl_cb		m				
Crossbeam bot flange thickness	br_t_bfl_cb		m				
Crossbeam centre-to-centre distance	br_ctc_cb		m				

Figure 4.4 Parameters OSD bridge





Top view



Red dots are the nodes in the model Black lines are the plate edges for the main girders and crossbeams Grey lines are the plate edges for the stiffeners.

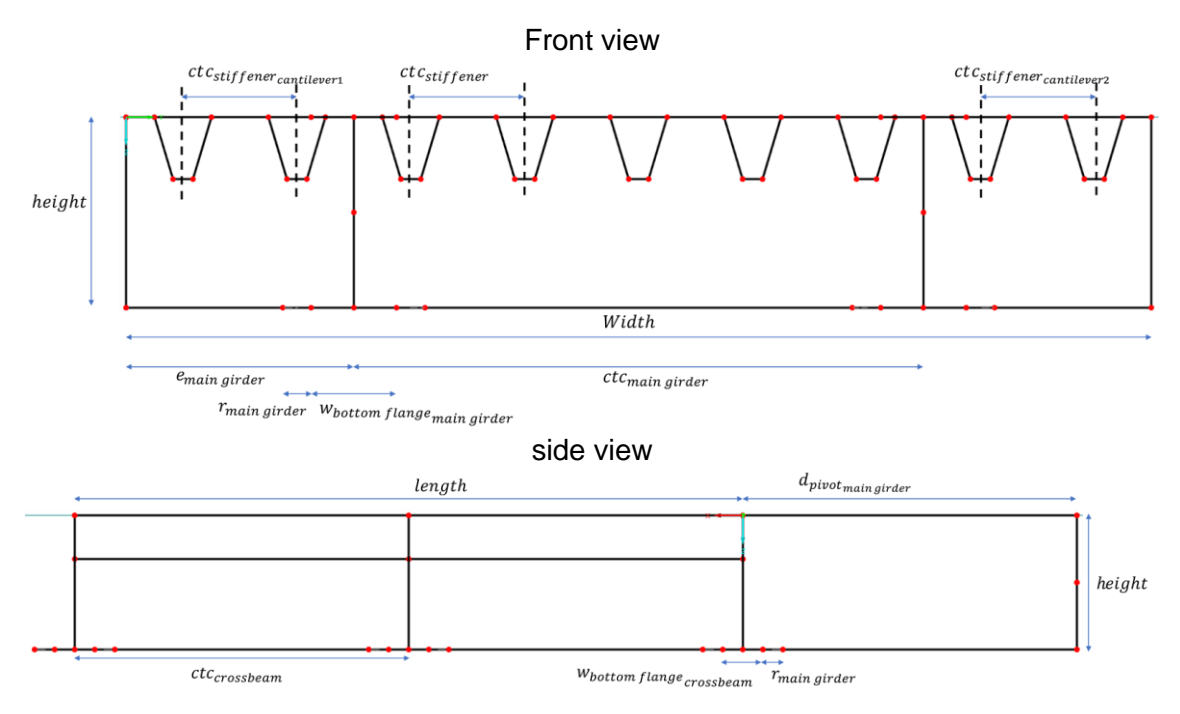


Figure 4.5 Cross-sections OSD bridge





The general dimensions include the width, span and height of the bridge together with the traffic lane lay-out. Three other general dimensions are the number of main girders, the distance between them and the distance to the edge of the bridge. All these parameters are project specific and will be fixed for a renovation project.

The span differs from 8 to 30 meters, height lies between 900 and 1600 mm. Usually there are 2 main girders with a distance of 7 to 9 meters between them (see Table 2.1).

Besides these parameters there are some parameters which could be altered but are highly unusual to differ from standard values for highway bridges. These include the dimensions of the stiffeners and the thickness of the deck plate which can be found in Figure 4.6.

The thickness is obtained from Table C.7, it is not a minimum value since the stiffeners are not continuous. For this thesis the thickness will however be fixed since local analysis of the deck-stiffener details are not conducted.

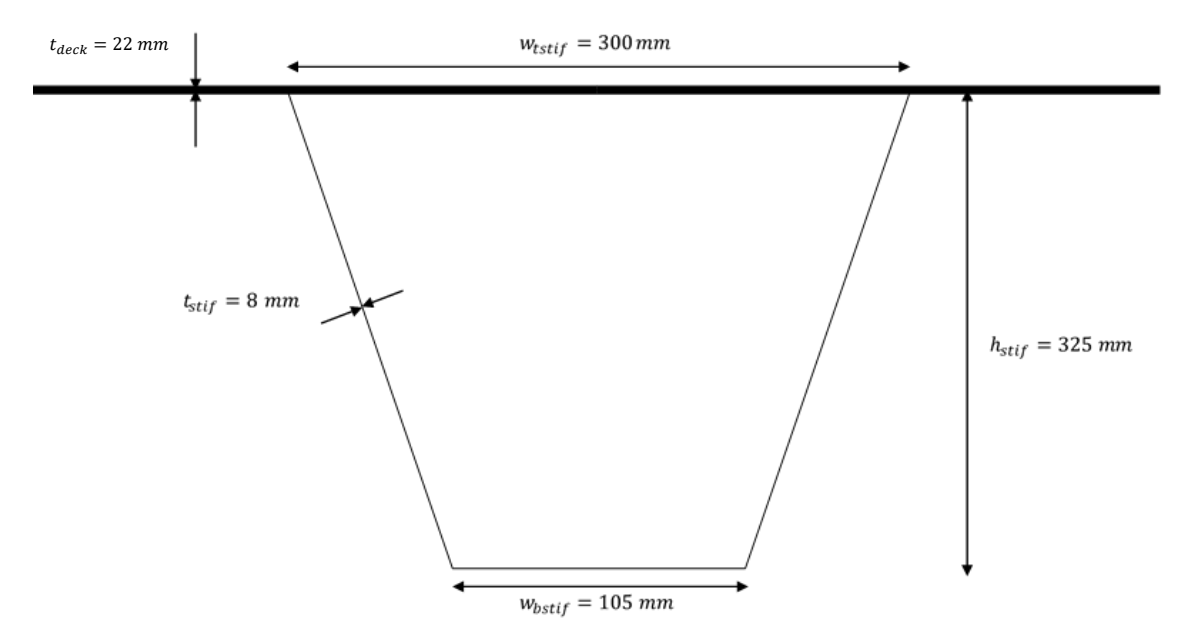


Figure 4.6 Dimensions stiffener and deck plate

The centre-to-centre distance of the stiffeners is often 300 mm. Only when this distance would result in a structure with odd situations around the main girders a deviation of this centre-to-centre distance would occur. Odd situations would be stiffener webs being to close (less than 100 mm from the main girder flange) or to far (more than 200 mm from the main girder flange) from the main girder flange.

The dimensions of the crossbeams and main girders mostly depend on the global parameters and an estimate is made for the dimensions of the crossbeam flange and web. The height of





the crossbeams and main girders is the same as the general height of the model. The dimensions of the flanges and webs can be given by the user, but a recommendation has been given with the help of existing welded beams.

In Table 4.1 ratios have been determined of width over thickness for both webs and flanges of I-beams made by manufacturer Steltech (Steltech, 2016). As an example boundaries have been determined for a beam with a height of 1 meter. For this height the following boundaries can be found according to this data.

$$12 \ mm(t_{web_{cb}}) \le t_{web} \le 16 \ mm(t_{web_{mg}})$$

$$235 \ mm(w_{flange_{cb}}) \le w_{flange} \le 437 \ mm(w_{flange_{mg}})$$

$$15 \ mm \le t_{flange_{cb}} \le 24 \ mm$$

$$28 \ mm \le t_{flange_{mg}} \le 45 \ mm$$

The upper range will be used as start value for the main girders and the lower range will be used as start value for the crossbeam. These values will also be used as start values, not as boundary values.

web height | web thick | ratio web height | Flange width | Ratio Flange width | Flange thick ratio 1200 16 75,00 Max 81.60 1200 500 2,40 May 4,25 500 40 12,50 Max 15,63 1192 16 74.50 Min 62,50 1192 500 2.38 Min 2,29 500 36 13.89 Min 9.8 1184 74,00 1184 500 2,37 500 32 16 15,63 1184 74,00 web_height 1184 400 2,96 web_height 1000 400 32 12,50 fl_width_mg 436,7 16 1000 1176 16 73,50 16,0 1176 400 2,94 max_fl_w 400 28 14.29 3,34 25 14,00 1170 16 73,13 1170 350 min_fl_w 350 27,9 1170 16 73,13 1170 275 4,25 275 25 11.00 32 fl_width_cb 235,0 1024 16 64,00 1024 400 2,56 400 12.50 2,54 1016 16 63.50 1016 400 400 28 14.29 max t 23.9 2,89 25 15,0 1010 16 63,13 1010 350 350 14,00 min t 1000 16 62,50 1000 300 3,33 300 20 15,00 924 12 77,00 924 400 2,31 400 32 12,50 916 12 76,33 916 400 2,29 400 28 14,29 910 12 75,83 910 350 2,60 350 25 20 14,00 900 12 75.00 3.00 15.00 900 300 300 816 10 81,60 816 300 2,72 300 28 10,71 810 81,00 810 275 2,95 275 25 11,00 10 800 10 80,00 800 275 2,91 275 20 792 10 79,20 250 3,17 250 16 15,63 792 716 71.60 716 2.60 10 275 275 28 9.82 250 2.84 250 25 710 10 71.00 710 10.00 700 10 70,00 700 250 2,80 250 20 12,50

Table 4.1 width over thickness ratio welded I-beams

The distance between crossbeams is often between two and three meters with a slightly smaller distance at the first and final crossbeam span. As a recommendation a distance of 2.6 meters will be used. The distance of the first and final span depend on the total length of the bridge, usually this distance is around 75% of the other spans.





The left over dimensions are needed for the main girders. The connection between the flanges of the main girders and crossbeams are often made with rounded corners. The radius of these corners can differ and will change the fatigue detail category. To obtain the highest detail category this radius must be 150 mm or larger, therefore the radius is set on 150 mm.

Than there are the main girder extensions to the pivot point. The distance is usually 2.5 meters. The dimensions of the web and flanges are kept the same as for the rest of the model.





4.2.1.2 Fatigue detail locations

As explained in annex C.1.6 there are many detail locations that must be considered for fatigue in bridges. Several of these details can be neglected decreasing the number of details that need to be analysed. The four details that will be analysed are stated first, the details that can be neglected will be stated afterwards.

Local detail 5 is often a critical detail in OSD bridges so an indicative value for this detail is desirable although a more detailed analysis is necessary to give a sound conclusion if failure will occur or not. This detail will be considered directly under a wheel load to create the best indicative damage value possible. For the OSD bridge this detail will be denoted as detail 1 as shown in Figure 4.7.

General detail 2 and 3 depend on the same stresses and coincide in some locations of the model where peak stresses can be expected (crossbeam to main girder connection). Therefore the lowest detail category will lead to the highest damage which makes it possible to neglect general detail 2. General detail 3 however must be considered with a detail category of 80. Stresses will be determined at the connection between the crossbeam web and the main girder web/flange. For the OSD bridge this detail will be denoted as detail 4 as shown in Figure 4.7.

General detail 5 can have a very low detail category, as low as 36. Therefore this detail will be included in the analysis. The detail category depends on the execution and finishing of the weld, in most cases this results in a detail category of 90. For the OSD bridge this detail will be denoted as detail 3 as shown in Figure 4.7.

General detail 6 could have a low detail category as well, possibly being as low as 50. Together with the fact that stress concentrations will occur near a curved edge this detail could be leading and will therefore be considered. As for detail 5 this detail category depends on the execution and finishing of the weld which often results in a category of 90 as well. For the OSD bridge this detail will be denoted as detail 2 as shown in Figure 4.7.

Figure 4.7 shows the four details that will be considered together with the detail category that coincides with the most used weld execution method. For detail 3 a correction factor k_s must be used as is given in equation (C.12).





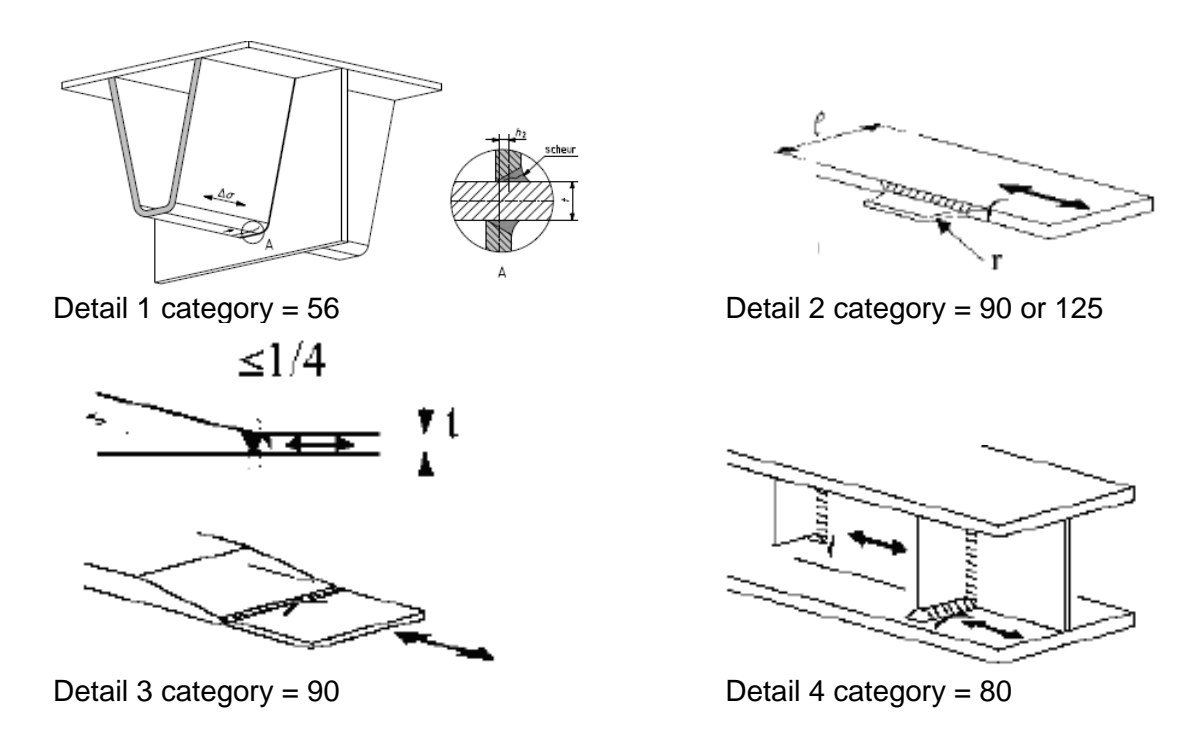


Figure 4.7 Details to consider for OSD bridge

The details that will not be considered are stated below.

Local details 1 and 2 can be neglected for deck plates thicker than 18 mm. For highway bridges a thickness of 22 mm is recommended nowadays therefore making these details obsolete. Local detail 4 is a weld failure to connect stiffeners to each other. For short spans such as a movable bridge this detail will not occur and can therefore be neglected.

Local detail 3 and 6 are local details that depend highly on the location of the wheel track. A local analysis is needed to determine the damage for these details, this is however outside the scope of this thesis and will therefore be neglected.

Several of the general details will be neglected as well. General detail 1 has the highest possible detail category. Chances are fairly low that this detail will result in considerable damage without other details being critical and will therefore be neglected.

General detail 4 is situated in the same location as detail 4 but takes into account stresses in the transverse direction. Significant stresses in this detail will only occur when the main girders have an immense torsional stiffness and the crossbeams have barely any stiffness at all. Since this is usually not the case this detail will be neglected.





4.2.2 Hybrid model

The hybrid model consists of plate elements just as the OSD model and is build up in the same order. The main girders and crossbeams are connected in the same way as the OSD model with the height of the main girders and crossbeams being the same. The sandwich panel is modelled using two face sheets and webs in between those face sheets as shown in Figure 2.9. The foam in the sandwich panel will not be modelled but will be taken into account for the weight per square meter. A PVC foam core of $80 \frac{kg}{m^3}$ will be considered. The lay-up and the dimensions of the sandwich panel will be determined in paragraph 4.2.3.

A challenge in the design of the hybrid model is the interaction between FRP and Steel. To create the most optimal structure a full hybrid interaction will be modelled. This means that a rigid bond between FRP and steel should be made.

Ideally this bond between the steel and FRP would be modelled along the complete contact surface. Several attempts have been made to do so but unfortunately it is not possible to create such a bond in RFEM for a large parametric model. Reasoning behind this can be found in Annex H. Therefore a different type of connection has been created in RFEM which should still ensure a full hybrid interaction.

The bond has been simulated with rigid plate elements in between the top flanges of the steel and the bottom face sheet of the FRP. As a result peak stresses are expected around this connections since it is not continuous. This will make verifications in the FRP around the connection irrelevant since the stress patterns do not compare to reality. Due to this workaround it is therefore impossible to verify the bonded joint (Annex C.2.1) as well as fatigue damage in FRP (Annex C.2.3) on a global scale. Figure 4.8 shows a close-up of the rigid links between the FRP sandwich panel and the steel substructure.





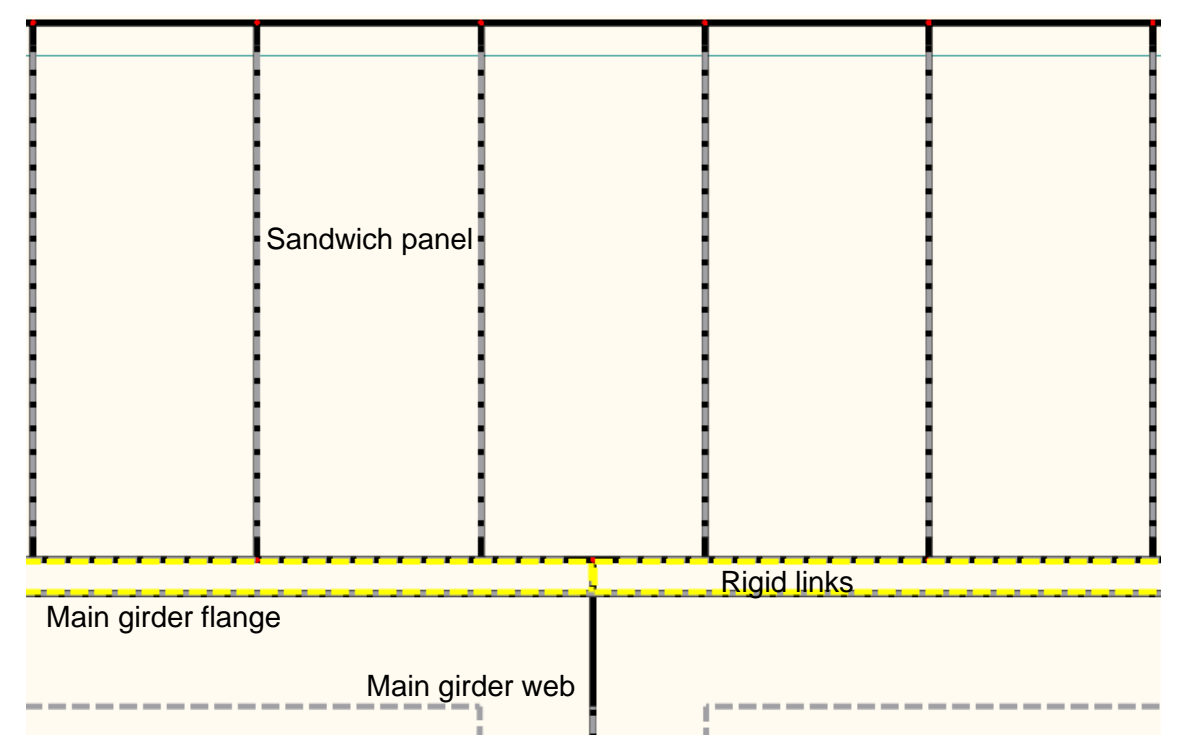


Figure 4.8 Hybrid model: rigid links

The effects of these rigid links on the rest of the model will be analysed in paragraph 4.3.2.

4.2.2.1 Parameters

The parameters for the hybrid bridge have similarities with the OSD bridge. The structure of main girders and crossbeams will be the same but also includes a top flange now. These top flanges will have fixed dimensions throughout the iterations.

The steel deck plate and stiffeners are replaced by the FRP sandwich panel. Five parameters are needed for this panel beside the material properties. These parameters are the height of the panel, thickness of both facings and the web and the distance between the webs. Optimizing this sandwich panel could be a thesis on its own, therefore the dimensions of the sandwich panel will be fixed.

Due to the slender nature of the sandwich panel webs and face sheets the panel is prone to buckling. The dimensions will therefore be determined depending on the buckling behaviour and will be elaborated in the next paragraph.

A list of all the parameters can be found in Figure 4.9, cross-sections can be found in Figure 4.10.





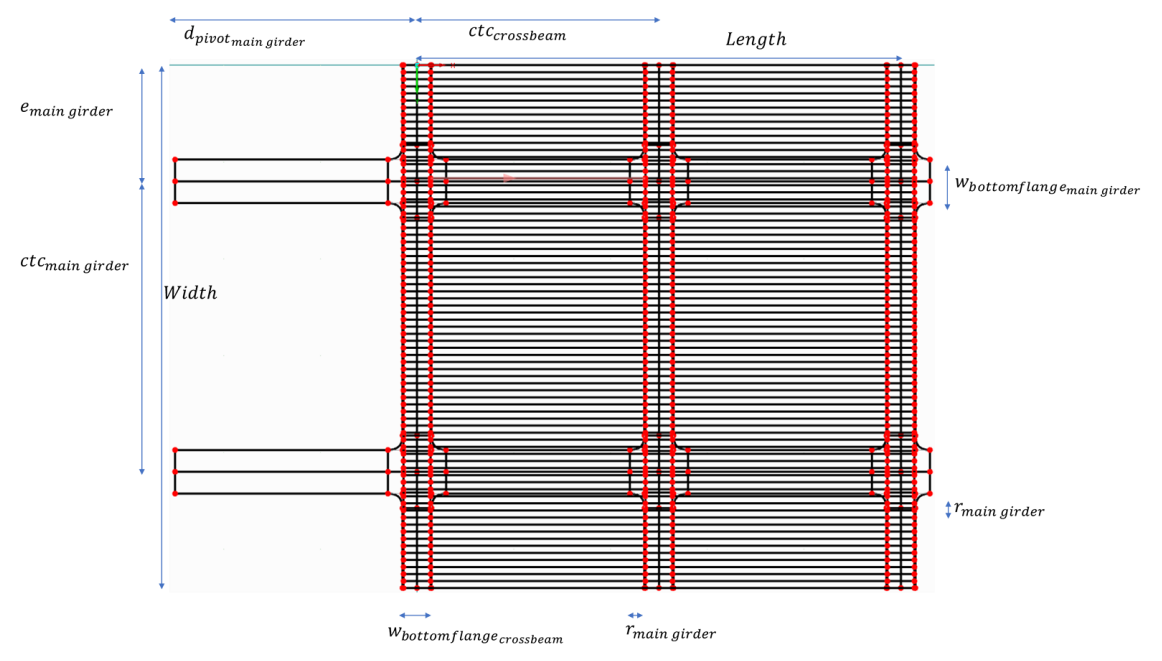
Input Parameters	In code	<u>value</u>	Unit	Input Parameters	In code	<u>value</u>	<u>Unit</u>
General				Main girders			
Span	br_l		m	Main girder height	br_h_mg		m
Width	br_w		m	Main girder connection radius	br_r_mg		m
Height	br_h		m	Main girder distance to pivot	br_piv_mg		m
Sandwich panel				Main girder top flange width	br_w_tfl_mg		m
Material properties	See "Sandwich deck"			Main girder top flange thickness	br_t_tfl_mg		m
Sandwich panel height (ctc)	br_h_sp		m	Main girder web thickness	br_t_web_mg		m
Sandwich panel top face sheet thickness	br_t_tfac_sp		m	Main girder bottom flange width	br_w_bfl_mg		m
Sandwich panel bot face sheet thickness	br_t_bfac_sp		m	Main girder bottom flange thickness	br_t_bfl_mg		m
Sandwich panel web thickness	br_t_web_sp		m	Number of main girders	br_n_mg		-
Sandwich panel centre-to-centre web	br_ctc_web_sp		m	Main girders centre-to-centre distance	br_ctc_mg		m
Nodes for sp-steel connection	nodes_link_e			Main girder distance to edge	br_e_mg		m
Crossbeams				Load cases			
Crossbeam height	br_h_cb		m	nr_lanes	Id_nr_lanes		m
Number of crossbeams	br_n_cb		-	Lanewidth	ld_w_lane		m
Crossbeam ctc distance first spans	br_ctc_cb2		m	Side parapet	ld_w_par		m
Crossbeam top flange width	br_w_tfl_cb		m				
Crossbeam top flange thickness	br_t_tfl_cb		m				
Crossbeam web thickness	br_t_web_cb		m				
Crossbeam bot flange width	br_w_bfl_cb		m				
Crossbeam bot flange thickness	br_t_bfl_cb		m				
Crossbeam centre-to-centre distance	br_ctc_cb		m				

Figure 4.9 Parameters hybrid bridge





Top view



Red dots are the nodes in the model Black lines are the plate edges for the main girders and crossbeams Grey lines are the plate edges for the sandwich panel.

Front view

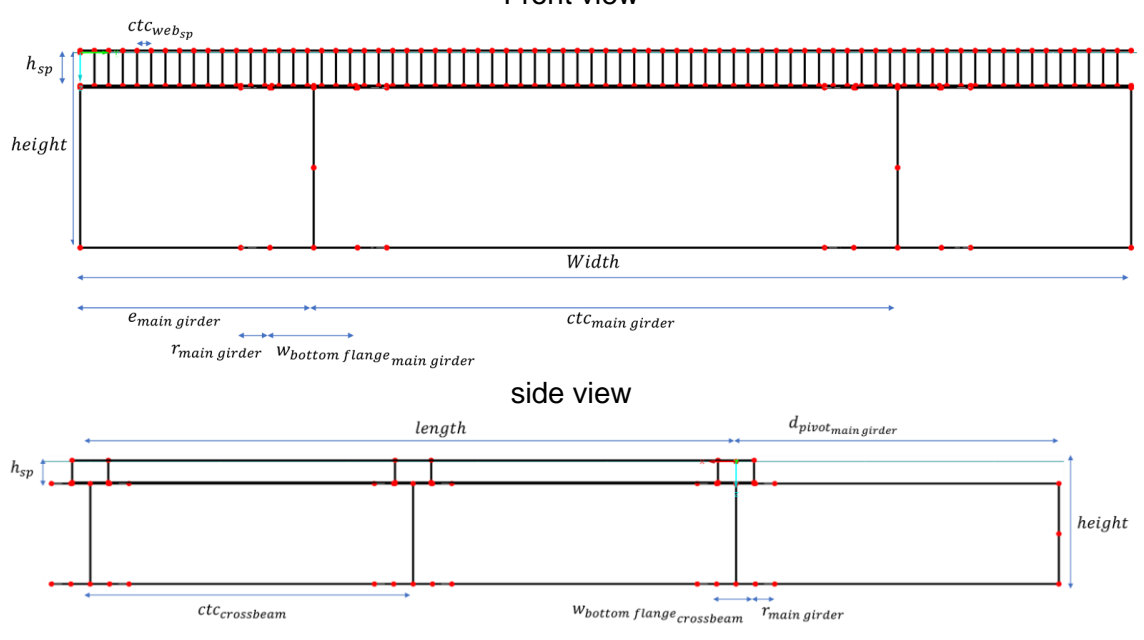


Figure 4.10 Cross-sections hybrid bridge





The following values can be used as starting values for the steel substructure, obtained from Table 4.1 for a height of 800 mm.

$$10 \ mm(t_{web_{cb}}) \le t_{web} \le 13 \ mm(t_{web_{mg}})$$

$$193 \ mm(w_{flange_{cb}}) \le w_{flange} \le 358 \ mm(w_{flange_{mg}})$$

$$12 \ mm \le t_{flange_{cb}} \le 20 \ mm$$

$$23 \ mm \le t_{flange_{mg}} \le 37 \ mm$$

The bridge, as a result of these parameters, has roughly the same dimensions as the Leeghwaterbrug (paragraph 2.2.3.4), although the Leeghwaterbrug has four main girders. The flange thickness of the main girders in the Leeghwaterbrug is higher (40 - 50 mm) as is the flange width (350 - 800 mm). The thickness of the web is also slightly thicker (16 mm). The dimensions of the crossbeams do coincide (200 - 300 mm).

The difference in values can be explained by two reasons. First off the Leeghwaterbrug does not consider shear interaction between the sandwich panel and the steel substructure. Therefore the steel is the only load bearing structure resulting in thicker and wider flanges to carry the loads. The second reason is that the steel height (820 mm) is very small compared to the span of the bridge. For a smaller span, when the ratio height/span is normal, these parameters will probably do fine but not for a large span. This means that dimensions must be increased to make sure deflection and stresses are low enough the obtain a unity check below 1.0.

Based on this information the values obtained from Table 4.1 will be increased to obtain the starting values for the hybrid model. The following dimensions will be used as start values (not as boundary values):

$$10 \ mm(t_{web_{cb}}) \le t_{web} \le 16 \ mm(t_{web_{mg}})$$

$$200 \ mm(w_{flange_{cb}}) \le w_{flange} \le 500 \ mm(w_{flange_{mg}})$$

$$12 \ mm \le t_{flange_{cb}} \le 20 \ mm$$

$$40 \ mm \le t_{flange_{mg}} \le 50 \ mm$$





4.2.2.2 Fatigue detail locations

Each of the details considered for the OSD bridge will be considered for the hybrid bridge except for the detail between the stiffener and the crossbeam. The details to consider are shown in Figure 4.11 with their detail category.

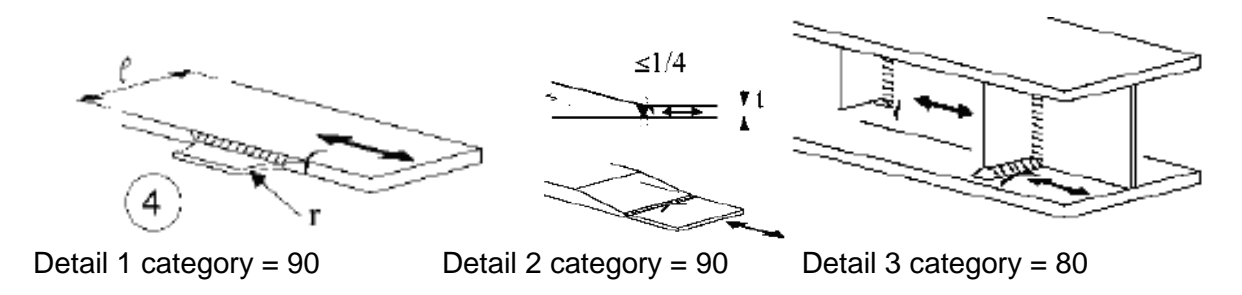


Figure 4.11 Details to consider for hybrid bridge

Fatigue damage in the FRP sandwich panel is unexpected but should be verified nonetheless. Fatigue damage often occurs in connections so verifying fatigue in a connection is most logical. In this model however, peak stresses are expected to occur around the bond between the sandwich panel and the steel structure due to the rigid plate elements needed for the connection. Therefore stress results in this location will not show any relevant results. A more detailed model should be created to verify the connection, but this is outside the scope of this thesis.





4.2.3 Sandwich panel properties

The properties of the sandwich panel will be discussed in this paragraph. Before looking at the dimensions of the panel it is necessary to know the lay-up of the laminates which will be explained first.

4.2.3.1 Material properties

The sandwich panel consists of face sheets and webs, both of them will have a separate layup and will be elaborated below. The laminate will be made out of glass fibres and polyester resin UD-plies, which is most used in sandwich panels.

The structural purpose of face sheets in a sandwich panel is transferring loads in longitudinal direction (0°) to the crossbeams. Having as many fibres as possible in the 0° direction is therefore desired. This results in an anisotropic layup, in this case the following layup has been chosen $[0^\circ(62.5\%) / +45^\circ (12.5\%) / 90^\circ(12.5\%) / -45^\circ(12.5\%)]$. This choice is a result of a recommendation stated in the CUR that in each main direction $[0^\circ / \pm 45^\circ / 90^\circ]$ a minimum fibre content of 12.5% must be present. This minimum will ensure that fatigue, creep and impact loads will not have the resin as a sole resisting member. The lay-up will be made symmetric to prevent torsion in the panel.

The structural purpose of the webs in a sandwich panel is to transfer loads between the top and bottom face sheet. The webs will therefore be focussed on the shear stresses between the face sheets. These stresses are best transferred by a quasi-isotropic laminate. Therefore a laminate layup of $[0^{\circ}(25\%) / +45^{\circ}(25\%) / 90^{\circ}(25\%) / -45^{\circ}(25\%)]$ will be used.

It turned out that it was not possible to use the laminate module in RFEM from excel, it can only be used within RFEM itself through manual input. Therefore a decision was made to model the sandwich panel as solid plates with average laminar properties. This should result in the same global deflections and stresses but makes it impossible to look into inter-laminar effects.

The FRP material properties will be determined by using laminate theory as explained in paragraph 2.2.1.4. The material properties depend on the lay-up of the UD-layers, this lay-up will not be considered in the optimization but will be fixed. The resulting laminate properties can be found in Table 4.2.





Table 4.2 Sandwich panel lay-up and parameters

UD-plie properties					
$V_f[-]$ 50%					
$E_x\left[\frac{N}{mm^2}\right]$ in longitudinal direction of span	371	75			
$E_y\left[\frac{N}{mm^2}\right]$ in transversal direction of span	113	352			
$G_{xy}\left[\frac{N}{mm^2}\right]$	35	13			
$v_{12}[-]$	0.2	29			
$\rho\left[\frac{kN}{m^3}\right]$	18492				
Material properties	Face sheets	Webs			
0°	62.5%	25%			
+45°	12.5%	25%			
90°	12.5%	25%			
-45°	12.5%	25%			
$E_x\left[\frac{N}{mm^2}\right]$ in longitudinal direction of span	28080	18973			
$E_y\left[rac{N}{mm^2} ight]$ in transversal direction of span	15560	18973			
$G_{xy}\left[\frac{N}{mm^2}\right]$	5333	7140			
$v_{12}[-]$	0.31	0.33			
$\rho \left[\frac{kN}{m^3} \right]$	18492	18492			

Using orthotropic material properties should not change any of the global analysis, only on local scale differences can be found. This has been verified in Annex G which compares simple models with a laminate lay-up or an orthotropic plate.

4.2.3.2 Dimensions determined by buckling

The sandwich panel will not be optimized in the model but will be fixed throughout each iteration. Therefore it is key to use a sandwich panel that will not collapse under loading. Due to the slender nature of the sandwich panel it is expected that failure will be caused by buckling behaviour. A buckling analysis will therefore be done to determine the dimensions of the face sheets and the webs.

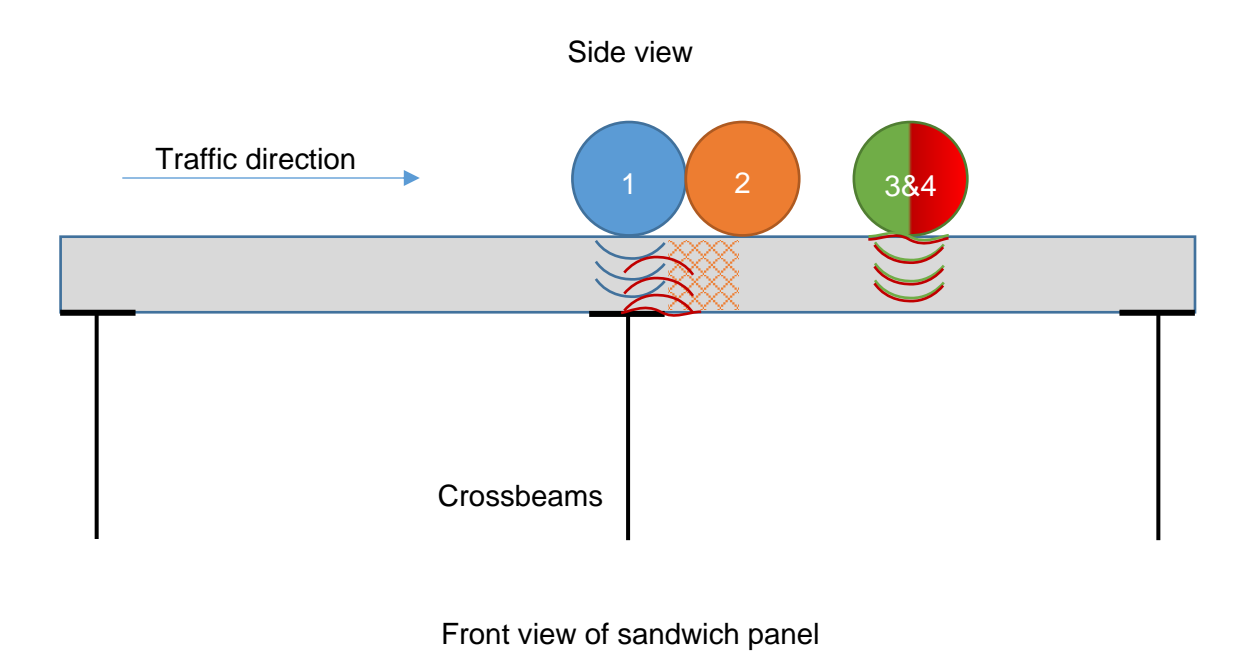
Buckling is a critical state of a structure at particular load levels at which the structure exhibits large displacements or collapse (Breuker, 2013). Buckling is most likely to occur in plates under compression but also shear buckling is possible.

There are three different wheel locations to be considered for the buckling analysis of a sandwich panel. The first location is with the wheel right on top of the main girder. The expected





buckling pattern is buckling in the webs of the sandwich panel. The second location is right beside the crossbeam. This location induces shear buckling failure in the webs. The third and final option is situated at mid span between the crossbeams. There are two failure modes to be expected for this location, namely buckling failure in the web and buckling failure in the top face sheet. The different locations and their possible failure modes have been drawn in Figure 4.12.



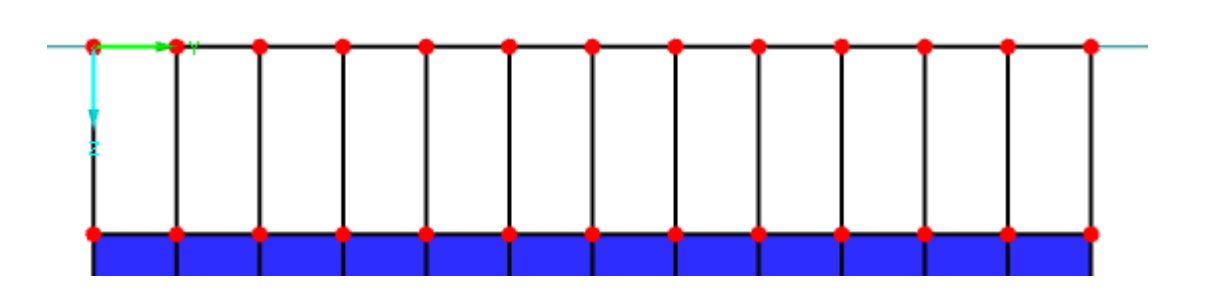


Figure 4.12 Buckling load locations and failure modes





73

Global deflections do not interact significantly with local buckling failures one and two. However for wheel location three global deflections will interact. This is mainly expected in the buckling of the top face sheet (4bi). A list of all the different failure modes are shown below with there locations shown Figure 4.12.

- 1. Buckling of the web due to wheel on top of the crossbeam (Blue)
- 2. Shear buckling due to wheel close to crossbeam (orange)
- 3. buckling due to wheel at midspan between crossbeams (green)
 - a. buckling of web
 - b. buckling of face sheet
- 4. Global buckling (red)
 - a. Buckling of web
 - i. At mid span
 - ii. At crossbeam
 - b. Buckling of face sheet
 - i. At mid span (top facing)
 - ii. At crossbeam (bottom facing)

The first four failure modes (1,2,3a and 3b) can be analysed in a local model. The other failure modes should be verified in a global model since the stresses due to global deflection will interact with the buckling modes. Both local and global analysis will be explained in this paragraph.





Local buckling analysis

For the local analysis the model as shown in Figure 4.12 will be used. The wheel load will be modelled as a square load of 200 by 200 mm with a distributed load of $1 N/mm^2$. This coincides with the distributed load of load model 1 and 2 as shown in equation (4.1).

$$LM1: \frac{Q}{A} = \frac{150.000}{400 * 400} = 0.9375 \frac{N}{mm^2}$$

$$LM2: \frac{Q}{A} = \frac{200.000}{350 * 600} = 0.9524 \frac{N}{mm^2}$$
(4.1)

The location of wheel one is directly above the crossbeam and for wheel three it is at mid span of the crossbeams. The location of wheel two is at a distance from the side of the crossbeam flange, this distance is the same as the height of the sandwich panel. The height of the crossbeams depends on the height of the sandwich panel, total of both must be 1 meter. The bottom flange has not been modelled. Instead the bottom of the crossbeam web has been clamped. As a result a slight increase in stiffness can be observed which will have a conservative result for wheels one and two. This might cause a slight underestimation for wheel three, however this wheel location will also be verified with a global model.

This table also shows the parameters of two reference projects (Souren, 2013, 2017). These bridges have a crossbeam span of 2310 mm and 1900 mm respectively. An optimization research on load bearing sandwich panels(Zarifis, 2018) show a safe design for a 4 meter span. The different parameters can be found in Table 4.3, Figure 4.13 shows the build up of the panel.

Five reference models have been created from this data, these models have a high thickness compared to the reference models which should ensure a safe estimate. The amount of web per meter of width is also given. The projects from Souren show a constant amount of web per meter but different distance and thickness. If this constant is determined somehow or is just a coincidence is unclear.





T. I. I. 40	D 11:			
l able 4.3	Buckling	sandwich	panei	parameters

case	height	thickness face sheets	thickness web	distance webs
number	(h) [mm]	$(t_{fac})[mm]$	(t_{web}) $[mm]$	$(d_{web})[mm]$
Leeghwater	180	12.22	5.64	$65.64 \left(86 \frac{mm \ web}{m \ span}\right)$
Nederweert	190	9.4	4.7	$54.7 \left(86 \frac{mm \ web}{m \ span}\right)$
Zarifis	215	15	5	$50\left(100\frac{mmweb}{mspan}\right)$
1	195	14	8	$80\left(100\frac{mmweb}{mspan}\right)$
2	210	14	8	$80\left(100\frac{mmweb}{mspan}\right)$
3	195	12	8	$80\left(100\frac{mmweb}{mspan}\right)$
4	195	14	7	$80\left(87.5\frac{mm\;web}{m\;span}\right)$
5	195	14	8	$85\left(94\frac{mm\ web}{m\ span}\right)$

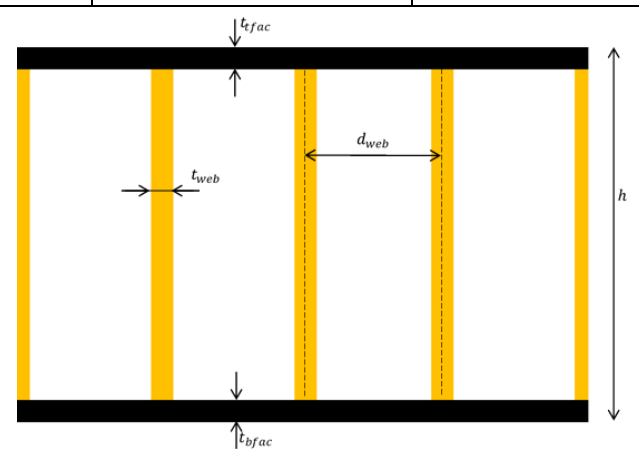


Figure 4.13 Buckling sandwich panel parameters

The results from the different analysis have been gathered in Table 4.4 with their respective buckling factors (λ) and maximum occurring stresses (σ or τ). Failure mode 3b didn't occur in any of the configurations (eigenmode number 15 as maximum) and is therefore omitted from the table.





Table 4.4 Buckling results					
case number	failure mode 1	failure mode 2	failure mode 3a		
1	$\lambda = 19.6$ $\sigma_{zz} = 14.5 \frac{N}{mm^2}$ $\sigma_{cr} = \lambda \sigma = 283.9 \frac{N}{mm^2}$	$\lambda = 23.0$ $\tau_{xz} = 8.0 \frac{N}{mm^2}$ $\tau_{cr} = \lambda \tau = 184.0 \frac{N}{mm^2}$	$\lambda = 28.3$ $\sigma_{zz} = 14.1 \frac{N}{mm^2}$ $\sigma_{cr} = \lambda \sigma = 345.4 \frac{N}{mm^2}$		
2	$\lambda = 14.9$ $\sigma_{zz} = 18.4 \frac{N}{mm^2}$ $\sigma_{cr} = \lambda \sigma = 273.2 \frac{N}{mm^2}$	$\lambda = 20.6$ $\tau_{xz} = 7.5 \frac{N}{mm^2}$ $\tau_{cr} = \lambda \tau = 154.1 \frac{N}{mm^2}$	$\lambda = 25.2$ $\sigma_{zz} = 13.7 \frac{N}{mm^2}$ $\sigma_{cr} = \lambda \sigma = 345.4 \frac{N}{mm^2}$		
3	$\lambda = 16.1$ $\sigma_{zz} = 18.9 \frac{N}{mm^2}$ $\sigma_{cr} = \lambda \sigma = 304.1 \frac{N}{mm^2}$	$\lambda = 22$ $\tau_{xz} = 8.2 \frac{N}{mm^2}$ $\tau_{cr} = \lambda \tau = 180.4 \frac{N}{mm^2}$	$\lambda = 27.1$ $\sigma_{zz} = 14.5 \frac{N}{mm^2}$ $\sigma_{cr} = \lambda \sigma = 392.2 \frac{N}{mm^2}$		
4	$\lambda = 11.3$ $\sigma_{zz} = 22 \frac{N}{mm^2}$ $\sigma_{cr} = \lambda \sigma = 247.7 \frac{N}{mm^2}$	$\lambda = 15.8$ $\tau_{xz} = 10.2 \frac{N}{mm^2}$ $\tau_{cr} = \lambda \tau = 161.0 \frac{N}{mm^2}$	$\lambda = 19.5$ $\sigma_{zz} = 15.7 \frac{N}{mm^2}$ $\sigma_{cr} = \lambda \sigma = 306.5 \frac{N}{mm^2}$		
5	$\lambda = 15.3$ $\sigma_{zz} = 17.5 \frac{N}{mm^2}$ $\sigma_{cr} = \lambda \sigma = 267.8 \frac{N}{mm^2}$	$\lambda = 21.3$ $\tau_{xz} = 9.5 \frac{N}{mm^2}$ $\tau_{cr} = \lambda \tau = 202.4 \frac{N}{mm^2}$	$\lambda = 26.2$ $\sigma_{zz} = 9.1 \frac{N}{mm^2}$ $\sigma_{cr} = \lambda \sigma = 238.2 \frac{N}{mm^2}$		

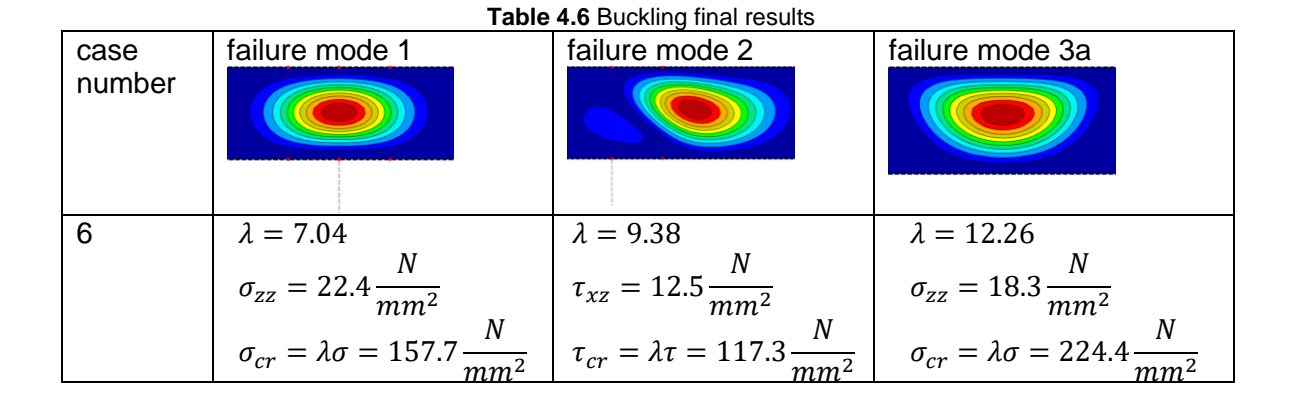
of these configurations show rather large buckling factors which means that the sandwich panels are overdimensioned. A sixth model has been created with slightly smaller dimensions as shown in Table 4.5. The results for the local analysis show smaller buckling factors as can be seen in Table 4.6.

Table 4.5 Buckling sandwich panel final parameters

case number	height (h) [mm]	thickness face sheets (t_{fac}) [mm]	thickness web (t_{web}) [mm]	$distance\ webs \ (d_{web})\ [mm]$
6	204	12	6	$80\left(75\frac{mm\ web}{m\ span}\right)$







Failure mode 3a still has the highest buckling factor, however this buckling mode will depend on the global deflections and stresses and not only on local effects.

Local buckling verification

An analytical approach can be used to verify the critical buckling stresses found for configuration 6. This can be done with the equations for buckling taken from the CUR as shown in Annex C.2.2.

Vertical buckling

Failure mode 1 and 3a are both buckling in the web in vertical direction. The critical buckling stress for these failure modes can be determined using equation (C.29) (Kassapoglou, 2013).

$$\sigma_{cr}(b=200) = 171.17 MPa \tag{4.2}$$

An analytical buckling stress of $171.17 \, MPa$ as shown in equation (4.2) can be found with a width of $b = 200 \, mm$, the same as the load width. This is slightly higher than the stress found for mode 1 but lower than for mode 3. This can be explained by a difference in effective width of the failure modes. This effective width is actually not equal to the width of the load but depends on the location of the load. Due to the stiffness of the crossbeam flange the effective width is slightly higher for failure mode 1 and the lower stiffness midspan causes the effective width to shrink. An increase or decrease in effective width of a few millimetres can have a significant effect due to the quadratic nature that it has in the equation as can be seen in equation (4.3) and (4.4).

$$\sigma_{cr}(b = 210) = 155.26 MPa$$

$$\sigma_{cr}(b = 180) = 211.32 MPa$$

$$(4.3)$$





Shear buckling

For shear buckling a different set of equations is needed. These have been taken from the CUR since these plate configurations coincide better with the problem at hand. The analytic results can be found in equation (4.5) and follow from Table C.10.

The critical shear buckling stress was 117.3 MPa which is close the analytical result for a clamped plate on two edges and free on the other two. In reality the plate under shear has two edges which could be modelled as stiff springs (top and bottom facing) and two edges which could be considered as rather weak springs (sides where the web continuous).

Global buckling analysis

Vertical buckling

The structure will be safe if the vertical stresses stay below the aforementioned vertical critical buckling stresses. Since global deformation will not effect the vertical stresses in the webs there is no need to read out results from the global model. The verification done in the local model is sufficient.

Horizontal buckling

Buckling due to horizontal stresses did not occur in the local model. Therefore analytical results will be used for the verification of the global model. The plate equations from the CUR can be used since aspect ratio $\frac{a}{b} > 5$. This must be done for both the face sheets as for the webs.

With the simplified plate configurations from the CUR (Table C.10) the critical buckling stresses stated in equation (4.6)* to (4.10)* can be expected for horizontal buckling of the webs.

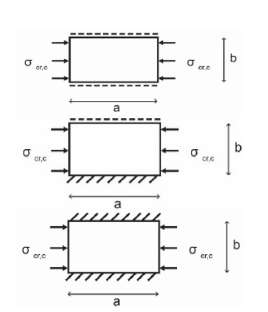


Table 4.7 FRP plate buckling under compression
$$\sigma_{cr,c} = 71.16 \ MPa \eqno(4.6)^*$$

$$\sigma_{cr,c} = 98.71 \, MPa \tag{4.7}^*$$

$$\sigma_{cr,c} = 128.37 \, MPa$$
 (4.8)*





$$\sigma_{cr,c} = 6.42 \, MPa$$

$$\sigma_{cr,c} = 23.82 \, MPa$$

$$K = 0.790 \, and \, v = 0.246$$

$$(4.9)^*$$

The third figure (equation (4.8)*) shows the most accurate horizontal critical buckling stress. The boundary conditions are fixed on either side of the web which is to be expected with the high stiffness of the face sheets.

Horizontal buckling of the face sheets can be determined by using the same formulas. The face sheet is under compression and the sides of the sheet can be assumed to be hinged in this case. There is some resistance from the webs and rest of the face sheet but assuming it to be fixed is an overestimation of the stiffness. Assuming a hinged edge is conservative. As a result a critical buckling stress of $7 * 10^6$ *GPa* can be expected as shown in equation (4.11).

$$\sigma_{cr,c} = 7 * 10^6 GPa \tag{4.11}$$

This critical buckling stress holds for both the top and bottom face sheets. This buckling stress is a more than a factor 1000 higher as for the webs. Therefore it is highly unlikely that the face sheets will buckle and this confirms the assumption of fixed boundary conditions for buckling of the webs.

In conclusion, the dimensions used for the sandwich panel are given in Table 4.8 with an explanation of the dimensions shown in Figure 4.14.





	_	O 1			
I ahle 4	×	Sandwich	nanel	dime	neinne
IUDICT		Carraviori	parior	unitio	11310113

Parameter		lue
Thickness top facing (t_{tfac})	12 mm	
Thickness bottom facing (t_{bfac})	12:	mm
Thickness webs (t_{web})	6 n	nm
Distance between webs (d_{web})	80 :	mm
Overall height of sandwich panel (h)	204 mm (192	ctc, 180 inner)
Weight of PVC per square meter $q_{pvc} = \rho_{pvc} * h * \frac{d_{web} - t_{web}}{d_{web}}$	$q_{pvc} = 80 * 0.18 * \left(\frac{80 - 6}{80}\right) = 13.32 \frac{kg}{m^2}$	
Material properties	Face sheets	Webs
$E_x\left[\frac{N}{mm^2}\right]$ in longitudinal direction of span	28080	18973
$E_y\left[rac{N}{mm^2} ight]$ in transversal direction of span	15560	18973
$G_{xy}\left[\frac{N}{mm^2}\right]$	5333	7140
v ₁₂ [–]	0.31	0.33
$ ho\left[rac{kN}{m^3} ight]$	18492	18492

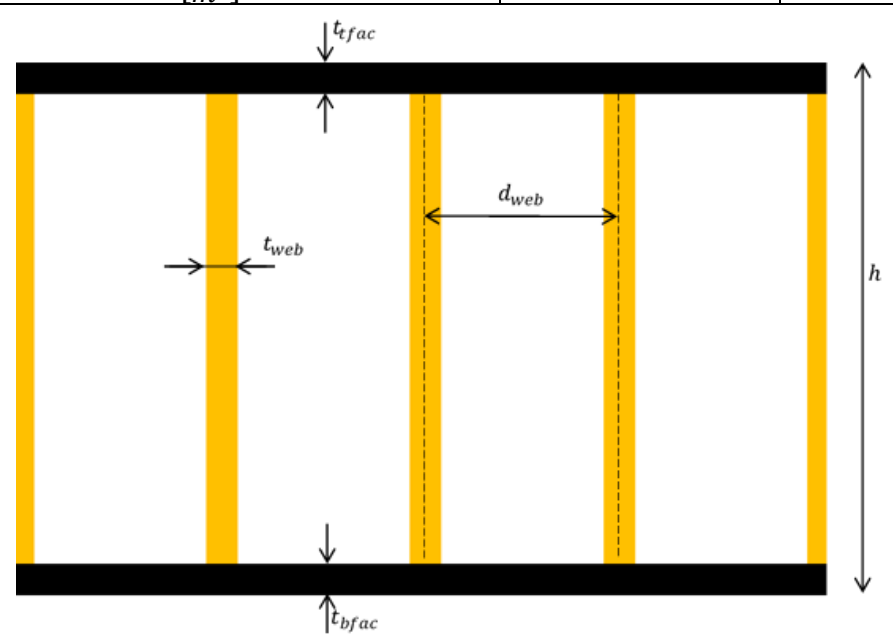


Figure 4.14 Sandwich panel cross-section





4.2.3.3 Fatigue verification

Fatigue damage in FRP has to be determined slightly different than for steel. The number of cycles that cause failure is determined by the maximum stress in a cycle instead of the stress range. The formula that determines this number of cycles (N) is stated in equation (4.12) and follows from equation (C.35).

```
N = 10^{\left[k*Log\left(\frac{\gamma_{Mf}*\gamma_{M}*\sigma_{max}}{\eta_{c}*B}\right)\right]} \tag{4.12} where k = -9 (CUR 96, 2017) (tabel 6.7) \gamma_{Mf} = 1.0 (CUR 96, 2017) (ch 2.4.4.3) \gamma_{M} = \gamma_{M1}*\gamma_{M2} = 1.35*1.2 = 1.62 (CUR 96, 2017) (tabel 2.1 and 2.2) \eta_{C} = \eta_{ct}*\eta_{cm} = 0.9*0.9 = 0.81 (CUR 96, 2017) (ch 2.4.5.2 and 2.4.5.3) B = 700*\frac{V_{f}}{0.55} = 636.4 (CUR 96, 2017) (tabel 6.7) \sigma_{max} = maximum\ occurring\ stress
```

The damage is determined with Miners rule (equation (C.36)) just as for steel.

The maximum occurring stress should be obtained for each different vehicle that transits the bridge. The CUR states that load model 4B should be used for FRP, LM4B is given in Table C.9 in paragraph C.1.5. A local model has been used for this analysis which is expected to be conservative compared to a full bridge span model. This is due to the fact that the maximum stress is needed. In the full bridge span the entire sandwich panel is in the compressive zone which will cause a decrease in stresses due to global deflections.

The sandwich panel dimensions determined by the buckling analysis will be used to verify the fatigue damage. This will be done using a local model with a width of 0.96 meter and a length of 10.6 meters (four crossbeam spans). The side edges have symmetry conditions to a complete axle load. The bottom of the crossbeams are supported in vertical direction only. A side view of the model is given in Figure 4.15.

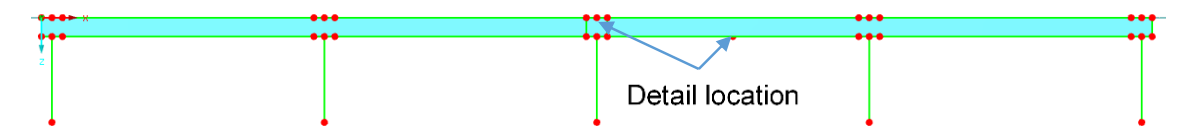


Figure 4.15 Fatigue model sandwich panel side view

A set of three wheels will be modelled that transit across the bridge. With a step size of 0.1 meters an influence line will be created for each of these wheels. These lines will be combined and factorized to form the load spectrum for the necessary vehicles as part of the post processing. A more extensive explanation on this process will be done in paragraph 5.1.4.





Model design

Fatigue damage will be determined in four locations, at mid span between crossbeams in the bottom facing and web and on top of the crossbeam in the top facing and web. Results are shown in Table 4.9. The biggest damage occurs in the bottom facing at midspan of the crossbeams. For each of the details vehicle three resulted in the most damage and caused approximately 50% of the total damage.

Table 4.9 FRP fatigue results

Detail	Total damage
Web at crossbeam	0,000007
Web at midspan	0,000019
Top facing at crossbeam	0,000072
Bottom facing at midspan	0,004830

These damage results are far below the maximum allowable value of 1.0 showing that FRP is not prone to fail due to fatigue. For this local analysis it shows that the sandwich panel is safe. Due to the rigid links it is irrelevant to do this analysis for the global model of the hybrid bridge. A more detailed list of the damages per vehicle can be found in Annex D.





4.3 Model verification

The models explained in paragraph 4.2.1 and 4.2.2 have been created in RFEM using excel vba. Load model 4 has been used for verification purposes of these models. In the next subparagraphs this verification will be shown for both the OSD and the hybrid model.

Verifications will be done for vertical displacement, stress-strain relations and the location of the neutral axis. This will be done with the help of classical beam theory (Hartsuijker, 2001).

4.3.1 OSD model verification

A model verification has been conducted using load model 4, a dead-load of $5 \, kN/m$ on the complete deck without self-weight. The dimensions that have been used for this verification can be found in Figure 4.16.

Input Parameters	In code	value	Unit
General			
Span	br_l	15	m
Width	br_w	12,0	m
Height	br_h	1,0	m
Deck			
Deck thickness	br_t_deck	0,020	m
Stiffeners			
Number of stiffeners	br_n_stif	20	-
Stiffener centre-to-centre cantilever	br_ctc_stif_can1	0,600	m
Stiffener centre-to-centre distance	br_ctc_stif	0,600	m
Stiffener centre-to-centre cantilever	br_ctc_stif_can2	0,600	m
Stiffener top width	br_w_tstif	0,300	m
Stiffener bottom width	br_w_bstif	0,105	m
Stiffener height	br_h_stif	0,325	m
Stiffener thickness	br_t_stif	0,008	m
Crossbeams			
Crossbeam height	br_h_cb	1,0	m
Number of crossbeams	br_n_cb	7	-
Crossbeam ctc distance first spans	br_ctc_cb2	2,300	m
Crossbeam web thickness	br_t_web_cb	0,012	m
Crossbeam bot flange width	br_w_bfl_cb	0,300	m
Crossbeam bot flange thickness	br_t_bfl_cb	0,200	m
Crossbeam centre-to-centre distance	br_ctc_cb	2,600	m
Main girders			
Main girder height	br_h_mg	1,0	m
Main girder connection radius	br_r_mg	0,150	m
Main girder distance to pivot	br_piv_mg	2,500	m
Main girder web thickness	br_t_web_mg	0,020	m
Main girder bottom flange width	br_w_bfl_mg	0,450	m
Main girder bottom flange thickness	br_t_bfl_mg	0,045	m
Number of main girders	br_n_mg	2	-
Main girders centre-to-centre distance	br_ctc_mg	8,400	m
Main girder distance to edge	br_e_mg	1,800	m
Load cases			
Lanewidth	ld_w_lane	3	m
Side parapet (zijberm)	ld_w_par	1,4	m
nr_lanes	ld_nr_lanes	3	-

Figure 4.16 Parameters OSD model verification





The side view shown in Figure 4.17 shows the imposed load and the location of the supports. The supports have been moved inwards from the pivot point to make sure the cross section is constant along the complete span. This is shown by the blue arrow, due to this moved support the cross section is constant and is shown in Figure 4.17.



Figure 4.17 side view OSD model verification

4.3.1.1 Vertical displacement

This test can be considered as a simply supported beam with a distributed load using beam theory. The vertical displacement u_z can be calculated using equation (4.13) according to classical beam theory.

 $u_{z} = \frac{5}{384} * \frac{q * l^{4}}{E * I}$ $u_{z} = vertical \ displacement \ [mm]$ $q = distributed \ load \ \left[\frac{N}{mm}\right]$ $l = length \ of \ span \ [mm]$ $E = stiffness \ \left[\frac{N}{mm^{2}}\right]$ $I = moment \ of \ inertia \ [mm^{4}]$

The E-modulus of steel is $210.000 \ N/mm^2$ and the span of the bridge is $15000 \ mm$. The dead load of $5 \ kN/m^2$ must be multiplied by the width of the model to form the distributed load q. This results in a distributed load of $60 \ N/mm$. The stiffeners will be left out of the equation to simplify the calculation of the moment of inertia. Figure 4.18 shows the simplified cross-section for the moment of inertia which is calculated by using equation (4.14).



Figure 4.18 cross-section OSD model verification

$$I = \sum_{1} \frac{1}{12} * bh^{3} + A * a^{2}$$

$$b = base or width of section$$
(4.14)

where





$$A = area \ of \ section$$

 $a = distance \ to \ neutral \ axis$

To determine the neutral axis equation (4.15) can be used. In this equation the distance d_n is the distance to the normal force centre from the top of the cross-section.

$$d_n = \frac{\sum A_i * z_i}{\sum A_i} = 141 \, mm \tag{4.15}^*$$

* An elaboration of the equation can be found in Annex A.

As a result the moment of inertia can be determined as shown in equation (4.16).

$$I = \sum_{1} \frac{1}{12} * bh^3 + A * a^2 = 3.11 * 10^{10} mm^4$$
 (4.16)*

Following equation (4.13) a displacement of approximately 6 mm can be expected as is shown in equation (4.17).

$$u_z = \frac{5}{384} * \frac{q * l^4}{E * I} = \frac{5}{384} * \frac{60 * 15000^4}{210000 * 3.11 * 10^{10}} = 6.06 \, mm$$
 (4.17)

Figure 4.19 shows the results from RFEM showing a maximum deformation of 7 mm, which is a difference of 15%. However, this deformation is also due to deformation of the deck plate which is not included in beam theory. Looking at the second figure, the deformation of the main girder, a deformation of 6.6 mm can be seen.





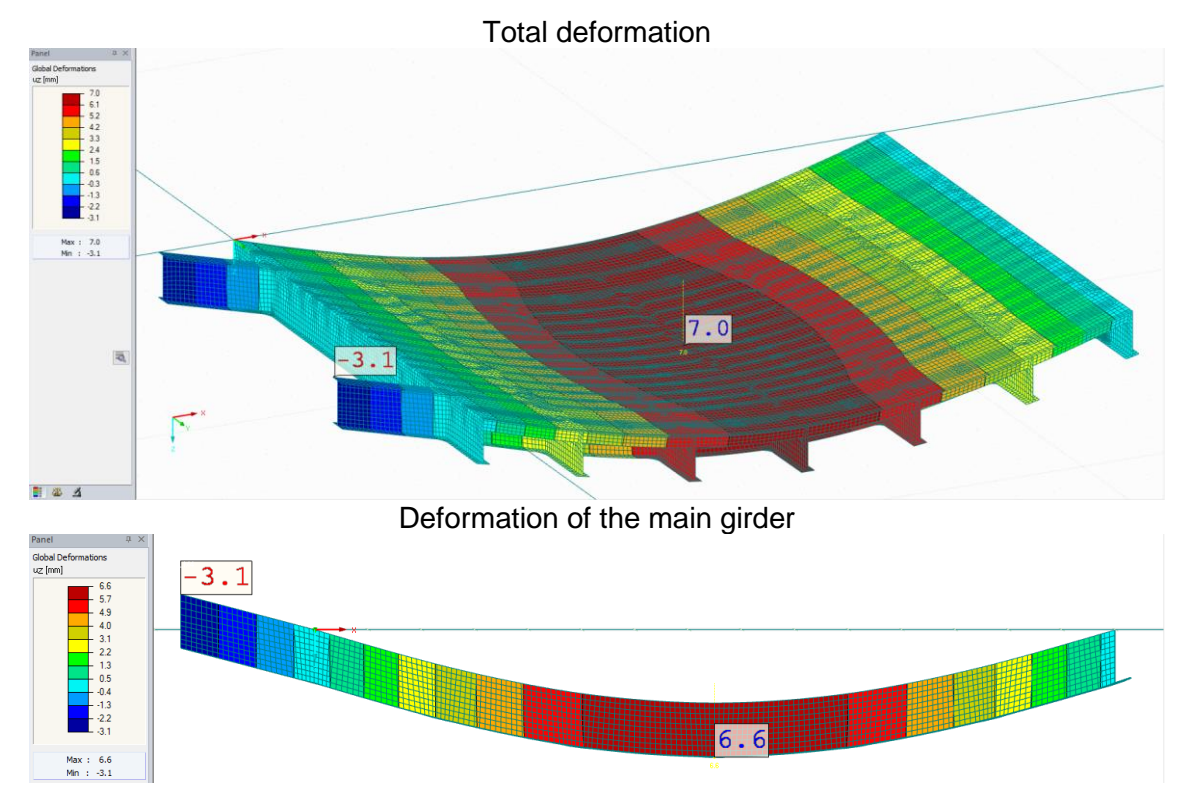


Figure 4.19 Vertical deformation OSD model verification

This is still not exactly the same as calculated with beam theory. The difference can be rectified by the fact that classical beam theory is used for cross sections where stresses at a certain height are the same everywhere in the cross-section. This is not the case for a large plate since stresses on the same height will differ across the width of the model.

This difference in stresses along the width of the model becomes clear in Figure 4.20 which shows the stresses in X-direction of the deck plate. Due to the stiffness of the main girders compression stresses are higher around the main girder then in mid span. As an effect the mid span of the deck contributes less in resisting deflection.

This effect is called effective width which essentially means that only a certain width of the deck contributes in the resistance. In this case approximately 60% of the deck is fully effective which can be verified by changing the width from 12 meters to 7.2 meters in equations (4.13) to (4.17).





87

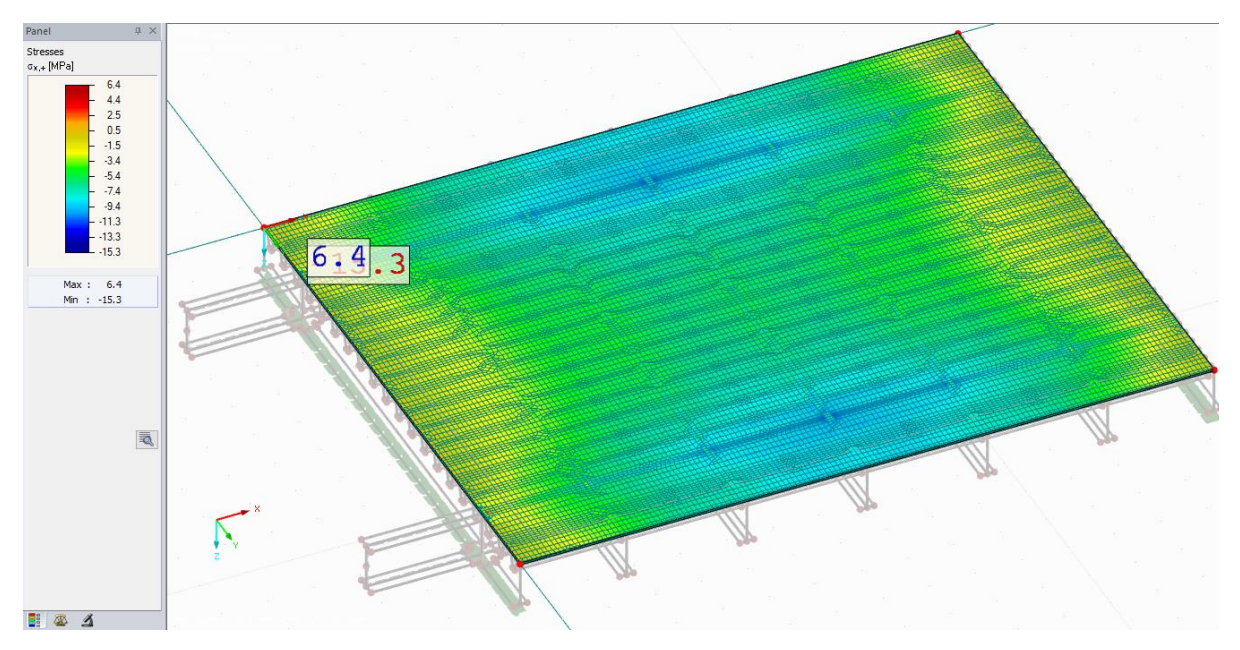


Figure 4.20 Sigma_x deck plate OSD model verification





4.3.1.2 Stress-strain relation

A verification will be done on the stress-strain relations in both models. This will be done in the main girder at mid span where the highest deformation occurs.

For the OSD bridge a linear strain curve is expected over the height. Since the main girder web has a constant dimension along the height the stress curve should be linear as well. Plotting the stresses against the strains should result in a linear relation which coincides with the E-modulus of the material.

Figure 4.21 shows the results from RFEM in the web of one of the main girders. The maximum strains occur close to mid span as expected and the strain pattern seems to be linear. Figure 4.22 shows the strains that have been retrieved from the model at midspan. This shows a linear curve of the strains over the height as expected.

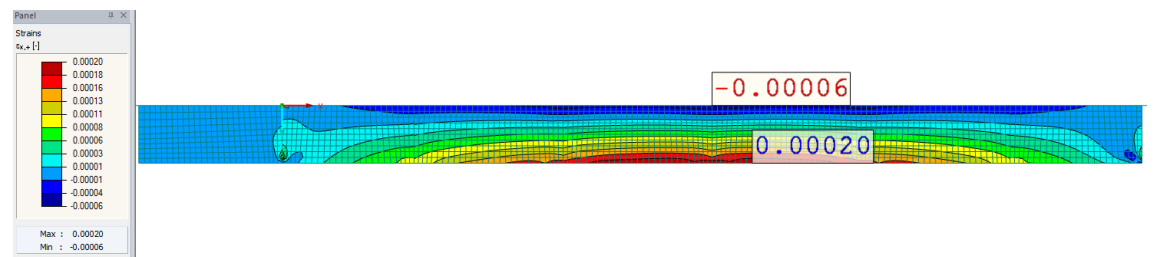


Figure 4.21 Strains OSD model verification

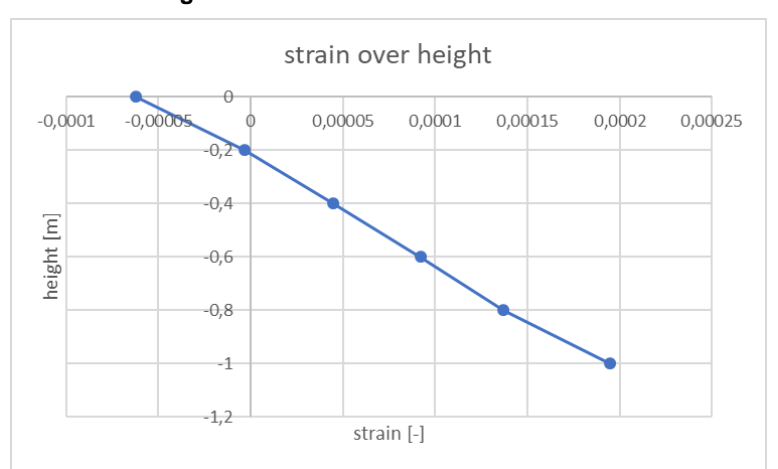


Figure 4.22 Strain diagram OSD model verification

Figure 4.23 and Figure 4.24 show the stresses at the same location, resulting in the expected linear diagram over the height of the web.





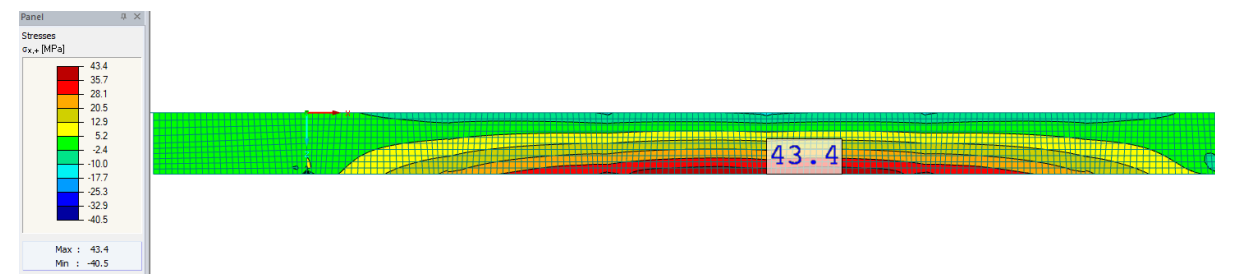


Figure 4.23 Stresses OSD model verification

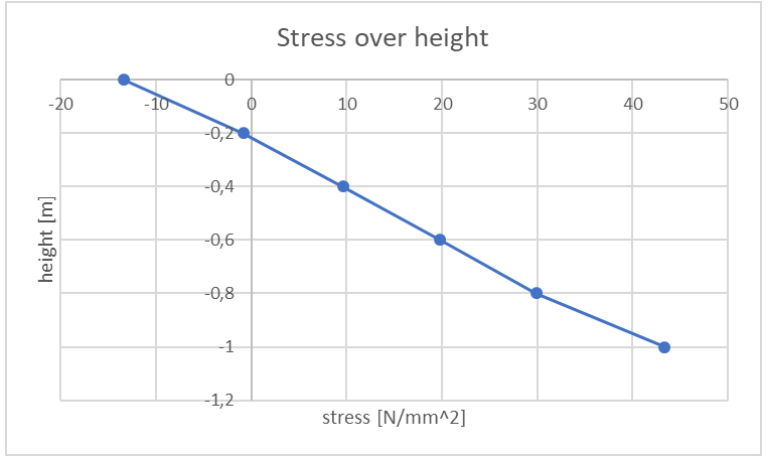


Figure 4.24 stress diagram OSD model verification

Plotting stress against strain results in Figure 4.25. The orange line represents the E-modulus of the material which almost coincides with the obtained results as is to be expected.

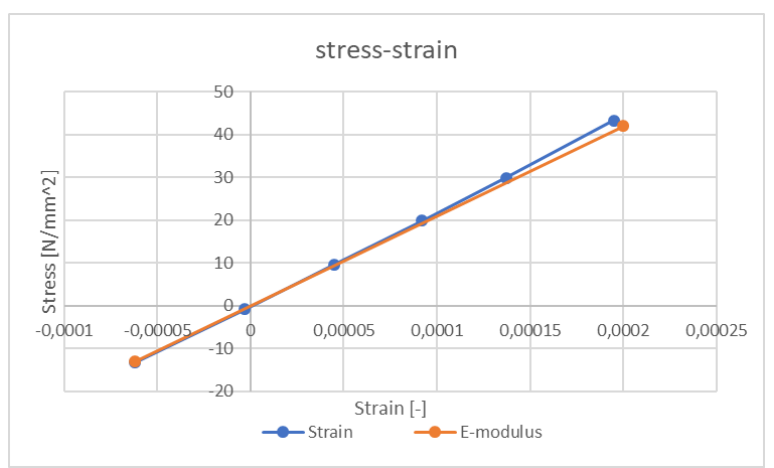


Figure 4.25 stress-strain diagram OSD model verification





4.3.1.3 Neutral axis

At the height where there is zero strain (and thus zero stress) lies the neutral axis. In load conditions where there is no external normal force this neutral axis should coincide with the normal force centre determined in paragraph 4.3.1. The height at which this neutral axis lies can be determined through linear interpolation using the data points stated in Figure 4.22.

Table 4.10 Stress and strain data OSD model verification

Stress	Strain	Z
43,3675	0,000195	-1
29,88436	0,000137	-0,8
19,83073	0,000092	-0,6
9,650939	0,000045	-0,4
-0,80262	-0,000003	-0,2
-13,3214	-0,000062	0

The linear interpolation is shown in equation (4.18) and shows that the neutral axis is situated at 213 mm from the top of the deck.

where
$$z = z_2 - \frac{s_2}{\alpha} = -0.2125m$$

$$\alpha = \frac{s_2 - s_1}{z_2 - z_1}$$
(4.18)*

The normal force centre from paragraph 4.3.1 has been determined analytically to be at 141 mm from the top of the deck (equation (4.15)*). For homogeneous models the normal force centre should coincides with the centre of gravity of the model. The difference with the neutral axis is to big to be caused by minor calculation or round off errors. A cause of this difference could be that the stiffeners and crossbeams have not been taken into account for the analytical results.

Including the stiffeners and the crossbeams the centre of gravity can be found at a distance of 250 mm from the top as shown in equation (4.19). This still does not coincide with the results from RFEM.

$$z_g = \frac{\sum V_i * a_i}{\sum V_i} = 0.25 m \tag{4.19}^*$$

The crossbeams do not contribute directly in the stiffness in X-direction, however the stiffeners do. Their stiffness is transferred to the main girders through the crossbeams, therefore a change in neutral axis can be expected around the crossbeams. Just as for the vertical displacement this will not be a full contribution due to the effective width principal.





If there is zero contribution of the stiffeners the neutral axis is expected at 0.141 meters. If there is full contribution of the stiffeners the neutral axis is expected to be at 0.25 meters. According to RFEM the neutral axis is at 0.2125 meters, which means that approximately 80% of the stiffener contributes to the stiffness.

Another effect can be seen in the strain distribution shown in Figure 4.26. The stiffeners contribute more around the crossbeams due to a better transfer of loads. In between the crossbeams the contribution is less, causing the neutral axis to move up slightly.

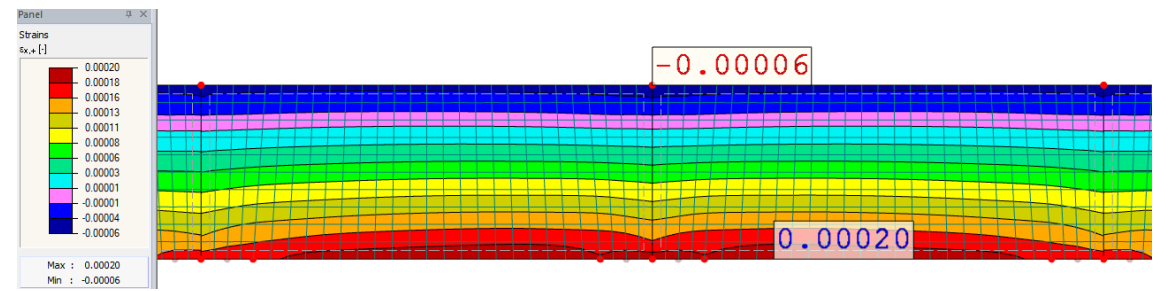


Figure 4.26 Strain distribution OSD model verification





4.3.2 Hybrid model verification

The same model verification as for the OSD model can be done for the hybrid model. The dimensions that have been used for this verification can be found in Figure 4.27.

Input Parameters	In code	value	Unit
General			
Span	br_l	15	m
Width	br_w	12,0	m
Height	br_h	1,0	m
Sandwich panel			
Material properties			
Sandwich panel height	br_h_sp	0,180	m
Sandwich panel top face sheet thickness	br_t_tfac_sp	0,012	m
Sandwich panel bot face sheet thickness	br_t_bfac_sp	0,012	m
Sandwich panel web thickness	br_t_web_sp	0,006	m
Sandwich panel centre-to-centre web	br_ctc_web_sp	0,073	m
Crossbeams			
Crossbeam height	br_h_cb	0,820	m
Number of crossbeams	br_n_cb	7	-
Crossbeam ctc distance first spans	br_ctc_cb2	2,300	m
Crossbeam centre-to-centre distance	br_ctc_cb	2,600	m
Crossbeam web thickness	br_t_web_cb	0,012	m
Crossbeam bot flange width	br_w_bfl_cb	0,300	m
Crossbeam bot flange thickness	br_t_bfl_cb	0,020	m
Crossbeam top flange width	br_w_tfl_cb	0,300	m
Crossbeam top flange thickness	br_t_tfl_cb	0,020	m
Main girders			
Main girder height	br_h_mg	0,820	m
Main girder connection radius	br_r_mg	0,150	m
Main girder distance to pivot	br_piv_mg	2,500	m
Main girder web thickness	br_t_web_mg	0,015	m
Main girder bottom flange width	br_w_bfl_mg	0,450	m
Main girder bottom flange thickness	br_t_bfl_mg	0,040	m
Main girder top flange width	br_w_tfl_mg	0,450	m
Main girder top flange thickness	br_t_tfl_mg	0,040	m
Number of main girders	br_n_mg	2	-
Main girders centre-to-centre distance	br_ctc_mg	8,400	m
Main girder distance to edge	br_e_mg	1,800	m

Figure 4.27 Parameters Hybrid model verification





93

4.3.2.1 Vertical displacement

In this hybrid model the stiffness modulus and moment of inertia have to be combined since it is a hybrid construction. Equation (4.20) has to be used to determine the location of the normal force centre.

$$d_n = \frac{\sum E_i S_i}{\sum E_i A_i} = 430 \ mm$$

$$E = E - modulus[N/mm^2]$$

$$S = first \ moment \ of \ inertia \ (A*z) \ [mm^3]$$

$$A = area \ [mm^2]$$
 (4.20)*

Using the top of the cross-section as reference and with the help of Figure 4.28 it can be found that the normal force centre is located at 430 mm from the deck as shown in equation (4.20)* with the E-modulus of FRP being 18.9 GPa.

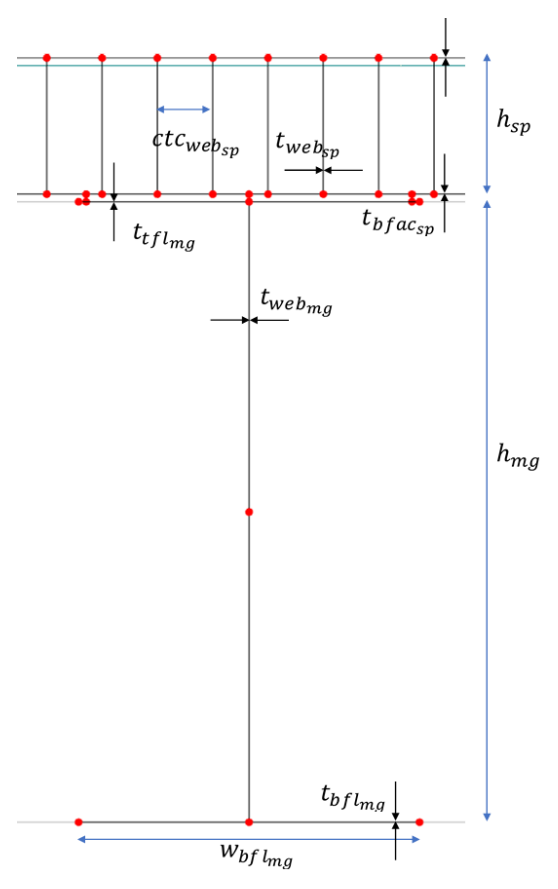


Figure 4.28 cross-section hybrid model verification





The cross sectional stiffness EI must be determined in the same manor as shown in equation (4.21).

$$EI = \sum_{i} E_{i} * I_{i} = 4.42 * 10^{15} \ kNm^{2}$$

$$I = stiffness \ modulus$$

$$E = E - modulus$$
 (4.21)*

Using the result of equation (4.21) a displacement of approximately 9 mm can be expected as is shown in equation (4.22) which calculates the deflection for a simply supported beam using beam theory.

$$u_z = \frac{5}{384} * \frac{q * l^4}{E * I} = \frac{5}{384} * \frac{60 * 15000^4}{4.42 * 10^{15}} = 8.94 \, mm$$
 (4.22)

Figure 4.29 shows the deformation determined by RFEM. As with the OSD model the deformations are slightly larger than determined with the beam theory. The difference is 15% with beam theory, which can be explained by the effective width principal just as for the OSD bridge.

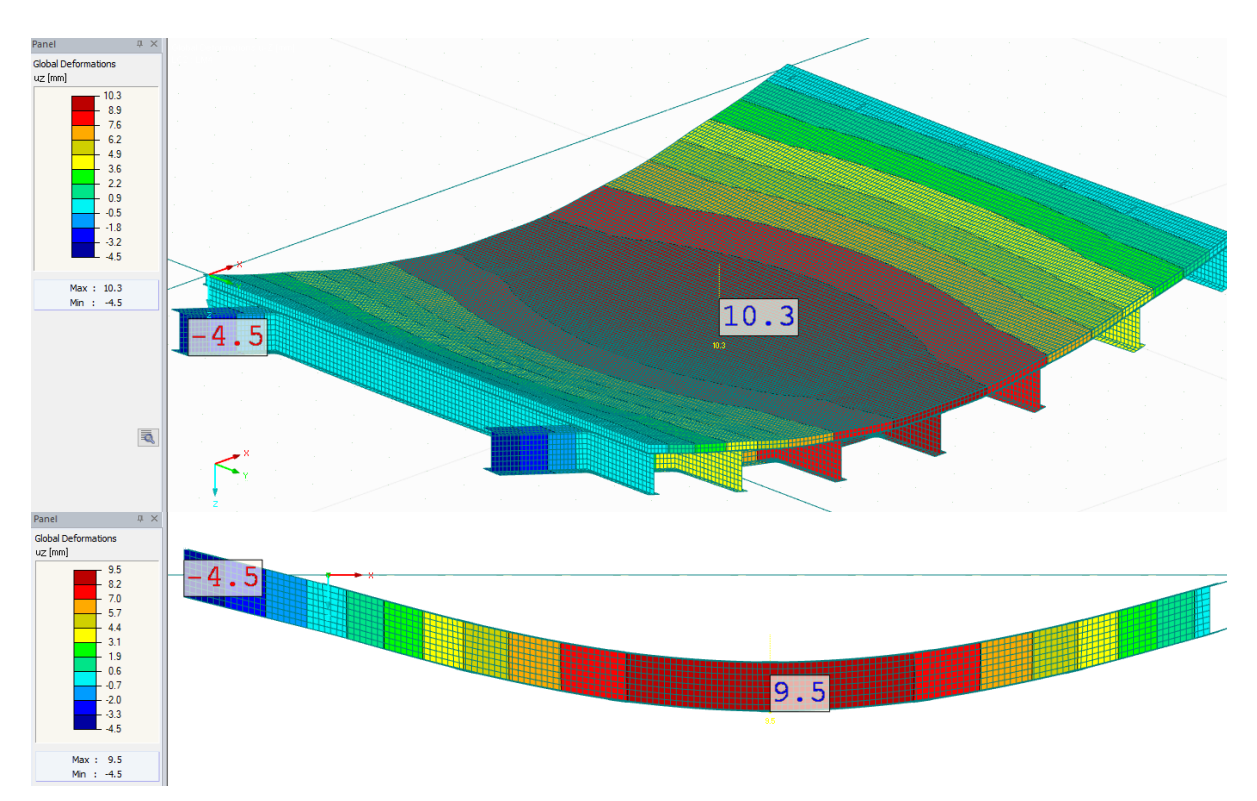


Figure 4.29 Vertical deformation hybrid model verification





4.3.2.2 Stress strain relation

For the hybrid bridge a linear strain curve is expected over the height. Due to the different E-moduli a clear kink should be visible at the Steel-FRP interface in the stress curve. Plotting the stresses against the strains should result in another bi-linear relation which coincides with the E-modulus of the material of FRP at one end and with the E-modulus of steel at the other.

Figure 4.30 shows the results from RFEM in the web of one of the main girders. The maximum strains occur close to mid span as expected and the strain pattern seems to be linear. Figure 4.31 shows the strains that have been retrieved from the model at midspan. This line is close to linear but has some distinct deviations. These are observed at the interface between the steel and FRP and are caused by the rigid links in the model. However, looking at Figure 4.30 it is clear that these effects are only local and will not effect the whole model.

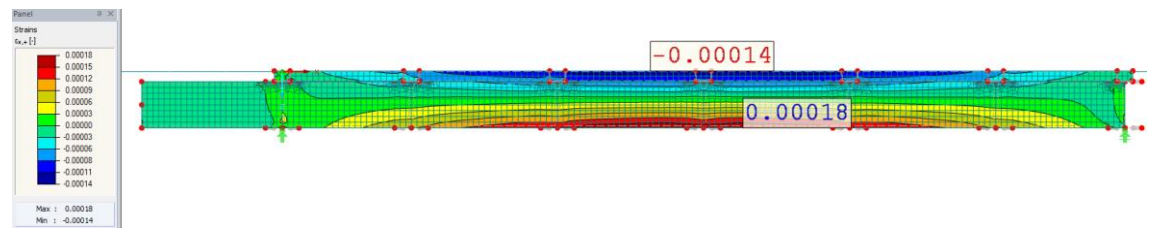


Figure 4.30 Strains hybrid model verification

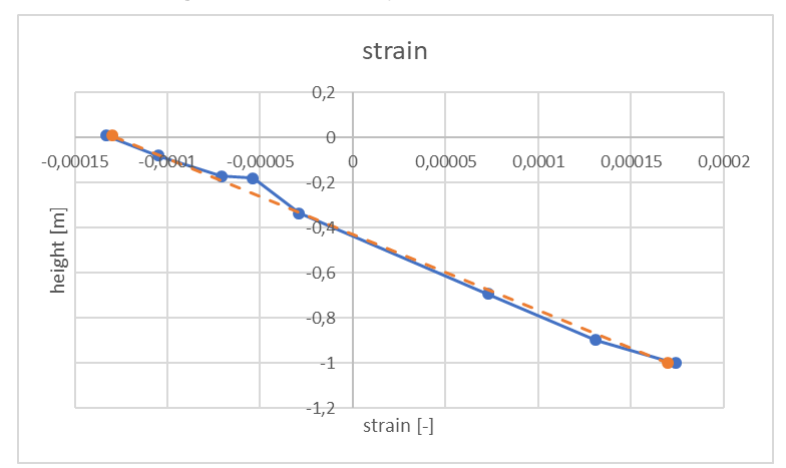


Figure 4.31 Strain diagram hybrid model verification

Figure 4.32 and Figure 4.33 show the stresses at the same location, resulting in the expected bi-linear diagram over the height of the web with a "jump" at the steel-FRP interface. Both "linear" parts of the diagram should coincide with the E-modulus of the material.

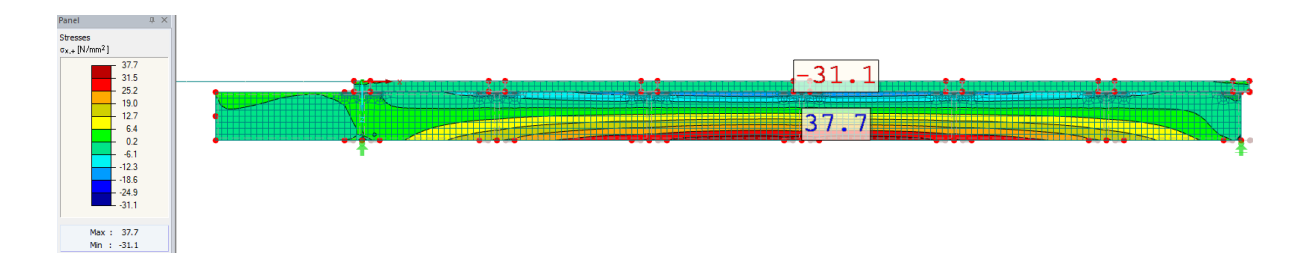






Figure 4.32 Stresses hybrid model verification

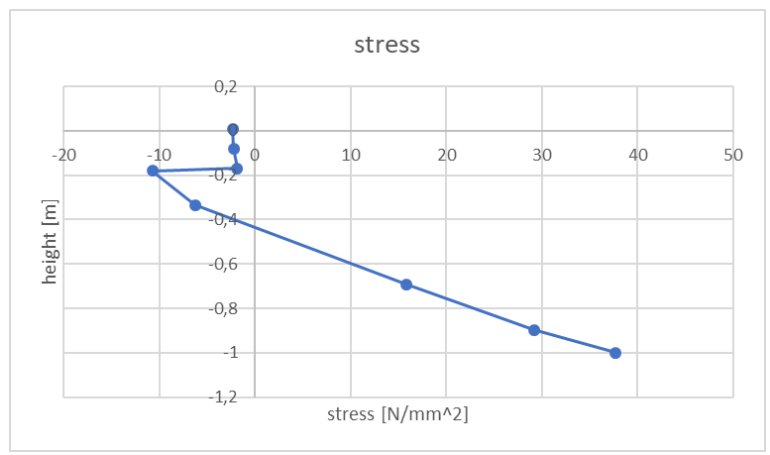


Figure 4.33 stress diagram hybrid model verification

Plotting stress against strain results in Figure 4.34. The orange line represents the E-modulus of steel and the grey line of FRP. As expected these lines almost coincide with the actual stress-strain curve.

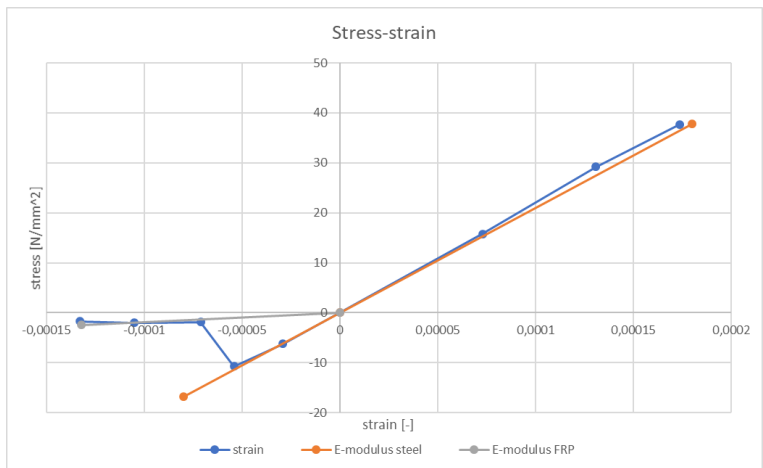


Figure 4.34 stress-strain diagram hybrid model verification





4.3.2.3 Neutral axis

Using equation (4.18) for the hybrid model with the data shown in Table 4.11 results in a neutral axis at 436 mm from the top of the deck.

Table 4.11 Stress and strain data hybrid model verification

Stress	strain	Z
37,73545	0,000174	-1
29,19437	0,000131	-0,8975
15,80234	0,000073	-0,6925
-6,23933	-0,000029	-0,33375
-10,7126	-0,000054	-0,18
-1,84763	-0,000071	-0,17
-2,23259	-0,000118	-0,08
-2,30093	-0,000153	0,01

In paragraph 4.3.2 a normal force location was found at 440 mm from the top. This value lies very close to the actual location of the neutral line. This would mean that the effective width of the sandwich panel is better than for the stiffeners in the OSD bridge.

The effect of the contributing width of the sandwich panel can also be seen in the hybrid model. However instead of the neutral axis going down around the crossbeams it moves upwards. This is due to the stiffening material, the sandwich deck, being above the neutral axis, whereas the stiffening material in the OSD bridge was below the neutral axis.

Figure 4.35 shows a close-up of the strain distribution with the neutral axis in the centre of the pink line. This changes very slightly from crossbeams to midspan of crossbeams which is to be expected for a stiffening material (sandwich panel) that has a better more constant effective width.

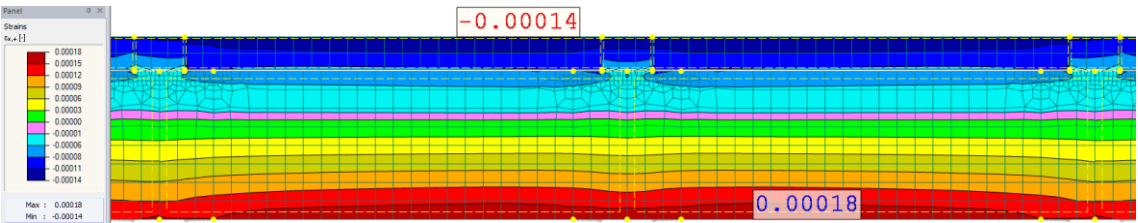


Figure 4.35 Strain distribution hybrid model verification





4.3.2.4 Effect of rigid links

The results shown in the verifications above show some disturbances around the connection between FRP and steel, mainly at the crossbeams. This is due to the rigid links, however the figures show that the disturbances are local and have no significant effects on a global scale. The effects can best be seen in Figure 4.33 and Figure 4.35.

Local effects in the connection between steel and FRP but also in the steel and FRP around the connection cannot be investigated with this model. A detailed model with 3D elements should be made if local effects are investigated.





4.4 Conclusion

Two different models have been designed in paragraph 4.2, one for the OSD bridge and one for the hybrid bridge. All the parameters necessary for these models have been elaborated in this paragraph. The parameters for the sandwich panel have been determined using a bucking analysis.

For the OSD model four fatigue detail locations have been chosen. One of these is a local detail situated in the stiffener to crossbeam connection. The other three details are situated around the crossbeam to main girder connection in the bottom flange. For the hybrid model only the three details in the crossbeam to main girder connection have been used for the fatigue analysis.

The model verification is done in paragraph 4.3 to validate the results calculated by RFEM. The verification is done for both the OSD model and the hybrid model and verified the vertical displacement, stress-strain relationship and the location of the neutral axis. This verification has been done with load model 4, a uniformly distributed load of $5 \, kN/m^2$ on the complete deck which had a span of 15 meters and a width of 12.

The vertical displacements that were obtained from RFEM have been verified with classical beam theory. A deviation of 15% has been found for both the OSD model and the hybrid model. This difference can be explained by looking into the effective width principal. The difference is small enough to interpret the results from RFEM as correct.

The verification of the stress-strain relationship in the OSD model was correct. A clear linear pattern was expected and it showed in the results as well. This linear pattern coincided with the E-modulus of steel as expected. For the hybrid model a slightly different behaviour was observed. A bi-linear stress-strain relationship was obtained from RFEM which followed the different E-moduli from the FRP and the steel. A slight distortion was observed at the bond between the FRP and steel. However, this distortion will have no significant effect on the global stresses and deformation but only on local effects near this bond. A solution for this distortion is possible but would result in a highly advanced model with an enormous amount of shell and solid elements resulting in a calculation time which will be to long. Since local effects are not investigated in this model there is no need to change this.

The verification of the neutral axis showed the expected results for both the OSD and the hybrid model. The neutral axis changed slightly over the span which is due to a slight increase of stiffness around the crossbeams.









5

Loading and results

This chapter elaborates steps eight to ten shown in Figure 4.1. First of are the load models that are implemented which follow from annex C.1 and are the same for the OSD and the hybrid bridge. Step nine is the export of results which shows how the output of RFEM is retrieved. Step ten shows how these results are used to make the necessary verifications that have to be done according to regulations (Annex C).

5.1 Load models

Each of the load models stated in annex C.1 will be considered for the model analysis. These only include traffic loads for static analysis and fatigue analysis. Other load cases such as dynamic loads, temperature loads and wind loads have not been integrated in this project.

The reasoning behind this decision is that dynamic and temperature loads will mainly effect the bond in the hybrid bridge between steel and FRP. Since this bond cannot be modelled well, see paragraph 4.2.2, these loads are irrelevant. Wind load is often the leading load case for the pivot point in the bridge and the main girders spanning between the pivot and the leaf of the bridge. This thesis focusses on the leaf of the bridge and is not made to verify stresses in and around the pivot point.

Temperature loads can however have significant effects on a hybrid bridge. Due to different expansion coefficients large deformations could occur not only in horizontal direction but also in vertical direction. FRP has a significantly higher expansion coefficient compared to steel which can result in an upwards curvature during a temperature increase. The effects of this curvature as well as the effects of a horizontal deformation should be investigated before building a hybrid bridge.





5.1.1 Vertical load models

There are four vertical load models to consider. Load model three is for special vehicles which is project specific therefor this load model is not considered. The other three load models will be elaborated in this paragraph.

Load model 1

Load model 1 includes axle loads that have to be modelled. This load should be modelled in the least favourable location. Since the main girders carry the load to the supports these are the main load bearing elements. Placing the load in the centre of their span will cause the highest global deflection and stresses. Some local effects due to the stiffeners and crossbeams might result in a slightly higher deflection, this is however not relevant in an early design stage.

The location in transverse direction of these axles depends on the number of notional lanes. Depending on the number of lanes several tandem systems must be modelled in transverse direction. An example is shown in Figure 5.1 for a bridge with a total of 3 traffic lanes, marked by the dashed lines, including the uniformly distributed loads.

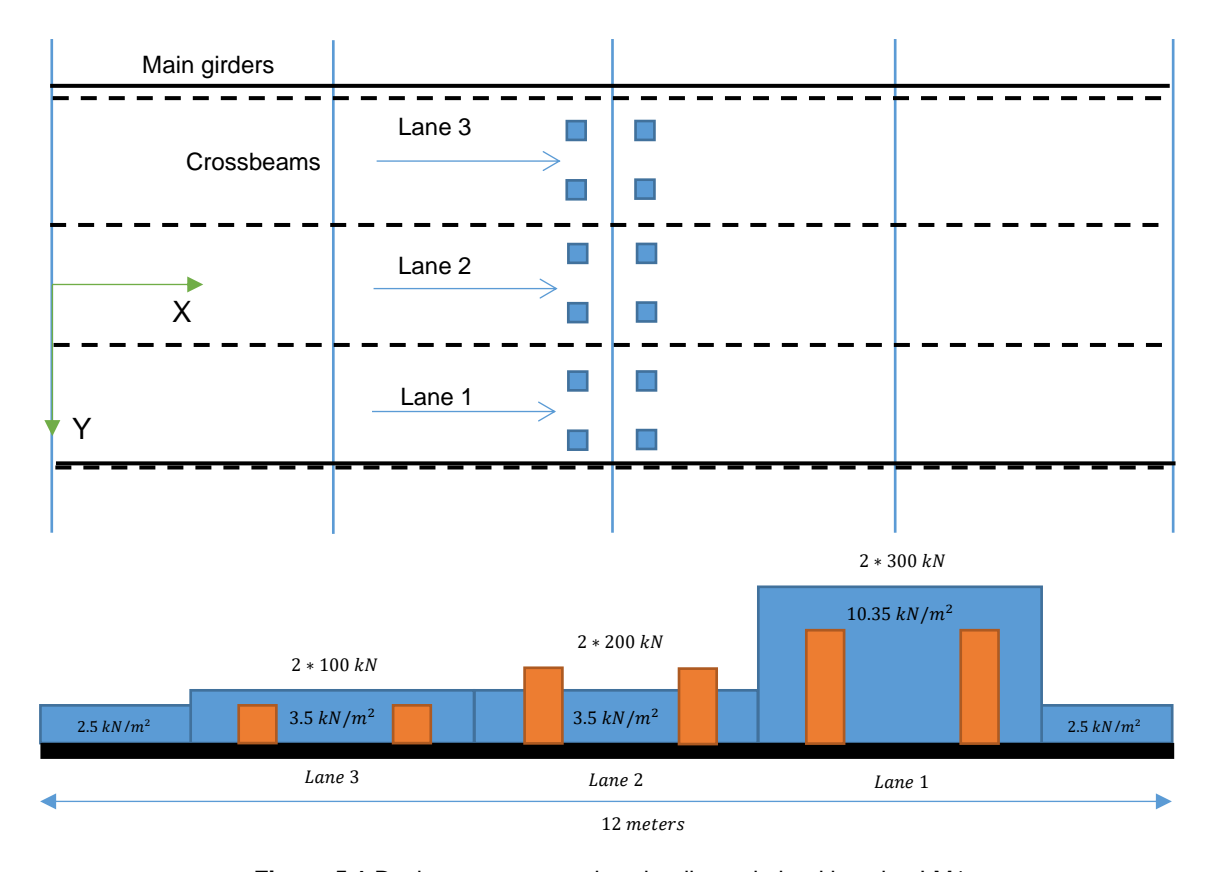


Figure 5.1 Deck geometry top view, leading axle load location LM1





The values stated in Figure 5.1 follow from equations (C.1) and (C.2). An elaboration of these equations can be found below in equations (5.1) and (5.2).

axle load lane
$$1 = 1.0 * 300 = 300 \, kN$$

axle load lane $2 = 1.0 * 200 = 200 \, kN$
axle load lane $3 = 1.0 * 100 = 100 \, kN$

$$UDL \, rest = 1.0 * 2.5 = 2.5 \frac{kN}{m^2}$$

$$UDL \ rest = 1.0 * 2.5 = 2.5 \frac{kN}{m^2}$$

$$UDL \ lane \ 1 = 1.15 * 9 = 10.35 \frac{kN}{m^2}$$

$$UDL \ other \ lanes = 1.4 * 2.5 = 3.5 \frac{kN}{m^2}$$
(5.2)

Load model 2

Load model 2 consists of a single axle load hence local deformations are important. Different locations could be leading for this load model depending on the configuration. Bridges with only two main girders will be considered since this is the case for almost all highway bridges. Placing the load in between the main girders will create maximum stresses and deflection in the bridge.

In longitudinal direction there are two possible locations, either on top of the crossbeam closest to midspan or in between crossbeams closest to midspan. The first option will cause maximum stresses and deflection in the crossbeam, the later option will cause this in the stiffeners. Since load model 1 already has significantly high loads on the deck the stresses in the crossbeams will probably be higher than for load model 2. Therefore load model 2 will be placed in between crossbeams on top of a stiffener in midspan of the main girders. Figure 5.2 gives a representation of load model 2 where the dashed lines are the stiffener legs.





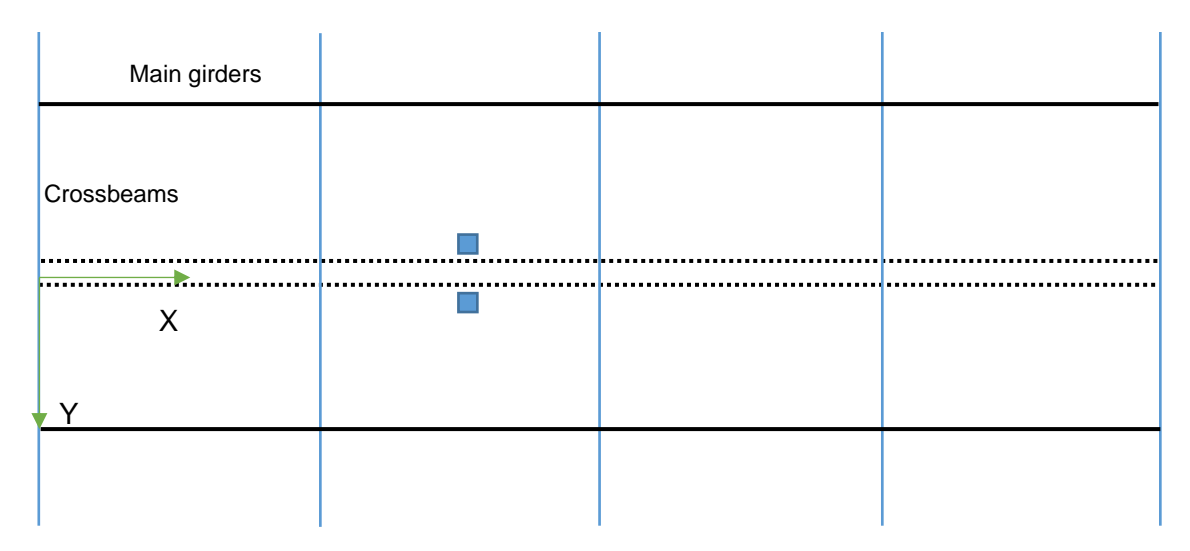


Figure 5.2 bridge geometry top view, leading axle load location LM2

Load model 4

Load model 4 consists of a uniformly distributed load of 5 kN/m^2 with a dynamic amplification factor already included. This load will be placed an top of the complete deck.





5.1.2 Horizontal load models

The loads due to braking and acceleration must be considered in the centre of any notional lane. The magnitude of the force depends on the vertical load from load model 1 on the first notional lane and has to be spread along the wheel print. Equation (5.3) is an example of the braking force for a bridge of 16 m length for one lane following equation (C.4).

$$Q_{lk} = 0.6 * 1.15 * (2 * 300) + 0.1 * 1.15 * 9 * 3 * 16 = 414 + 50 = 464$$
 (5.3)

This has to be done for each lane, the combined braking force is limited to 800 kN.

A skew braking force also has to be considered which is determined by taking 25% of the braking force. As a result a force of $464 \, kN$ must be considered in longitudinal direction together with 25% of this value in transverse direction due to skew braking. This results in a total force of $478 \, kN$ with an angle of 14° as is shown in equation (5.4).

$$Q_{trk} = 0.25 * 464 = 116 \, kN$$

$$Q_{k_{total}} = \sqrt{116^2 + 464^2} = 478 \, kN$$

$$\theta = Tan^{-1} \left(\frac{116}{464}\right) = 14^{\circ}$$
(5.4)

Horizontal forces only have to be considered for load model 1 as stated in Table C.5.





5.1.3 Groups of traffic loads

Six different load groups should be considered according to the Eurocode as shown in Table C.5. Each of the load groups will be explained below and result in the standard load cases that will be examined in this model.

Load group 1a (gr1a)

Load group 1a includes the characteristic value of load model 1, 0.8 times the characteristic value of horizontal forces and 0.4 time the characteristic value of evenly distributed loads. The evenly distributed load refers to biking or pedestrian lanes on the bridge. This will not be taken into consideration for highway bridges. Since there is one location of the axle loads only one load group 1a needs to be considered

$$LG_{1a} = LM_1 + 0.8 * Q_{k_{total}}$$

• Load group 1b (gr1b)

Load group 1b consists solely of the characteristic value of load model 2.

$$LG_{1b} = LM_2$$

Load group 2 (gr2)

Load group 2 consists of 0.8 times the characteristic value of load model 1 and the characteristic value of horizontal forces. Just as for LG_{1a} one version will be considered as shown below

$$LG_2 = 0.8 * LM_1 + Q_{k_{total}}$$

Load group 3 (gr3)

Load group 3 consists solely of the evenly distributed load from bike and pedestrian lanes. Since these do not occur on highway bridges it will not be considered.

Load group 4 (gr4)

Load group 4 consists solely of the characteristic value of load model 4.

$$LG_4 = LM_4$$





Load group 5 (gr5)

Load group five consists of 0.8 time load model 1, 0.8 times the horizontal forces and the characteristic value of load model 3. Load model 3 will not be considered in this project which results in load group five being equal to load group 1a but has a factor for load model 1 resulting in a lower total load. Therefore this load group will not be considered.

As a result a total of 4 different load groups will be considered, namely 1a, 1b, 2 and 4.





5.1.4 Fatigue load models

The fatigue load models must be modelled as explained in paragraph C.1.5. In almost any case fatigue load model 4 (FLM4), introduced on page 190, is leading. Therefore only FLM4 will be considered. For the steel sub-structure load model 4A needs to be considered.

To enhance the calculation time the load models will not be modelled completely. Per lane a set of three axles will be modelled that transit across the bridge. With a step size of 0.1 meters an influence line will be created for each of these axles. These lines will be combined and factorized to form the load spectrum for the necessary vehicles as part of the post processing. Overtaking traffic will also be considered during the post processing.

Further simplifications can be made for the load model of axle B. No local details that include the deck plate will be analysed, therefore the effects of modelling axle B as two wheels or four wheels will make no significant difference. Due to this, Axle B will be modelled as if it were two large wheels.

The frequency distribution of transverse location will be not be considered in this model. This would result in an extensive amount of different transverse wheel locations causing a long calculation time. This frequency distribution will have a big effect on local details, however on the general details the effect is minimal. Only for the detail including the stiffener to crossbeam connection the distribution is of importance, therefore results of this detail should be analysed more carefully in a later design stage.





5.2 Results export

By running the model in RFEM each load case will be calculated and results will be stored in a database. Figure 5.3 shows a workflow of the RFEM database and how to access it. First of the load case has to be selected, consecutively the surface in which the required mesh node is situated needs to be selected. The moment a surface is selected the complete data set of this surface will be retrieved from the database. Only then will it search for the node in this surface and for instance retrieve the stress in this node.

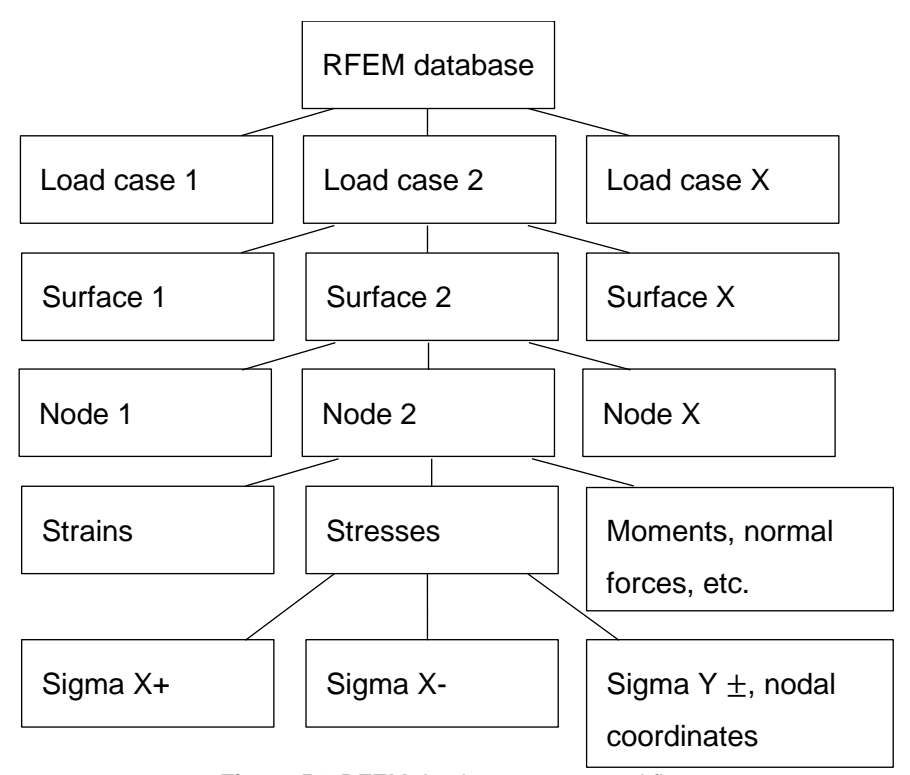


Figure 5.3 RFEM database access workflow

The export of results is done in Excel with the help of a vba code. This code is used to retrieve results from the RFEM database and store it in an excel sheet. For the standard load cases the results export exists of maximum deformations and maximum stresses. These values are exported with a value in [m] and $\left\lceil \frac{N}{m^2} \right\rceil$.

The results for the fatigue load models consist of stresses in a predefined location for the fatigue details. Stresses have to be obtained for each load step of an axle. An example can be seen in Figure 5.4 for fatigue location one of the OSD bridge with parameters stated in Figure 4.16. The first columns show the load case, load step and the nodal coordinates being requested. The following columns shows the stress results of wheel track A, B and C for lane one and wheel track A for lanes two and three which coincides with the fatigue load models stated on page 108.





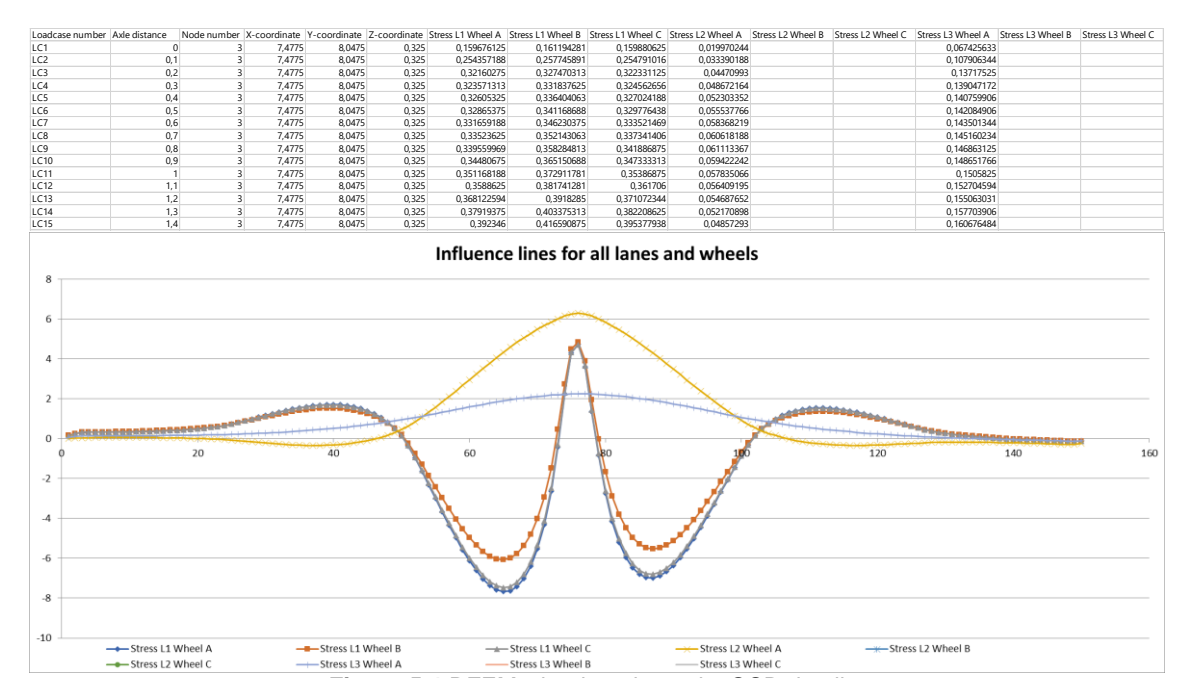


Figure 5.4 RFEM wheel track results OSD detail 1





5.3 Analysis of load models

The analysis of the results export is also done in Excel with the help of vba. Depending on the type of load cases being investigated different analysis or verifications are needed. For the standard load cases it is necessary to verify the maximum occurring stresses for an ULS check and a displacements verification is done as an SLS check as stated in annex C.1. For the fatigue load models a cumulative fatigue damage needs to be determined. This damage value will be determined as stated in annex C.1.5.

For the ULS check the maximum occurring stresses in the load bearing parts will be considered, which are the crossbeams and main girders.

For the SLS check a deflection verification will be done which is a limit states that concerns comfort of the user. In reality highway bridges have no comfort criteria but a deflection verification gives some good insights on the performance of the bridge. The maximum deflection of the bridge should be less then the span divided by 250 as shown in equation (C.6).

5.3.1 Standard load cases

Each of the standard load cases will have to be verified for serviceability limit state and ultimate limit state.

5.3.1.1 SLS verification

For the SLS verification a unity check will be made as shown in equation (5.5) which follows from equation (C.6). For this unity check a maximum allowable deflection of L/250 is used, however the user is free to change this deflection since there is no limit given in the Eurocode for highway bridges.

$$UC = \frac{u_{z,max}}{L/250} \le 1.0 \tag{5.5}$$

The maximum deflection will be determined for each of the load groups stated in annex C.1.4. An example of the results can be found in Table 5.1 where a unity check has been done for each of the four load combinations.





Table 5.1 OSD bridge: SLS verification

max allowable disp [mm]	58,33333333	
load combination	maximum displacement [mm]	Unity check
LC_1a	54,675	0,937
LC_1b	22,724	0,39
LC_2	45,203	0,775
LC_4	18,262	0,313

5.3.1.2 ULS verification

The unity check for an ULS verification is shown in equation (5.6) and follows from equation (C.7).

$$UC = \frac{\sigma_{max} * \gamma_Q}{f_y} \le 1.0 \tag{5.6}$$

This unity check should be done for each part in the bridge, however this is undesirable due to calculation time. Therefore the maximum stresses will be determined in predetermined locations for each different load case. An overview of the locations can be found in Table 5.2.





Table 5.2 ULS verification locations

	OSD bridge	Hybrid bridge
Load group 1a	In the bottom flange of the	In the bottom flange of the
	crossbeam closest to midspan of	crossbeam closest to
	the bridge	midspan of the bridge
Load group 1b	In the bottom flange of the stiffener	In the bottom flange of the
	midspan between crossbeams	crossbeam closest to
	closest to midspan of the bridge	midspan of the bridge
Load group 2	In the bottom flange of the main	In the bottom flange of the
	girder closest to midspan of the	main girder closest to
	bridge	midspan of the bridge
Load group 4	In the bottom flange of the	In the bottom flange of the
	crossbeam closest to midspan of	crossbeam closest to
	the bridge	midspan of the bridge

Besides the stresses the yield stress is needed. There are different steel grades which each have a different yield stress. For structural steel these are classes S235 up to S460 where the number represents the yield stress. A unity check will be done for each steel grade and the lowest possible steel grade that still fulfils the verification can be chosen. This can be done since fatigue does not depend on the steel grade for its stresses are far below the yield point.

An example of this verification can be found in Table 5.3. Steel class S275 will be enough in this example. However this would result in a unity check of 0.995 which is rather high so a higher steel class can be chosen as well. Most often a steel class of 355 is used in bridge construction.

Table 5.3 OSD bridge: ULS verification

Minimal steel class = S275		Steel class	235	275	355	420	460
load combination	maximum stress [N/mm2]		Unity check				
LC_1a	273,666944		1,165	0,995	0,771	0,652	0,595
LC_1b	214,629088		0,913	0,78	0,605	0,511	0,467
LC_2	229,127136		0,975	0,833	0,645	0,546	0,498
LC_4	84,30988		0,359	0,307	0,237	0,201	0,183
		UC_max	1,165	0,995	0,771	0,652	0,595





5.3.2 Fatigue load cases

The fatigue analysis can be split up in a four steps which will be elaborated in this paragraph. The first step is to create an influence line for each vehicle to be modelled. A peak-valley distribution can be determined from this influence line which is the second step. The third step is the so called rainflow counting algorithm to determine the stress ranges. The final step is to determine the fatigue damage from these stress ranges using an SN curve.

5.3.2.1 Influence line

From the influence line of the wheels as shown in Figure 5.4 an influence line for each vehicle on each lane can be created. This is done by multiplying the wheel influence lines to obtain the correct axle load and then combining them to obtain the correct vehicle configuration.

This has been done as an example for vehicle 4A_3 (Table C.8) on lane 1 using the wheel influence lines from Figure 5.4 and is shown in Figure 5.5. The two distinct peaks coincide with the moment that the first and second axles are on top of the detail location. The second is higher in this case since the axle load is higher as given by Table C.8.

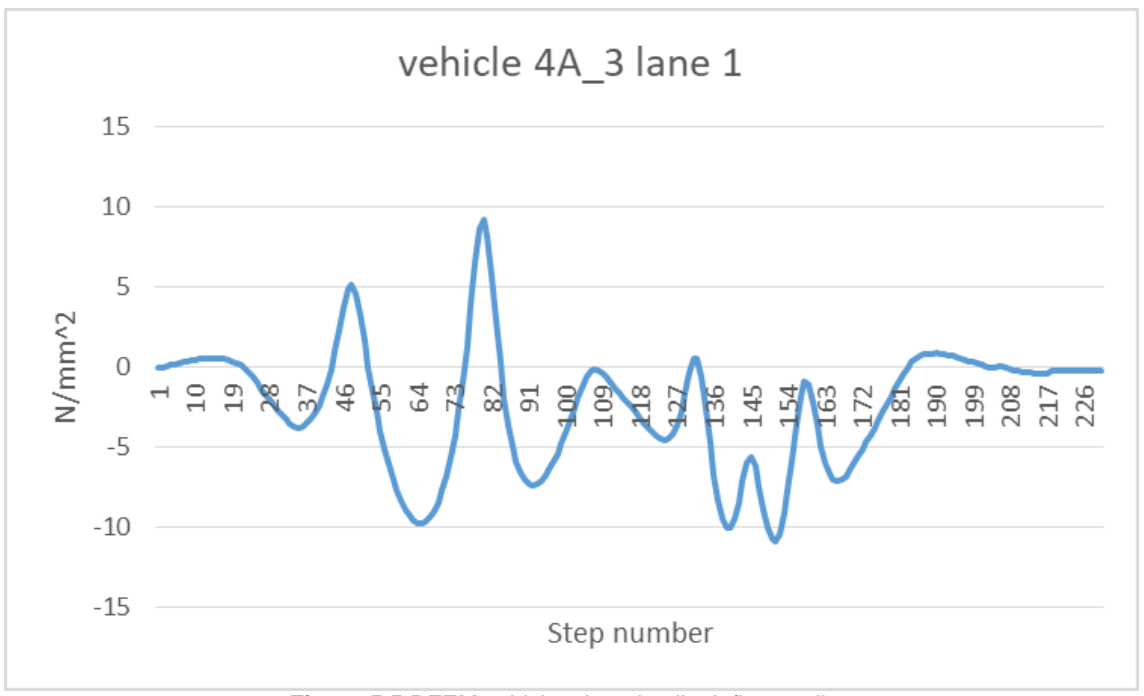


Figure 5.5 RFEM vehicle 4A_3 detail 1 influence line

Before going on to the next step it is necessary to sort this vehicle influence line in such a way that it will start with its maximum value. In this example it should start with the second peak with a value of $9 N/mm^2$. The result is shown in Figure 5.6.





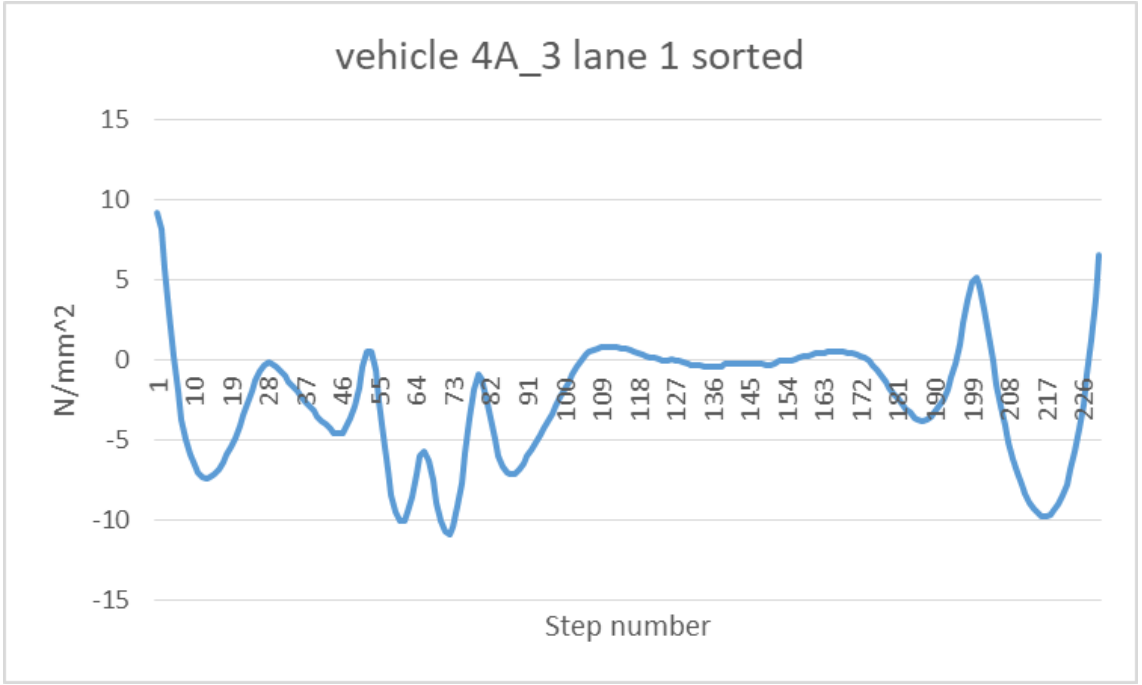


Figure 5.6 RFEM vehicle 4A_3 detail 1 influence line sorted

5.3.2.2 Peak-valley distribution

The peak-valley distribution simplifies the vehicle influence line to a line with only peaks and valleys. In short only the local maximum and minimum values remain of the influence line. This can be done by using a simple script that stores a value which is larger or smaller then both of its neighbouring values.

The result for vehicle 4A_3 for detail 1 can be found in Figure 5.7. This graph looks the same as the influence line with one important difference. The influence line starts with the highest occurring stress yet it finishes at a slightly lower stress. This is due to the fact that the influence line has been created by a step wise load instead of a continuous load.

For this reason an extra point has been added to the peak-valley distribution, the final peak stress is the same as the starting peak stress. The effects of this small change can be noticed in the rainflow counting and can have significant effects if forgotten.





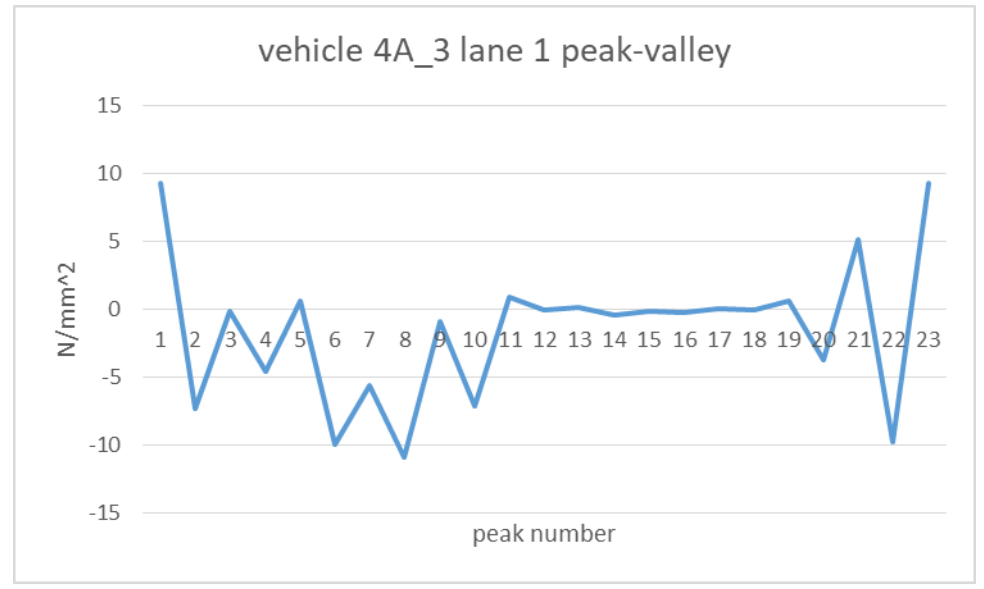


Figure 5.7 RFEM vehicle 4A_1 detail 1 peak-valley distribution

5.3.2.3 Rainflow counting method

The rainflow counting algorithm is a method to analyse fatigue damage and determines stress fluctuations from a peak-valley distribution. These fluctuations are also known as stress ranges. The rainflow counting method is a visual method that is easy to use by hand to determine stress ranges (as is shown in Annex E), however to automate this process is rather complex. A different method, the four point counting method, is used for this automation (Hiatt, 2016).

The four point counting method consists of a few steps elaborated below.

- 1. Chose four consecutive stress points (starting with nodes 1 to 4)
- 2. Determine if 2nd and 3rd stress points are inside the 1st and 4th

If this is the case an inner stress range has been found:

- 3.1. Determine and store stress range of 2nd and 3rd stress point
- 3.2. Remove 2nd and 3rd stress point from the list
- 3.3. Return to step 1

If this is not the case an incomplete cycle has been found:

7. Skip one (extra) node and return to step 1 (now considering nodes 2 to 5, 3 to 6, and so on)

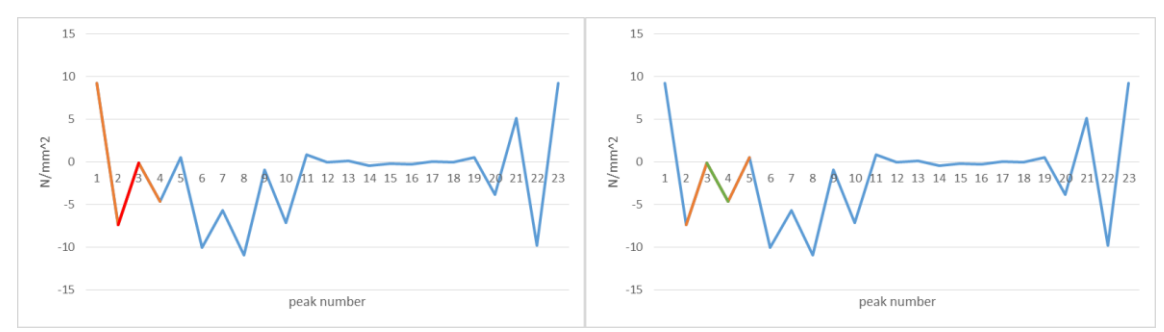
If there are no more inner stress ranges:

8. Determine residual stress ranges

This process has been illustrated in Figure 5.8 for the peak-valley distribution from Figure 5.7







Continue till inner stress range has been found, in this example for peak numbers 2 to 5.

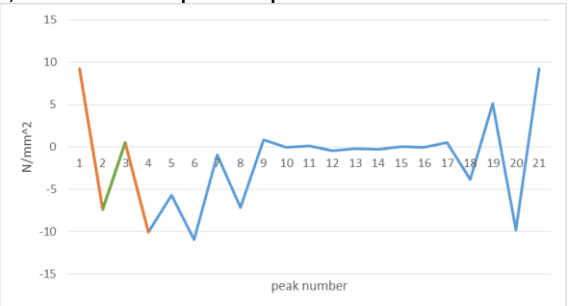
Inner stress range has been found.

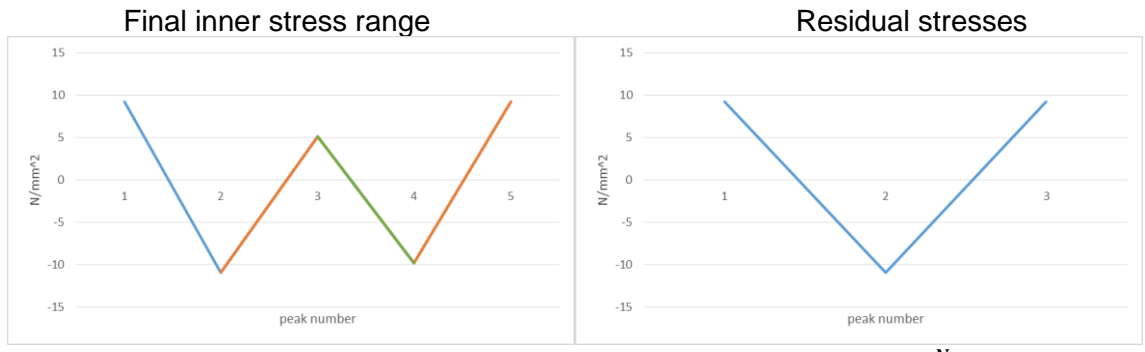
Stress range = $4.45 \frac{N}{mm^2}$

Remove stress range and start over.

Continue this process till no more inner

stress ranges can be found.





In this case only one residual stress range is left of $20.12 \frac{N}{mm^2}$.

Figure 5.8 RFEM vehicle 4A_3 detail 1 four point counting

As a result of this process a list of all the occurring stress ranges can be obtained. For this example the resulting stress ranges are shown in Table 5.4 in the order that they have been found. These stress ranges can now be used to determine the fatigue damage.





Table 5.4 Vehicle 4A_3 detail 1 stress ranges

	Stress range [N/mm^2]
Stress range 1	4.447836843
Stress range 2	7.90982287
Stress range 3	4.368877587
Stress range 4	6.226804972
Stress range 5	0.145205648
Stress range 6	0.071453473
Stress range 7	0.040448907
Stress range 8	0.989951048
Stress range 9	4.636080806
Stress range 10	14.89889244
Residual stress range	20.11962259

5.3.2.4 Fatigue damage calculation

Fatigue damage must be determined using the Palmgren-Miner rule as stated in annex C.1.5. For this rule it is necessary to know the number of vehicles that transit the bridge, this is stated in Table C.8. The other necessary information is the number of cycles till failure for the occurring stress ranges. For this the S-N curve needs to be determined with the cut-off limit and the constant amplitude fatigue limit (CAFL).

For stresses higher than the cut-off limit the number of cycles till failure need to be determined using equation (C.11). For this exemplary calculation a detail category of 56 is needed as stated in paragraph 4.2.1.2.

A detail category of 56 results in a cut-off limit of $19.71\frac{N}{mm^2}$ and a CAFL of $35.88\frac{N}{mm^2}$ as shown in equation (5.7).

$$\Delta \sigma_D = \left(\frac{2}{5}\right)^{\frac{1}{3}} * \frac{56}{1.15} = 35.88 \frac{N}{mm^2}$$

$$\Delta \sigma_L = \left(\frac{5}{100}\right)^{\frac{1}{5}} * 35.88 = 19.71 \frac{N}{mm^2}$$
(5.7)

One of the stress ranges is above the cut-off limit with a range of $20.12 \frac{N}{mm^2}$. This results in a number of cycles till failure of 37 million and 3.7 million respectively as shown in equation (5.8).

$$\begin{split} N_{Ri} &= \frac{\Delta \sigma_C^3}{\Delta \sigma_R^3} * 2 * 10^6 \ for \ \Delta \sigma_R > \Delta \sigma_D \\ N_{Ri} &= \frac{\Delta \sigma_C^5}{\Delta \sigma_R^5} * 5 * 10^6 for \ \Delta \sigma_L < \Delta \sigma_R \leq \Delta \sigma_D \end{split}$$





$$N_{Ri} = \frac{\frac{56}{1.15}}{19.71^{5}} * 5 * 10^{6} = 90,175,475 \ cycles$$
 (5.8)

Using the Palmgren-Miner rule this results in a damage of 0.00887 for the 800,000 vehicles that transit the bridge each year as shown in equation (5.9). This damage is lower than 1.0 so no failure will occur due to this vehicle. Even for a return period of 100 year, which is used for highway bridges, a damage of 0.887 is found which is still below 1.0 and therefore safe.

$$D = \sum_{i}^{n} \frac{n_{ei}}{N_{Ri}} = \frac{800000}{90175475} = 0.00887$$
 (5.9)

It can be said that fort his specific vehicle on this lane the design is safe, but close to 1.0. However this is just for one vehicle and only one lane. So each vehicle should be verified and combinations on multiple lanes should be considered. Table 5.5 shows the result overview for this example, the results for each lane and lane combination is given in Table 5.6.

Table 5.5 Vehicle 4A 3 excel results

damage vehicle 4A_3 lane 1	vehicle 4A_3 lane 1 stressrange_1	vehicle 4A_3 lane 1 peak-valley	vehicle 4A_3 lane 1 sorted	vehicle 4A_3 lane 1
0.88715917	4.447836843	9.222397695	9.222397695	-0.040448907
	7.90982287	-7.370911987	8.121926348	-0.033819893
	4.368877587	-0.158792455	5.679673223	0.005948215
	6.226804972	-4.606629297	2.871699105	0.080501528
	0.145205648	0.538910883	0.280057466	0.151250419
	0.071453473	-10.0290095	-1.938102112	0.219008451
	0.040448907	-5.660131911	-3.672691909	0.282398075
	0.989951048	-10.8972249	-4.980412639	0.340566696

Table 5.6 Detail 1 excel results

		Lane 2&1	0.218	Lane 3&2	(0.122
Lane 1	0.887	Lane 2	0.000	Lane 3	(0.000
Lane 1&2	1.017	Lane 2&3	0.122	Lane 3&4	(0.000

For lane 1 the damage is still below 1.0 showing that vehicle 3 is the only vehicle that causes damage. When including overtaking traffic it results in a damage higher than 1.0 meaning that the structure is unsafe.





5.3.3 Buckling of sandwich panel

The occurring stresses in the FRP sandwich panel will be verified with the critical buckling stresses for the sandwich panel, determined in paragraph 4.3.2.

As stated in this paragraph verification of vertical buckling is not necessary since the stresses will not be effected much by the global deflection. If a different sandwich panel will be used a new verification of the vertical buckling stresses is needed.

Shear stresses might change due to global deflection. However, due to the set-up of the model in RFEM the shear stresses near the crossbeams are disturbed. Therefore the shear stresses will not coincide with reality and are therefore useless to compare. This distortion is caused by the bond between FRP and steel which has been modelled as rigid links in certain locations, whereas in reality this bond is everywhere between FRP and steel. Peak stresses will occur at the modelled links which disturbs the actual occurring stresses and strains. Fortunately this has no effect on the global deflection but only on the local load transfer from FRP to steel.

Horizontal buckling stresses in the webs will be different in the global model due to global deformation. Therefore it is necessary to read out the maximum stresses in horizontal direction. As explained in paragraph 4.3.2 this should be done in two locations, underneath the wheel load in mid-span of the crossbeams and directly above the crossbeams. This latter one will not be accurate for the same reason that the shear stresses are not accurate. Horizontal stresses will therefore only be obtained at mid-span.

To maximize global effects the stresses will be obtained from load combination 1a, since this model results in the highest total deflection. The stresses will be obtained at the top of the webs directly under the wheel load. The buckling factor will be determined using equation (C.20) where $\sigma_{cr} = 104 \, MPa$ as given by equation (4.8)*. For buckling factors larger than 1.0 the structure will be safe.





5.4 Conclusion

All load models will be applied on both the OSD and hybrid bridge. There are two different types of load models that are considered, standard and fatigue load models. There are four standard load combinations modelled to determine the maximum displacement, maximum stresses and for the hybrid model one of these load cases is used to determine a buckling factor. The fatigue load models are step-wise loads that transit across the bridge on the predetermined notional lanes.

The results can be exported from RFEM to use in excel for a post calculation. This export is rather simple but due to the set-up of the RFEM database it costs a lot of time. Results are exported by first defining the load case, than the plate in which the required node lies and finally selecting the required node. The node selection is not done by number but by order. This means that node number 200 could be the first node if all the other node number are higher, as a result node 0 should be requested since it is the first node in the specific plate.

The result analysis can be split in three different parts, the analysis of the standard load cases, fatigue load cases and buckling (only for hybrid model).

The analysis of the standard load cases is done by two unity checks for each load case. The first being a unity check of the maximum deflection. This maximum deflection is the span divided by 250 if not specified otherwise. The second unity check is for the verification of the maximum allowable stress. This unity check will give the minimum steel class as a result (S235 to S460).

The analysis of the fatigue load cases is done for each of the detail locations, four for the OSD model and three for the hybrid model. This analysis is done with the help of the four point counting method which is a programmable approach of the visual rainflow counting method.

The analysis for buckling is only done for the hybrid model and results in a buckling factor for the sandwich panel. Due to the way the connection between the FRP and steel is modelled it is only possible to look into one of the global buckling modes.









6

Optimization

This chapter elaborates on the optimization of the models and the comparison between them. This comparison will be made for movable bridges with the same global dimensions (height, span and width). The goal however is to create a fair comparison and compare two "optimized" models with each other.

The optimization must be done after an analysis to create an even better model with the same global dimensions. This optimization will focus on a few parameters, namely the thickness and width of flanges of the main girders and crossbeams. The dimensions of the FRP sandwich panel will remain constant during this optimization. This optimization will decrease the amount of material used and thereby decrease the overall weight of the structure which is to be compared.

Depending on the results of the analysis certain optimizations can be made. It is expected that the fatigue load cases will be decisive so the optimization rests on those results while still verifying the standard load cases. A few example analysis have been conducted to determine the effects of the proposed alterations. The results of both the OSD and the hybrid model will be explained below.





Optimization OSD model 6.1

Seven models have been analysed to determine the effects of certain alterations. In each model one parameter has been changed to see the effect that it has on the fatigue damage. The other parameters of the reference models are shown in Figure 4.16. Table 6.1 shows the alterations for each of the models.

Table 6.1 OSD optimization: altered parameters

model nr.	Cros	sbeam dimension	ıs [mm]	Main girder dimensions [mm]			
	flange width	flange thickness	web thickness	flange width	flange thickness	web thickness	
1	300	20	12	450	45	20	
2	200	20	12	450	45	20	
3	300	15	12	450	45	20	
4	300	20	10	450	45	20	
5	300	20	12	350	45	20	
6	300	20	12	450	30	20	
7	300	20	12	450	45	15	

6.1.1 Results

The fatigue damage results of each detail (paragraph 4.2.1.2) have been gathered for each of the alternatives together with the total weight of the model in kilograms. An overview is given in Table 6.2 which also shows the percentage of difference with the reference model and the normalised difference percentage which includes the weight reduction.

Table 6.2 OSD optimization: fatigue damage results

model nr.	F	atigue dar	nage OS	D	Damage dif percentage of reference			V	Veight	damage dif	weight dif	
	Det1	Det2	Det3	Det4	Det1	Det2	Det3	Det4	[kg]	difference %	Det2	Det4
1	0	0,0432	0	0,0444	-	0,00%	-	0,00%	69.804	-	-	-
2	0	0,0408	0	0,0571	-	-5,60%	-	28,60%	68.469	1,91%	2,93%	-14,96%
3	0	0,0437	0	0,0448	-	1,02%	-	0,90%	68.923	1,26%	-0,81%	-0,71%
4	0	0,0436	0	0,0417	-	0,81%	-	-6,06%	68.460	1,93%	-0,42%	3,15%
5	0	0,0898	0	0,0829	-	107,77%	-	86,78%	68.241	2,24%	-48,13%	-38,76%
6	0	0,2425	0	0,2618	-	461,08%	-	489,66%	67.154	3,80%	-121,45%	-128,98%
7	0	0,0539	0	0,0618	-	24,69%	-	39,10%	68.204	2,29%	-10,77%	-17,06%

The last two columns show the normalised results where the difference in damage by a weight decrease of one percent has been determined. This has been done by linear interpolation, which is not the case in reality but does give some insight on the effects of the alterations. A positive value means that damage decreases while the weight decreases, a negative value means that damage increases while weight decreases.

Damage occurs in detail 2 and 4 which are the details that are determined by stresses in the bottom flange of the main girder. This explains the high damage increases for the alternatives with smaller main girder dimensions (alternative 5,6 an 7). It seems that reducing the thickness





of the web has the highest impact on weight reduction without increasing fatigue damage dramatically. The thickness of the bottom flange has the highest effect on damage increase.

To see what effect these alterations have on detail 1 and 3 a closer look into the influence lines of those details is needed. Table 6.3 shows the highest occurring stress range in the influence lines of the wheels (not the vehicles) per detail and the percentual difference with the reference model.

Table 6.3 OSD optimization: influence line stress range

model nr.	max single wheel stress range stress range dif percentage of reference					nce		
	Det1	Det2	Det3	Det4	Det1	Det2	Det3	Det4
1	12,167	15,172	2,397	14,690	-	ı	-	-
2	12,328	15,029	2,138	15,127	1,32%	-0,94%	-10,81%	2,97%
3	12,189	15,065	3,046	14,683	0,18%	-0,71%	27,08%	-0,05%
4	12,220	15,147	2,042	14,389	0,44%	-0,16%	-14,81%	-2,05%
5	12,193	17,583	2,339	16,269	0,21%	15,89%	-2,42%	10,75%
6	14,090	20,430	2,329	19,658	15,81%	34,66%	-2,84%	33,82%
7	12,363	15,863	2,442	15,429	1,61%	4,55%	1,88%	5,03%

None of the alterations have a significant influence on detail 1 except for the flange thickness reduction of model 6. This increase in the stress range is a result of the extra deformation that occurs due to less material in the flange of the main girder. For detail 3 only alternative 3, decrease in crossbeam flange thickness, causes a significant increase in damage. The other alternatives actually decrease the damage in detail 3.





6.1.2 Optimization

These results show that the simplest weight reduction without significant damage increase occurs when the thickness of both the crossbeam and main girder web is decreased. Reducing these webs has little effect on the global stiffness and deflection since this doesn't effect the moment of inertia as much as changing flange diameters. Therefore the webs will have a fixed thickness. For the crossbeams this will be 12 mm and for the main girders 16, these parameters can however be changed easily.

Changing the thickness of the crossbeam flange only has a significant effect on detail 3. However in this example the stress range of a wheel is only $3 N/mm^2$, this will not lead to significant damages with a detail category of 90. Changing this thickness will however effect the deflection of the bridge in between the main girders due to a reduction in the moment of inertia. Therefore this parameter needs to be checked with the standard load cases to verify whether the deflection and stresses are still within certain boundaries.

Changing the thickness of the main girder flange has significant effects on details 1, 2 and 4. The results show that it is better to reduce the width of the flange instead of the thickness. Reducing the width of the flange will have significant effects on warping and torsional stiffness so a good aspect ratio between the two is needed. The same thought process can be applied on the flange width of the crossbeam. To maintain this good aspect ratio a choice has been made to set the thickness of the flanges to 10% of the width of those flanges. This value coincides with the minimal aspect ratio found in Table 4.1.

The results and optimizations stated above can be summarised by the following choices

- Detail 1 has high damage → Increase stiffener thickness (and stiffener width if still not fulfilled)
- Detail 2 has high damage → Increase main girder flange width (and therefore flange thickness)
- Detail 3 has high damage → Increase crossbeam flange thickness
- Detail 4 has high damage → Increase crossbeam flange width





The model is optimized for each of the details every iteration. The optimization can be explained using the following steps:

- 1. Is the fatigue damage 0?
 - a. Yes: new dimension = old dimension 3 (mm for thickness, cm for width)
 - b. No: Go to 2.)
- 2. Is the fatigue damage between 0 and 0.8?
 - a. Yes: new dimension = old dimension $\left(\frac{1}{D}\right)^{\frac{1}{4}}$ (mm for thickness, cm for width)
 - b. No: Go to 3.)
- 3. Is the fatigue damage higher than 1.0?
 - a. Yes: new dimension = old dimension + $4*(D)^{\frac{1}{4}}$ (mm for thickness, cm for width)
 - b. No: The fatigue damage is between 0.8 and 1.0 which is fine, nothing changes.

This optimization changes the dimensions drastically if the damage is higher than 1.0. From there it will take smaller steps backwards to find an optimum.

A slightly different optimization is made for the stiffener. Changing the stiffener thickness by 1 mm has very large effects, therefore it will be changed with 1 mm at a time and it will only change if the fatigue damage is below 0.05. Furthermore, the width of the bottom of the stiffener will be increased if the detail in the stiffener results in damage for a thickness of 8 mm. This results in a stiffener which isn't mass produced which will result in an increase in cost, however the goal is to optimize for weight.

There are also boundaries for the dimensions of the changing parameters. They have been listed in Table 6.4. These boundaries have been determined from experience

Table 6.4 Boundaries for changing parameters

Parameter	Lower bound [mm]	Upper bound [mm]
Main girder flange width	300	-
Crossbeam flange width	200	-
Crossbeam flange thickness	12	-
Stiffener thickness	6	8
Stiffener width	105	210





6.1.3 Exemplary optimization

An exemplary optimization has been done for a 12 meter long bridge with two lanes. The optimized dimensions are given in Table 6.5.

Table 6.5 OSD optimization parameters

Input Parameters	In code	value	Unit	Input Parameters	In code	value	Unit
General				Main girders			
Span	br_l	12	m	Main girder height	br_h_mg	1,0	m
Width	br_w	9,6	m	Main girder connection radius	br_r_mg	0,150	m
Height	br_h	1,0	m	Main girder distance to pivot	br_piv_mg	2,500	m
Deck				Main girder web thickness	br_t_web_mg	0,016	m
Deck thickness	br_t_deck	0,022	m	Main girder bottom flange width	br_w_bfl_mg	0,430	m
Stiffeners				Main girder bottom flange thickness	br_t_bfl_mg	0,043	m
Number of stiffeners	br_n_stif	15	-	Number of main girders	br_n_mg	2	-
Stiffener centre-to-centre cantilever	br_ctc_stif_can1	0,600	m	Main girders centre-to-centre distance	br_ctc_mg	6,800	m
Stiffener centre-to-centre distance	br_ctc_stif	0,600	m	Main girder distance to edge	br_e_mg	1,400	m
Stiffener centre-to-centre cantilever	br_ctc_stif_can2	0,600	m	Load cases			
Stiffener top width	br_w_tstif	0,300	m	Lanewidth	ld_w_lane	3	m
Stiffener bottom width	br_w_bstif	0,105	m	Side parapet (zijberm)	ld_w_par	1,4	m
Stiffener height	br_h_stif	0,325	m	nr_lanes	ld_nr_lanes	2	-
Stiffener thickness	br_t_stif	0,008	m				
Crossbeams							
Crossbeam height	br_h_cb	1,0	m				
Number of crossbeams	br_n_cb	6	-				
Crossbeam ctc distance first spans	br_ctc_cb2	2,100	m				
Crossbeam web thickness	br_t_web_cb	0,010	m				
Crossbeam bot flange width	br_w_bfl_cb	0,270	m				
Crossbeam bot flange thickness	br_t_bfl_cb	0,012	m				
Crossbeam centre-to-centre distance	br_ctc_cb	2,600	m				

The results of each iteration is shown in Table 6.6. An optimum has been found after ten iterations.

Table 6.6 Hybrid optimization result

UC_max = 58 mm	Iteration 1	Iteration 2	Iteration 3	Iteration 4	Iteration 5	Iteration 6	Iteration 7	Iteration 8	Iteration 9	Iteration 10
Width mg flange	0,350	0,430	0,470	0,510	0,500	0,490	0,530	0,520	0,510	0,500
Thickness mg flange	0,035	0,043	0,047	0,051	0,050	0,049	0,053	0,052	0,051	0,050
Thickness cb flange	0,012	0,012	0,012	0,012	0,012	0,012	0,012	0,012	0,012	0,012
Width cb flange	0,190	0,270	0,310	0,300	0,280	0,270	0,260	0,240	0,220	0,220
Tickness stiffener	0,008	0,008	0,008	0,008	0,008	0,008	0,008	0,008	0,008	0,008
Width bottom stiffener	0,105	0,105	0,105	0,105	0,105	0,105	0,105	0,105	0,105	0,105
UC LM1A	0,401	0,331	0,305	0,286	0,292	0,297	0,279	0,285	0,290	0,295
UC LM1b	0,182	0,156	0,147	0,140	0,142	0,144	0,137	0,139	0,142	0,143
UC LM2	0,335	0,277	0,255	0,238	0,243	0,248	0,233	0,237	0,242	0,246
UC L4	0,145	0,121	0,112	0,105	0,107	0,109	0,103	0,104	0,106	0,108
UC max	0,401	0,331	0,305	0,286	0,292	0,297	0,279	0,285	0,29	0,295
Fat dam mg fl	16,04	3,83	1,82	0,40	0,47	1,44	0,29	0,37	0,44	0,52
Fat dam cb fl	0,00	0,00	0,00	0,00	0,00	0,00	0,00	0,00	0,00	0,00
Fat dam cb web	8,53	2,02	0,41	0,19	0,23	0,28	0,14	0,16	0,21	0,26
Fat dam stif	0,91	0,50	0,44	0,44	0,46	0,47	0,47	0,49	0,51	0,52
Fat max	16,04	3,83	1,82	0,44	0,47	1,44	0,47	0,49	0,51	0,52
Model weight [kg]	43749	45864	47054	48046	47635	47314	48320	47922	47529	47266
Model weight [kg/m2]	379,77	398,13	408,45	417,07	413,50	410,71	419,44	415,99	412,58	410,30
weight MG	5288	6457	7130	7864	7675	7490	8254	8057	7864	7675
weight CB	6416	5948	6164	6110	6002	5948	5895	5787	5679	5679
weight stif	8480	8480	8480	8480	8480	8480	8480	8480	8480	8480
weight deck	19768	19768	19768	19768	19768	19768	19768	19768	19768	19768





The first four iterations show an increase in the dimensions of the main girder. After that the bridge is slightly overdimensioned and starts to decrease the dimensions again. An optimum is found in the tenth iteration, another decrease in main girder dimensions would result in a jump in fatigue damage which can also be seen in iteration 5 and 6.

The resulting weight of the model per square meter is $410 \frac{kg}{m^2}$. As rule of thumb $450 \frac{kg}{m^2}$ is often used for OSD bridges, which is close to the result obtained.





6.2 Optimization hybrid model

Seven models have been analysed to determine the effects of certain alterations. In each model one parameter has been changed to see the effect that it has on the fatigue damage. The other parameters of the reference models are shown in Figure 4.27. Table 6.1 shows the alterations for each of the models.

6.2.1 Results

The same table as for the OSD model has been created for the Hybrid model. This shows the damage per detail, difference to the hybrid reference model, the weight and the damage over weight difference as shown in Table 6.7.

model nr. Damage dif percentage of Weight damage dif / weight dif Fatigue damage Det1 difference % Det2 Det3 Det1 Det2 Det3 [kg] Det1 Det2 0,248 0 0,2062 45.666 14,1% 16.9% 0,049 2 0.283 0,241 43.565 4,60% -3.07% 3 18.2% 0.1% 0,293 0,2065 -5,38% -0,04% 44.124 3,38% 4 15,7% -5,4% 2.23% 0.2869 0 0.1951 44.564 2.41% -6.50% 91,3% 5 0,4743 0 0,3329 61,4% 43.077 5,67% -16,10% -10,83% 6 0,8622 0 0,7473 247,7% 41.216 9,74% 262,4% -25,42% -26,93% 31,3% -7,34% 0,3256 0 0,2497 21,1% 44.354 2,87% -10,89%

Table 6.7 Hybrid optimization: fatigue damage results

The same dimensions of the flanges and webs have been used as for the OSD model. Due to the decreased height of the steel girders and a lower stiffness overall this results in higher fatigue damages. As for the OSD bridge detail 2 (in OSD detail 3) has no significant damage. The other details show the same effects when changing parameters as the OSD bridge but with different magnitude.

A significant difference can however be seen in the weight and weight difference. The OSD deck plate and stiffeners has been replaced by a FRP deck. This FRP deck is very light compared to the OSD deck plate and stiffeners. Therefore the percentual weight reduction by changing the parameters is higher for the hybrid bridge as for the OSD bridge. This in turn causes the damage over weight percentage to be lower opposed to the OSD percentages.

Table 6.8 shows the highest stress ranges from the wheel influence lines per detail to get a better understanding of the effects of alteration on detail 2. It is clear that for case number two and three an increase occurs, which if high enough might result in significant damage for this detail.





Table 6.8 Hybrid optimization: influence line stress range

model nr.	max single wheel stress range			stress ran	ge dif percentage	of reference
	Det1	Det2	Det3	Det1	Det2	Det3
1	19,429	6,716	19,111	-	-	-
2	18,896	9,471	19,768	-2,74%	41,03%	3,44%
3	19,209	8,433	19,094	-1,13%	25,57%	-0,09%
4	19,333	5,453	18,840	-0,49%	-18,81%	-1,42%
5	23,192	6,502	21,648	19,37%	-3,19%	13,28%
6	27,057	6,152	26,444	39,26%	-8,40%	38,37%
7	20,317	6,741	20,154	4,57%	0,38%	5,46%

Looking at the results from the OSD bridge (Table 6.3) a decrease in the stress range can be observed in detail 2 for case number 2 whereas for the hybrid bridge a large increase can be observed. This difference can be caused by the lack of transverse stiffness in the hybrid bridge. The FRP sandwich deck stiffness in longitudinal direction is way higher due to the webs then it is in transverse direction. Therefore a decrease in material of the crossbeam flanges has significantly more effect in the hybrid bridge then in the OSD bridge.

6.2.2 Optimization

Besides case number two (Table 6.8) the hybrid bridge shows the same effects as the OSD bridge, therefore the same optimization steps will be used. Since the hybrid bridge has no stiffeners this optimization step is skipped.

6.2.3 Exemplary optimization

An exemplary optimization has been done for a 12 meter long bridge with two lanes. The optimized dimensions are given in Table 6.9.





Table 6.9 Hybrid optimization parameters

Input Parameters	In code	value	Unit	Input Parameters	In code	value	Unit
General				Main girders			
Span	br_l	12	m	Main girder height	br_h_mg	0,808	m
Width	br_w	9,6	m	Main girder connection radius	br_r_mg	0,150	m
Height	br_h	1,0	m	Main girder distance to pivot	br_piv_mg	2,500	m
Sandwich panel				Main girder top flange width	br_w_tfl_mg	0,500	m
Material properties	See "Sandwich d	eck"		Main girder top flange thickness	br_t_tfl_mg	0,040	m
Sandwich panel height (ctc)	br_h_sp	0,192	m	Main girder web thickness	br_t_web_mg	0,016	m
Sandwich panel top face sheet thicknes	br_t_tfac_sp	0,012	m	Main girder bottom flange width	br_w_bfl_mg	0,580	m
Sandwich panel bot face sheet thickness	br_t_bfac_sp	0,012	m	Main girder bottom flange thickness	br_t_bfl_mg	0,058	m
Sandwich panel web thickness	br_t_web_sp	0,006	m	Number of main girders	br_n_mg	2	-
Sandwich panel centre-to-centre web	br_ctc_web_sp	0,080	m	Main girders centre-to-centre distance	br_ctc_mg	6,800	m
Nodes for sp-steel connection	nodes_link_e	0,012		Main girder distance to edge	br_e_mg	1,400	m
Crossbeams				Load cases			
Crossbeam height	br_h_cb	0,808	m	nr_lanes	ld_nr_lanes	2	m
Number of crossbeams	br_n_cb	6	-	Lanewidth	ld_w_lane	3	m
Crossbeam ctc distance first spans	br_ctc_cb2	2,100	m	Side parapet	ld_w_par	1,4	m
Crossbeam top flange width	br_w_tfl_cb	0,190	m				
Crossbeam top flange thickness	br_t_tfl_cb	0,012	m				
Crossbeam web thickness	br_t_web_cb	0,010	m				
Crossbeam bot flange width	br_w_bfl_cb	0,230	m				
Crossbeam bot flange thickness	br_t_bfl_cb	0,012	m				
Crossbeam centre-to-centre distance	br_ctc_cb	2,600	m				

The results of each iteration is shown in Table 6.10. An optimum was found after eight iterations.

Table 6.10 Hybrid optimization result

UC_max = 58 mm	Iteration 1	Iteration 2	Iteration 3	Iteration 4	Iteration 5	Iteration 6	Iteration 7	Iteration 8	Iteration 9	Iteration 10
Width mg flange	0,500	0,580	0,660	0,700	0,740	0,730	0,720	0,710	0,700	0,740
Thickness mg flange	0,050	0,058	0,066	0,070	0,074	0,073	0,072	0,071	0,070	0,074
Thickness cb flange	0,012	0,012	0,012	0,012	0,012	0,012	0,012	0,012	0,012	0,012
Width cb flange	0,190	0,230	0,220	0,220	0,220	0,220	0,220	0,220	0,220	0,220
UC LM1A	0,562	0,509	0,476	0,463	0,452	0,454	0,457	0,460	0,463	0,452
UC LM1b	0,350	0,330	0,319	0,315	0,311	0,312	0,313	0,314	0,315	0,311
UC LM2	0,467	0,422	0,394	0,383	0,373	0,376	0,378	0,380	0,383	0,373
UC L4	0,143	0,128	0,118	0,115	0,112	0,113	0,113	0,114	0,115	0,112
UC max	0,562	0,509	0,476	0,463	0,452	0,454	0,457	0,460	0,463	0,452
Fat dam mg fl	18,579	6,164	2,429	1,478	0,398	0,461	0,510	0,568	1,478	0,398
Fat dam cb fl	0,140	0,013	0,122	0,141	0,168	0,163	0,171	0,165	0,141	0,168
Fat dam cb web	2,266	0,290	0,112	0,000	0,000	0,000	0,000	0,000	0,000	0,000
Fat max	18,58	6,16	2,43	1,48	0,40	0,46	0,51	0,57	1,48	0,40
Buckling factor	2,38	2,41	2,42	2,43	2,44	2,44	2,44	2,43	2,43	2,44
Model weight [kg]	29533	32023	34528	35934	37421	37042	36667	36297,99	35934	37421
Model weight [kg/m2]	256,36	277,98	299,72	311,93	324,84	321,54	318,29	315,09	311,93	324,84
Main girders	14146	14146	16752	18145	19598	19229	18864	18502	18145	19598
Crossbeams	5895	5895	5841	5841	5841	5841	5841	5841	5841	5841
FRP	8339	8339	8339	8339	8339	8339	8339	8339	8339	8339
PVC Foam	1534	1534	1534	1534	1534	1534	1534	1534	1534	1534

After the five iteration the dimensions of the main girder were decreased again. After the 8th iteration this caused a fatigue damage over 1.0, as a result iteration 8 is an optimum.

The buckling factor of the sandwich panel web is at 2.43 which is safe enough but close to 1.0. Therefore a better inspection on the buckling behaviour is necessary in later design stage.

The resulting weight of the model per square meter is $315\frac{kg}{m^2}$. This is a reduction of 23% compared to the OSD bridge with a weight per square meter of $410\frac{kg}{m^2}$.





6.3 Comparison

When both the OSD and the hybrid bridge have been optimized and al verifications are safe, a comparison between the two can be made. For renovations one of the key factors to chose a certain bridge is weight if the foundations of the old bridge are re-used. Therefore one of the comparisons that will be made is a comparison of the total weight of the optimized bridge. This value can be retrieved from RFEM which uses of the material density to determine self-weight.

6.3.1 Results

Besides the self-weight a list of the verification results will be shown to make a better comparison between the two bridges. An example is shown in Table 6.11 for both bridges from paragraphs 6.1 and 6.2.

Table 6.11 OSD versus hybrid results comparison

UC_max = 58 mm	OSD	Hybrid
Width mg flange	0,500	0,710
Thickness mg flange	0,050	0,071
Thickness cb flange	0,012	0,012
Width cb flange	0,220	0,220
Tickness stiffener	0,008	-
Width bottom stiffener	0,105	-
UC LM1A	0,295	0,460
UC LM1b	0,143	0,314
UC LM2	0,246	0,380
UC L4	0,108	0,114
UC max	0,295	0,46
Fat dam mg fl	0,52	0,57
Fat dam cb fl	0,00	0,17
Fat dam cb web	0,26	0,00
Fat dam stif	0,52	-
Fat max	0,52	0,57
Buckling factor	-	2,43
Model weight [kg]	47266	36297,99
Model weight [kg/m2]	410,30	315,09
Weight MG	7675	18502
Weight CB	5679	5841
Weight stif	8480	-
Weight deck	19768	-
Weight FRP	-	8339
Weight Foam	-	1534

In the dimensions it is clear that the hybrid bridges main girders have significantly thicker and wider flanges. The dimensions for the crossbeams turned out to be the same for this model and both crossbeam dimensions are at their minimum value.





A maximum allowable deflection of 58 mm has been used for the standard load models. The result show that the deflection of the hybrid bridge is close to twice as high as the OSD bridge for load models 1 and 2. This is to be expected due to the lower stiffness of the FRP sandwich panel. The other load models show less difference between the bridges.

The fatigue damage for both models is around 0.55. Each of the models had another iteration after the optimal one which both showed failure. Therefore these models can be considered optimized for a pre-design face.

The buckling factor of the sandwich panel web is at 2.43 which is safe enough but close to 1.0. Therefore a better inspection on the buckling behaviour is necessary in later design stage but for now it can be considered to be safe.

These verifications conclude the analysis steps and show that both bridges are safe according to the design verifications done in this model.

6.3.2 Bridge choice

With the models optimized and verified it is possible to make a comparison and eventually a bridge choice. With weight being the main focus of this comparison it is clear that the hybrid bridge is preferable in this situation with a weight per square meter difference of $95 \frac{kg}{m^2}$. The hybrid model is more than 23% lighter than the OSD model while still maintaining the same safety for fatigue.

The only section where the hybrid model shows lesser results than the OSD model in this case is deflection. It is still well within the allowable boundaries but it can be expected that the hybrid model will show a unity check larger than 1.0 for bigger spans. This does not have to be an issues for highway bridges since deflection is only a criterion if bicycle or footpaths are on the same bridge or if it is necessary for ship clearance.

There are however other factors that are considered in the choice for a certain bridge type. These are among others the costs of the bridge and the environmental impact. These factors will both be elaborated in paragraph 7.3.





6.4 Conclusion

Optimizing a model is an extensive job to find the most optimal model. Since this analysis is used in an early design stage there is opted for a more simplistic optimization. This optimization will focus on a few predefined parameters and will alter them depending on the results from the analysis. A fixed amount of iterations will be done for each of the models, each iteration a few parameters will be altered to optimize the model.

Optimization of the sandwich panel is not included. If the buckling factor of the sandwich panel is critical a new buckling analysis must be conducted to be able to analyse a model with a different sandwich panel.

The optimization will be done with the results from the fatigue analysis since it is expected this will be leading. A unity check on the standard load cases will be done to verify this.

If the fatigue damage is higher than 1.0 is an optimization is done depending on which fatigue detail causes damage. For each detail a different parameter will be changed, mainly focussing on the flanges of the main girder and crossbeam. If the analysis result in a damage below 1.0 a reduction of material will be made to minimize material use while still maintaining a unity check below 1.0 for the standard load cases.

The results from both of the model analyses can be compared after the optimization. A comparison has been made between the two bridge types for an exemplary situation with a span of 12 meters and two traffic lanes. With weight being the main focus of this comparison it showed a clear advantage for the hybrid bridge with a difference in weight of $95 \frac{kg}{m^2}$. Deflection is however one of the weak points of the hybrid bridge and might result in a negative recommendation for the hybrid bridge in larger spans.









7

Comparison of results

To be able to answer the research question, shown below, it is necessary to run multiple simulations with different general parameters.

For which dimensions of movable highway bridges in the Netherlands is a hybrid bridge favourable as opposed to an orthotropic steel deck bridge when comparing weight?

The different general parameters will be stated in the first paragraph with an elaboration on the choices. The second paragraph will show the results of the simulations for both the OSD and the hybrid bridges. The final paragraph shows the comparison between the two different bridge types.

7.1 Simulation parameters

Currently most of the highway bridges in the Netherlands have two lanes (12 bridges) in both directions, some have three (4 bridges) and very few (2 bridges) have more than that (see chapter 2.1 Table 2.1). However, the vehicle fleet in the Netherlands is growing every year (Table 7.1), which means that chances are high that bridges will be extended during renovation to carry three traffic lanes. Therefore both two lane and three lane bridges will be considered. Bridges with 4 lanes are expected to be split in two bridges with two lanes instead of one bridge with 4 lanes.

Table 7.1 Vehicles in the Netherlands (CBS, 2019)

Year	Number of vehicles
2015	10 757 655
2016	10 908 581
2017	11 076 215
2018	11 287 017
2019	11 495 837





Using the data obtained from Rijkswaterstaat (Annex B) a set of general parameters can be created. Three different spans will be compared for the same number of lanes. An overview of the different parameters can be found in Table 7.2.

Table 7.2 General bridge parameters for comparison

Case number	Span [m]	Width [m]	main girder location [m]	Height [m]
1	12	9.6 (2 lanes)	1.4 - 6.8	1.0
2	15	9.6 (2 lanes)	1.4 - 6.8	1.0
3	20	9.6 (2 lanes)	1.4 - 6.8	1.0
4	12	12 (3 lanes)	1.8 - 8.4	L_tot/15
5	15	12 (3 lanes)	1.8 - 8.4	L_tot/15
6	20	12 (3 lanes)	1.8 - 8.4	L_tot/15
7	12	12 (3 lanes)	1.8 - 8.4	L_tot/17
8	15	12 (3 lanes)	1.8 - 8.4	L_tot/17
9	20	12 (3 lanes)	1.8 - 8.4	L_tot/17

For each of the analysis the maximum deformation will be set at total bridge length (span plus distance to pivot point) divided by 250. Although this unity check is not of significant importance since there is no actual deformation limit it does give a good insight on the performance of the bridge. Other results that will be shown are the fatigue damages for each of the details, the buckling factor (for the hybrid model) and the weight of the model as shown in the example in Table 6.11.





7.2 Results

The results will be given for both the OSD bridge and the hybrid bridge. Remarkable results will be elaborated.

7.2.1 OSD

The results for the nine different configurations of the OSD bridge can be found in Table 7.3. Remarkable results have been coloured orange and will be elaborated in this paragraph. This includes fatigue damage in the stiffeners, the weight per square meter and the width of the main girder flanges.

Table 7.3 OSD bridge configuration results

Case number	1	2	3	4	5	6	7	8	9
Iterations	10	5	8	10	9	9	10	10	10
UC LM1a	0,295	0,358	0,503	0,354	0,320	0,266	0,426	0,381	0,313
UC LM1b	0,143	0,169	0,217	0,163	0,147	0,119	0,194	0,172	0,139
UC LM2	0,246	0,297	0,421	0,295	0,268	0,222	0,355	0,319	0,262
UC L4	0,108	0,149	0,233	0,133	0,137	0,128	0,161	0,163	0,151
UC max	0,295	0,358	0,503	0,354	0,320	0,266	0,426	0,381	0,313
Fat dam mg fl	0,518	0,654	0,658	0,854	0,860	0,955	0,852	0,849	0,908
Fat dam cb fl	0	0	0	0	0	0	0	0	0
Fat dam cb web	0,258	0,461	0,464	0,375	0,553	0,167	0,433	0,564	0,159
Fat dam stif	0,920	1,025	1,019	1,017	1,103	1,142	1,179	1,063	1,091
Fat max	0,920	1,025	1,019	1,017	1,103	1,142	1,179	1,063	1,091
model weight [kg]	47507	61918	89881	59004	77523	116193	58521	76926	116380
model weight [kg/m2]	423	441	479	410	431	484	406	427	485
width mg flange [m]	0,500	0,580	0,730	0,540	0,570	0,710	0,580	0,62	0,79
thickness mg flange [m]	0,050	0,058	0,073	0,054	0,057	0,071	0,058	0,062	0,079
thickness cb flange [m]	0,012	0,012	0,012	0,012	0,012	0,012	0,012	0,012	0,012
width cb flange [m]	0,220	0,380	0,530	0,240	0,340	0,310	0,240	0,38	0,34
thickness stiffener [m]	0,008	0,008	0,008	0,008	0,008	0,008	0,008	0,008	0,008
width bottom stiffener [m]	0,210	0,210	0,210	0,210	0,210	0,210	0,210	0,21	0,21
fat dam stif lane 1	0,822	0,926	0,947	0,887	1,043	1,142	0,820	0,979	1,091





7.2.1.1 Fatigue damage stiffeners

The fatigue damage in the stiffeners shows two anomalies. All cases, except case 1, show fatigue damage higher than 1.0 for the connection between the stiffener and crossbeam which was not expected for these dimensions of the stiffener. As it turned out this damage occurred due to overtaking traffic, which is something that was not expected for a local detail.

The other anomaly is given in the bottom row of Table 7.3 which show the damage when all vehicles are on one lane and overtaking traffic is not considered. This shows damages below 0.9 for cases 4 and 7 which have a span of 12 meter. Cases 5 and 8 show damages close to 1.0 in lane 1 and higher damages when combining lanes 1 and 2. Cases 6 and 9 show damages above 1.0 even if only lane 1 is considered. This implies that not only overtaking vehicle but also the span of the bridge influences this local detail, something that is often not considered.

Both anomalies will be investigated and results will be explained below. Besides these anomalies it is worth to mention that it is often tried to circumvent this detail by creating a cope hole in the crossbeam. However, due to the limited height of these bridges this is not an option and a weld has to be made which is prone to fatigue failure.

Highest damage during overtaking

This anomaly will be explained with the results from case 4. The highest damage occurs for lane 1 with 10% of the time a vehicle on lane 2 as shown in Table 7.4 (indicated by "lane1&2").

Table 7.4 OSD stiffener results case 4 per lane						
		Lane 2&1	0,218	Lane 3&2	0,122	
Lane 1	0,887	Lane 2	0,000	Lane 3	0,000	
Lane 1&2	1 017	Lane 2&3	0.122	Lane 3&4	0.000	

Often engineering firms do not determine such local detail stresses from global models. Instead a small model is created in the same way as the buckling analysis for the sandwich panel (Paragraph 4.2.3) and only one lane or even just a few stiffeners are modelled. This way a second vehicle on the lane next to it is not modelled. This is done with the thought that the second vehicle is to far from the detail location to have any significant influence on this detail.

However results showed that damage in the stiffener is higher when overtaking is considered for all cases except case 6 and 9. This insinuates that this detail cannot be analysed with a local model which is often done. A closer look into the influence line will give a better understanding of the underlying reason, this has been done for vehicle three which turned out





to be most damaging. Figure 7.1 shows the influence lines of vehicle three for lane 1 and for lane 1 and 2 (during overtaking).

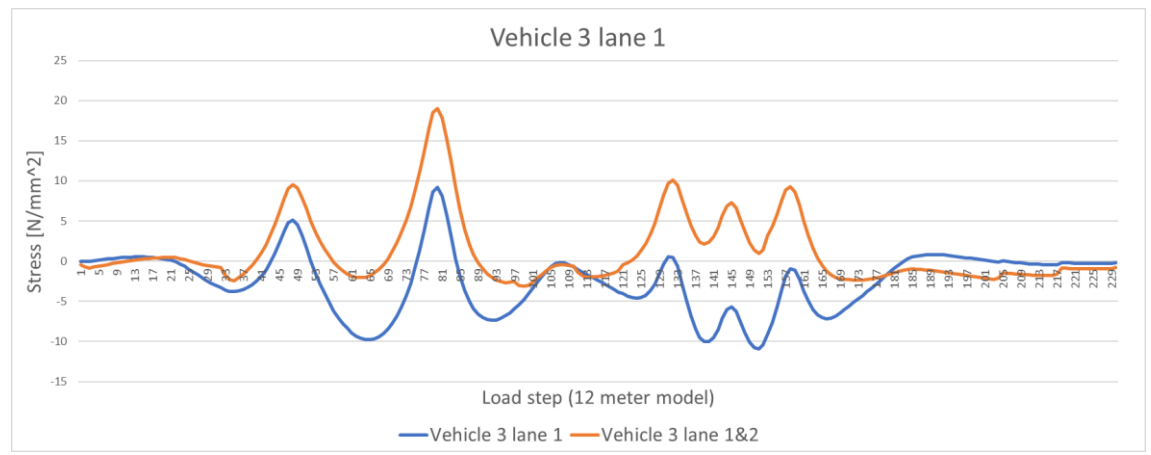


Figure 7.1 OSD detail 1 vehicle 3 lane 1 and lane1 and 2 combined

This figure shows that the combination of lanes 1 and 2 results in higher stresses overall which can be accounted for by the global deflection due to the presence of two vehicles on the bridge. The local effect of this is that the highest stress range that occurs in the bridge is $20.11 \frac{N}{mm^2}$ for lane 1 and $22.16 \frac{N}{mm^2}$ for lane 1 and 2 combined.

This increase in stress range is due to the fact that the vehicle in lane two causes a new lowest point which does not occur next to the fourth wheel (fourth peak) but in between the first and second peak. This new lowest point is primarily caused by wheels two and three from the vehicle on the second lane as shown in Figure 7.2.

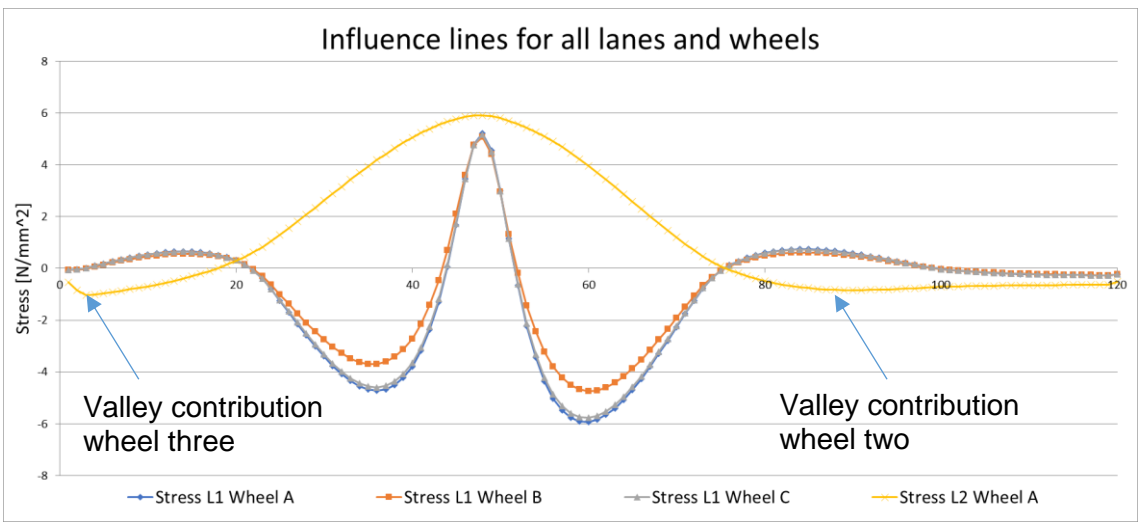


Figure 7.2 OSD detail 1 wheel influence lines

It can be concluded that it is necessary to test this detail with the presence of overtaking vehicles. The effect of neglecting this effect is an underestimate of the damage that will occur during the lifetime of the bridge. The damage that occurs now is higher than 1.0 however this





Results

does not mean that the stiffener will fail. The frequency distribution, see Figure C.5, is not included in this calculation and will have significant effects on a local detail.





Higher damage for bigger spans

Figure 7.3 shows the influence line of vehicle three in lane one of cases 4 and 5 with a span of 12 and 15 meters respectively. The influence line of case 5 has been shifted along the X axis to ensure the wheels transit the crossbeam at the same moment. It is clear that the stresses in the bigger span are lower overall. The maximum stress range in the 12m span is $20.11 \frac{N}{mm^2}$ and in the 15m span it is $20.78 \frac{N}{mm^2}$. The higher stress range explains the higher damage, however a closer look into the influence lines of the wheels is needed to explain this higher stress range.

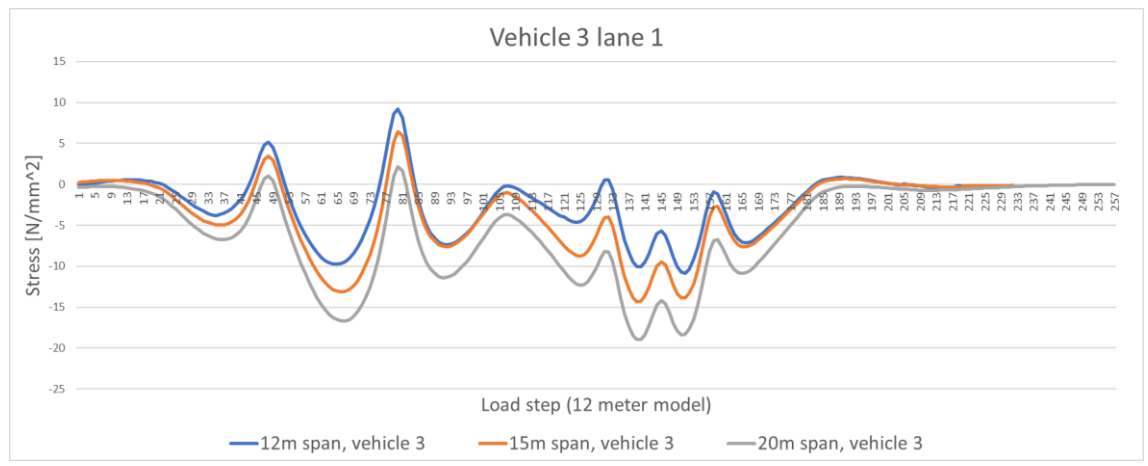


Figure 7.3 OSD detail 1 vehicle 3 lane 1 spans 12, 15 and 20

The influence lines of wheel A for bridge cases 4, 5 and 6 are shown in Figure 7.4. It shows the same distinct pattern around the location of the connection but for the larger spans the stresses move towards complete compression which is due to lowering of the neutral axis.

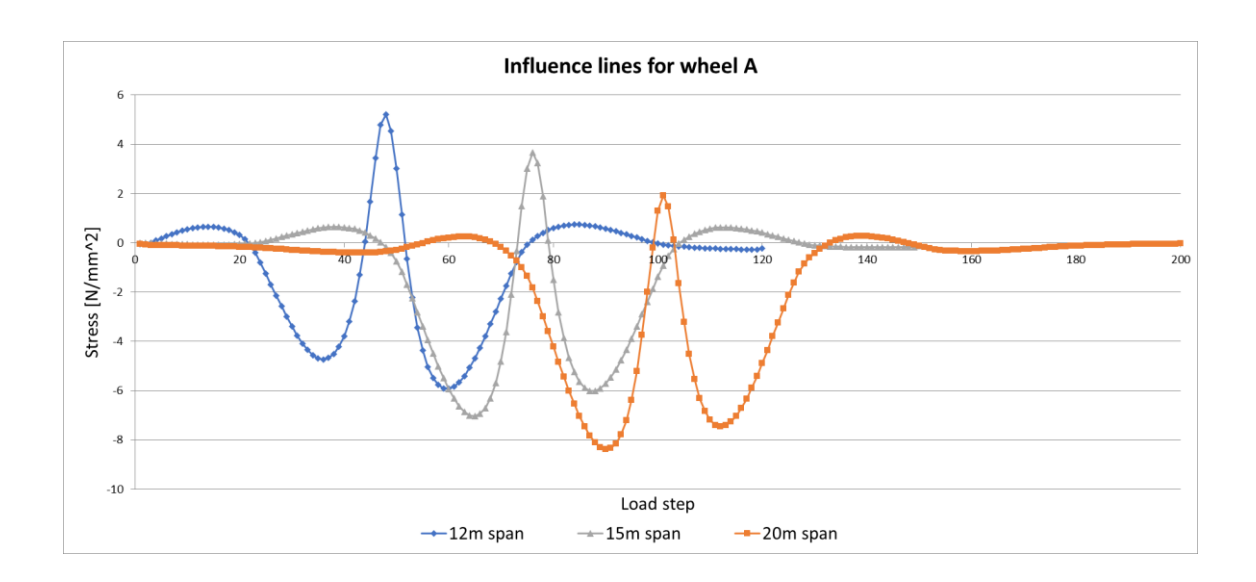






Figure 7.4 OSD detail 1 wheel A spans 12, 15 and 20

The maximum occurring stress ranges have been investigated for both the wheel influence lines and vehicle 3 influence lines. This showed odd results, the maximum stress range for the wheels decreased for longer spans, however for the vehicle influence line increased as is shown in Table 7.5.

Table 7.5 OSD stiffener stress ranges case 4 - 6

Maximum stress range	Wheel influence line	Vehicle 3 influence line
12m span	11.11 <i>MPa</i>	19.02 <i>MPa</i>
15m span	10.69 <i>MPa</i>	20.70 MPa
20m span	10.29 <i>MPa</i>	21.12 <i>MPa</i>

This means that the biggest stress range in the influence line is a result of wheel combinations for this vehicle and not the result of one wheel. Figure 7.5 shows the influence lines of each wheel of vehicle three for the case with a 20m span. It can be seen that the influence of the first two wheels (blue and orange) reach as far as the valley of the third wheel which causes the biggest valley in the influence line. This is not the case for the smallest bridge (12m span) and for the 15m span this effect only holds for the second wheel and not the first. This very minor influence does however result in a higher stress range for the bigger bridge span which in turn causes higher fatigue damage.

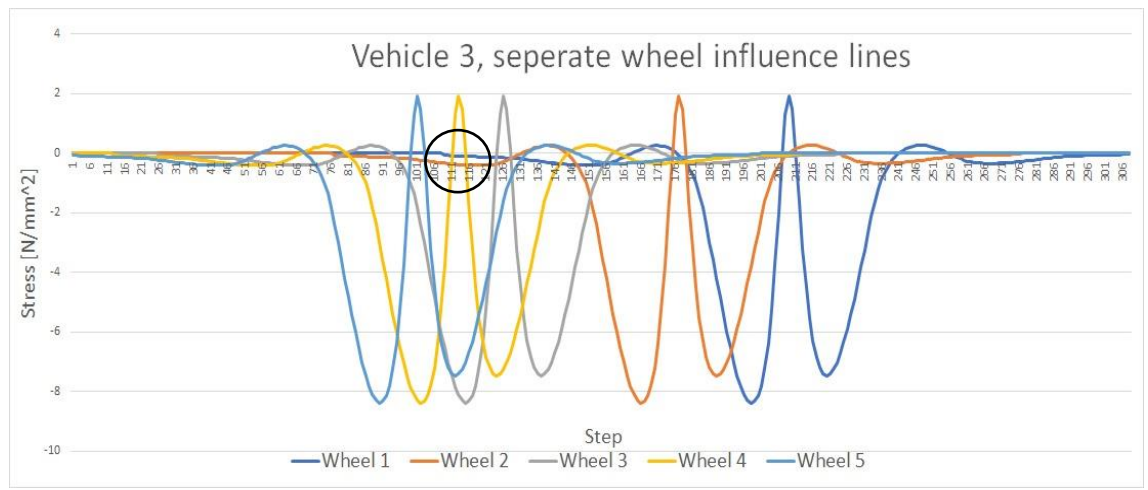


Figure 7.5 OSD detail 1 vehicle 3 separate wheel influence lines





7.2.1.2 weight per square meter

The weight per square meter is a good indicator of the efficiency of the material, the lower the better. If the bridge span increases the material needed per square meter increases to prevent high stresses and deformations. However, it seems that the width of the model does not influence the material per square meter that is needed for the smaller spans. A slight decrease can even be observed for the smaller spans $\left(\sim 10\frac{kg}{m^2}\right)$.

The difference in height of cases 4 to 6 and cases 7 to 9 has very little effect on the weight per square meter (compare case 4 with 7, 5 with 8 and 6 with 9). It can however be seen that the usage of material has changed slightly, for the higher bridges (4 to 6) there is more material in the crossbeam than there is for the bridges with les height (7 to 9) as shown in Table 7.6.

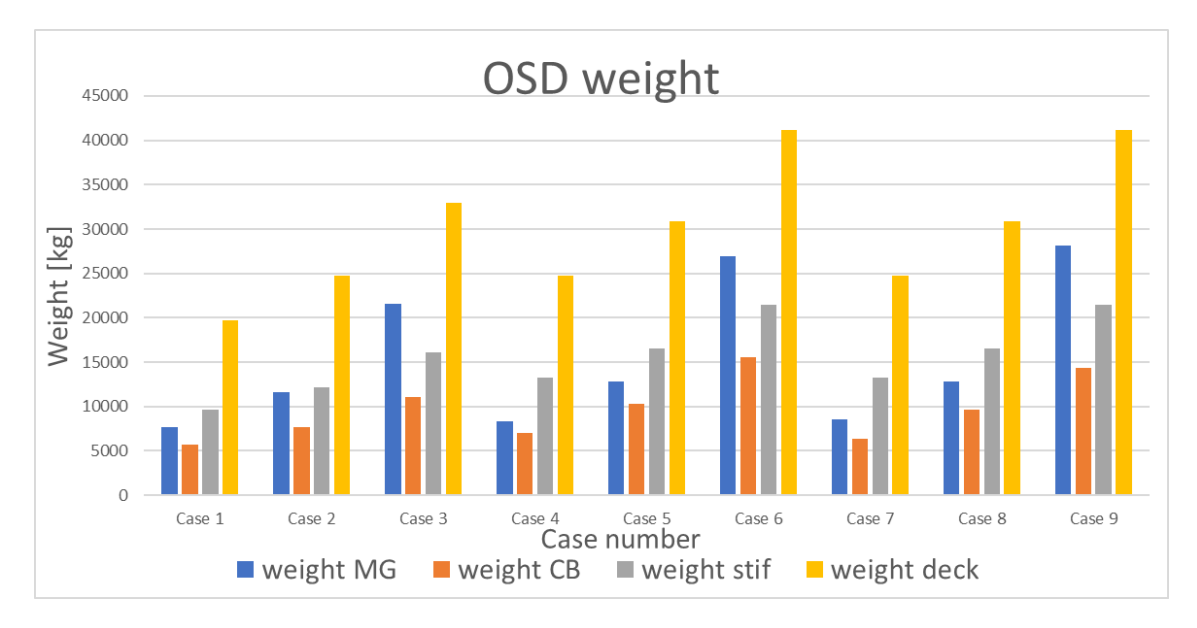
Case 1 Case 3 Case 8 Case number Case 2 Case 4 Case 5 Case 6 Case 7 Case 9 Span [m] Width [m] 9,6 9,6 9,6 0,97 1,03 1,32 Height [m] 1,17 1,5 0,85 kg/m^2 Tot weight weight MG weight CB weight stif weight deck

Table 7.6 OSD weight per part

The weight distribution per part is shown in Figure 7.6 in absolute values and percentages. Although the dimensions of the main girder and crossbeams differ in each of the cases it is clear that the highest impact of weight comes from the deck plate and stiffeners. The dimensions of the deck plate are however fixed and cannot be lower than 22 mm according to Eurocode (Table C.7). A reduction of this thickness is allowed if calculations show it is safe. Further investigation on this thickness useful since a reduction in thickness will have a big influence on the total weight of the bridge.







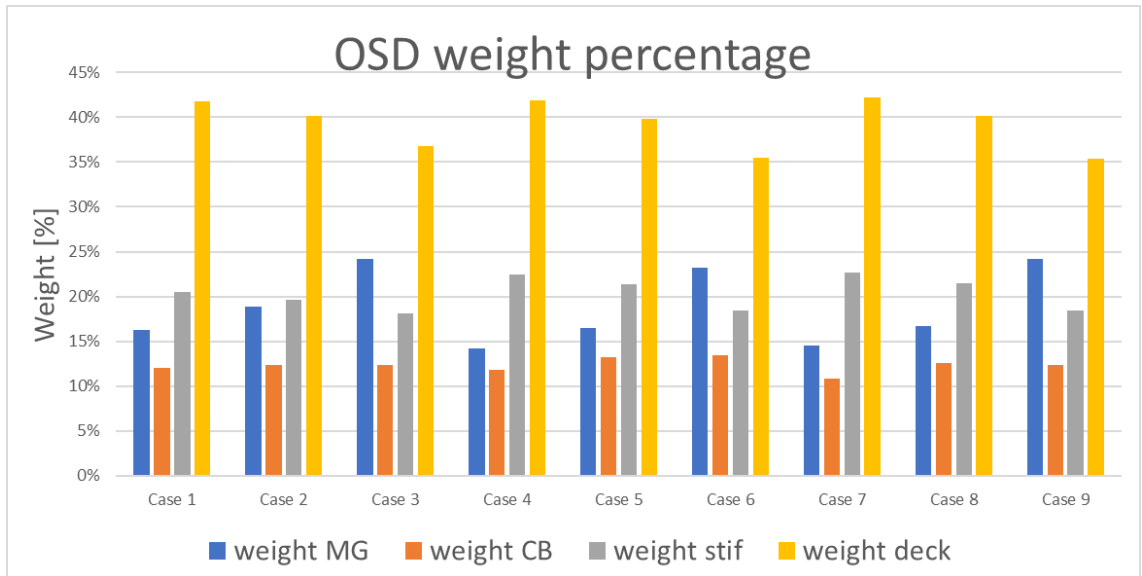


Figure 7.6 OSD weight distribution in absolute values and percentages

7.2.1.3 Width main girder flange cases 2,3 and 5,6

The main girder flange of cases 2 and 5 almost have the same size and the dimensions of the crossbeams are even lower for case number 5. For a bridge that is bigger both in span and width this is an unexpected result. This difference can be rectified by looking at the height of the bridge. For cases 5 and 6 this is 1.17 and 1.5 meter respectively whereas cases 2 and 3 have a height of 1 meter. This difference makes the main girder and crossbeam flanges far more effective in cases 5 and 6 since they result in a higher section modulus.





7.2.2 Hybrid

The results for the nine different configurations of the OSD bridge can be found in Table 7.7. Remarkable results have been coloured orange and will be elaborated in this paragraph. Remarkable results include the buckling factor and the weight per square meter.

Table 7.7 Hybrid bridge configuration results

Case number	1	2	3	4	5	6	7	8	9
Span [m]	12	15	20	12	15	20	12	15	20
Width [m]	9,6	9,6	9,6	12	12	12	12	12	12
Height [m]	1	1	1	0,97	1,17	1,5	0,85	1,03	1,32
UC LM1a	0,460	0,522	0,690	0,548	0,485	0,422	0,682	0,578	0,509
UC LM1b	0,314	0,323	0,372	0,355	0,297	0,236	0,419	0,339	0,271
UC LM2	0,380	0,431	0,576	0,453	0,399	0,350	0,563	0,476	0,422
UC L4	0,114	0,169	0,299	0,147	0,152	0,160	0,193	0,190	0,201
UC max	0,460	0,522	0,690	0,548	0,485	0,422	0,682	0,578	0,509
Fat dam mg fl	0,568	0,671	0,706	0,771	0,870	0,860	0,957	0,855	0,859
Fat dam cb fl	0,165	0,198	0,589	0,159	0,084	0	0,645	0,252	0
Fat dam cb web	0	0	0	0	0,117	0,120	0,000	0,104	0,103
Fat max	0,568	0,671	0,706	0,771	0,870	0,860	0,957	0,855	0,859
Buckling factor	2,43	2,32	2,07	2,33	2,34	2,29	2,24	2,26	2,2
model weight [kg]	37832	49542	77187	45365	55255	80020	46367	57765	81005
model weight [kg/m2]	328	344	402	315	307	333	322	321	338
width mg flange [m]	0,710	0,800	1,000	0,790	0,770	0,790	0,860	0,850	0,880
thickness mg flange [m]	0,071	0,080	0,100	0,079	0,077	0,079	0,086	0,085	0,088
thickness cb flange [m]	0,012	0,012	0,012	0,014	0,012	0,011	0,020	0,012	0,012
width cb flange [m]	0,220	0,220	0,190	0,270	0,240	0,270	0,190	0,260	0,220





7.2.2.1 Buckling factor

The buckling factor for the FRP web is close to one which is unusual for buckling. As a rule of thumb a factor of 10.0 is used for steel plates to ensure that a linear buckling analysis is valid. However for FRP a different minimal buckling factor should be used and can be determined using the CUR. Equation (7.1) shows the equation that is stated in the CUR to determine the critical buckling factor.

$$\lambda_{cr} = \frac{1}{\alpha * \frac{\eta_c}{\gamma_M}} \tag{7.1}$$

where

 $\alpha = reduction factor determined by tests$ $\eta_c = \eta_{ct} * \eta_{cm} * \eta_{cv} * \eta_{cf} = conversion factor$ $\gamma_M = \gamma_{M1} * \gamma_{M2} = material factor$

Since it is simple plate buckling a reduction factor of 1.0 can be used. The conversion factor depends on four other factors namely, temperature, moisture, creep and fatigue. For buckling all factors have to be taken into account. For creep a factor of 1.0 in the case of short term loads such as LM1a. The other factors are al 0.9 for this situation according to the CUR. The resulting conversion factor is 0.73 as shown in equation (7.2).

$$\eta_c = \eta_{ct} * \eta_{cm} * \eta_{cv} * \eta_{cf}
\eta_{ct} = 0.9, \eta_{cm} = 0.9, \eta_{cv} = 1.0, \eta_{cf} = 0.9
\eta_c = 0.9 * 0.9 * 0.44 * 0.9 = 0.729$$
(7.2)

The material factor can be .

$$\gamma_M = \gamma_{M1} * \gamma_{M2} = 1.15 * 1.35 = 1.5525 \tag{7.3}$$

As shown in equation (7.4) this results in a critical buckling factor of 2.13 to ensure a safe design for a hundred years.

$$\lambda_{cr} = \frac{1}{\alpha * \frac{\eta_c}{\gamma_M}} = \frac{1}{1 * \frac{0.73}{1.55}} = 2.126$$
 (7.4)

This criterium has not been met for each of the cases (case number 3 is 2.07) so the webs must be strengthened to prevent buckling. Adding two millimetres to the webs making them 8 millimetres thick should result in better bucking behaviour.





This increase in thickness results in an increase in the values of the D-matrix which in turn increase the critical buckling stress. As a result an increase of the critical buckling stress can be found as shown in equation (7.5).

$$\begin{split} D_{11} &= 1230191, D_{22} = 700352, D_{12} = 239639, D_{66} = 246677 \\ t &= 8 \ mm, b = 180 \ mm \\ \sigma_{cr,\text{new}} &= \frac{\pi^2}{tb^2} * \left[4.53 \sqrt{D_{11}D_{22}} + 2.44 (D_{12} + 2D_{66}) \right] = 228.21 \ \text{MPa} \\ \sigma_{cr,old} &= 128.37 \ MPa \\ increase &= \frac{228}{128} = 1.78 \\ \lambda_{cr} &= 2.13 * 1.78 = 3.78 \end{split} \tag{7.5}$$

The buckling factor is linearly dependent on the critical buckling stress which means that this increase of 2 millimetres will increase the buckling factor with almost a factor 2. The new critical buckling factor of 3.78 will ensure safety.

If this increase in the web thickness is necessary it will not change the results of the global weight analysis drastically. An increase of 2 mm results in an increase of weight per square meter of $8.5 \frac{kg}{m^2}$ as shown in equation (7.6).

weight increase =
$$\frac{1m \ (width)}{d_{web}} * h_{sp} * t_{web,extra} * 1m \ (length) * \rho$$

= $\frac{1}{0.08} * 0.18 * 0.002 * 1 * 1885 = 8.5 \frac{kg}{m^2}$ (7.6)

7.2.2.2 Weight per square meter

The general expectation is that an increase in span leads to an increase of the material needed per square meter. However case 5 shows a decrease in material needed as opposed to case 4. The reduction in material mainly comes from reduced dimensions of the main girder in case 5, which implies that the fatigue detail in the main girder is leading. A closer look in both cases showed that the crossbeams in the model were oriented in such a way that the fatigue detail in case 5 was in a different location than in case 4.

This is shown in Figure 7.7 by the blue circle with all values given in meters. In case 4 the detail is almost exactly in midspan of the bridge whereas in case 5 it deviates from midspan by 1.25 meter. This results in decreased stresses in this detail which in turn causes smaller damages. This makes it possible to have smaller main girder flanges which decreases the necessary material drastically.





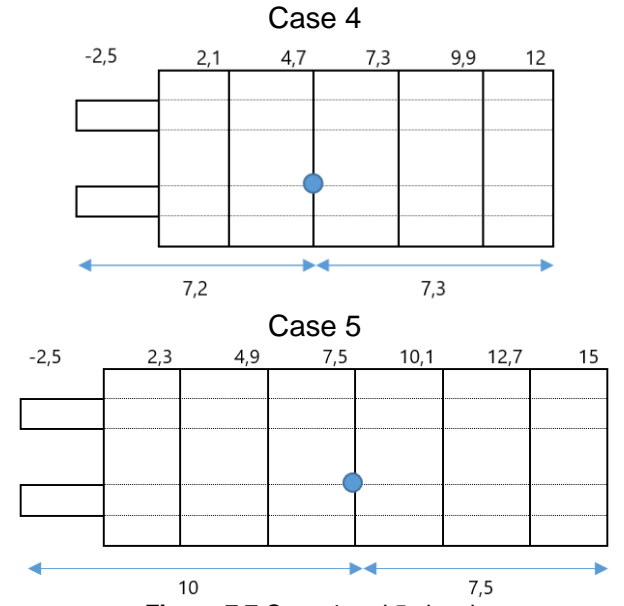


Figure 7.7 Case 4 and 5 sketch

Looking back at the OSD cases the same effect can be observed. The main girder flanges of case 5 are still bigger than case 4 but the difference is far less (30 mm) than between case 5 and 6 (140 mm). The same effect can be observed in both bridge types for cases 6 to 9. For the first three case s this effect cannot be observed as clearly which is due to the constant height whereas cases 4 to 9 have different heights depending on the span.

These results show that the location of the crossbeams have significant effects on the material that is necessary in a bridge. Creating bridges with an odd amount of crossbeams ensures that there is no crossbeam in midspan. Due to this the crossbeam to main girder connection is relocated to a location with lower stresses in the main girder flange which makes it possible to use less material.

Further research is needed to determine if it is worthwhile to change the distance between crossbeams to prevent an even number of crossbeams. Increasing this distance results in larger spans between crossbeams which in turn might create higher stresses in certain locations. Decreasing the distance would result in an extra crossbeam. Both options will decrease the needed amount of material in the main girder but increase material needed in other places such as the stiffeners or crossbeams. Whether the decrease of material in the main girders outweighs the increase in other parts must be investigated.





7.3 Comparison

Both models have been optimized to create a bridge with the lowest weight possible whilst still fulfilling all Eurocode norms. The results can now be compared to decide which bridge is better in terms of overall weight. Besides weight other factors play a role in the decision making process such as the price of the bridge and the environmental impact it has. Both of these factors will be elaborated in a simple way just to give an indication of the costs and the environmental impact.

From these three factors a decision can be made to do a more detailed analysis for one of the bridge types. These decisions will be summarised in a table together with a clear overview of the results of the factors for both bridge types. This table should lead to an answer on the research question:

For which dimensions of movable highway bridges in the Netherlands is a hybrid bridge favourable as opposed to an orthotropic steel deck bridge when comparing weight?





7.3.1 Weight comparison

Both bridge types have been optimized for weight and results can be compared using the data given in paragraph 7.2. The results have been summarised in Table 7.8. This table shows the overall dimensions of the bridge and the associated allowable deflection. The given unity check (UC) it for deflection. The fatigue damage is the maximum occurring fatigue damage without the stiffeners taken into account for the OSD bridge. The final rows show the weight per square meter and the percentual difference between the OSD and hybrid bridge.

Table 7.8 Weight comparison OSD vs hybrid

Case number	Case 1	Case 2	Case 3	Case 4	Case 5	Case 6	Case 7	Case 8	Case 9
Span [m]	12	15	20	12	15	20	12	15	20
Width [m]	9,6	9,6	9,6	12	12	12	12	12	12
Height [m]	1	1	1	0,97	1,17	1,5	0,85	1,03	1,32
Allowable deflection [mm]	58	70	90	58	70	90	58	70	90
OSD_UC_max	0,295	0,358	0,503	0,354	0,320	0,266	0,426	0,381	0,313
Hybrid_UC_max	0,460	0,522	0,690	0,548	0,485	0,422	0,682	0,578	0,509
OSD_fat_max	0,518	0,654	0,658	0,854	0,860	0,955	0,852	0,849	0,908
Hybrid_fat_max	0,568	0,671	0,706	0,771	0,870	0,860	0,957	0,855	0,859
Hybrid_buckling factor	2,43	2,32	2,07	2,33	2,34	2,29	2,24	2,26	2,2
OSD_weight [kg/m2]	423	441	479	410	431	484	406	427	485
Hybrid_weight [kg/m2]	328	344	402	315	307	333	322	321	338
Weight difference [kg/m2]	95	97	77	95	124	151	84	106	147
Weight difference [%]	22%	22%	16%	23%	29%	31%	21%	25%	30%

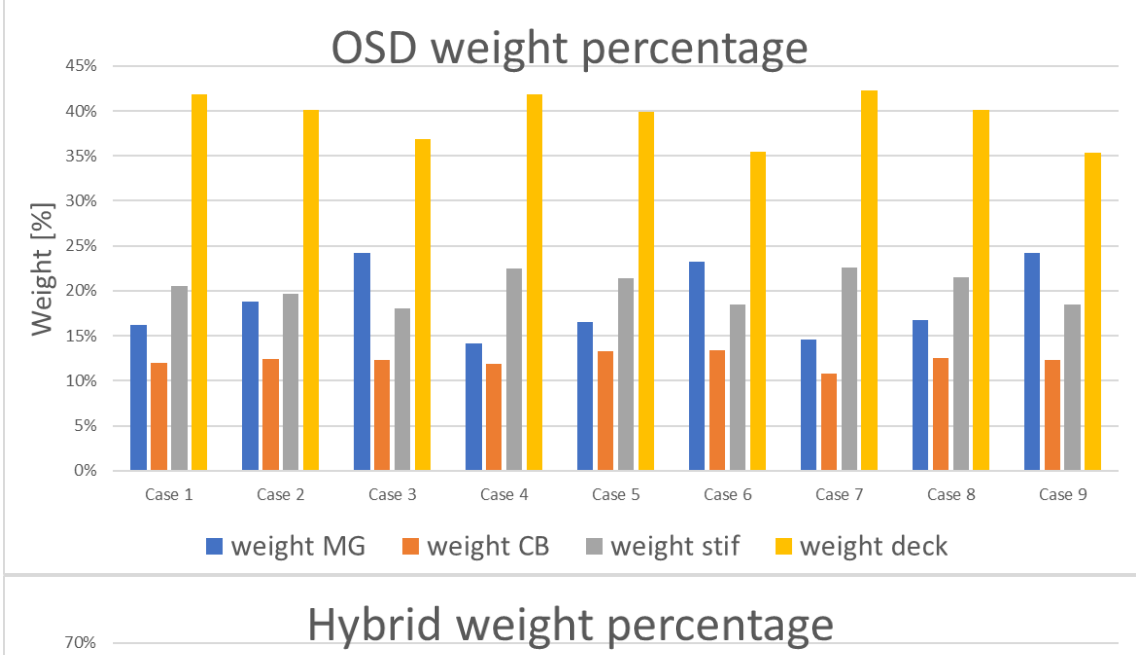
These results show a clear favour towards the hybrid bridge with a reduction of weight ranging from 15% to 30%. The weight saving occurs in the deck structure of the bridge. For OSD bridges this deck consists of a steel plate and stiffeners which make up more than half of the total weight of the structure For the hybrid bridge the deck structure consists only of the FRP sandwich panel which only makes up 20% of the total weight. An overview of this data can be found in Table 7.9 and Figure 7.8.

This reduction of up to 30% shows that it is worthwhile to invest time into the design of a hybrid steel-FRP bridge instead of an OSD bridge.





Table 7.9 OSD and hybrid weight distribution													
OSD													
kg/m^2	410	428	466	410	431	484	406	427	485				
Tot weight	47266	61617	89479	59004	77523	116193	58521	76926	116380				
weight MG	7675	11616	21618	8364	12804	26960	8525	12851	28121				
weight CB	5679	7632	11025	7065	10339	15770	6391	9736	14557				
weight stif	9934	12418	16557	13246	16557	22076	13246	16557	22076				
weight deck	19768	24710	32947	24710	30888	41184	24710	30888	41184				
HYBRID													
kg/m^2	328	344	402	315	307	333	322	321	332				
Tot weight	37832	49542	77187	45365	55255	80020	46367	57765	79657				
weight MG	18502	27361	50834	21408	26544	40366	23866	29989	44224				
weight CB	5841	6814	8518	7829	9867	15374	7514	9107	13748				
weight FRP	8339	10423	13898	10423	13029	17372	10423	13029	17372				
weight Foam	1534	1918	2557	1918	2398	3197	1918	2398	3197				



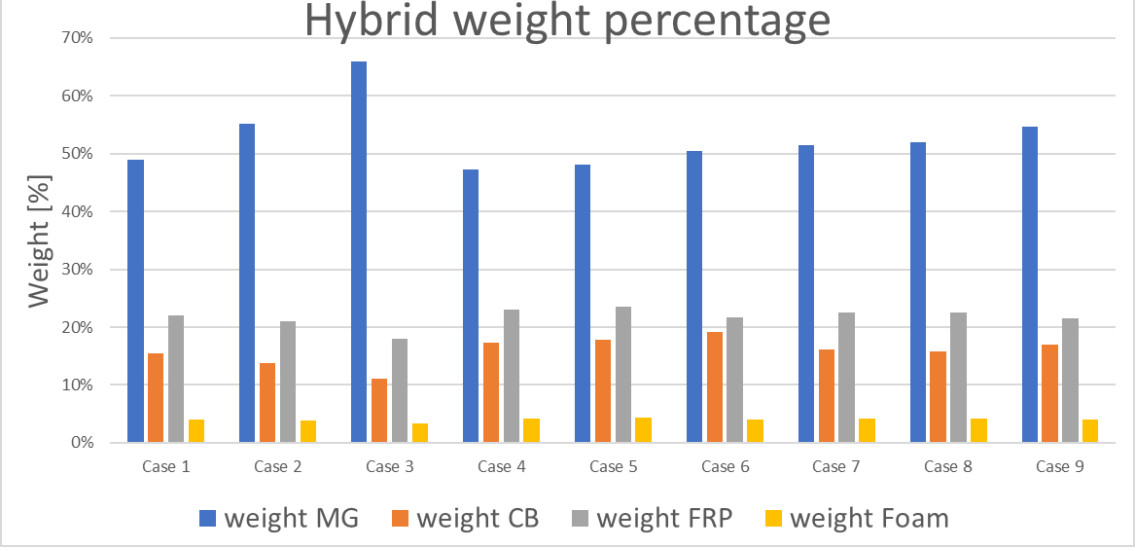


Figure 7.8 OSD and hybrid weight distribution





7.3.2 Cost comparison

Creating a clear estimate of the costs for a bridge are difficult in an early design stage. It depends on many factors such as the location, transportation, dimensions, production process and more. An indicative value will be determined mainly on the material and production costs. Estimating further costs depends on to many different factors and will not be elaborated in this thesis.

The weight for each material in both bridges has been split up as shown in Table 7.10. An estimate weight of the ballast has been determined by multiplying the weight of the bridge leaf by 1.5. This information can be used to determine a cost estimate with indicative cost values. These values are often used in the pre-design phase, the end values can deviate from these indicative values.

Case 1 Case 2 Case 3 Case 4 Case 5 Case 6 Case 7 Case 8 Case 9 Span [m] Width [m] 9,6 9,6 9,6 0,85 1,03 0.97 1.17 1,5 1.32 Height [m] (total) OSD bridge steel [kg] OSD bridge balast [kg] Hybrid FRP [kg] Hybrid foam [kg] Hybrid steel [kg] Hybrid bridge balast [kg]

Table 7.10 Cost comparison material weight

The cost indicative value for steel in the leaf is $\in 5$, -/kg which includes welding and manufacturing costs. For the steel used in the ballast a value of $\in 2,50/kg$ will be used since manufacturing costs are lower and cheap steel can be used. These value are used by engineers in an early design stage. Such a value is difficult to determine for FRP due to a lack of experience.

Therefore a price will be determined by using the reference case "Leeghwaterbrug" (paragraph 2.2.3.4). The FRP sandwich panel had a cost of $\&pmath{\in}800$, $-/m^2$ including the bolted connection that has been used. The sandwich panel from the models uses slightly more material and a different connection method is needed to ensure full hybrid interaction. Therefore a conservative square meter price of $\&pmath{\in}1200$, $-/m^2$ will be used.

The costs for each part as well as a cost per square meter can be found in Table 7.11 for both bridge types. At the bottom the difference is shown in percentages.





Table 7.11 Cost comparison results

	Case 1	Case 2	Case 3	Case 4	Case 5	Case 6	Case 7	Case 8	Case 9
Span [m]	12	15	20	12	15	20	12	15	20
Width [m]	9,6	9,6	9,6	12	12	12	12	12	12
Height [m] (total)	1	1	1	0,97	1,17	1,5	0,85	1,03	1,32
Steel	€ 237.535	€ 309.591	€ 449.403	€ 295.020	€ 387.615	€ 580.965	€ 292.605	€ 384.630	€ 581.900
Steel balast	€ 178.151	€ 232.193	€ 337.053	€ 221.265	€ 290.711	€ 435.724	€ 219.454	€ 288.473	€ 436.425
Steel per m2	€ 2.062	€ 2.150	€ 2.341	€ 2.049	€ 2.153	€ 2.421	€ 2.032	€ 2.137	€ 2.425
Steel per m2 with balast	€ 3.608	€ 3.762	€ 4.096	€ 3.585	€ 3.768	€ 4.236	€ 3.556	€ 3.739	€ 4.243
Steel	€ 139.797	€ 186.001	€ 303.659	€ 165.121	€ 199.141	€ 297.255	€ 170.130	€ 211.692	€ 302.181
Sandwich panel	€ 138.223	€ 172.779	€ 230.372	€ 172.779	€ 215.974	€ 287.965	€ 172.779	€ 215.974	€ 287.965
Steel balast	€ 141.872	€ 185.781	€ 289.451	€ 170.120	€ 207.206	€ 300.075	€ 173.878	€ 216.619	€ 303.769
Hybrid per m2	€ 2.413	€ 2.492	€ 2.781	€ 2.347	€ 2.306	€ 2.438	€ 2.381	€ 2.376	€ 2.459
Hybrid per m2 with balast	€ 3.645	€ 3.782	€ 4.289	€ 3.528	€ 3.457	€ 3.689	€ 3.589	€ 3.579	€ 3.725
Difference without balast	17%	16%	19%	15%	7%	1%	17%	11%	1%
Difference with balast	1%	1%	5%	-2%	-8%	-13%	1%	-4%	-12%

It shows that for each case the hybrid bridge is more expensive when only the bridge leaf is considered. However when the ballast is included in the cost indication it shows that the hybrid bridge is competitive and even cheaper in some cases. A difference of up to 13% can be observed in favour of the hybrid bridge where a higher difference is observed for larger spans. The maximum difference is obtained for the larger bridge spans with a considerable height (case 6 and 9). If the height is really small (case 3) the opposite effect can be observed where the cost difference grows in favour of the OSD bridge.

There are however many uncertainties in these values. These uncertainties include, among others, the costs for testing of the hybrid structure. Since it is not yet an established construction material with its own Eurocode it is often requested to provide test results. These tests can be expensive and often need samples which add to the material costs. However, when FRP is a well established construction material these costs will disappear and a prove of safety using only calculations will suffice.

All together it seems that the OSD bridge and hybrid bridge are competitive in this early design stage. However there are many uncertainties that could result in one of the bridge types being significantly more expensive than the other. More experience with FRP and the hybrid interaction is needed to create better cost indications in such an early design stage.





Comparison

7.3.3 Environmental impact comparison

Besides cost and weight the environmental impact of a bridge is considered during the decision making process. A life cycle analysis is one of many assessment methods to determine the environmental impact that a structure has. This analysis includes all stages of the life cycle from cradle to gate. For this research only a small part will be considered, namely the environmental impact of the materials that are used and their production. The Dutch method has been established by "stichting Bouwkwaliteit" which uses the "GWW" database. This method aims to quantify the environmental performance of constructions and civil engineering works (Stichting Bouwkwaliteit, 2014). Another method only looks into the CO₂ footprint and has been used in recent research conducted by the TU Delft.

Take make a good comparison an weight estimate will be made for the complete movable bridge including counterweight. As a rule of thumb the counterweight is 1.5 times as heavy as the leaf of the bridge. This can differ depending on the size of the bascule and therefore the arm that the counterweight has to the trunnion. This counterweight is often made from steel due to it's high density.

GWW method

Data from master course "Materials and Ecological Engineering" at the TU Delft has been used to determine a quantitative value for each of the designs. This value represents the cost that is needed to undo the damage that the structure causes. These costs are determined for ten categories such as global warming, ozone layer depletion and human toxicity. The shadow prize for each category together with the equivalent emissions per kilogram of material can be found in Annex I.

The results given in Table 7.12 show that for each of the cases the hybrid bridge has a lower impact value than the OSD bridge which means it is more environmentally friendly. The difference is due to the extra weight that makes up the OSD bridge which is also needed in the counterweight. The difference in weight ranges from 20% to 30%.





Table 7.12 Environmental impact (GWW) OSD vs hybrid

	Cas	se 1	Ca	se 2	Ca	se 3	Cas	se 4	Ca	se 5	Ca	se 6	Cas	se 7	Ca	se 8	Cas	se 9
Abiotic depletion	€	298	€	389	€	564	€	370	€	487	€	729	€	367	€	483	€	730
Global warming (GWP100)	€	10.864	€	14.159	€	20.554	€	13.493	€	17.728	€	26.571	€	13.383	€	17.591	€	26.614
Ozone layer depletion (ODP)	€	0	€	0	€	1	€	0	€	0	€	1	€	0	€	0	€	1
Human toxicity	€	40.466	€	52.741	€	76.559	€	50.259	€	66.033	€	98.972	€	49.848	€	65.525	€	99.131
Fresh water aquatic ecotox.	€	5.284	€	6.887	€	9.997	€	6.563	€	8.622	€	12.923	€	6.509	€	8.556	€	12.944
Marine aquatic ecotoxicity	€	15.478	€	20.174	€	29.284	€	19.224	€	25.258	€	37.857	€	19.067	€	25.063	€	37.918
Terrestrial ecotoxicity	€	225	€	293	€	426	€	280	€	367	€	551	€	277	€	365	€	552
Photochemical oxidation	€	221	€	288	€	418	€	275	€	361	€	541	€	272	€	358	€	542
Acidification	€	3.615	€	4.711	€	6.839	€	4.490	€	5.899	€	8.841	€	4.453	€	5.853	€	8.855
Eutrophication	€	1.467	€	1.912	€	2.776	€	1.822	€	2.394	€	3.589	€	1.807	€	2.376	€	3.594
Total OSD	€	77.919	€	101.555	€	147.418	€	96.776	€	127.150	€	190.574	€	95.983	€	126.170	€	190.881
Abiotic depletion	€	264	€	344	€	529	€	318	€	388	€	558	€	324	€	404	€	564
Global warming (GWP100)	€	9.838	€	12.812	€	19.628	€	11.857	€	14.489	€	20.770	€	12.086	€	15.063	€	20.995
Ozone layer depletion (ODP)	€	0	€	0	€	1	€	0	€	1	€	1	€	0	€	1	€	1
Human toxicity	€	35.479	€	46.267	€	71.170	€	42.709	€	52.150	€	74.940	€	43.563	€	54.288	€	75.779
Fresh water aquatic ecotox.	€	3.846	€	5.058	€	7.982	€	4.593	€	5.580	€	8.146	€	4.705	€	5.859	€	8.255
Marine aquatic ecotoxicity	€	11.492	€	15.099	€	23.759	€	13.738	€	16.700	€	24.334	€	14.065	€	17.518	€	24.655
Terrestrial ecotoxicity	€	181	€	237	€	369	€	218	€	265	€	384	€	222	€	277	€	388
Photochemical oxidation	€	177	€	232	€	361	€	212	€	259	€	375	€	217	€	270	€	379
Acidification	€	3.251	€	4.235	€	6.494	€	3.917	€	4.786	€	6.864	€	3.994	€	4.977	€	6.939
Eutrophication	€	1.219	€	1.593	€	2.468	€	1.464	€	1.785	€	2.576	€	1.495	€	1.863	€	2.606
Total hybrid	€	65.748	€	85.877	€	132.759	€	79.027	€	96.403	€	138.946	€	80.670	€	100.520	€	140.562

This value is not the end value of the environmental impact since transportation and installation costs should be included as well. However due to the light weight of the hybrid bridge it is safe to assume that transport and installation impacts will be lower than for the OSD bridge. Therefore the conclusion can be drawn that the hybrid bridge has a lower environmental impact than the OSD bridge with a difference of approximately 20% when only considering material and production impact. Emissions for each of the materials per bridge can be found in Annex I.

CO₂ footprint method

The CO_2 footprint method that has been used by the TU made use of LCA experts from RHDHV and data from the European eco invent database. In their research a CO_2 equivalent per tonne of material has been determined. The equivalent value for steel was 2.8 and for vacuum infused FRP it was 4.0. Using these values for the weights of both the OSD and hybrid bridge result in a CO_2 equivalent which can be compared with each other. The results are given in Table 7.13 where the weight of the PVC foam has been added to the weight of FRP.

Table 7.13 CO₂ footprint OSD vs hybrid

	Case 1	Case 2	Case 3	Case 4	Case 5	Case 6	Case 7	Case 8	Case 9
tCO2eq OSD	333	433	629	413	543	813	410	538	815
tCO2eq Hybrid	277	362	560	332	405	585	339	423	592
percentual difference	17%	17%	11%	20%	25%	28%	17%	21%	27%

Both methods show a difference in favour of the hybrid bridge with percentages ranging from 10% to 30%.





7.3.4 Conclusion

Results showed a clear favour towards the hybrid bridge for all of the spans and widths investigated when comparing weight and environmental impact. The cost of a new bridge leaf is however bigger when using a hybrid configuration instead of a steel orthotropic configuration.

The difference in weight of the hybrid bridges showed a decrease of 15 to 30% as opposed to the orthotropic option. This decrease in weight is just for the leaf which means an even bigger decrease will be observed when including the counterweight of the bascule bridge. More details about the weight and weight distribution can be found in Annex J.

The OSD bridge and hybrid bridge are competitive in pricing in an early design stage. However there are many uncertainties that could result in one of the bridge types being significantly more expensive than the other. More experience with FRP and the hybrid interaction is needed to create better cost indications in such an early design stage.

With the use of life cycle analysis established by "Stichting bouwkwaliteit" an environmental impact value has been quantified for the materials needed in the bridges. A different method that determines the CO₂ footprint has also been used. Both methods showed a difference ranging from 10% to 30% percent in favour of the hybrid bridge. This is mainly due to the large amount of steel needed for the bridge leaf which also means that more material is needed for the counterweight.





8 Conclusion

8.1 OSD or hybrid

For which dimensions of movable highway bridges in the Netherlands is a hybrid bridge favourable as opposed to an orthotropic steel deck bridge when comparing weight?

For movable bridges tested for vehicle loading and fatigue loading a hybrid steel-FRP bridge with full hybrid interaction showed to be favourable for spans ranging from 12 to 20 meters with two or three notional lanes.

Results showed a clear favour towards the hybrid bridge for all of the spans and widths investigated. This ensures applicability to most other vehicle bridges in the Netherlands as well. The difference in weight of the hybrid bridges showed a decrease of 15 to 30% as opposed to the OSD bridge.

Depending on the dimensions of the bridge the OSD bridge resulted in a weight per square meter ranging from $405\frac{kg}{m^2}$ to $485\frac{kg}{m^2}$. For the hybrid bridge these values were smaller and ranged from $307\frac{kg}{m^2}$ to $402\frac{kg}{m^2}$. Although the hybrid bridge is far lighter than the OSD bridge both bridges have more material per square meter than the current bridges made in the 50's and 60's have. The average weight per square meter at that time ranges from $200\frac{kg}{m^2}$ to $300\frac{kg}{m^2}$. Therefore it is necessary to verify the load carrying capacity of the concrete pillars and foundation before replacing the bridge, but either way it shows that the hybrid bridge is lighter and will be more suited for renovation projects than OSD bridge leaves if weight is a limiting factor.

However weight is not the only factor for which a design is chosen. Both costs and environmental impact have a big influence on the decision making process. The cost comparison showed that the OSD bridge and hybrid bridge are competitive in pricing in an early design stage. However there are many uncertainties that could result in one of the bridge types being significantly more expensive than the other. More experience with FRP and the hybrid interaction is needed to create better cost indications in such an early design stage.





With the use of life cycle analysis established by "Stichting bouwkwaliteit" an environmental impact value has been quantified for the materials needed in the bridges. A different method that determines the CO₂ footprint has also been used. Both methods showed a difference ranging from 10% to 30% percent in favour of the hybrid bridge. This is mainly due to the large amount of steel needed for the steel orthotropic bridge leaf which also means that more material is needed for the counterweight.

While this research showed a clear favour for hybrid bridges over orthotropic bridges in terms of weight and environmental impact and no significant difference in cost more research is needed before this type of bridge is used more often. The results in this research have been obtained for a hybrid bridge with full hybrid interaction in the bond between steel and fibre reinforced polymer. This interaction comes with a lot of uncertainties due to the novelty of the bond. Hence, this is not yet defined in the Dutch or European requirements. Further research on the bond in bridge engineering is required to be implemented in norms and regulations.

Furthermore the analyses conducted in this research should be carried out with a software package that supports modelling of this interaction. This way a better understanding of the interaction can be obtained. It also makes it possible to model other loads such as temperature loads and see the effect it has on the interaction between steel and FRP.

Further investigation is necessary to convince engineers to apply hybrid bridges of steel and fibre reinforced polymers. Results from this report are however a first step towards more usage of these type of hybrid structures.





161

8.2 Finite element software

Initially it seemed that RFEM had the capabilities needed for this project. Unfortunately as the project advanced it became clear that RFEM has some limitations due to the way it is set up. The software has all the necessary options to model hybrid bridges and to create verification load models, but it lacks in the options to parametrize the models. There are many add-ons that are needed for the verifications which are only accessible from within the program, not from an external program such as excel.

This lack of accessibility is due to the way RFEM has been created. The fundamental parts of RFEM are easily accessible through other programs such as excel. However, RFEM has created many modules over the years to enhance there program. These modules are extra add-ons and not (yet) accessible for parametric use. This means only fairly basic parametric models can be created.

This is an issue that is not to be expected with SOFiSTiK since it is a text based software package. New parts of the software are directly implemented in the code and therefore easily accessible to the users. Recreating this research in SOFiSTiK will therefore give more freedom to the researcher to add more calculations or create a better export of results. However, the possibilities of modelling laminates and interfaces in SOFiSTiK seems limited so other programs might be more useful.









9

Recommendation

Several recommendations can be given for further research and will be elaborated below. The paragraphs which led to the recommendation are stated in the bullet points.

Full hybrid interaction (paragraph 4.2.2)

The model that has been made for the hybrid bridge assumed full interaction between steel and FRP. Full interaction is expected to be possible with both a bolted and bonded connection. Further investigation into this bond must be done to verify this assumption and might give better insight in specific failure mechanisms that might occur in the connection. If there is more information available about the connection it is also possible to make the comparison between hybrid bridges with and without interaction and the (dis)advantages of them. When this interaction can be modelled it will also be useful to model temperature loads and see the effects of the different expansion coefficients of the materials.

FRP sandwich panel optimization (paragraph 4.2.3)

The FRP sandwich panel has been determined with the help of a local buckling and fatigue analyses. The dimensions that have been chosen resulted in a safe design but are far from optimized. More research is needed to determine the most optimal dimensions of the sandwich panel. This can be done on a local scale but must also be done for a global scale since differences in the sandwich panel will influence global effects.

Distance between crossbeams (paragraph 7.2.2.2)

Results showed that having a crossbeam at midspan of the bridge resulted in high stresses in the flange connection of main girders and crossbeams. Further research is needed to determine if it is worthwhile to change the distance between crossbeams to prevent a crossbeams at midspan. Increasing this distance results in larger spans between crossbeams which in turn might create higher stresses in certain locations. Decreasing the distance would result in an extra crossbeam. Both options will decrease the needed amount of material in the main girder but increase material needed in other places such as the stiffeners or crossbeams.





Whether the decrease of material in the main girders outweighs the increase in other parts, such as crossbeams or sandwich panel, must be investigated.

Detailed analysis stiffener to crossbeam connection (paragraph 7.2.1.1)

The stiffener to crossbeam connection in the OSD bridge showed resulting damages higher than 1.0 which means it will fail. Since this detail reacts drastically to minor stress changes due to its low detail category further investigation is needed to show safety of the detail. This should include the frequency distribution which has not been implemented in this report. However it should also include a full length bridge and overtaking traffic since results in this report showed that this effects influences the stress and therefore the damage in a negative way.

Different FEM software (paragraph 4.2)

Several problems occurred during this thesis due to the chosen software RFEM. These problems occurred due to limitations by the program when using it parametrically from Excel. Problems occurred during the modelling of the connection between steel and FRP where it was impossible to create a simple laminate of FRP and steel. Instead a small rigid link had to be modelled between two plates which increased the number of mesh elements significantly. Other issues occurred during the extraction of data from RFEM which were caused by the way the database is created. These issues might be resolved by using different software such as SOFiSTiK or Diana.





10

Bibliography

- Afsluitdijk, D. (2017). Swing bridge Afsluitdijk. Retrieved from https://deafsluitdijk.nl/nieuws/draaibruggen-kornwerderzand-weer-in-gebruik/
- Alkhrdaji, T. (2015). Strengthening of Concrete Structures Using FRP Composites. Retrieved from https://www.structuremag.org/?p=8643
- AZoM.com. (2001). *E-Glass Fibre*. Retrieved from https://www.azom.com/article.aspx?ArticleID=764
- Breuker, R. de. (2013). What is buckling? Retrieved from https://ocw.tudelft.nl/course-lectures/what-is-buckling/
- CBS. (2019). Vehicle fleet. Retrieved from https://opendata.cbs.nl/statline/#/CBS/nl/dataset/82044NED/table?dl=1B320
- CUR 96. (2017). Vezelversterkte kunststoffen in bouwkundige en civieltechnische draagconstructies.
- Engineering, P. (2018). FRP reinforcement of structures. Retrieved from https://www.build-on-prince.com/frp-reinforcement.html
- Flink, P. (2015). *Composite Bridge Design* (TU Delft). Retrieved from https://repository.tudelft.nl/islandora/object/uuid:dd28e122-0fab-4730-8ad4-5c7c88d3a57d/datastream/OBJ/download
- Freitas, S. T. de. (2011). Figures. Retrieved from https://www.researchgate.net/figure/Orthotropic-steel-bridge-deck-a-cross-section-b-underside-view_fig1_258158240
- Hartsuijker, C. (2001). Toegepaste mechanica deel 2.
- Hiatt, J. (2016). Rainflow counting. Retrieved August 7, 2019, from Siemens website: https://community.plm.automation.siemens.com/t5/Testing-Knowledge-Base/Rainflow-Counting/ta-p/383093





- Kassapoglou, C. (2013). Design and Analysis of Composite Structures.
- Koglin, T. L. (2003). *Movable Bridge Engineering*. Retrieved from https://books.google.nl/books?id=_cyqkMJ7QDgC&printsec=frontcover&redir_esc=y#v= onepage&q&f=false
- Li, M. (2014). Figures. Retrieved from https://ascelibrary.org/doi/10.1061/%28ASCE%29BE.1943-5592.0000610
- Luigi Ascione, Jean-François Caron, João Ramô Correia, E. (2016). *Prospect for New Guidance in the Design of FRP*. 172. https://doi.org/10.2788/22306
- Mouroulis, D. Y. (2018). A Feasibility Study on Weight Saving in Bascule Bridge Design by Implementing an FRP-deck A Feasibility Study on Weight Saving in Bascule Bridge Design by Implementing an FRP-deck. TU Delft.
- NEN-EN1991-2. (2015). Belastingen op constructies Deel 2: Verkeersbelasting op bruggen.
- NEN-EN1991-2NB. (2011). Belastingen op constructies Deel 2: Verkeersbelasting op bruggen.
- NEN-EN1993-2NB. (2019). *NEN-EN 1993-2 + C1 / NB*. (december 2011).
- NEN1993-1-9. (2012). Ontwerp en berekening van staalconstructies Deel 1-9: Vermoeiing.
- NOS. (2015). Vertical lift bridge, Botlek. Retrieved from https://nos.nl/artikel/2075482-botlekbrug-viert-jubileum-50e-storing.html
- Partov, D., Pasternak, H., Petkov, M., Nikolov, R., & Dimitrova, A. (2018). *About the history of orthotropic bridge decks. 4*, 295–311.
- Pavlovic, M. (2018a). Fibre Reinforced Polymer Structures. Retrieved from https://online-learning.tudelft.nl/courses/frp-composites-in-structural-engineering/
- Pavlovic, M. (2018b). Options for Finite Element Analysis of FRP composite structures. (September), 1–9. Retrieved from https://brightspace.tudelft.nl/d2l/le/content/125878/viewContent/1152572/View
- Pillwein, V. (2015). *An Introduction to Finite Element Methods*. 19–20. https://doi.org/10.1145/2755996.2756685
- Provincie Noorhd-Holland. (2018). *N242 Leeghwaterbrug*. Retrieved from https://www.noord-holland.nl/Onderwerpen/Verkeer_vervoer/Projecten_Verkeer_en_Vervoer/N242_Leegh waterbrug/Over_het_project
- Reis, E. M., & Rizkalla, S. H. (2008). Material characteristics of 3-D FRP sandwich panels.





- Construction and Building Materials, 22(6), 1009–1018. https://doi.org/10.1016/j.conbuildmat.2007.03.023
- Rijkswaterstaat. (2017). *Richtlijnen Ontwerp Kunstwerken*. (April), 1–255. Retrieved from https://staticresources.rijkswaterstaat.nl/binaries/RTD1001_ROK1.4_BijlageA_april2017 _tcm21-108742.pdf
- Rijkswaterstaat. (2019a). Database (p.). p. .
- Rijkswaterstaat. (2019b). Fairway Information Services. Retrieved March 19, 2019, from www.vaarweginformatie.nl/fdd/main/infra/vin
- SCIA. (2016). SCIA Engineer. Retrieved from https://help.scia.net/17.1/en/sr/composite_analysis_model/02-tb_composite_analysis_model.htm
- Souren, W. (2013). UO Berekening dek van Brug 15 te Nederweert.
- Souren, W. (2017). Ontwerp composiet brugdek Leeghwaterbrug B te Alkmaar.
- Steltech. (2016). WELDED BEAMS AND COLUMNS.
- Stichting Bouwkwaliteit. (2014). Assessment Method Environmental Performance

 Construction and Civil Engineering Works (GWW). (November), 89. Retrieved from

 https://www.milieudatabase.nl/imgcms/SBK_Assessment_method_version_2_0_TIC_versie.pdf
- TU-Delft. (n.d.). *Vermoeiing van brugdekken*. Retrieved from http://mstudioblackboard.tudelft.nl/bruggenentrends/inhoud/vermoeiing/vermoeiing1.htm
- Vacmobiles. (2012). Vacuum infusion process. Retrieved from https://www.vacmobiles.com/resin_infusion.html
- Wateren, M. van der. (2019). Parametric design of steel orthotropic bridge decks for fatigue calculations. Retrieved from https://repository.tudelft.nl/islandora/object/uuid%3Aec7b7b01-d252-4c1b-b635-7ea6b39206f1?collection=education
- Zarifis, G. G. (2018). *Application of bio-based FRP on a road traffic bridge* (TU Delft). Retrieved from https://repository.tudelft.nl/islandora/object/uuid%3A311d536e-542d-45b5-97d9-f52b2dd4abf3?collection=education









Annex A

Calculation elaborations

In this annex the elaborations of several calculations from this thesis can be found sorted by occurrence in this thesis.

$$t = 6 \, mm, \, a = 180 \, mm, \, b = 200 \, mm \qquad (4.2)$$
 Web layup of UD-plies $[0/45/90/-45]^{\rm s}$ $[25\%/25\%/25\%/25\%]$
$$D_{11} = 518987, D_{12} = 101098, D_{22} = 295461, D_{66} = 104067$$

$$\lambda = \frac{a}{b} \left(\frac{D_{22}}{D_{11}}\right)^{\frac{1}{4}} = \frac{180}{200} \left(\frac{295461}{518987}\right)^{\frac{1}{4}} = 0.78$$

$$K = \frac{4}{\lambda^2} + \frac{2(D_{12} + 2D_{66})}{\sqrt{D_{11}D_{22}}} + \frac{3}{4}\lambda^2$$

$$K = \frac{4}{0.78^2} + \frac{2*(101098 + 2*104067)}{\sqrt{518987*295461}} + \frac{3}{4}*0.78^2$$

$$K = 6.5746 + 1.5794 + 0.4563 = 8.61$$

$$\sigma_{cr} = \frac{\pi^2}{tb^2} * \sqrt{D_{11}D_{22}} * K = \frac{\pi^2}{6*200^2} * \sqrt{518987*295461} * 8.61$$

$$\sigma_{cr} = 171.17 \, MPa$$

Web layup of UD-plies
$$[0/45/90/-45]^s$$
 $[25\%/25\%/25\%/25\%]$ to $D_{11} = 518987, D_{12} = 101098, D_{22} = 295461, D_{66} = 104067$ (4.10)
$$K = \frac{2D_{66} + D_{12}}{\sqrt{D_{11}D_{22}}} = \frac{2*104067 + 101098}{\sqrt{518987 * 295461}} = 0.790$$

$$v = \frac{D_{12}}{2D_{66} + 2D_{12}} = \frac{101098}{2*104067 + 2*101098} = 0.246$$

$$\sigma_{cr,c} = \frac{\pi^2}{tb^2} * \left[2\sqrt{D_{11}D_{22}} + 2(D_{12} + 2D_{66})\right] = 71.16 \text{ MPa}$$

$$\sigma_{cr,c} = \frac{\pi^2}{tb^2} * \left[3.125\sqrt{D_{11}D_{22}} + 2.33(D_{12} + 2D_{66})\right] = 98.71 \text{ MPa}$$

$$\sigma_{cr,c} = \frac{\pi^2}{tb^2} * \left[4.53\sqrt{D_{11}D_{22}} + 2.44(D_{12} + 2D_{66})\right] = 128.37 \text{ MPa}$$

$$\sigma_{cr,c} = 12*\frac{D_{66}}{tb^2} = 6.42 \text{ MPa}$$

$$\sigma_{cr,c} = \frac{1}{tb^2}\sqrt{D_{11}D_{22}}\left[15.1K\sqrt{1-v} + 7(1-K)\right] = 23.82 \text{ MPa}$$

$$\tau_{xy,cr} = \frac{4}{tb^2} \sqrt[4]{D_{11}D_{22}}\left[15.07 + 7.08K\right] = 144.6 \text{ MPa}$$





$$t = 12 \ mm, b = 80 \ mm$$

$$D_{11} = 5324357, D_{12} = 522972, D_{22} = 1762849, D_{66} = 546724$$

$$\sigma_{cr,c} = \frac{\pi^2}{th^2} * \left[2\sqrt{D_{11}D_{22}} + 2(D_{12} + 2D_{66}) \right] = 7 * 10^6 \ GPa$$
(4.11)

$$d_{n} = \frac{\sum E_{i}S_{i}}{\sum E_{i}A_{i}}$$

$$d_{n} = \frac{(ES_{frp} + ES_{steel})}{EA_{frp} + EA_{steel}}$$

$$ES_{frp} = E_{frp} * \left(n_{webs} * t_{web_{sp}} * \frac{h_{sp}^{2}}{2} + w * t_{bfac_{sp}} * h_{sp}^{2}\right)$$

$$w = width ; n_{webs} = \frac{w}{ctc_{web_{sp}}} ; h = height$$

$$ES_{steel} = 2 * E_{steel}$$

$$* \left(t_{tfl_{mg}} * w_{tfl_{mg}} * h_{sp} + t_{web_{mg}} * h_{mg} * \left(h_{sp} + \frac{h_{mg}}{2}\right)\right)$$

$$+ t_{bfl_{mg}} * w_{bfl_{mg}} * h\right)$$

$$EA_{frp} = n_{webs} * t_{web_{sp}} * h_{sp} + w * \left(t_{tfac_{sp}} + t_{bfac_{sp}}\right)$$

$$EA_{steel} = 2 * \left(t_{tfl_{mg}} * w_{tfl_{mg}} + t_{web_{mg}} * h_{mg} + t_{bfl_{mg}} * w_{bfl_{mg}}\right)$$

$$d_{n} = \frac{5.46 * 10^{8} + 1.20 * 10^{10}}{8.79 * 10^{9} + 2.03 * 10^{10}} = 430 mm$$





 $EI = \sum E_i * I_i = 4.42 * 10^9 \tag{4.21}$

		<u> </u>		
FRP	1/12*bh^3	A*a^2	El	Unit
I_tfl	0,0000017	0,0266765	5,04E+08	Nm^2
I_web	0,0004782	0,0205246	3,97E+08	Nm^2
I_bfl	0,0000017	0,0090296	1,71E+08	Nm^2
		SUM	1,07E+09	Nm^2
Steel	1/12*bh^3	A*a^2	El	Unit
I_tfl	0,0000048	0,0022574	4,75E+08	Nm^2
I_web	0,0013784	0,0006265	4,21E+08	Nm^2
I_bfl	0,0000048	0,0116795	2,45E+09	Nm^2
		SUM	3,35E+09	Nm^2
		Total	4,42E+09	Nm^2









Annex B

Bridge data Rijkswaterstaat

Ketelbrug NOORD Top width bot width height thick Scharsterfinbrug 300- 250 Scharsterfinbrug 307- 250 Stevinsluizen 307- 325- Kruiswaterbrug 300 105 325- Schipholbrug 300 105 325 Schipholbrug 300 100 325 Burg over het Zijkanaal C Old drawings 300 326 Schipholbrug 300 100 325 Burg over het Zijkanaal C Old drawings 300 326 Schinkelbrug 300 100 325 Glessenbrug 300 105 325 Haringvlierbrug 300 105 325 Averagers 300 100 325	Stiffener			Cro	Crossbeam		
NOORD 300 25	height thickness	c.t.c. (hoh) Trog type	Aantal height	Web thick		flange width	flange thick
Signature 300 - 256 256	250 6	900	7		3325		
izen uizen uizen uizen uizen uizen uizen uizen uug brug brug brug brug and and and and and and and an	250 6	600 Koker rond	7 less then mg	mg	3325		
Pen		600 Koker rond	4	938 12	2,53 (2,36)	250	20
brug and brug br							
Serbrug Serb							
and the training and the training and traini							
105 322 322 322 323 323 323 324 324 325							
Proteg Old drawings Intel Zijkanaal C Old drawings Intel Zijkanaal C 300 200 32 Brug 300 105 32 Brug 300 105 32 Etbrug 300 105 32 Etbrug Aantal Neight Web thick Brug Aantal Neb thick Abt thick Inbrug 2 938 12 (20) 32 Inbrug 2 1537 15 (20) 32 Inbrug 2 1537 15 (20) 32 Increase 2 1537 15 (20) 32 Increase 3 2 1537 15 (20) 32 Increase 3 3 3 3 3 Increase 3 3 3 3 3 Increase 3 3 3 3 3 Increase 3 3 3 3 3 3 Increase 3		609 Koker	5	1275	3,53		25
Pret Zijkanaal C Old drawings Prug							
brug 300 200 320							
Section Sect							
Page		600 Koker	8		4000 (1*2685)		
December 300 100 32, 102 32, 103 32, 103 32, 103 32, 103 32, 103 32, 103 32, 103 32, 103 33, 103 33, 103 33, 103 33, 103 33, 103 33, 103 33, 103 33, 103 33, 103 33, 103 103 33, 103 33, 103 33, 103 33, 103 33, 103 103 33, 103 33, 103 33, 103 33, 103 33, 103 33, 103 33, 103 33, 103 33, 103 33, 103 103 33, 103 103 33, 103							
rug 300 105 322 brug 302 105 322 brug 300 105 322 brug Aantal height Web thick g AUID Aantal Neb thick g AUID 2 33 12 (20) g AUID 2 33 12 (20) g Auis 2 1537 15 (20) 15 (20) g Isen 1537 15 (20) 15 (20) 15 (20) g Internal 15 (20) 15 (20)		600 koker met uitsparing	veel				
brug etbrug brug brug brug brug syllo	325	608 koker	2	1000	2830	300	30
brug brug brug brug brug swoorb swoorb struct rug rug brug brug shura brug brug brug brug brug brug brug struct s		l-profiel					
brug bbrug bbrug s NOORD s NOORD s NOORD s Light s							
Antal height Web thick signal of the control of the		l-profiel					
NOORD Noor							
Sample S							
NoORD Neight Web thick		600 koker	×	1000	3000	300	25
Antal height Web thick g NOORD g ZUID g ZUID rijnbrug g Tuizen grbrug g Thrug							
Antal height Web thick NOORD	Main girder		Deck		Overall (m)		
s NOORD s ZUID s ZUID rijnbrug zen izen uizen srbrug strug het Zijkanaal C nug nug shenoordbrug	c.t.c.	flange width flange thick	Thickness Length	Width (road)	RW	lanes	Height
### STAID ### ST			12 2		12410	2	
rijnbrug 2 938 izen 8 938 izen 938 srbrug 2 1537 srug 6 1537 srug 7018 7018 7018 7018 7018 7018 7018 7018				21147 17900	10135+6155	4	-
izen uizen erbrug g nug nug nug nug erbrug nug erbrug brug brug brug erbrug brug	88 12 (20) 8600	400 20	20	9950 14950	12250	2	938
srbrug 2 1537 and 2 1537 and 2 1537 and 3 1537 and 4 1538 and 6 1537 and 8 1576 brug 6 1576 brug 7 1576 brug 7 1576 brug 8 1576 brug 8 1576 brug 8 1576						2	
rerbrug 2 1537 nug 2 1537 nug 2 1576 rug 2 1576 cut 3 1576 cut 4 1576 cut 6 1576 cut 7 1576 cut 8 1576 cut 8 1576 cut 8 1576 cut 9 1576 cu						2	_
3 1537 The t Zijkanaal C						2	-
Zijkanaal C						2	
Zijkanaal C	15 (20) 7489	450 50	15	15200 10929	10229	3	1537
Zijkanaal C ordbrug 2 1576 2 8						3	-
ordbrug 2 1576 2 8 8 3 8						3	
ordbrug 2 1576 2 8 8						5	-
oordbrug 2 1576 ug 8 8 orug 8 ug 1576	13950		2	28175 24120	24120 2*8250	2	
enoordbrug 2 1576 brug 8 1576 tibrug 1576 intg						2	
ug 2 1576 brug 8 ttbrug 1576 trug 1576						4*3	-
brug tibrug rug	76 16,20,30 8700	600	20	12529 14695	11104	3	1576
Haringvlietbrug Volkerakbrug aagbrug						2	-
Volkerakbrug Gagbrug						2	
kaagbrug Durde Riinhrus						2	
a sinda Bilaharia						2	
Spira	_			_		2	
Averages 2 1500 15		450 40	20	18000 14000	11000	2-3	1500









Annex C

Norms and regulations

There are many norms and regulations to be considered to verify the structural requirements of a bridge. In Europe these regulations are stated in the Eurocode. Since FRP is a rather new material in civil engineering no Eurocode exists yet. There are however several recommendation documents, one of which is the Dutch recommendation CUR. This is used as a basis for the Eurocode under construction for FRP.

Besides the Eurocode and the CUR many countries have additions or alterations to the Eurocode. In the Netherlands this is the ROK (design guidelines for civil engineering works, Dutch: Richtlijnen ontwerp kunstwerken). The ROK is the leading document for civil engineering works in the Netherlands, but the Eurocode is a foundation for this document.

The following list of rules and regulations are needed to conduct a thorough research on highway bridge design.

- EN1990 → Basis of structural design
- ► EN1991 → Actions on structures
 - Part 1-4 → Wind actions
 - Part 1-5 → Thermal actions
 - Part 2 → Traffic loads on bridges
- EN1993 → Design of steel structures
 - Part 2 → Steel bridges
- NEN 6786 (Dutch) → Rules for the design of movable parts of civil structures
 - Part 1 → Movable bridges
- CUR 96 (Dutch) → FRP in structural and civil engineering structures
- ROK (Dutch) → Design guidelines for civil engineering works

Considering all types of loading would result in an unnecessarily extensive model for an early design stage. Therefore a decision has been made to focus on traffic loads, wind and thermal actions will not be considered. Also the NEN6786 about movable parts, which focusses on the opening and closing of the bridge, will not be considered. These loads should be considered in a later design stage.





C.1 Load models

There are many loads that have to be considered for bridge building such as thermal loading, wind loads and traffic loads. Only the traffic loads will be considered for this thesis.

Traffic loads on bridges are stated in EN1991-2 and are independent of the bridge type except for the fatigue load models. The load cases given in this code will be considered for both steel and hybrid bridges. The national annex and Eurocode can be split up in several parts:

- Factors (Annex C.1.1)
- Vertical loads (Annex C.1.2)
- Horizontal loads (Annex C.1.3)
- Groups of traffic loads (Annex C.1.4)
- Fatigue load models (Annex C.1.5)

Each part will be discussed in the next paragraphs. Alterations due to the Dutch national annex have been incorporated in the (Dutch) tables and text. Certain definitions hold for each load case and will be specified below.

The **width** w **of notional lanes** on a carriageway and the number of lanes is defined in Table C.1

Width of the Carriageway width Number of notional Width of a notional lanes lane w_i remaining area w w < 5.4 m3 mw-3m $n_1 = 1$ $5.4 m \le w < 6 m$ $n_2 = 2$ 0 2 $n_i = Int\left(\frac{w}{3}\right)$ $6 m \leq w$ 3 m $w - 3 * n_i$

Table C.1 Number and width of notional lanes (NEN-EN1991-2, 2015)

Where the carriageway on a bridge is physically divided into two parts separated by a central reservation, then each part should be divided into notional lanes. Roads wider than 42 meters should always be divided (NEN-EN1991-2NB, 2011).

The **location of notional lanes** should not be necessarily related to their numbering. Location of notional lanes should be chosen so that the effects from the load models are the most adverse, the most unfavourable lane should be numbered as lane 1, second unfavourable lane as lane two, etc. For fatigue representative values and models, the location and the numbering





of the lanes should be selected depending on the traffic to be expected in normal conditions (NEN-EN1991-2, 2015).

In the case of separate parts on two independent decks each part should be considered as a carriageway.

C.1.1 Factors

Different factors need to be included in a calculation. Each factor will be elaborated in this paragraph to obtain the correct calculation and verification values.

Material factors

The material factor γ_m should be taken as 1.0 unless described otherwise and should be implemented as shown in equation

Adjustment factors

Certain load models need adjustment factors α_{Q1} and α_{q1} which depend on the span length and number of heavy vehicles and is depicted in Table C.2 (tables from the Dutch national annex have not been translated).

Aantal vrachtwagens per α_{Q1} en α_{q1} jaar per rijstrook voor Lengte van de overspanning of invloedslengte (L) zwaar verkeer Nobs a 20 m50 m100 m $\geq 200 m$ $\geq 2~000~000$ 1.0 1.0 1.0 1.0 200 000 0.97 0.97 0.95 0.95 20 000 0.95 0.94 0.89 88.0 2 000 0.91 0.91 0.82 0.81 200 0.88 0.87 0.75 0.74

Table C.2 Correction factors (NEN-EN1991-2NB, 2011)

According to the Dutch national annex α_{q1} must be taken as 1.15 in the case that a traffic lane is designated to heavy traffic. When a carriageway consists of three or more lanes and has an $N_{obs} \geq 2~000~000~per~year~\alpha_{qi} = 1.4~for~i > 1$.

^a Tussengelegen waarden mogen worden geïnterpoleerd.





Fatigue factors

There are multiple factors that need to be considered for fatigue. This includes the partial factor for fatigue, the dynamic amplification factor.

Partial factor for fatigue

The Partial factor for fatigue strength, γ_{MF} , is a factor specific to fatigue in steel structures and follows from Table C.3. For movable bridge decks this factor will be equal to 1.35 for general details and 1.15 for local details (stiffeners).

Table C.3 Partial factors for fatigue strength

Pagardalingamathada	Gevolgen van	het bezwijken
Beoordelingsmethode	Gering	Groot
Schade-tolerant	1.00	1.15
Veilige-levensduur	1.15	1.35

Dynamic amplification factor

The dynamic amplification factor, φ_{fat} , is a multiplication factor for fatigue assessment. This factor depends on the expected roughness of the road surface and on any dynamic amplification already included in the records. This factor is used for road bridge assessment based on recorded traffic and should be taken as 1.2 for surfaces of good roughness and 1.4 for surfaces of medium roughness.

An additional dynamic amplification factor, $\Delta \varphi_{fat}$, must be applied if one or more vehicle axles are within 6 m from an expansion joint. If this is the case, $\Delta \varphi_{fat}$ can be taken as a constant value of 1.15 and must be applied on each axle of that vehicle. This factor is also used for load model 2.





C.1.2 Vertical loads

This load model is associated with the ultimate limit state verification and particular serviceability verifications and consists of load models 1 to 4.

Load model 1

Load model 1 consists of two partial systems, a tandem system (TS) and a uniformly distributed load (UDL). No more than one TS should be taken into account per notional lane and only complete tandem systems should be taken into account. The TS is shown in Figure C.1 and the axle load can be calculated as shown in equation (C.1). Equation (C.2) shows the uniformly distributed load.

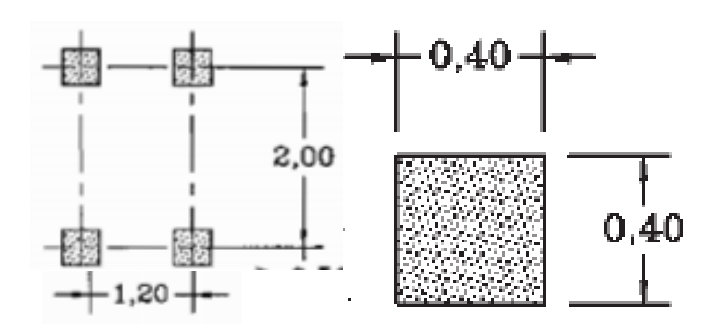


Figure C.1 Application of tandem system

$$axle\ load = \alpha_Q Q_{ik} \tag{C.1}$$

$$UDL = \alpha_q q_{ik} \tag{C.2}$$

$$\alpha = adjustment\ factor\ (chapter\ C.\ 1.1)$$

$$Q = axle\ load$$

Where

 $q = distributed \ load$ s for Q_{ij} , and q_{ij} , are given in Table C 4 and values

Values for Q_{ik} and q_{ik} are given in Table C.4 and values for α_Q and α_q can be found in Table C.2 (paragraph C.1.1).

Table C.4 Load model 1: characteristic values (NEN-EN1991-2, 2015)

Location	Tandem system TS	UDL system
	Axle loads Q_{ik} (kN)	$q_{ik} (kN/m^2)$
Lane Number 1	300	9
Lane Number 2	200	2.5
Lane Number 3	100	2.5
Other lanes	0	2.5
Remaining area (q_{rk})	0	2.5





Load model 2

Load model 2 consists of a single axle load of $400\,kN$ and should include a dynamic amplification at all times. When relevant, only one wheel of $200\,kN$ may be taken into account. The contact surface of each wheel should be taken into account as a rectangle of sides $0.35\,m$ and $0.60\,m$ as shown in Figure C.2. Equation (C.3) shows the calculation for the single axle load where $\Delta \phi_{fat}$ is an additional dynamic amplification factor in the vicinity of expansion joints.

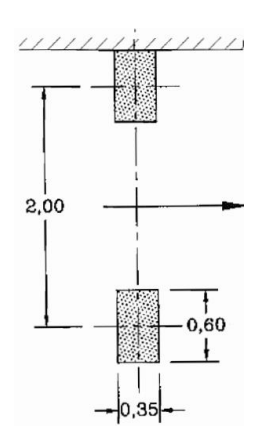


Figure C.2 Load model 2(NEN-EN1991-2, 2015)

Single axle load =
$$\Delta \phi_{\text{fat}} * \alpha_{Q1} * Q_{ak}$$
 with $Q_{ak} = 400 \text{ kN}$ (C.3) $\Delta \phi_{\text{fat}} = \text{dynamic amplification factor (paragraph C. 1.1)}$

Where

Load model 3

Where relevant, models of special vehicles should be defined and taken into account. This will not be taken into account in this report.

Load model 4

Load model 4 is for crowd loading and consists of a uniformly distributed load of $5 \, kN/m^2$ which includes dynamic amplification. This load model should be applied on all relevant parts including the central reservation.





Dispersal of concentrated loads

The wheel loads associated with LM1 and LM2 should be taken as uniformly distributed an dispersal through the pavement should be taken into account. The dispersal has a spread-to-depth ratio of 1:1 down to the level of the centroid of the structural top plate.

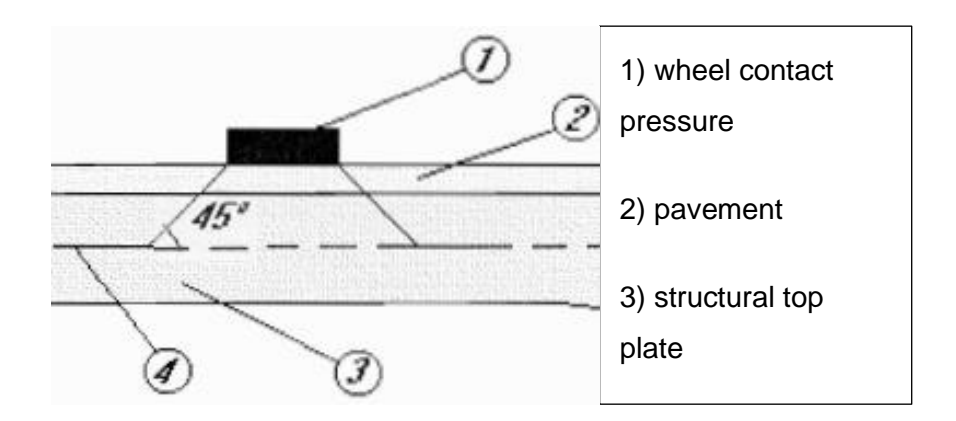


Figure C.3 Dispersal of concentrated loads through pavement and structural top plate (NEN-EN1991-2, 2015)



Where



C.1.3 Horizontal loads

Horizontal loads occurring on the deck might have severe consequences for a hybrid bridge deck. These forces can cause large shear stresses in the bond between the two materials. When exceeding the shear strength of the bond the hybrid interaction disappears lowering the load bearing capacity.

Braking and acceleration forces

A breaking force, Q_{lk} , shall be taken as a longitudinal force acting at the surfacing level of the carriageway and has a characteristic value limited to $800 \, kN$ for the total width of the bridge. The characteristic value of Q_{lk} can be determined by equation (C.4).

$$Q_{lk} = 0.6\alpha_{Q1}(2Q_{1k}) + 0.1\alpha_{q1}q_{1k}w_{1}L$$

$$180\alpha_{Q1}(kN) \le Q_{lk} \le 800 (kN)$$

$$w = width \ of \ lane \ 1$$

$$l = span \ length$$
(C.4)

This force should be taken into account as a force located along the axis of each lane. Acceleration forces should be taken into account as well, with the same magnitude but another sign (negative instead of positive). Horizontal forces transmitted by expansion joints or applied to structural joins are defined by equation (C.5).

$$Q_{lk} = 0.6\alpha_{01}(2Q_{1k}) \le 800 \, kN \tag{C.5}$$

Centrifugal and other transverse forces

Bridges with a horizontal radius of the carriageway will not be taken into account in this report. This results in a centrifugal force equal to zero.

Transverse forces due to skew braking or skidding will be taken into account. A transverse braking force, Q_{trk} , equal to 25% of the longitudinal braking or acceleration force Q_{lk} , should be considered to act simultaneously with Q_{lk} at the finished carriageway level.





C.1.4 Groups of traffic loads

For combination with non-traffic loads such as wind or thermal actions load groups must be defined. Simultaneity of the loading systems is defined in Table C.5. Each of these group of loads, which are mutually exclusive, should be considered as defining a characteristic action for combination with non-traffic loads.

Table C.5 Assessment of groups of traffic loads (NEN-EN1991-2NB, 2011)

Belastings- type				Rijwe	eg			Voet- en fietspaden
		Verticale krac	hten	Horizontale	Alleen verticale krachten			
Verw	/ijzing	4.3.2	4.3.3	4.3.4	4.3.5	4.4.1 4.4.2		5.3.2.1
	stings- teem	BM1 (TS en UDL)	BM2 (enkele as)	BM3 (bijzondere voertuigen)	BM4 (mensen- menigte)	Rem- en versnellings- krachten	Centrifugaal- krachten en krachten in dwarsrichting	Gelijkmatig verdeelde belastingen
	gr1a	Karakteristieke waarde				0,8× Karakteristieke waarde	0,8× Karakteristieke waarde	0,4× Karakteristieke waarde
ingen	gr1b		Karakteristieke waarde					
Groepen van belastingen	gr2	0,8× Karakteristieke waarde				Karakteristieke waarde	Karakteristieke waarde	0,4× Karakteristieke waarde
en va	gr3							Karakteristieke waarde ^a
Groep	gr4				Karakteristieke waarde ^b			
gr5		0,8× Karakteristieke waarde °		Karakteristieke waarde		0,8× Karakteristieke waarde °	0,8× Karakteristieke waarde °	
a 7:-		De gearceerde behorend bij de	e groep)			. ,		

^a Zie 5.3.2.1. Er behoort slechts één voetpad als belast te zijn beschouwd, indien het effect hiervan ongunstiger is dan bij belasting op twee voetpaden.

These group loads should be verified for both serviceability limit state (SLS) and ultimate limit state (ULS).

For the SLS verification the maximum deflection will be verified using equation (C.6).

$$u_{z,max} < \frac{L}{250}$$
 (C.6) where
$$u_{z,max} = deflection \ in \ z - direction$$

$$L = length \ of \ the \ span \ (local \ or \ global)$$

For the ULS check the maximum stresses will be verified with the material properties. The occurring stress should be lower than the yield stress of the material, including safety factors as shown in equation (C.7).

b Inclusief de belasting op voet- en fietspaden.

^c Vast te stellen voor afzonderlijke projecten.





(C.7)

where

 $\sigma_{max} * \gamma_Q < f_y$ $\sigma_{max} = maximum occurring stress$ $\gamma_Q = Safety \ factor = 1.35 \ (chapter \ 177C. \ 1.1)$ $f_y = Yield \ point$





C.1.5 Fatigue load models

Since fatigue is the main reason for current bridges to be renovated it must be taken into account in the calculation of the replacement bridge. Fatigue damage is caused by micro cracks in the material which propagates due to repetitive stress changes. The micro cracks are caused by impurities in the material. Impurities occur everywhere but welding causes a local increase in the number of impurities. These micro cracks will propagate despite stress changes being far below the maximum allowable stress. This is due to the repetitive nature that slightly increases the crack length each time. The amount of fatigue damage can be quantified by a numeric value by following specific rules stated in Eurocode 1993-1-9 (NEN1993-1-9, 2012).

Fatigue damage can be determined using the Palmgren-Miner rule shown in equation (C.8) with the help of the fatigue strength curve, also known as the SN-curve. For damage values below 1.0 the structure is considered safe.

$$D = \sum_{i}^{n} \frac{n_{ei}}{N_{Ri}} \tag{C.8}$$

where

 $n_{ei} = number\ of\ cycles\ associated\ with\ the\ stress\ range\ N_{Ri} = endurence\ in\ cycles\ obtained\ from\ SN\ curve$

The SN-curve quantifies the relationship between a stress range and the number of cycles needed till fatigue failure occurs. This curve can be constructed using the detail category of the fatigue detail and is represented by a bi-linear curve an a log-log scale. For this bi-linear curve 2 values, beside the detail category, must be calculated. These are the cut-off limit, which shows the minimum stress range to result in damage and the constant amplitude limit which shows the minimum stress range needed to result in damage for constant amplitude loads. The formulas can be found in equation (C.9) and (C.10).

$$\Delta \sigma_D = \left(\frac{2}{5}\right)^{\frac{1}{3}} * \frac{\Delta \sigma_C}{\gamma_{Mf}} \tag{C.9}$$

where

 $\Delta \sigma_D = constant$ amplitude fatigue limit $\Delta \sigma_C = detail$ category

$$\Delta \sigma_{L} = \left(\frac{5}{100}\right)^{\frac{1}{5}} * \Delta \sigma_{D}$$

$$\Delta \sigma_{L} = cut - off \ limit$$
(C.10)

where

As a result of these formula's the graph as shown in Figure C.4 can be constructed for several detail categories ranging from 36 being the lowest to 160 being the highest. To determine the endurance N_{Ri} for a certain stress range equation (C.11) must be used.





$$\begin{split} N_{\mathrm{Ri}} &= \frac{\Delta \sigma_{C}^{3}}{\Delta \sigma_{R}^{3}} * 2 * 10^{6} \ for \ \Delta \sigma_{R} > \Delta \sigma_{D} \\ N_{\mathrm{Ri}} &= \frac{\Delta \sigma_{C}^{5}}{\Delta \sigma_{R}^{5}} * 5 * 10^{6} \ for \ \Delta \sigma_{L} < \Delta \sigma_{R} \leq \Delta \sigma_{D} \\ \Delta \sigma_{R} &= stress \ range \end{split}$$
 (C.11)

where

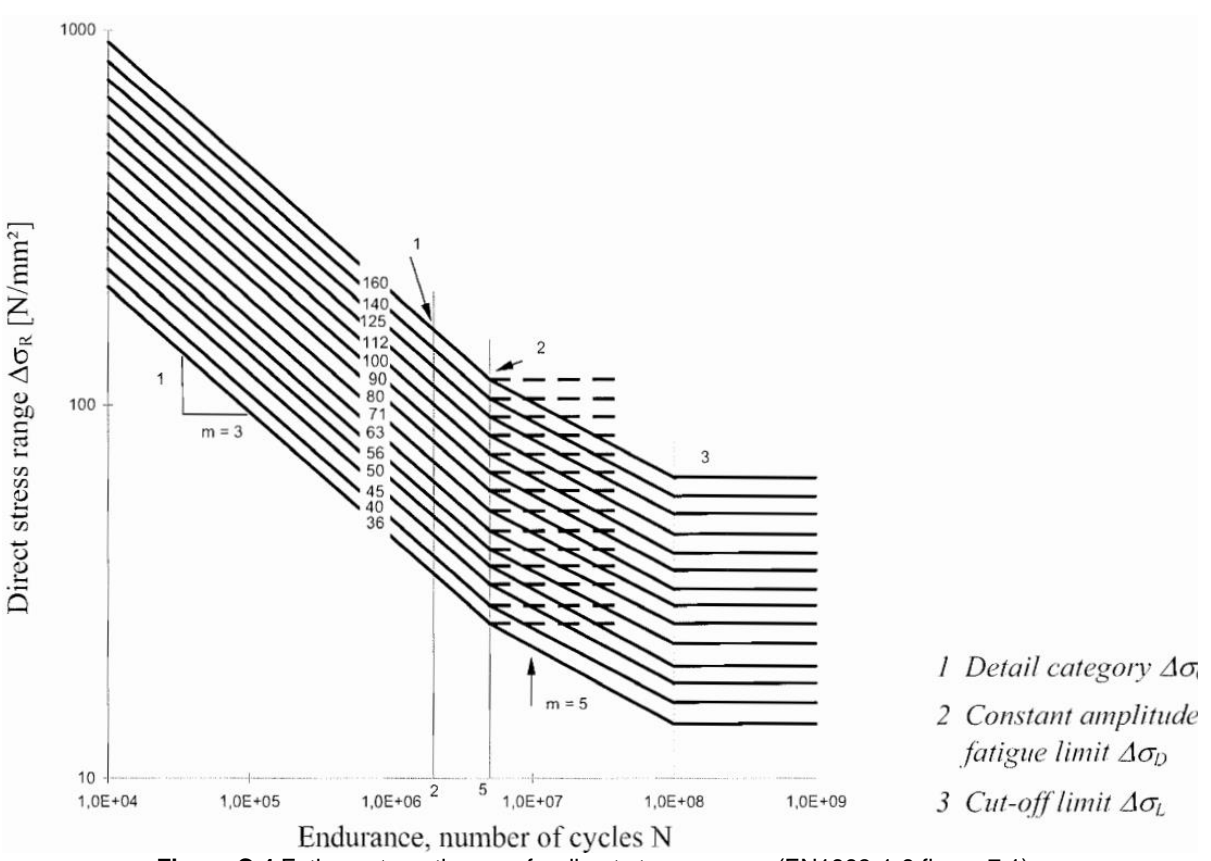


Figure C.4 Fatigue strength curve for direct stress ranges (EN1993-1-9 figure 7.1)

The occurring stress range depends on the geometry of the vehicle, axle loads, vehicle spacing, composition of traffic and its dynamic effects. For load models 1 and 2 the stress range must be determined by obtaining the maximum and minimum stress caused by the two worst possible load arrangements on the bridge. The stress ranges of Load models 3 and 4 need to be obtained from the transit of the model along the bridge. This transit will cause a stress spectrum of that specific load model, also called an influence line. Stress ranges need to be obtained from this influence line with the help of either the rainflow method or the reservoir method. The rainflow method is explained in Annex E.

Besides the stress range it is important to know how many vehicles actually transit along the bridge. The traffic category on a bridge defines this number of "heavy" vehicles, N_{obs} , that transit per year per heavy traffic lane and can be found in Table C.6.





Table C.6 Indicative number of heavy vehicles expected per year and per slow lane (NEN-EN1991-2NB, 2011)

Ve	erkeerscategorie	$N_{obs,a,ai}$				
		per jaar en per rijstrook				
		voor zwaar verkeer				
1	Autosnelwegen (A-wegen) en wegen met twee of meer	$2.0*10^{6}$				
	rijstroken per richting en met intensief vrachtverkeer					
2	(Auto)wegen met gemiddeld vrachtverkeer (zoals N-	$0.5 * 10^6$				
	wegen)					
3	Wegen met weinig vrachtverkeer	$0.125 * 10^6$				
4	Wegen met weinig vrachtverkeer en bovendien	$0.05*10^6$				
	uitsluitend bestemmingsverkeer					
OI	OPMERKING De aantallen zware voertuigen per jaar en per rijstrook voor zwaar					
ve	rkeer $N_{obs,a,ai}$ zijn inclusief trend.					

The traffic category is also used for a lower bound thickness of the deck plate which is stated in (NEN-EN1993-2NB, 2019). This states that the thickness for decks with closed stiffener, with a width of 300 mm, continuous through the crossbeams should be at least the thickness given in Table C.7.

Table C.7 Deck thickness as a function of design life (NEN-EN1993-2NB, 2019)

	rscategorie overeenkomstig tabel	Dekplaatdikte			
NB.5 va	ın NEN-EN 1991-2+C1/NB	mm			
			Asfalt, mastieklaag		ijtlaag met
		of hogesterktebeton		een minii	male dikte
		met een minimale		van 8 mm	
		dikte van 60 mm			
Cat. nr	t. nr Ontwerplevensduur		100 jaar	50 jaar	100 jaar
1.	Autosnelwegen (A-wegen) en	N.v.t.	18	N.v.t.	22
	wegen met twee of meer				
	rijstroken per richting en met				
	intensief vrachtverkeer				
2.	(Auto)wegen met gemiddeld	18	N.v.t.	20	N.v.t.
	vrachtverkeer (zoals N-wegen)				
3.	` ,		N.v.t.	18	N.v.t.
4.			N.v.t.	15	N.v.t.
	en bovendien uitsluitend				
	bestemmingsverkeer				

According to the Dutch national annex an extra vehicle must be modelled on the lane next to the heavy traffic lane in 10% of the cases to simulate overtaking. This vehicle must be assumed to be the same as the vehicle on the heavy traffic lane. This means that a total of $110\% N_{obs}$ vehicles transit the bridge. Depending on the location of the heavy traffic lane this overtaking traffic can be on the left or right side of the heavy traffic lane (NEN-EN1991-2NB, 2011).

Another important factor is the location of the vehicles in transverse direction (the width of the bridge). For the assessment of general action effects (e.g. in main girders) all fatigue load





models should be placed centrally on the notional lanes. For the assessment of local action effects (e.g. in slabs) the models should be centred on notional lanes assumed to be located anywhere on the carriageway. However, where the transverse location is significant a statistical distribution of this transverse location should be used for load models 3, 4 and 5. This statistical distribution or frequency distribution is shown in Figure C.5.

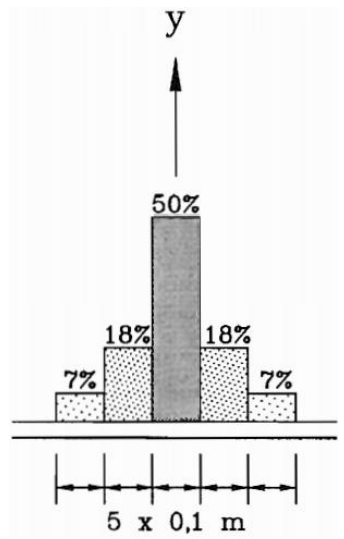


Figure C.5 Frequency distribution (NEN-EN1991-2, 2015)

For this analysis only general action effects will be considered. The vehicles will therefore be situated centrally on the notional lanes.

Fatigue load models 1 to 4 include dynamic load amplification as explained in paragraph C.1.1.

Fatigue load model 1

Fatigue load model 1 has the configuration of load model 1 defined previously. The TS loads have been lowered by a factor 0.7 and the UDL has been lowered by a factor 0.3. Maximum and minimum stresses ($\sigma_{FLM,max}$ and $\sigma_{FLM,min}$) should be determined from the possible load arrangements of the model on the bridge.





Fatigue load model 2

Fatigue load model 2 consists of a set of idealised lorries called frequent lorries and are shown in Figure C.6 together with the geometrical definition of the wheel and axle types. The maximum and minimum stresses should be determined from the most severe effects of different lorries.

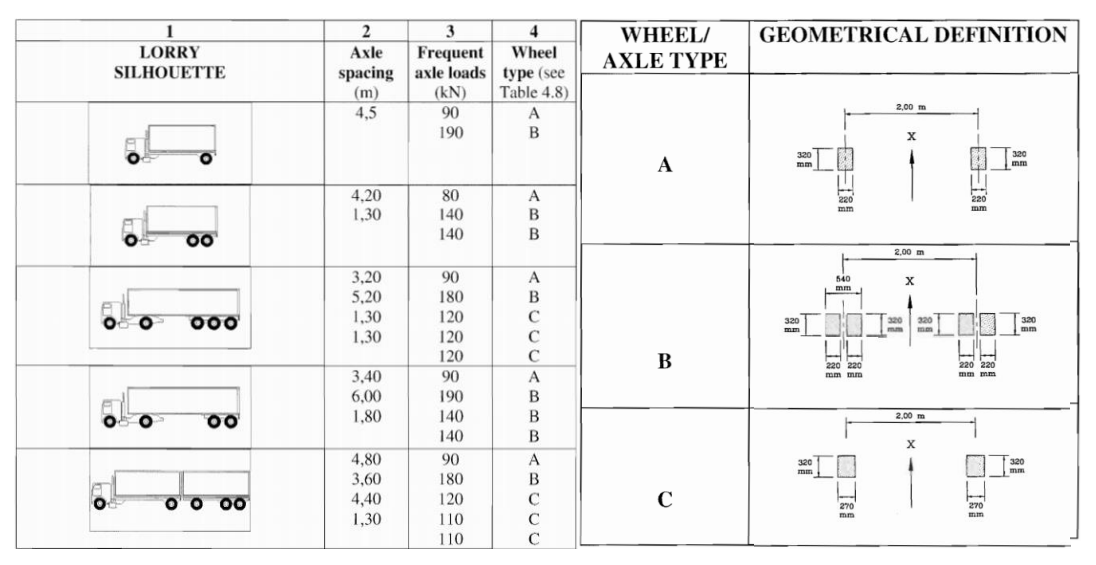


Figure C.6 Set of frequent lorries (FLM2) and wheel/axle type(NEN-EN1991-2, 2015)

Axle type B consists of 4 wheels. When, due to dispersion, two of the surface areas meat the surface area can be modelled by a single wheel with dimensions of $320 \ mm \ x \ 540 \ mm$ before dispersion calculation is done.

Fatigue load model 3

Fatigue load model 3 consists of four axles with identical wheels and has an axle load of $120 \, kN$. The geometrical definition is shown in Figure C.7





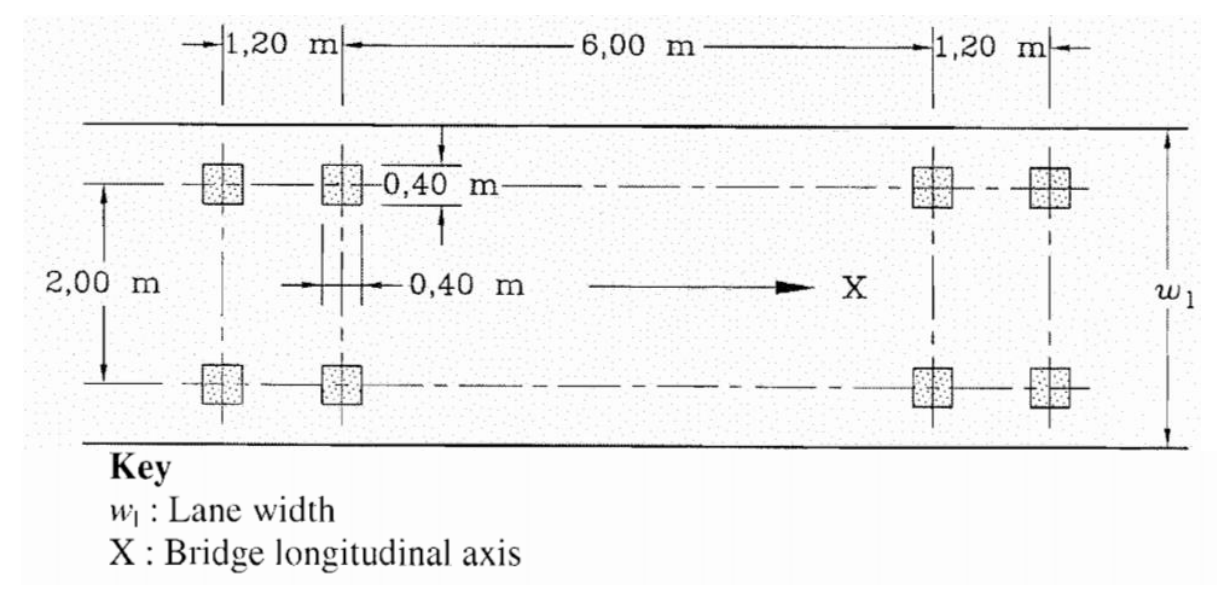


Figure C.7 Fatigue load model 3(NEN-EN1991-2, 2015)

The maximum and minimum stresses and the stress ranges for each cycle should be calculated as a result of the transit of the model along the bridge. Where relevant, two vehicles in the same lane should be taken into account, the second vehicle should have an axle load of $36 \, kN$ and the distance between vehicles should be no less than $40 \, m$.

Fatigue load model 4

Fatigue load model 4 consists of sets of standard lorries which together produce effects equivalent to those of typical traffic on European roads. Fatigue load model 4A is used for materials that only depend on the stress range to suffer from fatigue damage such as steel and has been taken from the Dutch national annex (NEN-EN1991-2NB, 2011). Fatigue load model 4B is used for materials which depend on the stress range and the maximum stress such as concrete and FRP and has been taken from the ROK(Rijkswaterstaat, 2017).

These load models produce a stress spectrum in the bridge which is unique for each location. The corresponding number of cycles from each fluctuation during the passage of individual lorries on the bridge should be determined by the Rainflow or Reservoir counting method (see Annex E).





Table C.8 Set of equivalent lorries for load model 4A (NEN-EN1991-2NB, 2011)

Тур	e voertuig			Verkeerstype		
Afbeelding van de vrachtwagen	Afstand tussen de assen	Gelijkwaardige aslast	Lange afstand	Middellange afstand	Lokaal verkeer	Wiel- type
viaciitwageii	m	kN	% ^a	% ^a	% ^a	
Srafte"	4,5	70 130	20,0	50,0	80,0	A B
"Heavy- Iraffic"	4.20 1,30	70 120 120	5,0	5,0	5,0	A B B
"Heavy- Sreffic"	3,20 5,20 1,30 1,30	70 150 90 90 90	40,0	20,0	5,0	A B C C C
Heavy South	3,40 6,00 1,80	70 140 90 90	25,0	15,0	5,0	A B C C
Heavy Suffic	4,80 3,60 4,40 1,30	70 130 90 80 80	10,0	10,0	5,0	A B C C
^a Percentage vrachtwagens.						

Table C.9 Set of equivalent lorries for load model 4B (Rijkswaterstaat, 2017)

Voertuigtype	Asafstand [m]	Equivalente aslast [kN]	Wieltype	Equivalent voertuiggewicht [kN]	Aantal per jaar
1	4.5	70 130	A B	200	750.000
2	4.2 1.3	70 120 120	A B B	310	600.000
3	3.2 5.2 1.3 1.3	70 150 90 90 90	A B C C	490	600.000
4	3.2 1.3 4.4 1.3 1.3 1.3	70 90 70 70 70 70 70 70	A C A A A A A	580	230.000
5	1.5 2.4 1.3 9.5 1.3	70 70 170 160 70	A A B B A A	750	66.000





	1.3	70	А		
		70	Α		
6	1.7	70	Α	950	3.100
	3.3	70	Α		
	1.3	180	В		
	3.5	190	В		
	3.5	70	Α		
	1.3	180	В		
		190	В		
7	2.4	170	В	1.090	500
	1.3	170	В		
	5.5	200	В		
	1.3	180	В		
	1.3	180	В		
		190	В		
8	2.5	130	В	1.220	200
	1.3	160	В		
	5.2	170	В		
	1.3	220	В		
	1.3	200	В		
	1.3	170	В		
		170	В		
9	1.4	130	В	1.280	100
	2.6	130	В		
	1.3	180	В		
	6.1	180	В		
	1.9	220	B B		
	1.9	220	B		
		220	В		
10	2.4	90	С	1.410	100
	1.3	90	C B B		
	1.3	240	B		
	9.5	220			
	1.3	200	В		
	1.3	180	В		
	1.3	190	В		
		200	В		

Fatigue load model 5

Fatigue load model 5 is based on recorded road traffic data and will therefore not be taken into account in this report.





C.1.6 Fatigue detail locations

Fatigue can occur in many different locations. For a correct model verification the Eurocode gives certain detail locations that have to be considered.

The following details are from the Dutch national annex for steel bridges. These details include locations in stiffeners, deck and crossbeams and exclude the main girders.

Local detail 1 is cracking in the deck plate at mid span between crossbeams and is shown in Figure C.8. This detail has a detail category of 125 and can occur on either side of the stiffener leg.

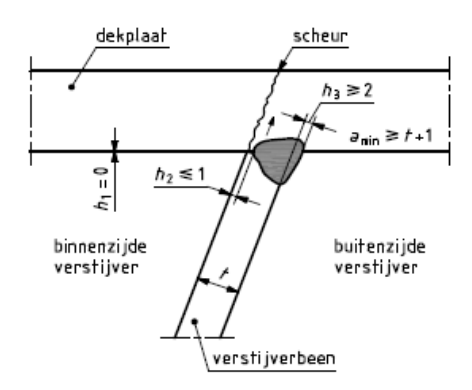


Figure C.8 Local detail 1 (NEN-EN1993-2NB, 2019)

Local detail 2 is cracking in the deck plate on top of the crossbeam and is shown in Figure C.9. This detail has a detail category of 125 and must be determined with a local hot spot stress. This is one of the few details that has caused many problems over the years and has been investigated thoroughly. This research concluded that for deck plates thicker then 18 mm this detail will not result in significant damages.

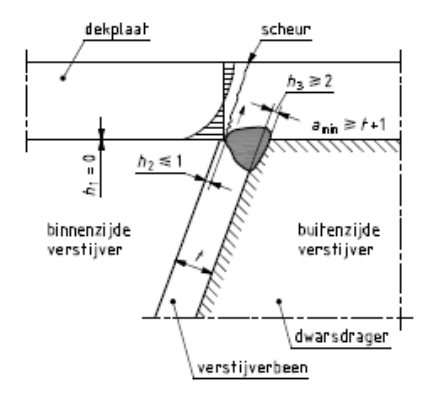


Figure C.9 Local detail 2 (NEN-EN1993-2NB, 2019)





Local detail 3 is weld failure between the stiffener and deck plate at mid span between crossbeams and is shown in Figure C.10. Depending on the weld type this detail has a category of 100 (automated weld process) or 90 (handweld).

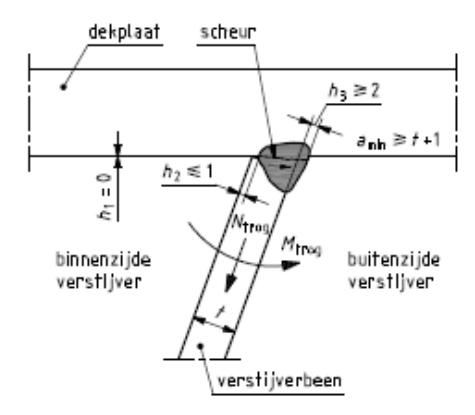
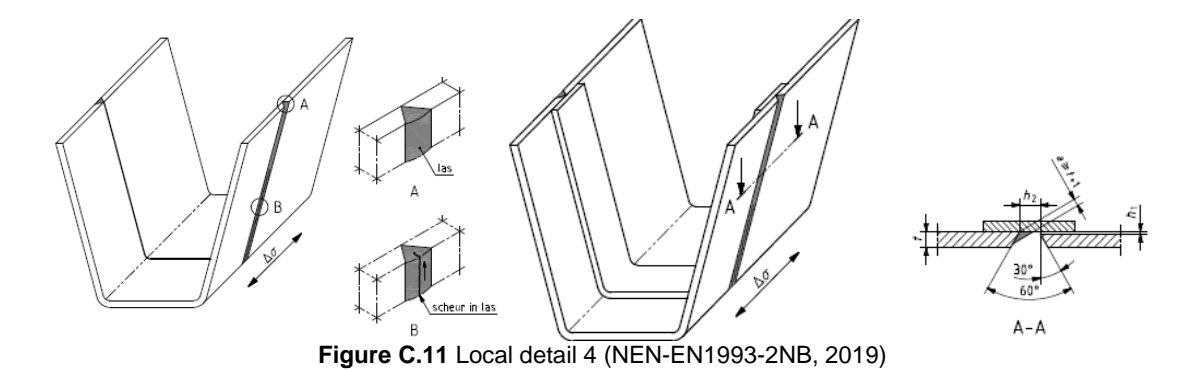


Figure C.10 Local detail 3 (NEN-EN1993-2NB, 2019)

Local detail 4 is weld failure in a butt-weld in the stiffener as shown in Figure C.11. The detail category ranges from 80 to 112 depending on the weldtype and detailing with or without backplate.



Local detail 5 is weld failure between stiffener and crossbeam as shown in Figure C.12. Depending on the local detailing the detail category is 56 for the left detailing or 71 tot 125 for the right detailing. For the left detailing the stiffeners are located in between the crossbeams, in the right detailing the crossbeams run through the stiffeners. This latter option is used in cases where the height of a bridge deck is not important. The left detailing is used for bridges with a limited deck height.

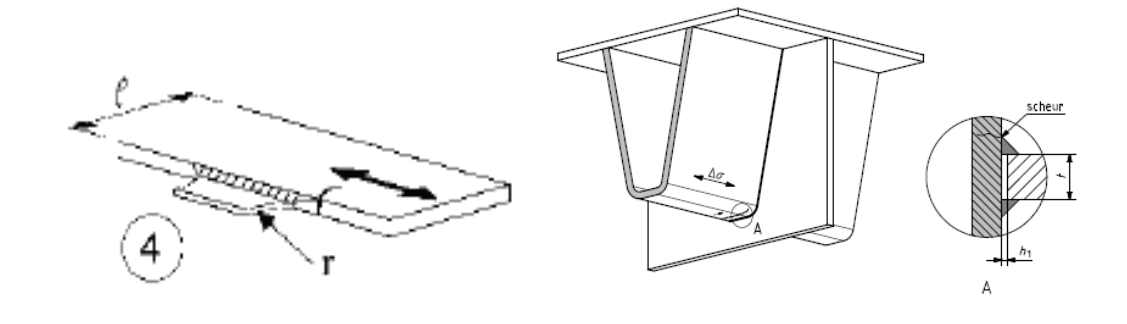






Figure C.12 Local detail 5 (NEN-EN1993-2NB, 2019)

Local detail 6 is also in the connection between stiffener and crossbeam but failure occurs in the crossbeam as shown in Figure C.13. Both detail configurations have a detail category of 80.

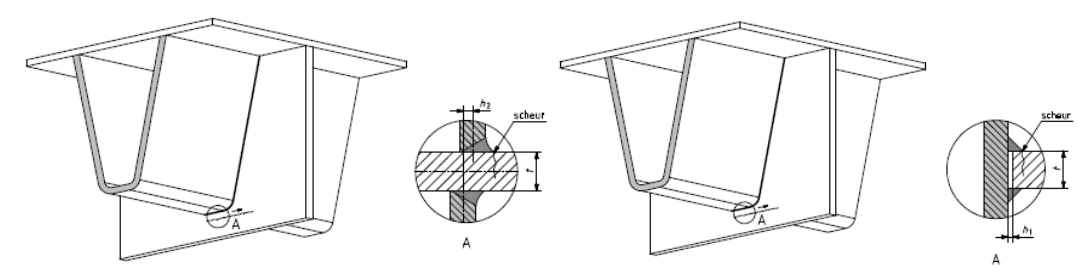


Figure C.13 Local detail 6 (NEN-EN1993-2NB, 2019)

Other details, including general action effects, that must be considered are taken from the Eurocode for fatigue (NEN1993-1-9, 2012)

General detail 1 is plate failure that can occur anywhere in a steel plate as shown in Figure C.14. Usual verification locations are in the bottom of the stiffeners or the deck plate at midspan of the bridge. This detail has the highest category which is 160.



Figure C.14 General detail 1 (NEN1993-1-9, 2012)

General detail 2 is weld failure in longitudinal direction as shown in Figure C.15. These details occur in the main girders and crossbeams. Depending on the weld type a detail category ranging from 100 to 125 must be considered.

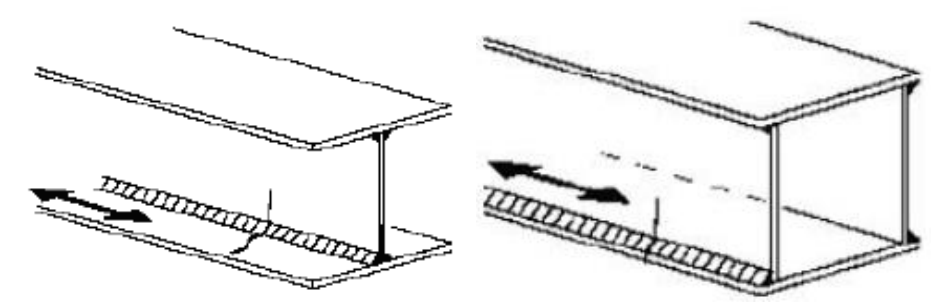


Figure C.15 General detail 2 (NEN1993-1-9, 2012)





General detail 3 is weld failure in transverse direction as shown in Figure C.16. This detail can be found in the connection between crossbeam and deck plate as well as crossbeam and main girder. This detail has a category of 80.

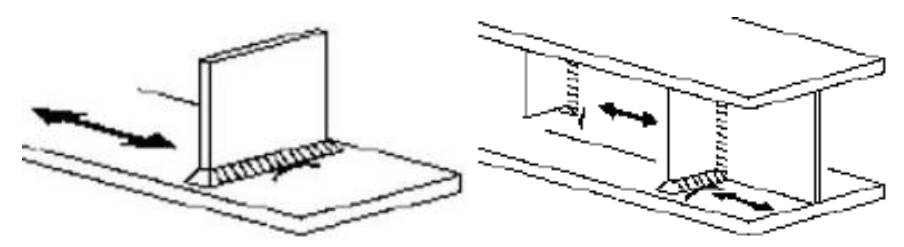


Figure C.16 General detail 3 (NEN1993-1-9, 2012)

General detail 4 is weld failure due to a pulling force as shown in Figure C.17. This detail can be found in the connection between crossbeam and main girder webs and has a detail category ranging from 40 to 80. This category depends on the thicknesses l and t. For OSD bridges a detail category of 80 holds if the thickness of the main girder web is less than 50 mm.

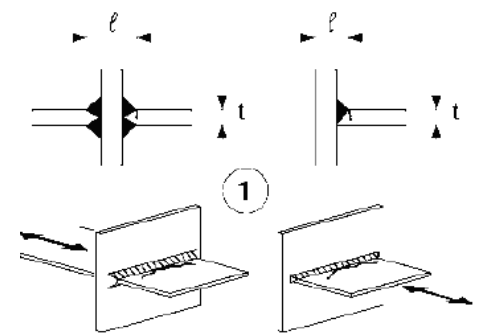


Figure C.17 General detail 4 (NEN1993-1-9, 2012)

General detail 5 is weld failure in the connection between crossbeam and main girder flange as shown in Figure C.18. This detail only occurs if the main girder and crossbeam have the same height. The detail category ranges from 36 to 112 depending on weldtype. Usually this detail category is 90 for OSD bridges. A correction factor k_s must be used if the thickness of the crossbeam flange is larger than 25 mm. k_s must be determined with equation (C.12).

$$k_{s} = \left(\frac{25}{t}\right)^{0.2} \quad \text{for } t > 25 \, \text{mm}$$

$$k_{s} = 1 \quad \text{for } t < 25 \, \text{mm}$$

$$k_{s} = \text{correction factor}$$

$$t = \text{crossbeam flange thickness}$$
(C.12)

where





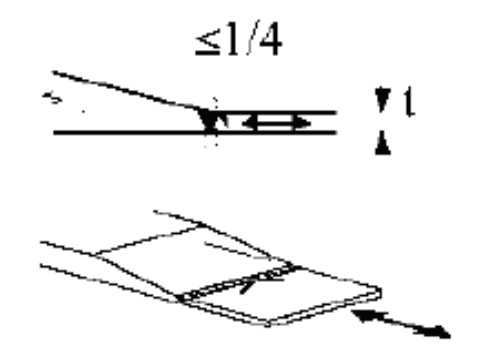


Figure C.18 General detail 5 (NEN1993-1-9, 2012)

General detail 6 is failure in the round-off from main girder to crossbeam flange as shown in Figure C.19. This detail only occurs if the main girder and crossbeam have the same height. The detail category is either 125 or 140 for unwelded round-off or ranges from 50 to 90 for welded round-off. For a welded detail with a radius larger than 150 mm a detail category of 90 must be used. For an unwelded round-off a detail category of 125 is often used.

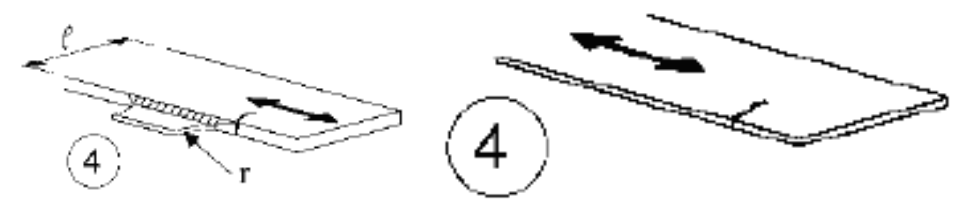


Figure C.19 General detail 6 (NEN1993-1-9, 2012)





C.2 FRP norms and regulations

Current norms for other materials do not compare to FRP which makes verification of design difficult. Different organizations have started to create rules and regulation for the use of FRP. These rules and regulations are mostly country bound but collaboration does happen. At the moment "CUR aanbeveling 96 (CUR 96, 2017)" is the Dutch recommendation and the latest version has been published in 2017 ((Luigi Ascione, Jean-François Caron, João Ramô Correia, 2016)). Another guideline that will be used in this report is the Prospect for New Guidance in the Design of FRP which has been published in 2016 (Luigi Ascione, Jean-François Caron, João Ramô Correia, 2016). This Prospect for New Guidance is a collaboration between different guidelines and is the first step towards a European code.

C.2.1 Bonded joints

In CUR 96 multiple recommendations can be found on the usage of adhered connections and will be stated below.

The influence of aging, water(vapour) and temperature on the adhesive strength must be considered by using conversion factors or obtaining values through testing. The adhesive must be valid for the adherend materials and conditions it will be used in. Connections should be protected from water(vapour) and moisture intrusion as much as possible. The following properties of an adhesive are of influence for the strength and must be considered in the design verification:

- Used materials
- Surface treatment
- Application method end hardening of the adhesive (pressure and environment conditions)
- Geometry of the adhesive connection
 - Type of connection (e.g. single or double lap)
 - Adhesive thickness
 - o Stiffness and chamfer of the adherends
 - o Fillet of the adherend
 - Overlap length

Temperatures of thermohardening and thermoplastic adhesives cannot exceed the usage temperature of the structure during the hardening process.

Adhesives must have a maximum usage temperature that exceeds the constructions usage temperature by a minimum of 20°C.





The overlap length should have a minimum length that coincides with equation (C.13).

$$L_{overlap,min} = 10 * t_{lam} for single lap joints L_{overlap,min} = 5 * t_{lam} for double lap joints t_{lam} = adherend thickness [mm]$$
 (C.13)

With:

Pre-surface treatment of the adherends and the thickness of the adhesive layer should be in accordance with the suppliers specifications. An optimal adhesive thickness can be approximated by equation (C.14).

$$t_a = \frac{G_{Ic} * E_a}{\pi * f_{y,a}^2} \tag{C.14}$$

with:

 $t_a = adhesive thickness [mm]$

 $G_{IC} = strain\ energy\ release\ rate\ [N/mm]$

(in accordance with NEN5528 or NEN - ISO15024)

 $f_{v,a} = adhesive yield stress [N/mm^2]$ $E_a = adhesive E - modulus [N/mm^2]$

Strength verifications for the adhesive bond should fulfil equations (C.15) to (C.18).

$$\frac{\sigma_{3a,Ed}}{f_{3a,Rd}} \le 1 \tag{C.15}$$

$$f_{3a,Rd} = \frac{\eta_{ca} * f_{3a,Rk}}{(C.16)}$$

$$\frac{\tau_{13a,Ed}}{\tau} \le 1 \tag{C.17}$$

$$\frac{\sigma_{3a,Ed}}{f_{3a,Rd}} \le 1$$
(C.15)
$$f_{3a,Rd} = \frac{\eta_{ca} * f_{3a,Rk}}{\gamma_{Ma}}$$
(C.16)
$$\frac{\tau_{13a,Ed}}{\tau_{13a,Rd}} \le 1$$
(C.17)
$$f_{13a,Rd} = \frac{\eta_{ca} * f_{13a,Rk}}{\gamma_{Ma}}$$
(C.18)

with:

 $\sigma_{3a,Ed} = out \ of \ plane \ stress$

 $f_{3a,Rd} = characteristic adhesive tensilte stress (test results)$

 $\eta_{ca} = conversion factor$ $\tau_{13a,Ed} = shear stress$

 $\tau_{13a,Rd} = characteristic shear stress$

 $\gamma_{Ma} = partial \ safety \ factor$

For combined stresses equation (C.19) should be fulfilled.

$$\left(\frac{\sigma_{3a,Ed}}{f_{3a,Rd}}\right)^2 + \left(\frac{\tau_{13a,Ed}}{\tau_{13a,Rd}}\right)^2 \le 1 \tag{C.19}$$





C.2.2 Buckling

Due to the slender nature of FRP plate structures stability issues can occur easily. A simple verification can be done to determine the buckling factor which should by higher than 1.0, the verification can be found in equation (C.20).

$$\lambda = \frac{\sigma_{cr}}{\sigma}$$

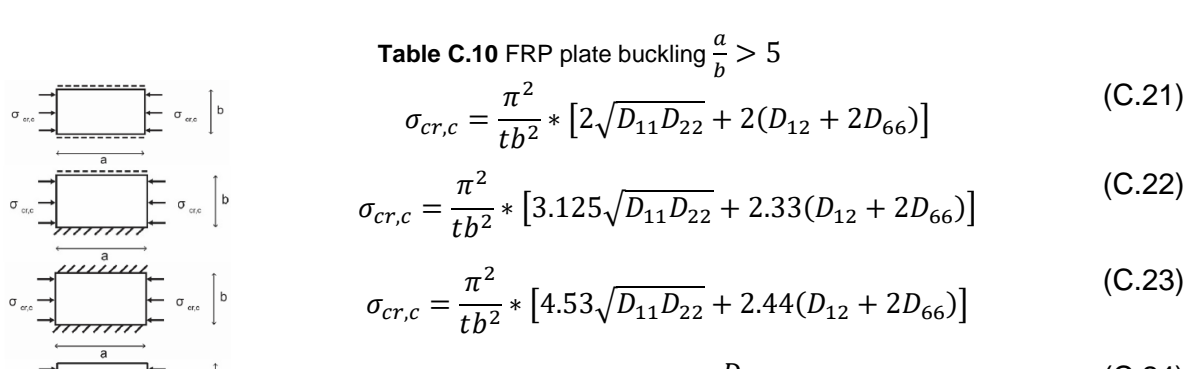
$$\lambda = buckling \ factor$$

$$\sigma_{cr} = critical \ buckling \ stress$$

$$\sigma = Actual \ stress$$
(C.20)

where

Analytical formulas have been constructed for simple FRP plate configurations which depend on the boundary conditions and type of loading. The critical buckling stresses for plates under compression and under shear loading can be found in Table C.10. These formula's only hold for plates where length (a) can be considered as infinite. This is true if $\frac{a}{b} > 5$ and holds for buckling in longitudinal direction of the FRP sandwich panel.



$$\sigma_{cr,c} = 12 * \frac{D_{66}}{tb^2} \tag{C.24}$$

$$\sigma_{cr,c} = \frac{1}{tb^2} \sqrt{D_{11}D_{22}} \left[15.1K\sqrt{1-v} + 7(1-K) \right] if \ K \le 1$$

$$\sigma_{cr,c} = \frac{1}{tb^2} \sqrt{D_{11}D_{22}} \left[15.1K\sqrt{1-v} + 6(K-1)(1-v) \right] if \ K > 1$$
(C.25)

$$K = \frac{2D_{66}^{CD} + D_{12}}{\sqrt{D_{11}D_{22}}} \text{ and } v = \frac{D_{12}}{2D_{66} + 2D_{12}}$$

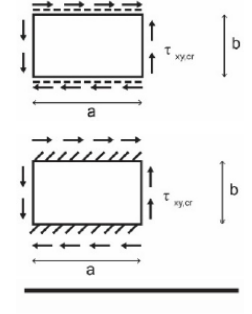
$$\tau_{xy,cr} = \frac{4}{tb^2} \sqrt[4]{D_{11}D_{22}^3 (8.125 + 5.045K) if K \le 1}$$

$$\tau_{xy,cr} = \frac{4}{tb^2} \sqrt[4]{D_{22}(D_{12} + 2D_{66})} \left(11.7 + \frac{1.46}{K^2}\right) if K > 1$$
(C.26)

$$\tau_{xy,cr} = \frac{1}{tb^2} \sqrt[4]{D_{22}(D_{12} + 2D_{66})} \left(11.7 + \frac{1.16}{K^2}\right) if K > 1$$

$$\tau_{xy,cr} = \frac{4}{tb^2} \sqrt[4]{D_{11}D_{22}^3 (15.07 + 7.08K) if K \le 1}$$

$$\tau_{xy,cr} = \frac{4}{tb^2} \sqrt[4]{D_{22}(D_{12} + 2D_{66})} \left(18.59 + \frac{3.56}{K^2}\right) if K > 1$$
(C.27)



Free edge Hinged edge D_{ij} are obtained from the D-matrix obtained from the laminate theory as shown in paragraph 2.2.1.4.





These formulas are not true for a sandwich panel since the boundary conditions are not fixed, hinged nor free but somewhere in between. However, these formulas can give good insight on the magnitude of the critical stresses that can be expected when using finite element software to determine the critical buckling stresses.

For plates with a ratio of $\frac{a}{b}$ < 5 a different set of formulas must be used. These are formulas from the aerospace industry and are shown in Table C.11 (Kassapoglou, 2013). These formulas can be used for buckling in vertical direction of the webs.





Table C.11 FRP plate buckling $\frac{a}{b} < 5$

	Table C.11 FRP plate buckling $\frac{1}{h} < 5$	
ss b ss ss	$\sigma_{cr} = \frac{\pi^2}{ta^2m^2} * [D_{11}m^4 + 2(D_{12} + 2D_{66})m^2(AR)^2 + D_{22}(AR)^4$	(C.28)
where	$m = number\ of\ half\ sines, m = 1$ is probably most critical	
	$AR = \frac{a}{b}$, (Aspect Ratio)	
→ c ↑ ss c ←	$\sigma_{cr} = \frac{\pi^2}{tb^2} * \sqrt{D_{11}D_{22}} * K$ $K = \frac{4}{\lambda^2} + \frac{2(D_{12} + 2D_{66})}{\sqrt{D_{11}D_{22}}} + \frac{3}{4}\lambda^2 \text{ for } 0 < \lambda < 1.662$	(C.29)
where	$K = \frac{4}{\lambda^2} + \frac{2(D_{12} + 2D_{66})}{\sqrt{D_{11}D_{22}}} + \frac{3}{4}\lambda^2 \text{ for } 0 < \lambda < 1.662$	
	$K = \frac{m^4 + 8m^2 + 1}{\lambda^2(m^2 + 1)} + \frac{2(D_{12} + D_{66})}{\sqrt{D_{11}D_{22}}} + \frac{\lambda^2}{m^2 + 1} $ for $\lambda > 1.662$	
	$\lambda = \frac{a}{b} \left(\frac{D_{22}}{D_{11}} \right)^{\frac{1}{4}}$	
→ ss b c ss ←	$\sigma_{cr} = \frac{\pi^2}{tb^2} * \sqrt{D_{11}D_{22}} * K$	(C.30)
where	$K = \frac{m^2}{\lambda^2} + \frac{8(D_{12} + 2D_{66})}{\sqrt{D_{11}D_{22}}} + \frac{16}{3}\lambda^2$ $\sigma_{cr} = \frac{\pi^2}{tb^2} * \sqrt{D_{11}D_{22}} * K$ $K = \frac{4}{\lambda^2} + \frac{8(D_{12} + 2D_{66})}{\sqrt{D_{11}D_{22}}} + 4\lambda^2 \text{ for } 0 < \lambda < 1.094$	
→ c ↑ c c ←	$\sigma_{cr} = \frac{\pi^2}{tb^2} * \sqrt{D_{11}D_{22}} * K$	(C.31)
where	$K = \frac{4}{\lambda^2} + \frac{8(D_{12} + 2D_{66})}{\sqrt{D_{11}D_{22}}} + 4\lambda^2 \text{ for } 0 < \lambda < 1.094$	
	$K = \frac{m^4 + 8m^2 + 1}{\lambda^2(m^2 + 1)} + \frac{2(D_{12} + D_{66})}{\sqrt{D_{11}D_{23}}} + \frac{\lambda^2}{m^2 + 1} $ for $\lambda > 1.094$	
ss b ss +	$\sigma_{cr} = \frac{\pi^2}{tb^2} * \sqrt{D_{11}D_{22}} * K$	(C.32)
where	$\sigma_{cr} = \frac{\pi^2}{tb^2} * \sqrt{D_{11}D_{22}} * K$ $K = \frac{12}{\pi^2} + \frac{D_{66}}{\sqrt{D_{11}D_{22}}} + \frac{1}{\lambda^2}$ $\tau_{cr} = \frac{4}{tb^2} * (D_{11}D_{22}^3)^{\frac{1}{4}} * K$	
ss b ss ss		(C.33
where	$K = 8.2 + 5 * \frac{D_{12} + 2D_{66}}{\sqrt{D_{11}D_{22}}} * \frac{1}{\frac{A}{B} + B\beta}$	
	$\beta = \left(\frac{D_{11}}{D_{22}}\right)^{\frac{1}{4}}, \lambda = \frac{a}{b}\left(\frac{D_{22}}{D_{11}}\right)^{\frac{1}{4}}$	
	$A = -0.27 + 0.185 * \frac{(D_{12} + 2D_{66})}{\sqrt{D_{11}D_{22}}}$	
	$B = 0.82 + 0.46 * \frac{D_{12} + 2D_{66}}{\sqrt{D_{11}D_{22}}} - 0.2 \left(\frac{D_{12} + 2D_{66}}{\sqrt{D_{11}D_{22}}}\right)^2$	





C.2.3 Fatigue

Fatigue must be considered for constructions with cyclic loading with more than 5000 cycles or a maximum cyclic load which is higher than 40% of the failure load. Cyclic loads can be considered as a load with constant amplitude if the alternating stresses differ no more than 5% from the average stress range. In all other cases the fatigue load has to be considered as a variable amplitude load.

The fatigue life for constant amplitude loads can be determined using a fatigue strength curve which is expressed by a R-value. The R-value van be determined using equation (C.34). This fatigue strength curve is specific for a material and fatigue load type. So called "constant life diagrams" (in Dutch: constante levensduur diagram or CLD) exist if there is no fatigue strength curve for a situation at hand. These CLDs can be used to interpolate between existing fatigue strength curves.

$$R = \frac{\sigma_{min}}{\sigma_{max}} \tag{C.34}$$

To construct a CLD some fixed R values can be used for specific cases as stated below.

- R = 0.1 for alternating tensile forces (0 < R < 0.8)
- R = -1 for alternating tensile & compression forces (-10 < R < 0)
- R = 10 for alternating compression forces (1.2 < R < 10)

The fatigue strength curve itself can be constructed using equation (C.35). This equation is given by the CUR and holds for situations in which the spread of stresses is less than 10%-20%.

$$\log(N) = k * \log\left(\frac{\gamma_{Mf} * \gamma_{M} * \sigma_{max}}{\eta_{c} * B}\right)$$
 (C.35)

with

N = number of cycles till failure

k = regression paramter, can be deduced from tests

B = characteristic strength of laminate after 1 cycle

$$B = 700 * \frac{V_f}{0.55}$$

 $\sigma_{max} = maximum \ occurring \ stress \ during \ a \ cycle$

 $\gamma_{Mf} = material fatigue factor$

Standard values for k and B are recommended by the CUR for laminates with a volume fraction between 35% and 65% and a minimum fibre percentage in the four main directions of 12.5%. These standard values can be found in Table C.12 and hold for a number of cycles between 10^2 and 10^6 .





Table C.12 Regression parameters k and B for UD-laminates

UD-plies		Glass/epoxy		Glass/polyester		Carbon/epoxy
	k	В	k	В	k	В
R = -1	-10	$600*\left(\frac{V_f}{0.55}\right)$	-9	$700*\left(\frac{V_f}{0.55}\right)$	-15	$900*\left(\frac{V_f}{0.55}\right)$
R = 0.1	-10	$1100*\left(\frac{V_f}{0.55}\right)$	-7	$1300*\left(\frac{V_f}{0.55}\right)$	-30	$1200*\left(\frac{V_f}{0.55}\right)$
R = 10	-18	$750*\left(\frac{V_f}{0.55}\right)$				

The actual damage due to fatigue must be calculated using Miners rule as shown by equation (C.36). A component must be considered as failed if the damage value D is larger or equal to 1.

$$D = \sum \frac{n_i}{N_i} \le 1.0 \tag{C.36}$$

Where

 $D = \sum \frac{n_i}{N_i} \leq 1.0$ $n_i = number\ of\ cycles\ of\ a\ specific\ stress\ range\ and\ R-value$ $N_i = number\ of\ cycles\ till\ failure\ for\ that\ specific\ n_i$





Annex D

Sandwich panel fatigue results

						_ •	abi		<u> </u>		ariu	WIC	<u>''' </u>	an	CI 1	aแ	guc	; re	Sui							
	Damage	2,59E-07	6,25E-06	3,88E-05	3,47E-06	7,80E-06	1,26E-06	3,28E-06	7,09E-06	4,17E-07	3,31E-06	7,19E-05			Damage	1,04E-03	4,07E-04	2,40E-03	2,44E-04	5,28E-04	1,31E-04	3,48E-05	1,17E-05	4,31E-06	3,10E-05	4,83E-03
	n_occur	7,50E+07	6,00E+07	6,00E+07	2,30E+07	6,60E+06	3,10E+05	5,00E+04	2,00E+04	1,00E+04	1,00E+04	mage			n_occur	7,50E+07	6,00E+07	6,00E+07	2,30E+07	6,60E+06	3,10E+05	5,00E+04	2,00E+04	1,00E+04	1,00E+04	mage
ssbeam	N_failure r	2,90E+14	9,60E+12	1,55E+12	6,62E+12	8,46E+11	2,46E+11	1,52E+10	2,82E+09	2,40E+10	3,02E+09	Total damage		nidspan	N_failure r	7,20E+10	1,48E+11	2,50E+10	9,42E+10	1,25E+10	2,36E+09	1,44E+09	1,71E+09	2,32E+09	3,22E+08	Total damage
top face crossbeam	Max stress N	7,87	11,49	14,07	11,97	15,05	17,26	23,51	28,36	22,36	24,58			bottom face midspan	Max stress N	19,78	18,27	22,25	19,20	24,03	28,46	30,56	29,99	28,98	36,09	
	Vehicle	damage vehicle 4B_1 =	damage vehicle 4B_2 =	damage vehicle 4B_3 =	damage vehicle 4B_4 =	damage vehicle 4B_5 =	damage vehicle 4B_6 =	damage vehicle 4B_7 =	damage vehicle 4B_8 =	damage vehicle 4B_9 =	damage vehicle 4B_10=				Vehicle	damage vehicle 4B_1 =	damage vehicle 4B_2 =	damage vehicle 4B_3 =	damage vehicle 4B_4 =	damage vehicle 4B_5 =	damage vehicle 4B_6 =	damage vehicle 4B_7 =	damage vehicle 4B_8 =	damage vehicle 4B_9 =	damage vehicle 4B_10=	
		3	7	9	7	7	7	7	7	3	7							9	7	5	7	7	~	8	7	
	Damage	1,88E-08	5,43E-07	3,86E-06	3,36E-07	7,09E-07	1,11E-07	2,44E-07	4,83E-07	2,66E-08	2,21E-07	6,56E-06			Damage	4,30E-06	1,64E-06	9,68E-06	1,26E-07	2,06E-06	5,29E-07	1,41E-07	4,28E-08	1,60E-08	1,20E-07	1,87E-05
	n_occur	7,50E+07	6,00E+07	6,00E+07	2,30E+07	6,60E+06	3,10E+05	5,00E+04	2,00E+04	1,00E+04	1,00E+04	mage			n_occur	7,50E+07	6,00E+07	6,00E+07	2,30E+07	6,60E+06	3,10E+05	5,00E+04	2,00E+04	1,00E+04	1,00E+04	mage
beam	N_failure r	3,99E+15	1,10E+14	1,55E+13	6,85E+13	9,30E+12	2,78E+12	2,05E+11	4,14E+10	3,76E+11	4,53E+10	Total damage		span	N_failure r	1,74E+13	3,66E+13	6,20E+12	1,82E+14	3,20E+12	5,86E+11	3,54E+11	4,67E+11	6,23E+11	8,33E+10	Total damage
Web crossbeam	Max stress	2,88	8,76	10,89	9,23	11,53	13,18	17,62	21,04	16,47	18,67			Web midspan	Max stress	10,75	06′6	12,06	8,28	12,98	15,40	16,57	16,07	15,57	19,47	
	Vehicle	damage vehicle 4B_1 =	damage vehicle 4B_2 =	damage vehicle 4B_3 =	damage vehicle 4B_4=	damage vehicle 4B_5 =	damage vehicle 4B_6=	damage vehicle 4B_7 =	damage vehicle 4B_8=	damage vehicle 4B_9=	damage vehicle 4B_10 =				Vehicle	damage vehicle 4B_1 =	damage vehicle 4B_2 =	damage vehicle 4B_3 =	damage vehicle 4B_4=	damage vehicle 4B_5 =	damage vehicle 4B_6=	damage vehicle 4B_7 =	damage vehicle 4B_8=	damage vehicle 4B_9=	damage vehicle 4B_10 =	









Annex E

Rain flow method

The stress ranges, or so-called fatigue ripples, can be determined from the vehicle spectrum in multiple ways, one of which is the rain-flow counting method. This method consists of multiple steps and will be explained below. Here an example has been used from an existing fatigue calculation of vehicle type three from Table C.8. This example has been taken from my own internship report at Royal HaskoningDHV (Wateren, 2019).

1. Rearrange the vehicle spectrum or vehicle influence line to start with the highest peak. The stress spectrum given for a certain vehicle must be rearranged to start with the highest peak. This results in a graph as shown in Figure E.1 for example.

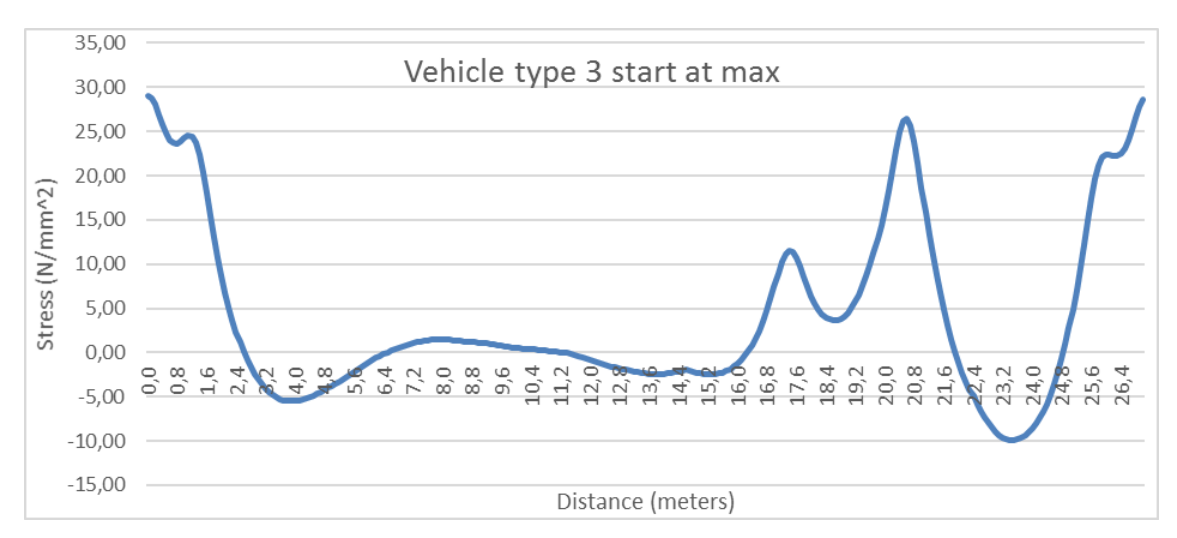


Figure E.1 Vehicle spectrum start at max

2. Find all the peaks and valleys and create a new graph from this data.

With the help of excel a simple IF() statement can be used to see whether the next value is smaller than the current value. The moment it returns a false value instead of a true value a valley has been found. The moment it returns a true value after a false value a peak has been found. These peaks and valleys arranged after each other results in Figure E.2 and has a close resemblance to Figure E.1.







Figure E.2 Rainflow diagram from vehicle spectrum

3. Rotate the graph clockwise 90° and count the stress ranges.

Each stress range from peak to valley has been numbered and gathered in Figure E.3





4. Sea each peak/valley as a source of water and let water drip down (Figure E.3)

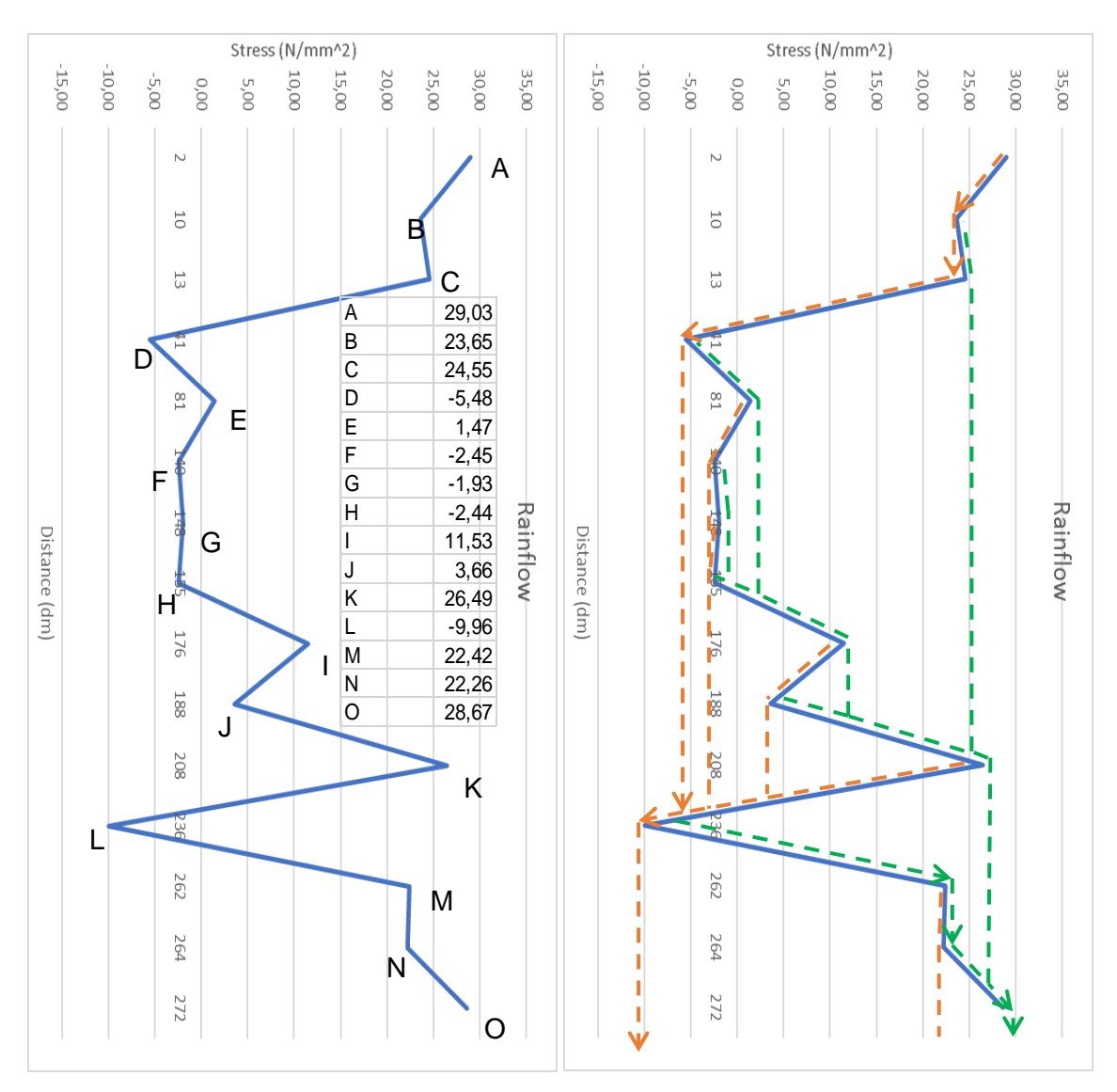


Figure E.3 Stress range and rain flow for stress range

For each valley in the graph the water will drip down to the right (green lines) for each peak the water will drip down to the left (orange lines). In case of the red lines the highest peak must be found first and water starts dripping down from there. This results in a line of water running from A through B and D to L with a stress range of $29.03 - -9.96 = 38.99 \, MPa$ as is shown by the red arrows. The next biggest range will start from the next peak, in this case K and will run until it finds the already existing flow. The results in a stress range running from K to D before it merges with the already existing flow of water. This process is repeated until there are no peaks left as a water source. Then the same process is done starting from the valleys as is shown by the green lines.





5. Count the number of occurrences of each stress range.

Since the bigger the stress ranges the bigger the damage the task is to find the highest stress ranges possible without using the same line twice. An overview can be found in Table E.1 and is in accordance with the lines shown in Figure E.3.

Table E.1 Stress range overview

Start	Finish	Stress	Start	Finish	Stress	Stress range	Stress	Occurrence
Α	L	38,99	L	0	38,63	$\Delta\sigma_1$	38,99	1
K	D	31,97	D	K	31,97	$\Delta\sigma_2$	38,63	1
I	J	7,88	J		7,88	$\Delta\sigma_3$	31,97	2
Е	F	3,91	F	Е	3,91	$\Delta\sigma_4$	7,88	2
С	В	0,90	В	С	0,90	$\Delta\sigma_5$	3,91	2
G	Н	0,51	Н	G	0,51	$\Delta\sigma_6$	0,90	2
М	N	0,16	M	Ν	0,16	$\Delta\sigma_7$	0,51	2
						$\Delta\sigma_8$	0,16	2

The different stress ranges have been rearranged to form a list of stress ranges in descending order. Next to this a column is added which sums up the number of occurrences of that specific stress range. The two biggest stress ranges will always result in a single occurrence, all the others will result in 2 occurrences. These occurrences can also be called the number of half-cycles.





Annex F

FEM elements and analysis

Finite element types

There are different type of elements that have different properties but they can be categorized in three main groups, 1D, 2D or 3D.

1D elements are the simplest elements as shown in Figure F.1. Depending on the order of the element it can be a straight (linear) or curved (2nd order or higher) line. These elements can be used when designing a model for global loads. For instance an I-beam can be modelled as a 1D element if global analysis is desired.

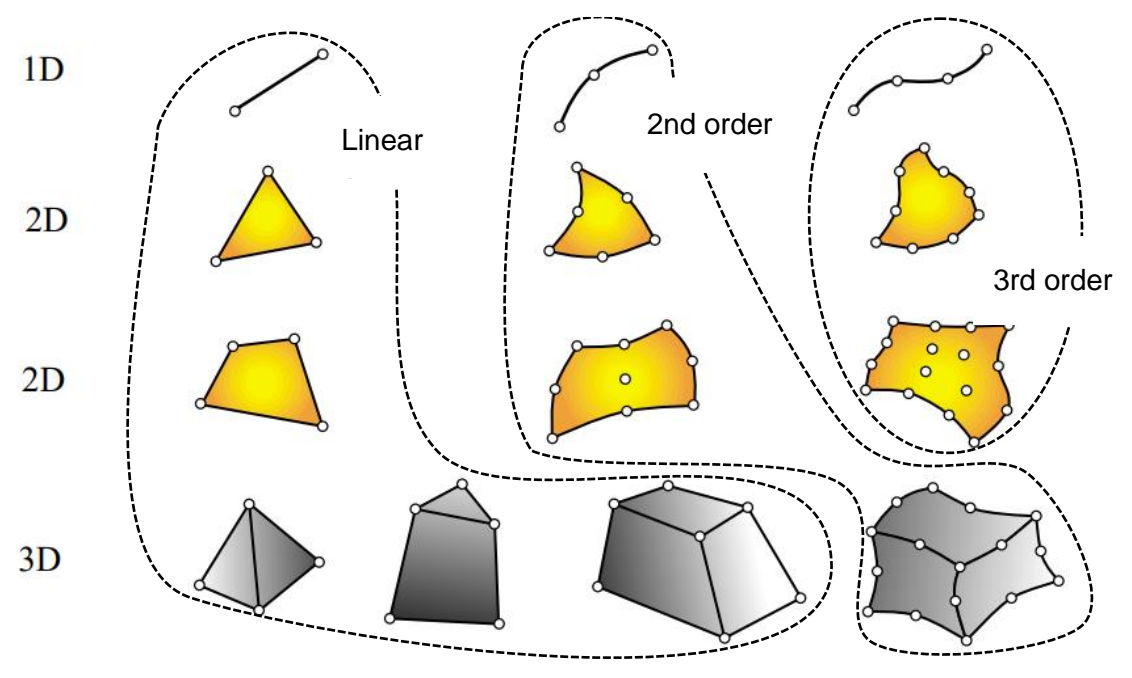


Figure F.1 FEM elements (Pillwein, 2015)

For a slightly more detailed analysis 2D elements or so called plate elements are used. Most used is the 4 node quadrilateral shell element. These elements can have a thickness and through linear interpolation stresses and strains can be calculated at the bottom or top of the element. The 2nd order 2D element, also known as the Lagrange quadrilateral, and result in a higher accuracy. This increase in accuracy comes with a higher calculation time, usually a 4 node quadrilateral is accurate enough.





These 2D elements are very useful for finite element analysis but do have their limitations. Laminate characteristics can be assigned to these elements which can result in correct results for a global analysis. Local analysis however cannot be done. The laminate is modelled as one solid layer and interlaminate failure (delamination) cannot be modelled.

To model these local failures such as delamination 3D elements are needed. With the use of 3D elements each separate ply within the laminate can be modelled and interface conditions can be added to define the failure characteristics of the resin. These so called volume elements can either be linear (8 nodes) or quadratic (20) nodes.

Deciding on which element to use depends on the goal and the desired calculation time. Using higher order or higher dimension elements (usually) results in a more realistic outcome, however calculation times increases. Between modelling a plate with 4-node quadrilateral elements or with 8-node volume elements doubles calculation time. Using 2nd order elements instead of 1st order increases the calculation time even more.

For this project which is mainly focussing on a global scale 3D elements are unnecessary but 1D elements are to simplistic. Therefore 2D elements must be used with enough accuracy but without increasing calculation time drastically.

Analysis types

Multiple ways of analysis can be done for different structures and load cases. Depending on the loading, type of structure and desired goal different analysis must be conducted. A few analysis types will be explained in this paragraph (Pavlovic, 2018b).

By using **linear analysis** material properties are defined as linear elastic. Results produced are stresses, deformations and forces which can than be used to perform SLS or ULS verifications. This type of analysis is very useful to determine maximum stresses or strains occurring for a certain load-case. However, if an element of the structure would fail no redistribution will occur since element properties are linear elastic without any failure point.

The **linear buckling analysis** determines critical buckling modes with the use of eigenvalue analysis of the linear system. Only load distribution, not intensity, will influence the buckling modes and linear buckling analysis assumes each load to be proportional. Distinguishing dead loads from live loads is not possible due to this assumption.

By doing a **material nonlinear analysis** progressive failure can be analysed. Plasticity or damage to materials is considered in this analysis which means that a redistribution of forces





will occur if a part of the structure fails. For laminates this can be used to determine ultimate resistance of the laminate even after one of the plies fails or resin failure occurs. This is however an analysis that is conducted on a small scale. Since this project is working on a more global scale this analysis type is not needed.

A **geometrically nonlinear analysis** is often combined with material nonlinearity and is a step wise analysis that uses the deformed shape of the previous step. Combining these nonlinear analysis can be done to perform a **nonlinear buckling analysis**. With the same reasoning as the material nonlinear analysis this analysis is not needed.









Annex G

Validation of RFEM laminate

The validation of laminates in RFEM will be done in several steps. The first validation will show that a simple laminate plate gives the same results as an orthotropic plate with properties defined by the laminate theory shown in chapter 2.2.1.4. Table G.1 shows the material properties that will be used for this validation, on the left the properties of the laminate and on the right the resulting orthotropic plate properties calculated with the laminate theory.

Ply properties and ply built-up Orthotropic plate properties Top flange Top flange output Variable value Variable Value unit Unit E1 37200 MPa t tot mm E2 MPa 18,90 11400 Ex Gpa G 18,90 MPa 3400 Ey **GPa** v12 0,29 7,09 Gxy GPa alpha 11 1,05E-05 0,33 /deg K VXY alpha 22 Rekgrens Trek /deg K 5,08E-05 1,2% mm **0,125** 0 (X-direction) Rekgrens Druk 1,2% Layer 1 thick Layer 2 thick mm 0,125 45 Rekgrens Afschuif 2,4% Layer 3 thick 0,125 90 (Y-direction) 226,76 Sig xt Mpa mm 0,125 -45 Layer 4 thick MPa 226,76 mm Sig_xc 0,125 -45 MPa 170,10 Layer 5 thick mm Tau 12 2,12E-05 Layer 6 thick 0,125 90 alpha x /deg K mm 0,125 45 Layer 7 thick mm alpha_y /deg K 2,12E-05 Layer 8 thick 0,125 0 alpha_xy /deg K 0,00E+00 mm

Table G.1 Validation material properties

The simplest verification that can be done is verifying the displacement due to a line load using classical beam theory. A beam is modelled in RFEM with a width of 100 mm, a span of 3000 mm and a height of 50 mm as is shown in Figure G.1.



Figure G.1 Validation beam model

The beam is supported on both sides in Y and Z-direction and on one side in X-direction.





A distributed load is placed upon the beam causing it to deform. The deformation should coincide with the expected deformation as calculated by the forget-me-nots. For a simply supported beam the forget-me-not shown in equation (G.1) must be used.

$$w = \frac{5}{384} \frac{q * l^4}{EI} \tag{G.1}$$

with

w = deformation [mm] $q = distributed load \left[\frac{N}{mm}\right]$ l = length [mm] $E = E - modulus \left[\frac{N}{mm^2}\right]$ $I = moment of inertia [mm^4]$

The moment of inertia in this case is $1.04 * 10^6 mm^4$ as shown in equation (G.2).

$$I = \frac{1}{12} b * h^{3} = \frac{1}{12} * 100 * 50^{3} \cong 1.04 * 10^{6} mm^{4}$$

$$b = width [mm]$$

$$h = height [mm]$$
(G.2)

with

With this the expected deformation for a distributed load of $0.1 \frac{N}{mm}$ will be $5.36 \ mm$ as shown in equation (G.3)

$$w = \frac{5}{384} \frac{0.1 * 3000^4}{18900 * 1.04 * 10^6} = \frac{5}{384} * \frac{8.1 * 10^{12}}{19.69 * 10^9} = 5.36 \, mm \tag{G.3}$$

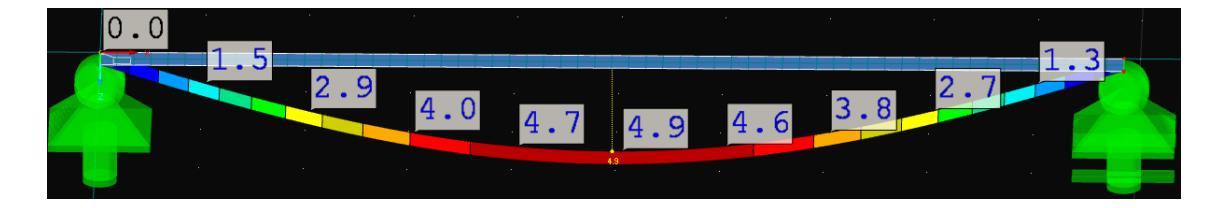
Figure G.2 shows the results from RFEM. A different result can be seen for laminates with different ply thicknesses. This can be explained by looking at the effect fibres have in bending. The outer fibres will deform the most and will therefore have a bigger effect on the restraining of deformation. Using thick plies results in a thicker layer of fibres in the span-direction which restrain the deformation more then fibres in other directions do.

Lowering the ply thickness to a more realistic value (for instance 0.125 mm) results in a deformation that coincides with the expected deformation from the forget-me-not. The deformation of the orthotropic plate also results in the same deformation and thereby validates the capabilities of RFEM for modelling laminates in a basic way.

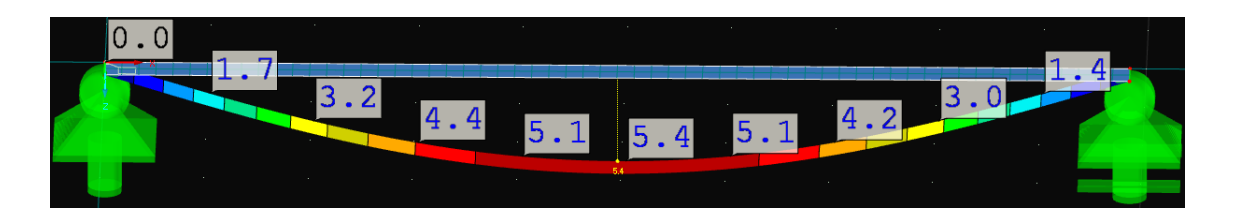
Laminate plate (16 layers of 3.125 mm)







Laminate plate (400 layers of 0.125 mm)



Orthotropic plate

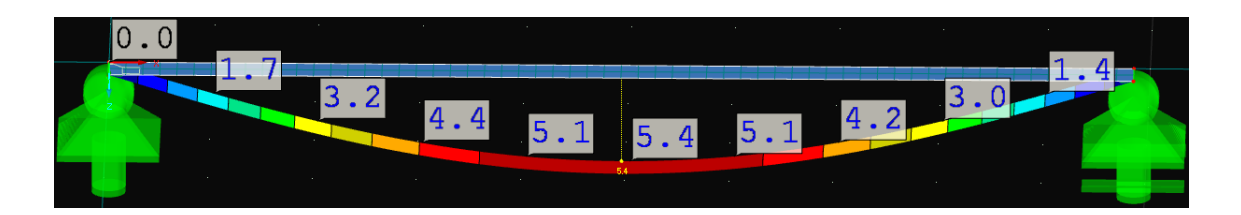
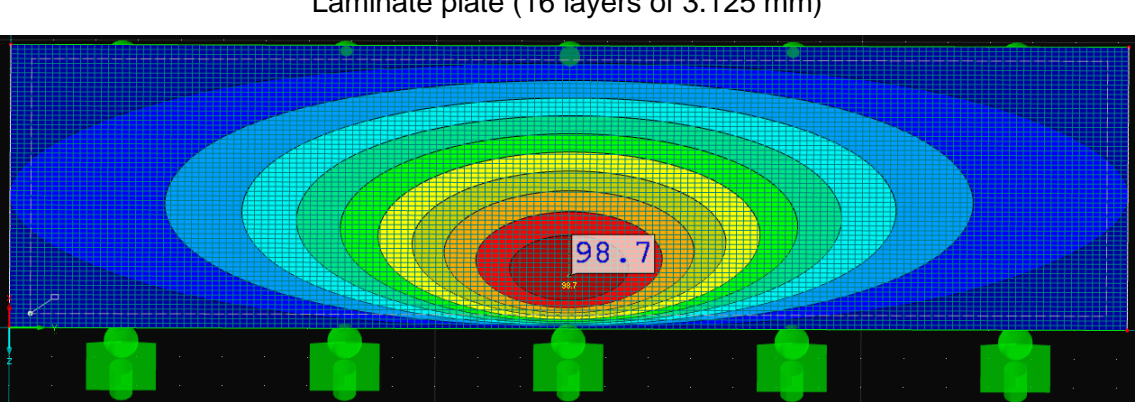


Figure G.2 Validation beam model results

When extending the width of the beam a wide plate can be modelled with a width of $8000 \ mm$. As an example a single wheel load of $200 \, kN$ is placed in the centre of the plate and deformations are compared as shown in Figure G.3. Once more it can be seen that there is a necessity for small ply thicknesses to ensure a correct analysis. The orthotropic plate differs slightly from the laminate plate (0.29%). This difference can be considered as negligible.

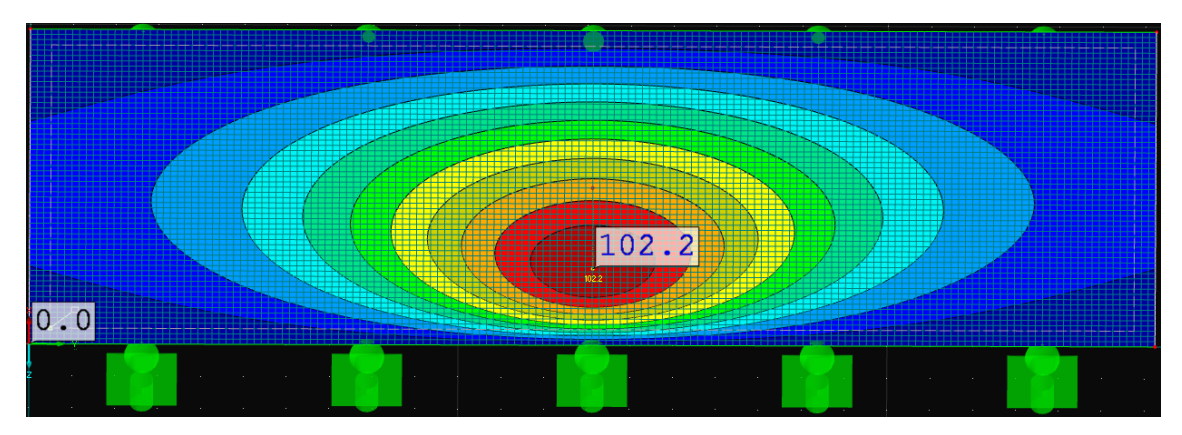


Laminate plate (16 layers of 3.125 mm)

Laminate plate (400 layers of 0.125 mm)







Orthotropic plate

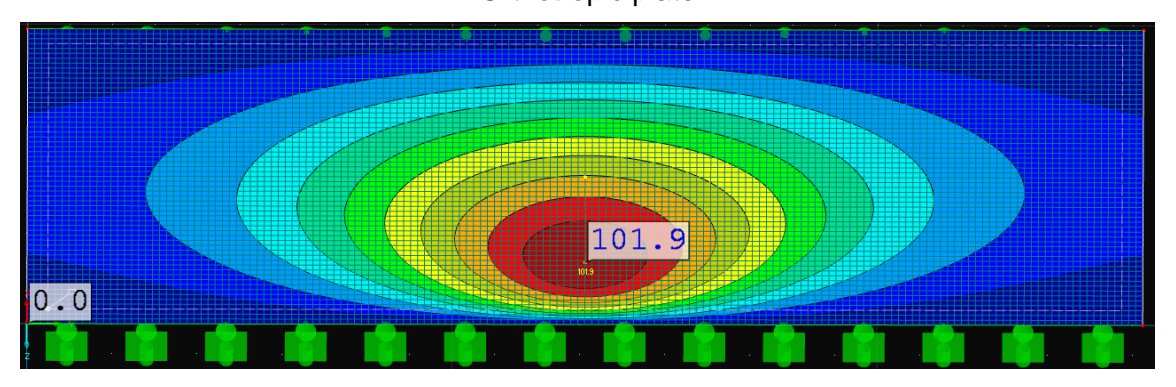


Figure G.3 Validation plate model results





The next step is to validate results for a complete sandwich panel. The parameters for this validation can be found in Figure G.4. The webs run in the direction of the span which coincides with the X-direction in the RFEM model.

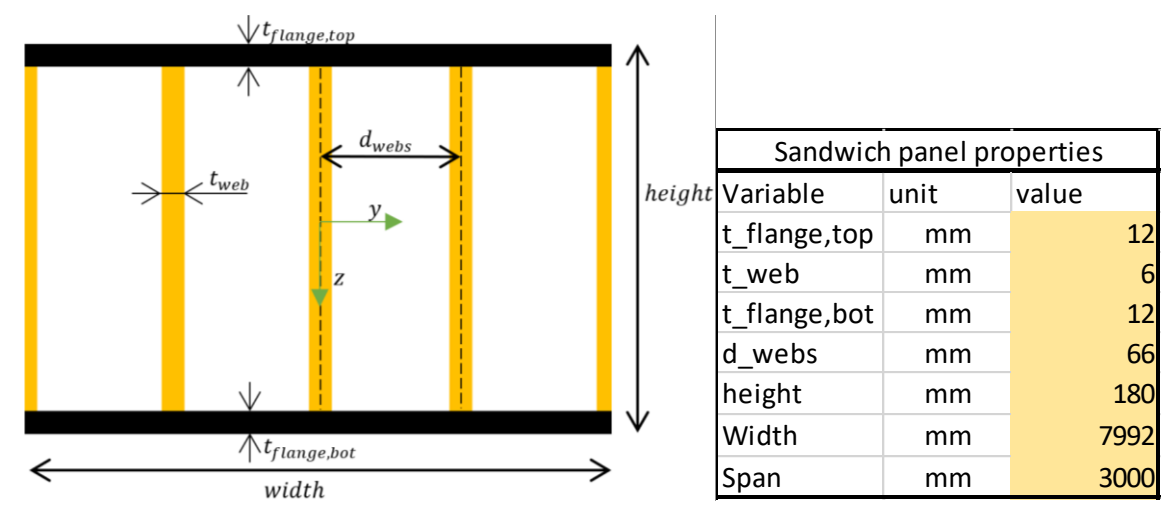


Figure G.4 Validation sandwich model parameters

The same wheel load has been applied as in the previous validation together with the corresponding horizontal forces. The horizontal forces are added to verify that both decks react the same when lateral forces are applied and loads are transferred correctly through the webs. The results are shown in Figure G.5. The figures on the left are from the laminate sandwich panel, the figures on the right from the orthotropic sandwich panel. No differences can be found in the deformations hence validating the laminate module in RFEM.

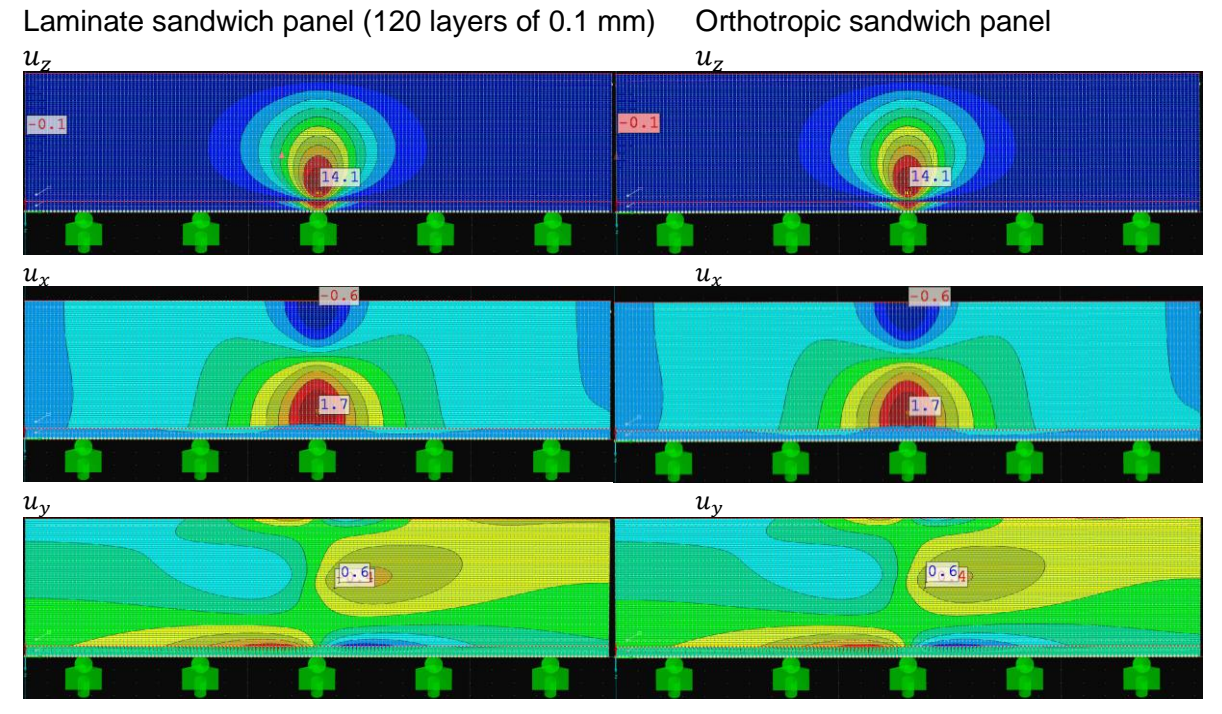


Figure G.5 Validation sandwich model results









Annex H

Validation RFEM release mechanism

This annex gives an explanation on the release mechanisms that can be implemented in RFEM. It starts of with an explanation on what a release mechanism is. After that a set of examples is given for a 2D release, 3D release and a 3D release with bolts.

Release mechanisms

Laminates can be modelled by RFEM as shown in the previous paragraph. The next question is what the capabilities are for RFEM to model bolted and/or bonded connections. To model this so called node or line releases are needed. These release mechanisms make sure that certain elements in a model are connected when fulfilling specific requirements. Explaining this mechanism can best be done using an example as shown in Figure H.1.

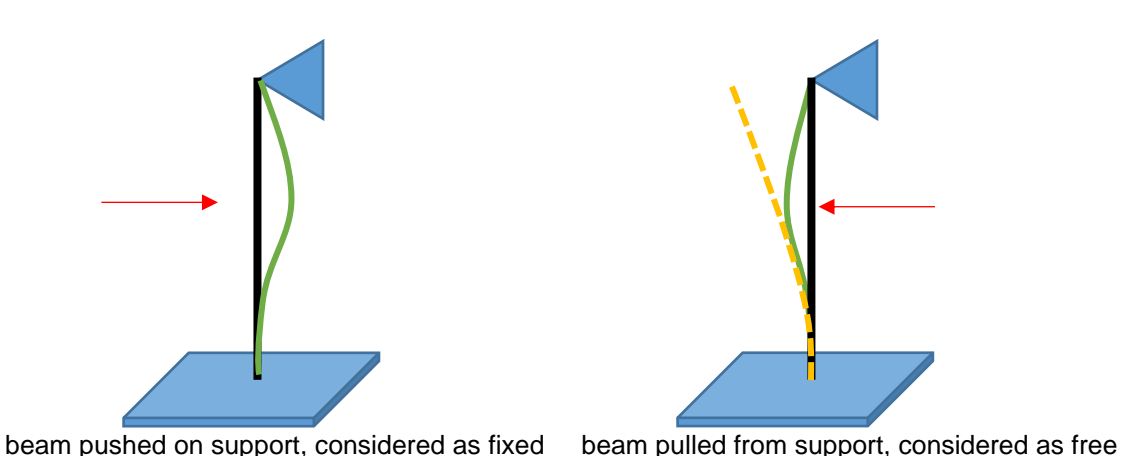


Figure H.1 Node release example

The left figure shows a rod that is being pushed on the top support. As expected the support prohibits the rod from displacing in lateral direction. Turning the force (red arrow) in the other direction causes a mirrored displacement field (green). If a nodal release mechanism is considered at the top support the displacement could look like the yellow dashed line. In this case a release mechanism has been programmed that releases the rod if a pulling force occurs.





This mechanism can be used for nodes and lines and can be programmed in many different ways. The example above shows a sudden release, other possibilities may include elastic or plastic release, tear, etc. In the case of an adhered Steel-FRP bridge deck a tear release can be considered. The bond will deform due to stresses in the material up until a certain threshold, after that the bond fails causing a tear. After this tear a load can only be transferred through friction or a pressure load perpendicular to the surface.

2D release mechanism

A simple example has been created to verify this release mechanism in RFEM. For this the model parameters as shown in Figure G.4 are used. Instead of one span two spans are used and the supports have been replaced by a part of the cross beam. The release mechanisms are created between the top flange of the cross beam and the bottom flange of the sandwich panel. An illustration of the set-up can be seen in Figure H.2.

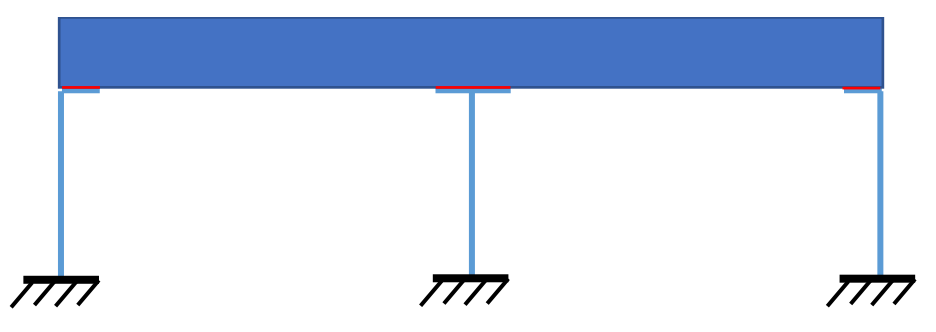


Figure H.2 release mechanism example

Figure H.3 shows the results, the top figure without a release mechanism and the bottom figure with a release mechanism. A distributed load has been placed on top of the right span. Without a release mechanism the sandwich panels stays attached to the crossbeam, comparable to an infinitely stiff bonded or bolted connections. Wit the release mechanism the sandwich panel parts with the cross beam. This can be compared with a sandwich panel placed upon crossbeams without any bonding.





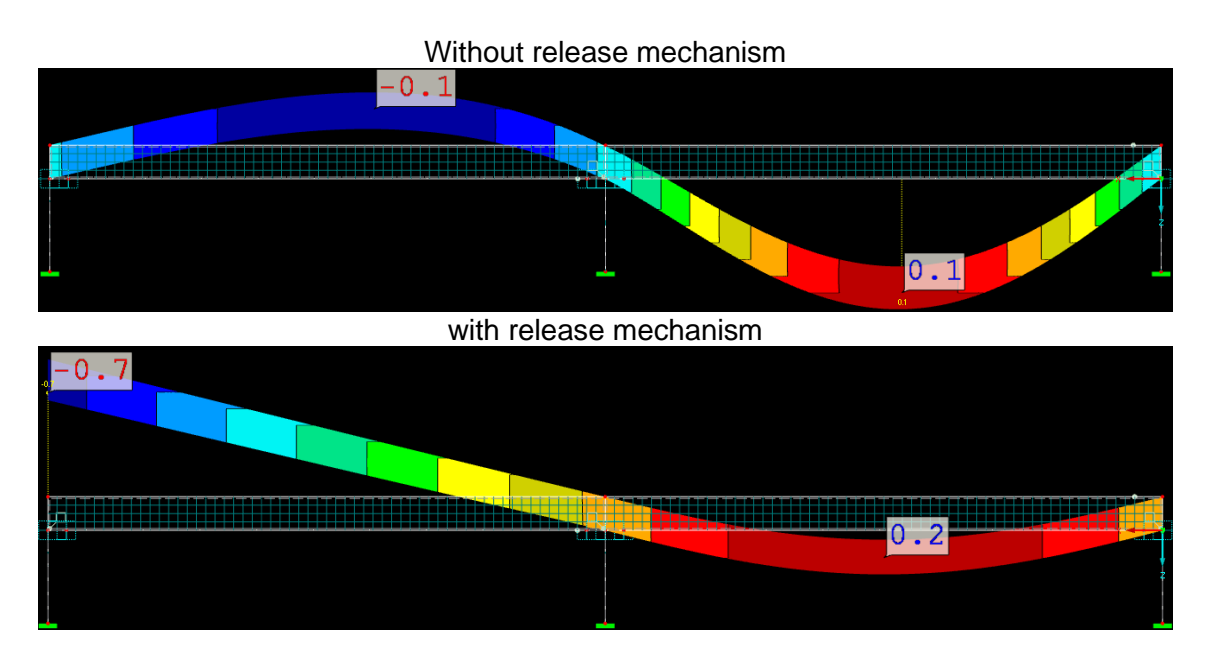


Figure H.3 release mechanism 2D example results

3D release mechanism

The same has been done for a 3D model with a slight alteration. Instead of a downward force which causes uplift in the neighbouring span an upward force is modelled in one span. Releases have been modelled on one of the main girders and the crossbeams in that span. This is shown in Figure H.4 where it became clear that the job was more tedious than for a 2D model.





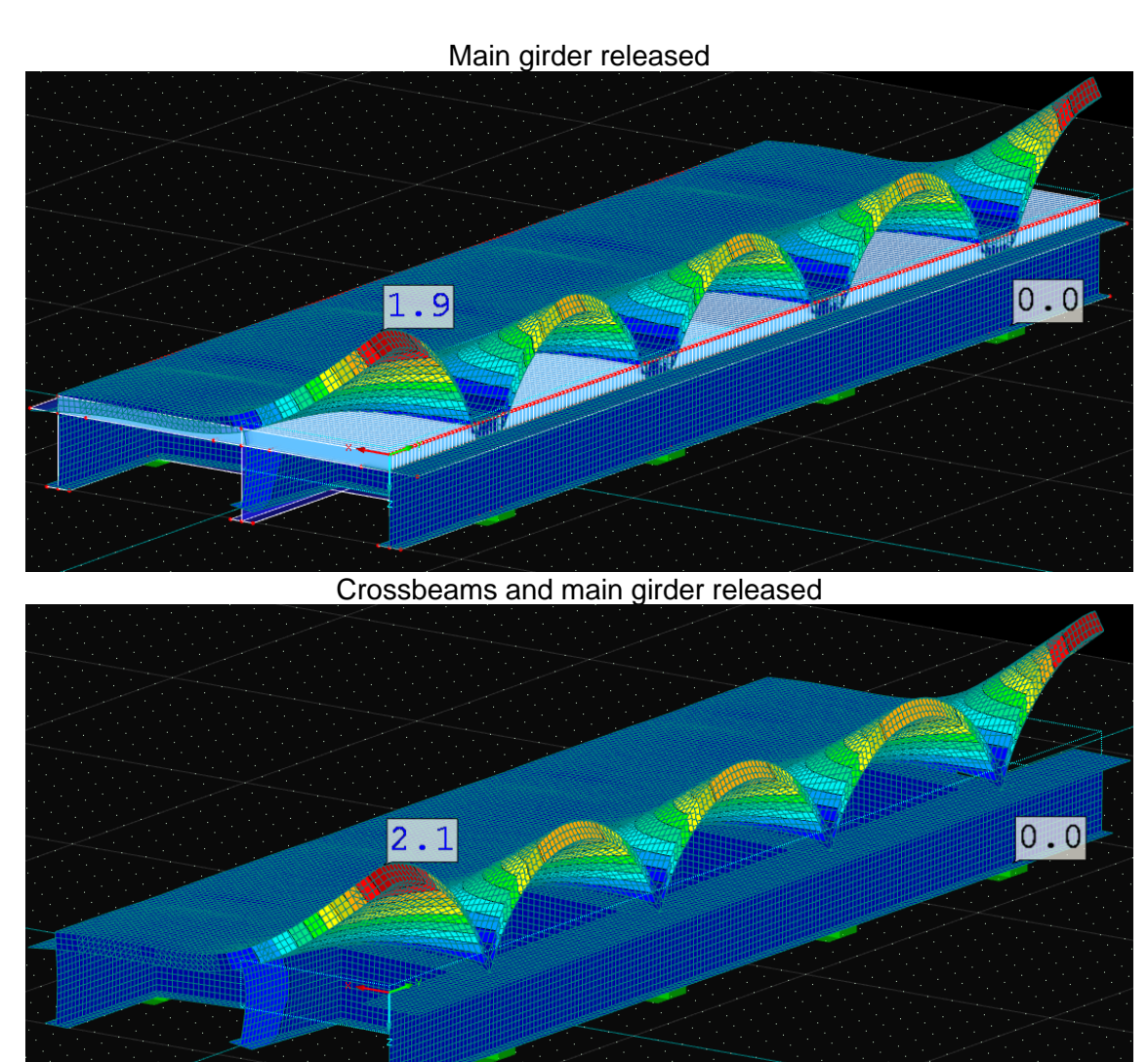


Figure H.4 release mechanism 3D example results surface release

Releases had to be defined for nodes separately, just surface releases did not work as shown in Figure H.5.





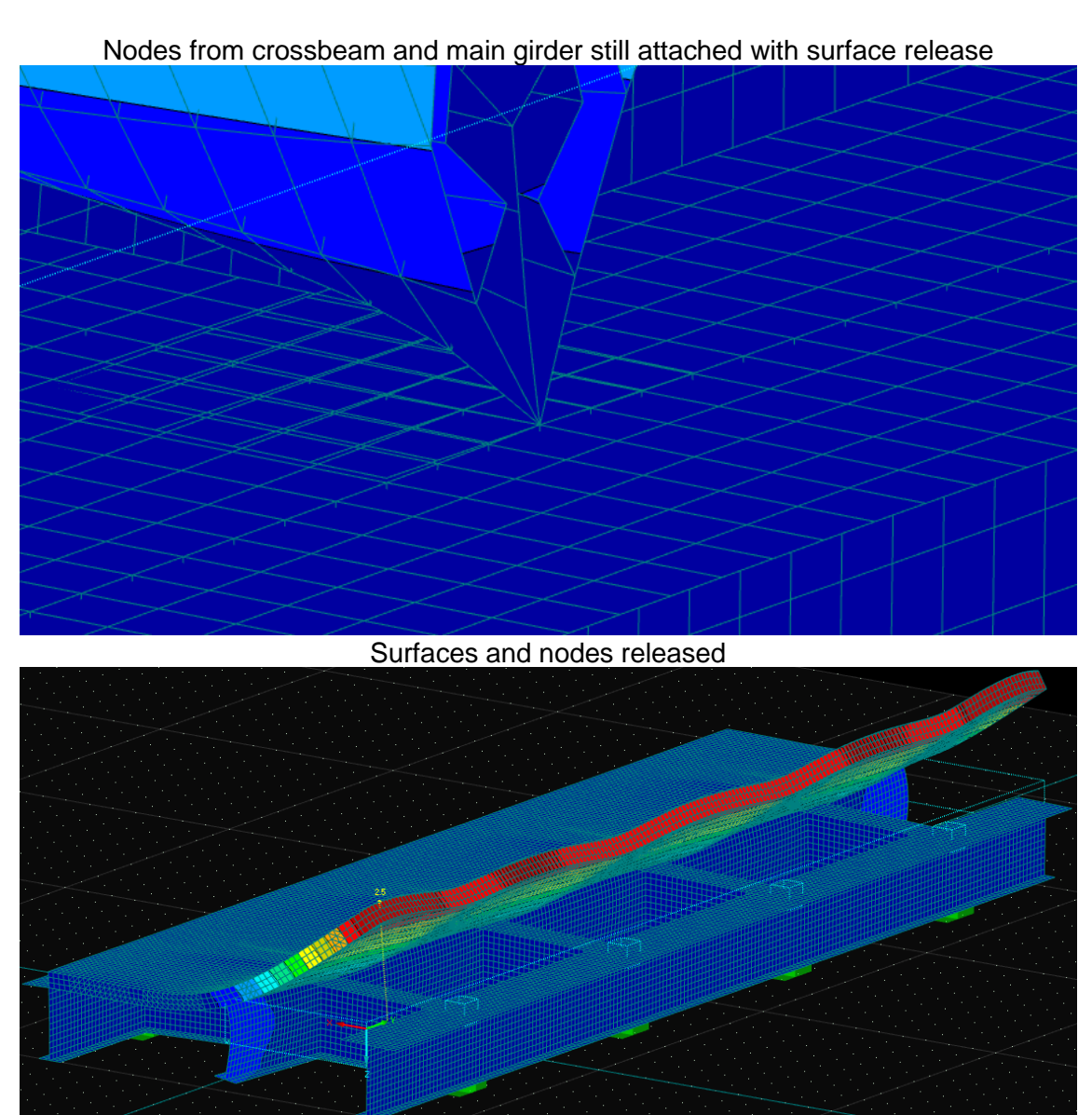


Figure H.5 release mechanism 3D example results nodal release

The next step was to create a spring release instead of complete release upon tension forces in the interface. This resulted in endless errors that could not be solved due to the size of the model. The releases worked for several surfaces but not for all which is probably a result of surfaces not overlapping correctly. This is something that could not be solved on this large scale. A more detailed model could be made to analyse local effects but this is outside of the scope for this thesis.





3D release mechanism with bolts

The choice has been made to look into a bolted connection since complete release of the model was possible. With this complete release "bolts" can be implemented as circular locations where the steel flange and FRP face sheet would be connected infinitely stiff. This should result in a correct interaction on global results, however this is not a correct representation for local results. Since the scope of this thesis is on global analysis this is no problem.

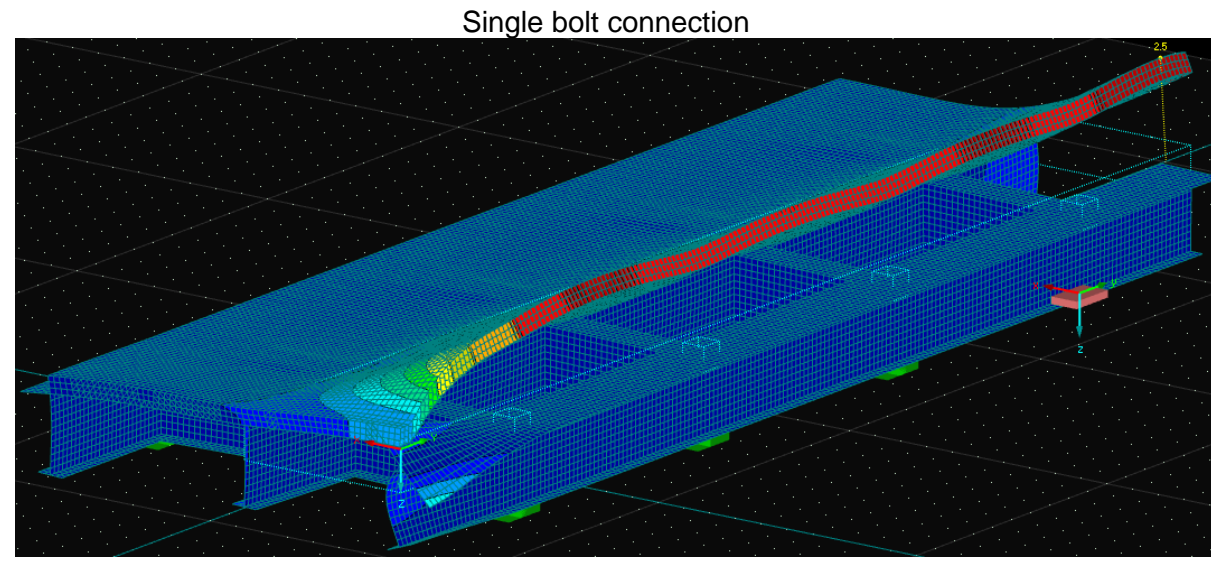
For simplicity a model had been created with just a single bolt to see if these bolts can be modelled in this way. The results can be seen in Figure H.6. The single bolt can be modelled however due to the complete release mechanism the crossbeam flange "punctures" the sandwich panel as can be seen by the black line.

In the case of two bolt rows, which is always the case in bolted connections, this would not occur since both plates will have the same deformation. This has been attempted to model on one main girder. Unfortunately this caused to many errors in the mesh of the model that mesh size became so small that calculation times became to large.

Since there are many load cases to model for this project it is undesirable to have one load case take up 20 minutes which was the case for this example. A simplification has been made where a row of rigid plate elements is modelled on both the crossbeams and main girder connecting the steel to the FRP. These rigid plate elements that have been used are elaborated in paragraph 4.2.2.







Crossbeam flange "punctures sandwich panel

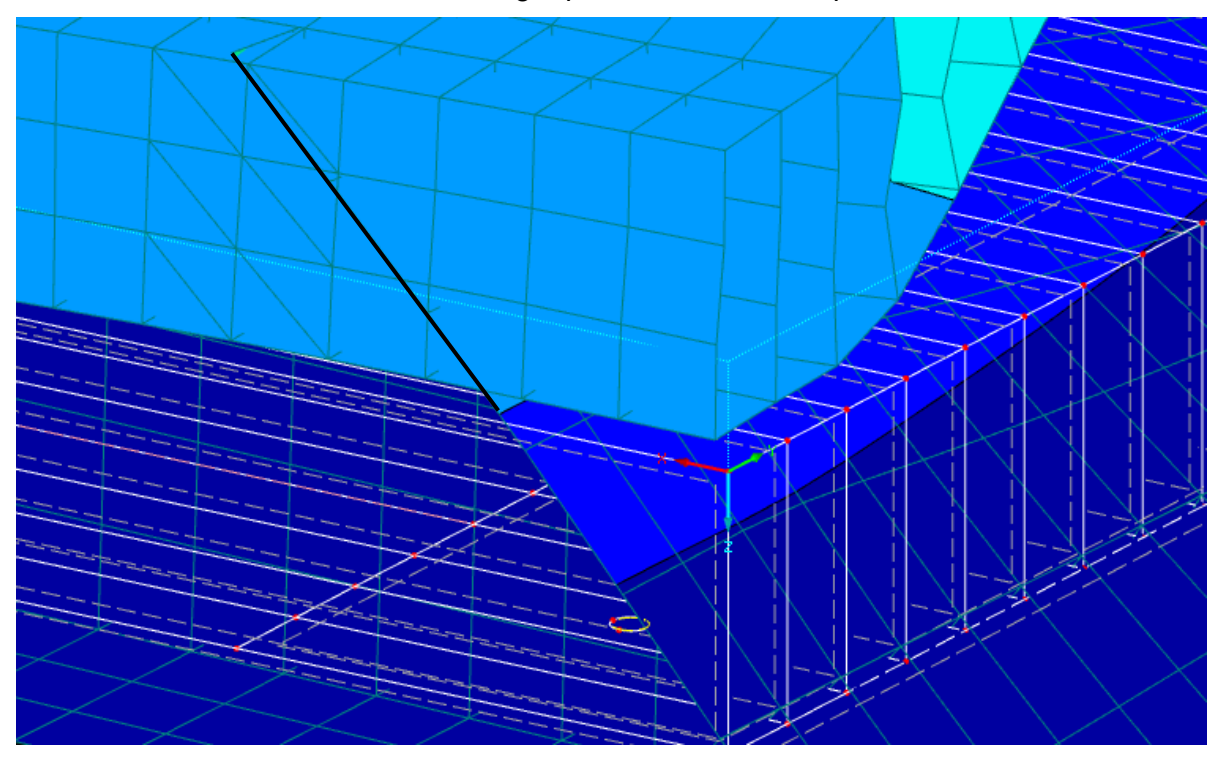


Figure H.6 release mechanism 3D example results single bolt









Annex I

Environmental impact (GWW)

Table I.1	GWW	environmental	impact val	ues
-----------	------------	---------------	------------	-----

GWW Materials											
Shadow prize (Euro) per kg equivalents		€ 0,16	€ 0,16 € 0,05 €	€ 30,00 €	0,09	€ 0,03	€ 0,00 €	€ 0,06 €	€ 2,00 €	€ 4,00 €	€ 9,00
			Global	Ozone layer		Fresh water Marine	Marine				
		Abiotic	Abiotic warming depletion	depletion	Human	aquatic	aquatic	Terrestrial Photochemic	Photochemic		Eutrophicatio 5
Impact category	unit	depletion	unit depletion (GWP100) (ODP)	(ODP)	toxicity	ecotox.	ecotoxicity	ecotoxicity ecotoxicity al oxidation Acidification n	al oxidation	Acidification	L
Unit		kg Sb eq	kg CO2 eq	kg Sb eq kg CO2 eq kg CFC-11 eq kg 1,4-DB eq kg 1,4-DB eq kg 1,4-DB eq kg 1,4-DB eq kg C2H4 kg SO2 eq kg PO4 eq	kg 1,4-DB eq	kg 1,4-DB eq	kg 1,4-DB eq	kg 1,4-DB eq	kg C2H4	kg SO2 eq	kg PO4 eq
Fibre Reinforced Polymer, glass fibre in epoxy	ķ		3,59E-02 4,42E+00	4,53E-07	7,41E+00	7,41E+00 2,60E+00 4,06E+02	4,06E+02	4,09E-02		8,93E-04 2,51E-02	2,84E-03
Fibre Reinforced Polymer, glass fibre in polyester	ķ	3,43E-02	3,43E-02 4,65E+00	7,54E-07	8,71E+00	2,80E-01	5,36E+02	4,04E-02	1,10E-03	1,92E-02	2,15E-03
Fibre Reinforced Polymer, glass fibre in vinylester	ķ	3,19E-02	kg 3,19E-02 3,44E+00	2,06E-07	5,73E+00	1,56E-01	2,83E+02	2,54E-02	7,68E-04	1,32E-02	1,02E-03
PVC (averaged)	ķ	2,26E-02	kg 2,26E-02 1,96E+00	2,95E-09	5,93E-01	1,53E-01	4,09E+01	6,84E-03	3,13E-04	5,35E-03	7,60E-04
Steel GWW (averaged)	ķ	1,54E-02	kg 1,54E-02 1,79E+00	7,17E-08	3,81E+00	1,49E+00	1,32E+03	3,18E-02	9,27E-04	7,38E-03	1,34E-03
Steel reinforcement net FeB 500 HKN	ķ	1,27E-02	kg 1,27E-02 1,49E+00	5,65E-08	6,59E-01	6,33E-01	5,90E+02	2,75E-02	8,47E-04	5,16E-03	1,05E-03
Steel slag	ķ	1,26E-02	kg 1,26E-02 1,80E+00	1,73E-07	8,63E-01	3,98E-02	1,50E+02	2,62E-03	2,81E-04	1,03E-02	2,15E-03
Steel, heaw duty - 90% Beam steel (BlastFurnace	ş	1,56E-02	Furnace kg 1,56E-02 1,82E+00	5,66E-08	6,02E-01	4,57E-01	4,27E+02	1,08E-02	1,08E-03	6,16E-03	1,32E-03





Table I.2 Case results GWW impact values

	_									ipact va								
	Cas		Case		Ca	se 3	Cas	se 4	Ca	se 5	Ca	se 6	Cas	se 7	Cas	se 8	Cas	
OSD steel kg	-	118768		154796	-	224702	-	147510		193808	-	290483	-	146303	-	192315		290950
Hybrid	+																	
Hybrid FRP kg		8339		10423		13898		10423		13029		17372		10423		13029		17372
Hybrid foam kg		1534		1918		2557		1918		2398		3197		1918		2398		3197
Hybrid steel kg		84708		111513		176512		101072		122711		179481		103577		128986		181944
Abiotic depletion	€	298	€	389	€	564	€	370	€	487	€	729	€	367	€	483	€	730
Global warming (GWP100)	€	10.864		14.159	€	20.554	€	13.493	€	17.728	€	26.571	€	13.383	€	17.591	€	26.614
Ozone layer depletion (ODP)	€	0	€	0	€	1	€	0	€	0	€	1	€	0	€	0	€	1 00 424
Human toxicity	€	40.466		52.741	€	76.559	€	50.259	€	66.033	€	98.972	€	49.848	€	65.525	€	99.131
Fresh water aquatic ecotox.	€	5.284	€	6.887	€	9.997	€	6.563	€	8.622	€	12.923	€	6.509	€	8.556	€	12.944
Marine aquatic ecotoxicity	€	15.478		20.174	€	29.284	€	19.224	€	25.258	€	37.857	€	19.067	€	25.063	€	37.918
Terrestrial ecotoxicity	€	225	€	293	€	426	€	280	€	367	€	551	€	277	€	365	€	552
Photochemical oxidation	€	221	€	288	€	418	€	275	€	361	€	541	€	272	€	358	€	542
Acidification Eutrophication	€	3.615	€	4.711	€	6.839	€	4.490	€	5.899 2.394	€	8.841	€	4.453	€	5.853	€	8.855
	<u> </u>	1.467	€	1.912	€	2.776	€	1.822	€		€	3.589	Ť	1.807	€	2.376	€	3.594
OSD Steel	€	77.919	€ 1	01.555	€	147.418	€	96.776	€	127.150	€	190.574	€	95.983	€	126.170	€	190.881
Abiotic depletion	€	46	€	57	€	76	€	57	€	72	€	95	€	57	€	72	€	95
Global warming (GWP100)	€	1.939	€	2.424	€	3.231	€	2.423	€	3.029	€	4.039	€	2.424	€	3.029	€	4.039
Ozone layer depletion (ODP)	€	0	€	0	€	0	€	0	€	0	€	0	€	0	€	0	€	0
Human toxicity	€	6.536	€	8.170	€	10.894	€	8.170	€	10.213	€	13.617	€	8.170	€	10.213	€	13.617
Fresh water aquatic ecotox.	€	70	€	88	€	117	€	88	€	110	€	146	€	88	€	110	€	146
Marine aquatic ecotoxicity	€	447	€	558	€	744	€	558	€	698	€	930	€	558	€	698	€	930
Terrestrial ecotoxicity	€	20	€	25	€	34	€	25	€	32	€	42	€	25	€	32	€	42
Photochemical oxidation	€	18	€	23	€	31	€	23	€	29	€	38	€	23	€	29	€	38
Acidification	€	640	€	800	€	1.067	€	800	€	1.000	€	1.333	€	800	€	1.000	€	1.333
Eutrophication	€	162	€	202	€	269	€	202	€	253	€	337	€	202	€	253	€	337
Hybrid FRP	€	9.878	€	12.347	€	16.463	€	12.347	€	15.434	€	20.579	€	12.347	€	15.434	€	20.579
		_	_		_		_		_		_		_		_	_	_	
Abiotic depletion	€	6	€	7	€	9	€	7	€	9	€	12	€	7	€	9	€	12
Global warming (GWP100)	€	150	€	188	€	251	€	188	€	235	€	313	€	188	€	235	€	313
Ozone layer depletion (ODP)	€	0	€	0	€	0	€	0	€	0	€	0	€	0	€	0	€	0
Human toxicity	€	82	€	102	€	136	€	102	€	128	€	171	€	102	€	128	€	171
Fresh water aquatic ecotox.	€	7	€	9	€	12	€	9	€	11	€	15	€	9	€	11	€	15
Marine aquatic ecotoxicity	€	6	€	8	€	10	€	8	€	10	€	13	€	8	€	10	€	13
Terrestrial ecotoxicity	€	1	€	1	€	1	€	1	€	1	€	1	€	1	€	1	€	1
Photochemical oxidation	€	1	€	1	€	2	€	1	€	2	€	2	€	1	€	2	€	2
Acidification	€	33	€	41	€	55	€	41	€	51	€	68	€	41	€	51	€	68
Eutrophication	€	10	€	13	€	17	€	13	€	16	€	22	€	13	€	16	€	22
Hybrid foam	€	296	€	370	€	494	€	370	€	463	€	617	€	370	€	463	€	617
Abiotic depletion	€	213	€	280	€	443	€	254	€	308	€	451	€	260	€	324	€	457
Global warming (GWP100)	€	7.748		10.200	€	16.146	€	9.245	€	11.225	€	16.417	€	9.474	€	11.799	€	16.643
Ozone layer depletion (ODP)	€	0	€	0	€	0	€	0	€	0	€	0	€	0	€	0	€	0
Human toxicity	€	28.861		37.994	€	60.140	€	34.437	€	41.809	€	61.152	€	35.290	€	43.948	€	61.991
Fresh water aquatic ecotox.	€	3.769	€	4.961	€	7.853	€	4.497	€	5.459	€	7.985	€	4.608	€	5.739	€	8.095
Marine aquatic ecotoxicity	€	11.039		14.533	€	23.004	€	13.172	€	15.992	€	23.391	€	13.499	€	16.810	€	23.712
Terrestrial ecotoxicity	€	161	€	211	€	335	€	192	€	233	€	340	€	196	€	245	€	345
Photochemical oxidation	€	158	€	208	€	329	€	188	€	228	€	334	€	193	€	240	€	339
Acidification	€	2.578	€	3.394	€	5.372	€	3.076	€	3.735	€	5.463	€	3.152	€	3.926	€	5.538
Eutrophication	€	1.046	€	1.378	€	2.181	€	1.249	€	1.516	€	2.217	€	1.280	€	1.594	€	2.248
Hybrid steel	€	55.574	€	73.159	€	115.803	€	66.310	€	80.506	€	117.751	€	67.953	€	84.623	€	119.366
Hybrid	€	65.748		85.877	€	132.759	€	79.027	€	96.403	€	138.946	€	80.670	€	100.520	€	140.562
OSD	€	77.919	€ 10	01.555	€	147.418	€	96.776	€	127.150	€	190.574	€	95.983	€	126.170	€	190.881





Annex J

Graphic weight results

Table J.1 OSD weight distribution

OSD [kg]	Case 1	Case 2	Case 3	Case 4	Case 5	Case 6	Case 7	Case 8	Case 9
weight MG	7675	11616	21618	8364	12804	26960	8525	12851	28121
weight CB	5679	7632	11025	6998	10260	15568	6324	9658	14354
weight stif	9693	12117	16156	13246	16557	21466	13246	16557	21466
weight deck	19768	24710	32947	24710	30888	41184	24710	30888	41184

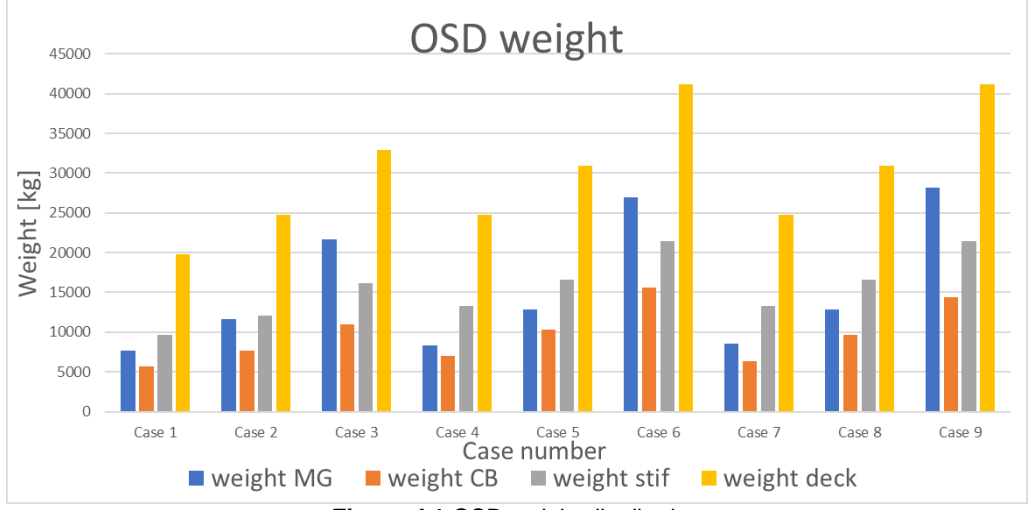


Figure J.1 OSD weight distribution

Table J.2 Hybrid weight distribution

Hybrid [kg]	Case 1	Case 2	Case 3	Case 4	Case 5	Case 6	Case 7	Case 8	Case 9
weight MG	18502	27361	50834	21408	26544	40366	23866	29989	44224
weight CB	5841	6814	8518	7829	9867	15374	7514	9107	13748
weight FRP	8339	10423	13898	10423	13029	17372	10423	13029	17372
weight Foam	1534	1918	2557	1918	2398	3197	1918	2398	3197

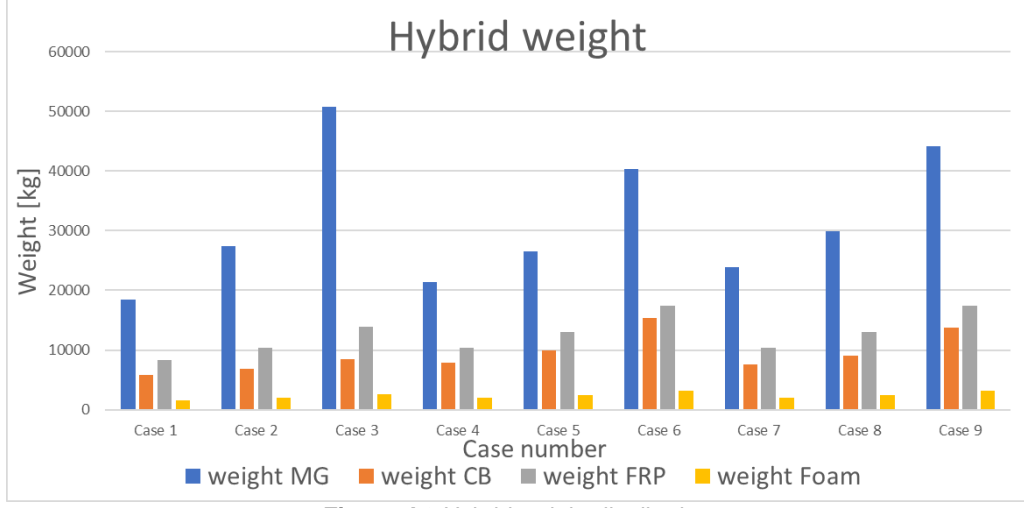


Figure J.2 Hybrid weight distribution

Table J.3 OSD weight percentage distribution





OSD [%]	Case 1	Case 2	Case 3	Case 4	Case 5	Case 6	Case 7	Case 8	Case 9
weight MG	16%	19%	24%	14%	17%	23%	15%	17%	24%
weight CB	12%	12%	12%	12%	13%	13%	11%	13%	12%
weight stif	21%	20%	18%	22%	21%	18%	23%	22%	18%
weight deck	42%	40%	37%	42%	40%	35%	42%	40%	35%

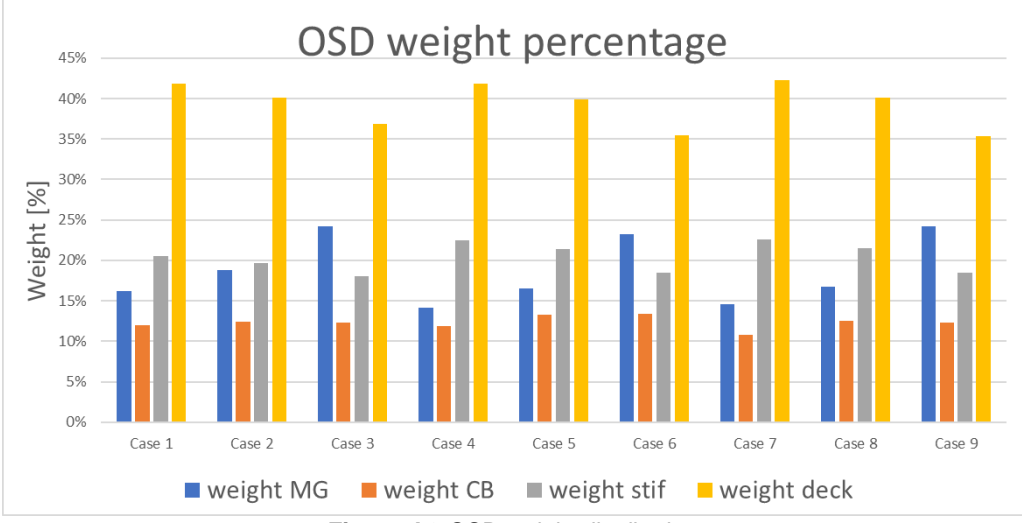


Figure J.3 OSD weight distribution

Table J.4 Hybrid weight percentage distribution

Hybrid [%]	Case 1	Case 2	Case 3	Case 4	Case 5	Case 6	Case 7	Case 8	Case 9
weight MG	49%	55%	66%	47%	48%	50%	51%	52%	55%
weight CB	15%	14%	11%	17%	18%	19%	16%	16%	17%
weight FRP	22%	21%	18%	23%	24%	22%	22%	23%	21%
weight Foam	4%	4%	3%	4%	4%	4%	4%	4%	4%

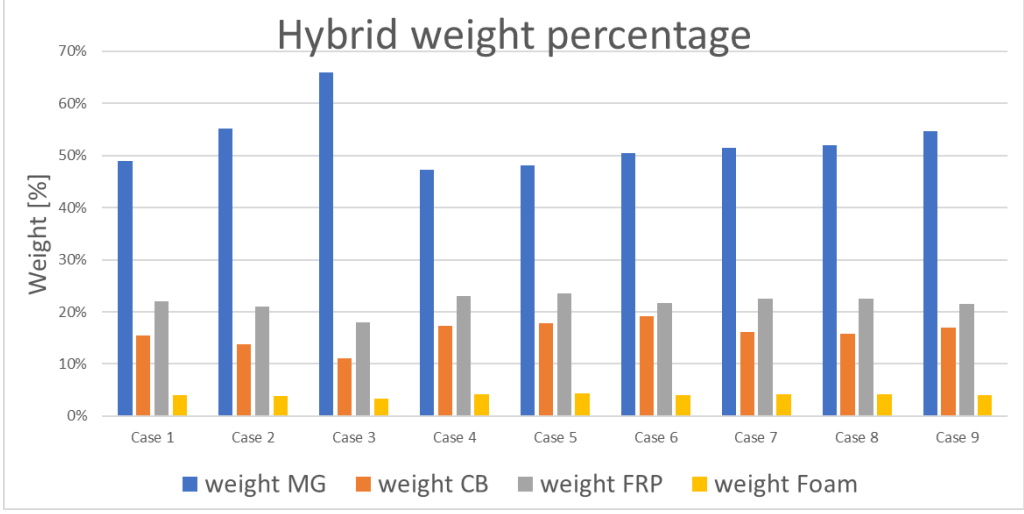


Figure J.4 Hybrid weight distribution





Table J.5 OSD weight per square meter distribution

OSD [kg/m^2]	Case 1	Case 2	Case 3	Case 4	Case 5	Case 6	Case 7	Case 8	Case 9
weight MG	67	81	113	58	71	112	59	71	117
weight CB	49	53	57	49	57	65	44	54	60
weight stif	84	84	84	92	92	89	92	92	89
weight deck	172	172	172	172	172	172	172	172	172

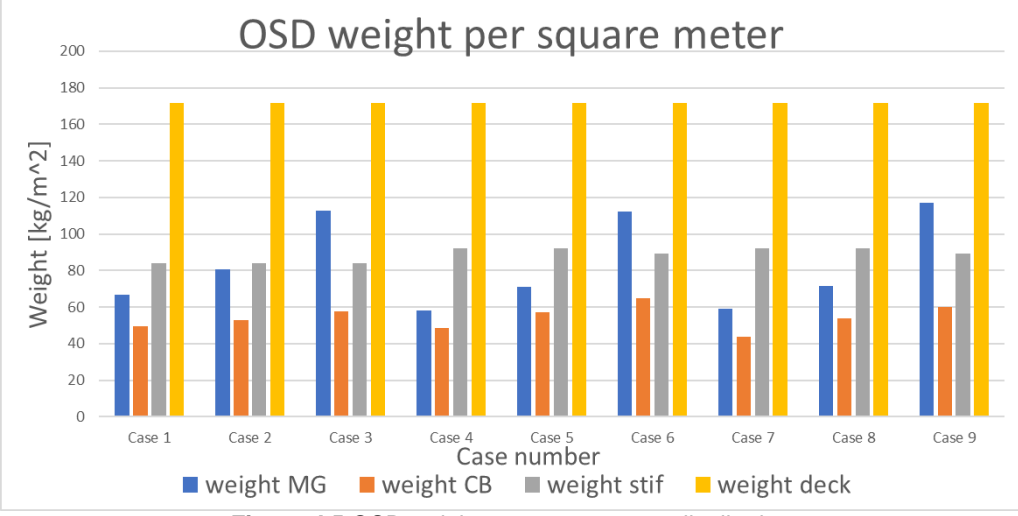


Figure J.5 OSD weight per square meter distribution

Table J.6 Hybrid weight per square meter distribution

Hybrid [kg/m^2]	Case 1	Case 2	Case 3	Case 4	Case 5	Case 6	Case 7	Case 8	Case 9
weight MG	161	190	265	149	147	168	166	167	184
weight CB	51	47	44	54	55	64	52	51	57
weight FRP	72	72	72	72	72	72	72	72	72
weight Foam	13	13	13	13	13	13	13	13	13

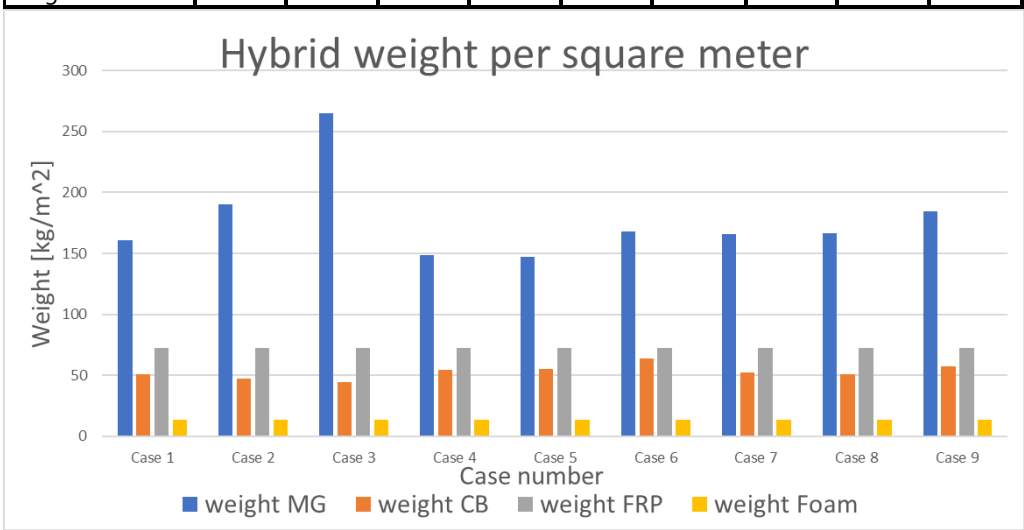


Figure J.6 Hybrid weight per square meter distribution